A STUDY OF A CYLINDRICAL, PULSED, SOLID FUEL MICROTHRUSTER

by

WILLIAM GFANT SEEGLITZ

B.S., Harvey Mudd College

1970

SUBMITTED IN PARTIAL FULFILLMENT OF THE REQUIREMENTS FOR THE DEGREES OF

MASTER OF SCIENCE

and

ENGINEER IN AERONAUTICS AND ASTRONAUTICS

at the

MASSACHUSETTS INSTITUTE OF TECHNOLOGY

February, 1973

Signature of Author _____

Department of Aeronautics and Astronautics
February, 1973

Certified by _____

Thesis Supervisor

Accepted by _____

Chairman, Departmental Committee on Graduate Studies

A STUDY OF A CYLINDRICAL, PULSED, SOLID FUEL MICROTHRUSTER

by

William Grant Seeglitz

Submitted to the Department of Aeronautics and Astronautics on January 24, 1972, in partial fulfillment of the requirements for the degrees of Master of Science and Engineer of Aeronautics and Astronautics.

ABSTRACT

A pulsed ablative solid fuel microthruster has been studied, which relies upon gasdynamic expansion of a heated teflon plasma for its thrust. Through a series of experiments the dependence of the thruster's performance upon the discharge energy and the discharge chamber geometry was investigated. It was found that the impulse bit and the mass ablated/shot were proportional to the discharge energy and the length of the discharge chamber. Their dependence upon the chamber diameter was weak. Typical values for the specific thrust range from 7.0 micropounds/watt to 11.9 micropounds/watt. The mass ablated/shot varies from 100 micrograms/shot to 300 micrograms/shot. The specific impulse of the thruster was found to be proportional to the inverse of the square root of the chamber length. Its dependence upon the chamber diameter and the discharge energy was much weaker. Typical values for the specific impulse range from 250 seconds to 400 seconds. The efficiency was found to be relatively constant, regardless of configuration changes. It had values between 6% and 10% The addition of nozzles, without converging section, generally improved the performance of the thruster, by as much as 30%. Polyethylene was tried as a propellant and produced a specific impulse greater than teflon but with a much lower impulse bit.

A feed mechanism, employing Negator springs, was designed, to permit long-life tests of the thruster. A life test of about 510,500 shots was conducted in which two and one-half inches of teflon (48 grams) were fed and ablated successfully. Problems with uneven ablation were encountered and since corrected by changing the discharge energy. Material investigations showed Mallory 1000 to be the best electrode material and quartz the best discharge chamber side wall material. The application of such a thruster to satellite control is discussed.

A model is proposed and expressions derived which relate the thruster's performance to its discharge energy and chamber geometry. They predict, to first order, the general trends found by experimentation.

Thesis Supervisor: Albert Solbes
Title: Associate Professor of Aeronautics and Astronautics

ACKNOWLEDGEMENT

The author wishes to express his sincere appreciation to Professor Solbes for his assistance and advice during the course of work on this thesis. His many helpful suggestions and insights contributed much towards successful completion of this work. The author would like to express his gratitude to Mr. John Stevens and Mr. John Barley, for the very helpful technical advice and assistance they provided.

The author would also like to give a very special thanks to his parents for their support and guidance over the years which have made all of this possible.

To the author's wife, Linda, goes his sincerest thanks and appreciation for bearing with him during the work for this thesis and for the considerable help, including the typing of the manuscript, which she has given him in completing this thesis.

Finally, a word of thanks to the Air Force and M.I.T. Lincoln Laboratory, who provided the funds with which this research was performed.

TABLE OF CONTENTS

Chapter No.		Page No.
1	Introduction	13-16
2	Thruster Design	17-29
3	Performance Evaluation	31-41
4	Data & Analysis--Review of Experimental Results	42
	Data and Analysis	43-56
	Analysis--Theoretical Considerations	57-64
	Data and Analysis--Summary of Experimental Results	65-67
	Table 1: Summary of Experimental Results	68-89
	Table 1: Comments on Configurations	90-93
5	Satellite-Thruster System	94-99
6	Conclusion	100-101
Appendix	Error Analysis	102-104
Figures		105-172
References		173-175

List of Figures

Figure No.		Page No.
1	Schematic of Thruster Components	105
2	Front View of Test Thruster--Circular Configuration	106
3	Slant View of Test Thruster--Circular Configuration	107
4	Ignition Circuit Schematic	108
5	Bendix Ignitor Plug	109
6	Circular Configuration Modified for Fuel Feed	110
7	Two Nozzles Based on Rao[12] Calcualtions	111
8	Five-inch, Sectioned 30° Full Angle Test Nozzle--Full Size	112
9	Rectangular Nozzle--Aluminum, Scale 2:1	113
10	Discharge Waveform (High Damping)	114
11	Discharge Waveform (Low Damping)	115
12	Slant View of Test Thruster--Rectangular Configuration	116
13	Side View of Thruster--Rectangular Con-Configuration	117
14	Rectangular Test Thruster Disassembledto Show Component Placement	118
15	Thruster Attached to Pendulum	119
16	Thruster Stand--Showing Thruster Mounted on Pendulum Resting on Cradles	120
17	Thrust Stand--Showing Laser--Mirror Arrangement	121
18	Thrust Stand/Vacuum System--Showing Meter Stick Laser--Arrangement	122
19	Triggering Circuit Schematic	123
20	Meter Stick Reading Vs. Time	124

Figure No.		Page No.
21	RLC Representation of Thruster Discharge Circuit	125
22	Discharge Waveform (Low Damping)	126
23	Discharge Waveform (High Damping)	127
24	Discharge Waveform (Over Damped)	128
25	Schematic of Life Test Triggering (Pulser) Circuit	129
26	Impulse Bit & Specific Impulse vs. Discharge Energy	130
27	Mass Ablated/Shot & Efficiency vs. Discharge Energy	131
28	Specific Thrust & Specific Mass/ Shot vs. Discharge Energy	132
29	Specific Impulse vs (Discharge Energy)$^{1/2}$	133
30	Impulse Bit vs Chamber Diameter	134
31	Specific Impulse vs. Chamber Diameter	135
32	Specific Thrust & Efficiency vs. Chamber Diameter	136
33	Mass Ablated/Shot & Specific Mass Ablated/Shot vs. Chamber Diameter	137
34	Impulse & Specific Impulse vs Length of Discharge Chamber	138
35	Efficiency vs. Chamber Length	139
36	Mass Ablated/Shot vs. Chamber Length	140
37	Specific Thrust vs. Chamber Length	141
38	Specific Impulse vs. Chamber Length	142
39	Efficiency vs. Chamber Length	143
40	Mass Ablated/Shot vs. Chamber Length	144

Figure No.		Page No.
41	Specific Thrust vs. Nozzle Length	145
42	Specific Impulse vs. Nozzle Length	146
43	Efficiency vs. Nozzle Length for 15° half angle nozzle	147
44	Specific Thrust vs. Hydraulic Diameter ---Rectangular Geometry	148
45	Specific Impulse vs. Hydraulic Diameter ---Rectangular Geometry	149
46	Specific Impulse vs. (Hydraulic Diameter)$^{1/2}$	150
47	Specific Mass Ablated/Shot vs. Hydraulic Diameter---Rectangular Geometry	151
48	Specific Mass Ablated/Shot vs (Hydraulic Diameter)$^{-1}$---Rectangular Geometry	152
49	Efficiency vs. Hydraulic Diameter--- Rectangular Geometry	153
50	Erosion of Super-mica Sidewall	154
51	Erosion & Mica Deposits on Stainless Steel Cathode	155
52	Uneven Teflon Ablation Profile--Side View	156
53	Uneven Ablation of Teflon--Slant View	157
54	Front View--Teflon Ablation Profile	158
55	Ablation Profile--Energy Effects	159
56	Ablation Profile--Chamber Diameter Effects	160
57	Resistance & Inductance vs. Chamber Diameter	161
58	Inductance vs. Chamber Diameter	162
59	Resistance vs. Chamber Diameter	163

Figure No.		Page No.
60	Resistance vs. (Chamber Diameter)$^{-1}$	164
61	Resistance & Inductance vs Chamber Length	165
62	Resistance & Inductance vs. Hydraulic Diameter---Rectangular Geometry	166
63	Resistance vs. (Hydraulic Diameter)$^{-1}$ ---Rectangular Geometry	167
64A	Thruster Performance Range	168
64B	Mass Ablated/Shot vs. hE/D--Circular and Rectangular Geometries	169
65	Schematic of 4-wall Teflon Feed Thruster	170
66	Typical Thrusting for East-West Station-Keeping	171
67	Typical Thrusting for North-South Station-Keeping	172

SYMBOLS

Latin Letters

a = Diameter described by capacitor electrodes in circular configuration

A_{EXIT} = Exit area of nozzle

A_{THROAT} = Cross-sectioned area of nozzle throat

c = Dimension (height) of rectangular chamber cross-section

C = Main storage capacitor capacitance; Centigrade degrees--temperature

cc = cubic centimeter

C_p = heat capacity at constant pressure

D = Diameter of circular chamber cross-section

E = Discharge Energy

ev = electron volts

f = firing frequency, friction coefficient; $\bar{f}$ = average friction factor

g = acceleration due to gravity = 9.81 m/sec^2

h = length of discharge chamber

h_v = heat transfer coefficient

H_p = total enthalpy per unit mass of plasma

H.D. = Hydraulic Diameter

i(t) = Discharge current

I = Impulse bit

I_{sp} = Specific impulse

I/E = Specific thrust

$\bar{J}$ = Current density in chamber

K = Kelvin degrees--temperature

Latin Letters(cont).

ℓ = length of nozzle, distance from axis of rotation to center of the pendulum assembly

ℓ' = distance from axis of rotation to center of thrust

L_c = capacitor internal inductance

L_{cir} = circuit inductance

L_p = plasma inductance

m = total mass ablated during a run

M = mass of pendulum thruster assembly; Flow Mach number

M_o = total satellite mass

M_p = total propellant mass

$\dot{m}$ = rate of mass ablation

$\Delta m/E$ = specific mass ablated/shot = $M/(N \cdot E)$

$\Delta m/shot$ = mass ablated/shot = M/N

ma = milliamperes

mhos = $(ohms)^{-1}$

q = heat transferred from plasma to walls

N = total number of shots fired during a run

R = Universal gas constant

R_c = capacitor internal resistance

R_{cir} = circuit resistance

R_p = plasma resistance

S_D = slope of direct fire curve

S_R = slope of retro-fire curve

SCR = silicon-controlled rectifier

St = Stanton number = $hv/(\rho u C_p)$

Latin Letters

t = time

T = thrust, period of pendulum assembly

t_{max} = time of maximum overshoot of discharge waveform

t_f = firing ends

t_i = firing begins

T_e = electron temperature

T_p = plasma temperature

T_w = wall temperature

u = mass averaged flow velocity, average exhaust velocity $= I_{sp} \cdot g$

V_c = voltage applied across the capacitors

V_m = voltage applied to storage capacitors, measured voltage

ΔV = satellite velocity increment

w = dimension(width) of rectangular chamber cross-section

Greek Letters

α = deflection angle of pendulum from rest position

α_f = angle at which firing ends

α_i = angle at which firing begins

α_∞ = asymptotic value of α as time increases indefinitely

α_n = maximum deflection after N^{th} shot

ε = energy required for ablation of a mass Δm of teflon

η = efficiency of thruster = $1/2(I/E)(I_{sp}) \cdot g$

ϕ = phase angle of current discharge waveform

γ = ratio of specific heats

Greek Letters

λ = heat of ablation of teflon = 2180 joules/gm

μ = micro-10^{-6} (μlb-sec--micro-pound seconds = 10^{-6} pound sec)

ν = damping constant of pendulum

ω = angular frequency of pendulum

$\omega_c = \omega/(1-\nu^2/\omega^2)$

ω_n = natural frequency of voltage discharge waveform = $1/LC$

ρ = plasma density

ξ = damping voltage discharge waveform = $R/2L\omega_n$

σ = conductivity of plasma

CHAPTER I

INTRODUCTION

Recent spacecraft designs have shown a trend toward multi-year missions requiring long term positioning and attitude control. To meet this requirement, reliable, accurate, and long-life propulsion systems are being developed, with special emphasis being placed on low system weights and high specific impulses. These propulsion systems deliver thrust in the micro- and millipound levels and may be required to operate in either a steady or a pulsed mode.[1] In view of the need for long lifetimes and high specific impulses, electric thrusters are being considered instead of chemical systems for many auxillary propulsion applications. One candidate for such a low power, high performance system is the pulsed ablative thruster. In a recent survey,[2] this type of thruster was compared with a number of other propulsion devices and, on the basis of critical components and subsystems, it was rated the most reliable system. An electric thruster, it can operate in either of two ways, by the action of electromagnetic body forces, or by expansion of a propellant heated electrically. This thesis is concerned with the development of this latter type of thruster.

Advantages of such systems are:[3]

1. Simplicity and ruggedness; the only moving part is a spring-driven fuel rod.
2. High reliability and long life; lifetimes of tens of millions of shots have been achieved for pulsed ablative thrusters.
3. Solid propellant advantages:
    a). No tanks, heaters, feed lines or valves are required.
    b). Simple feed systems; no special requirements for

zero-g or vacuum conditions.

c). Long shelf-life (very low vapor pressure)

4. Discrete impulse bits; with pulse mode firing, the thruster is adaptable to either 3-axis stabilized or spin stabilized satellites. Steady thrust may be obtained by firing at a sustained pulse frequency.
5. Zero warm-up time; little or no standby power is required.
6. Fail-safe failure mode; an inoperative thruster will produce no thrusts. There are no escaping gases to cause forces or moments on the spacecraft.
7. Power availability; necessary power is obtainable from low voltage output solar cells with the use of a power conditioner.
8. Specific thrusts greater than 11 micropounds/watt(91 watts/ millipound) have been obtained.

Two main drawbacks to the pulsed ablative thruster are the problems of redundancy and storage capacitor weight. In order to achieve redundancy with this system, not only are a separate set of nozzles and electrodes needed, but in addition a separate fuel element must be added. A new fuel element is necessary because, in event of a chamber failure, the fuel rod in that chamber cannot be switched to a new chamber, as can gaseous propellants with a valve. There is no apparent way of circumventing this problem.

Capacitors are a critical component of this system. To achieve long lifetimes ($>10^7$ pulses), very reliable capacitors must be used, which add a weight penalty. Presently capacitors have an energy density of about 20 joules/

kilogram for a lifetime of 10^7 pulses with 0.96 reliability.[4] Undergoing tests now are capacitors with lifetimes of 10^{11} pulses and a specific weight of ~13 joules/kgm .[5] Therefore, at the present time, although basically very reliable, the capacitor weight and the non-switchable fuel feed tend to penalize redundancy in this type of propulsion system. In some cases, this makes the pulsed ablative system less desirable than other types of thrusters.[6]

The LES-6 thruster,[7] which has been flight tested, is a typical electromagnetic pulsed ablative thruster. Using virgin teflon for its solid fuel, the thruster is pulsed the necessary number of times to produce the desired thrusts (on the order of hundreds of thousands pulses for pound-second changes in momentum). However, while high specific impulses have been obtained using such thrusters, in general their specific thrust has been low, ∿4 μlb/watt, and their impulse bit has been small, ∿7 μlb-sec for LES-6 and 70 μlb-sec for the LES-7 thruster,[8] (a higher powered version of LES-6). With investigation it has been found that the thrust of the LES-6 type of thruster is about evenly divided between gas-dynamic and electromagnetic contributions.[9] Starting from this point, my thesis has been concerned with the development of a purely gas dynamic pulsed ablative thruster, with a high specific thrust and a large impulse bit. The high specific thrust is desired to keep the power conditioner weight low. The high impulse bit is necessary in order to lower the number of times the thruster must be pulsed (cycled) to produce a given impulse change, thereby increasing the lifetime of the thruster components, in particular, the capacitors.

In addition to designing a thruster with a high specific thrust and a high specific impulse, attention must be given to the integration of the

thruster into the spacecraft and the types of mission that it is capable of performing. Some items that must be examined are the power conditioner, efficient utilization of the required satellite volume, and thruster noise and exhaust effects upon the spacecraft.

CHAPTER II

THRUSTER DESIGN

The principle of operation of cylindrical pulsed ablative thrusters is as follows. A high voltage electrical discharge occurs along the surface of the teflon propellant, which forms the discharge chamber. Teflon molecules are ablated and heated forming a hot plasma that exhausts from the open end of the chamber, producing thrust. Dissociation and ionization of the teflon molecules also occur to some extent. The level of ionization is about 10% for the LES-6 thruster and is probably comparable for the cylindrical design studied here. Singly, doubly, and triply ionized atoms of carbon and fluorine are present in the exhaust gases, as well as the teflon polymers, monomers, and free radicals. The electrical discharge occurs axially in the same direction as the thrust. The thrust is produced by gasdynamic forces. The major Lorentz forces ($\vec{J} \times \vec{B}$ forces) are perpendicular to the direction of flow and have small effect upon the plasma compared to the effect of the gasdynamic forces.

TEST THRUSTER

The test thruster was designed and constructed to fit the thrust stand (See Chapter III) and to permit relatively easy changes in thruster configurations for the purposes of testing. The basic design consists of six-2 microfarad capacitors for main energy storage, an ignition circuit, the cathode and anode, and the teflon fuel. (See Figure 1).

The sequence of events that occur for one shot is as follows;

1. The six-2 microfarad main energy capacitors are charged to the desired voltage (typically 1825 volts (20 joules)). The 1 microfarad trigger capacitor (ignition circuit) is charged

to 500 volts (1/8 joule).

2. To fire the thruster , a command impulse (6 volts, 10 millisecond duration) switches a silicon-controlled rectifier (SCR) which connects the trigger capacitor to the primary of the transformer. The energy is transferred to the secondary coil causing a spark at the surface of the ignitor plug.
3. The spark produced causes particles to be ejected into the gap between the main electrodes.
4. An electrical breakdown occurs between the anode and the cathode and is fed by energy in the main storage capacitors. The current is on the order of 10,000 amperes.
5. Teflon molecules on the exposed surface of the fuel are ablated and partially dissociated and ionized by the high energy discharge. The resulting plasma is heated (Joule heating) and exhausts through the open end of the thrust chamber.

This sequence of events then repeats itself. One pulse, gives typically an impulse bit on the order of 200 micro-pound-second. The electrical discharge lasts approximately 1-3 microseconds. The gaseous efflux continues for a time after the discharge is over[10] and approximately $2 \cdot 10^{-7}$ kilograms of teflon are ablated. In actual operation the thruster would be pulsed enough times to produce the desired amount of thrust, some multiple of 200 μlb-second. By pulsing the thruster at a sustained frequency, a steady thrust can be developed, its value is given by,

$$T = I \cdot f \qquad (2\text{-}1)$$

where:

T = thrust

I = impulse bit

f = firing frequency

The basic thruster configuration is shown in Figure 2 and 3. This circular arrangement was used during most of the testing. It consists of the six-2 microfarad capacitors in a circle, with the teflon fuel piece between them at the center of the thruster. The front and back plates are aluminum. The ignition circuit, SCR, and transformer are mounted on the back plate, while, depending upon the configuration, the spark plug is either press-fit into the cathode (attached to the base plate), or attached to an inert wall of the discharge chamber. The two ignition circuit capacitors are strapped alongside of the main storage capacitors.

The main discharge capacitors are high quality capacitors rated at 2000 volts, 2 microfarads each, (Dearborn Hi-Jul Energy Capacitors, ESXP 205J20001). They are tubular approximately 2" in diameter by 2 1/2" long. Their leads are size 10-32 bolts extending about 3/4" from either end. These leads were placed, into the front and back plates and bolted to them. From Waltz[11], each capacitor has an internal inductance of approximately 34 nanohenries and an internal resistance of 0.034 ohms.

The ignition circuit is the same one used for the LES-6 and LES-7 thrusters. Its schematic is shown in Figure 4. A six volt pulse to the SCR, shorts the trigger storage capacitor to ground through the primary of the transformer. The voltage is increased by a factor of three and from the secondary is applied to the electrodes of the spark plug. The spark plug

(Bendix #10-380704-1, ignitor plug), consists of a round stainless steel center electrode approximately 0.25" in diameter. This is surrounded by an annulus of semiconductor material about 0.05" thick. This is surrounded by an annulus of steel about 0.75" across on the outside, which is the other electrode. See Figure 5. When triggered, the spark jumps from one electrode to the other across the surface of the semiconductor material, ejecting particles into the discharge chamber. The outer electrode is at the same potential as the back plate and serves as the cathode when the chamber diameter is less than 0.75".

The back plate consists of two pieces, one 3/16" thick aluminum disc and one 1/8" thick stainless steel disc. The stainless steel disc is of a small enough diameter to fit between the capacitors in the thruster. It is movable, axially, to accomodate varying lengths of fuel. In the majority of runs, the spark plug was pressed through a hole in the center of the stainless steel disc, fitting very tightly. The teflon discharge chamber is then centered over the spark plug. With sufficient pressure forcing the teflon against the plate, an effective seal could be made allowing no appreciable plasma leakage. In cases where the fuel chamber diameter is less than the spark plug center electrode diameter, a cover plate is placed over the front of the stainless steel disc. Approximately 1/8" thick, this plate has a small hole, 1/8" in diameter, drilled through its center. The spark plug side of this hole is flared out to the diameter of the semiconductor material. In this way, the ejected particles can be funnelled into the discharge chamber.

The front plate was designed to accept a variety of cathode configuations and nozzles. It consists simply of a 3/16" thick aluminum annulus to which

the capacitors, electrode holders, and nozzles can be bolted. It rests against the front surface of the capacitors and remains stationary to accomodate different lengths of teflon.

The circular configuration was modified to accept the teflon feed by replacing the front aluminum plate with a plexiglas plate. The stainless steel back plate was mounted to the front of this. Copper leads connected the capacitor terminals to the anode and cathode. (See Figure 6). The spark plug was placed in two positions, in the cathode, as before, and in an inert wall in the discharge chamber.

Optimization

Some of the main considerations in designing a thruster for a spacecraft are its thrust to weight ratio, its thrust to power ratio, or specific thrust, and its specific impulse. These last two can be combined to define an efficiency for the thruster. In addition, the volumetric size of the thruster is important. The first three of these considerations arise from the fact that for every pound of thruster, fuel, or power conditioner weight needed, a pound of satellite payload weight is taken away. The last consideration is based on the limitation placed on the satellite volume by the booster used.

The thruster to weight ratio will determine the thruster weight once the thrust level needed for the spacecraft mission is determined. The higher this ratio, the lighter will be the unit for any given thrust level. Although difficult to determine, an estimate of this number can be made from the previous pulsed thruster engines, LES-6 and LES-7, which were carried through to the flight test stage of design.

The specific thrust, I/E, will determine the power conditioner size for a given level of thrust. Here also, the larger the ratio, the larger are the weight savings for the thruster system. For example, if it is important that the time necessary for a given maneuver be kept small, a pulsed thruster will have to be pulsed at a fast enough frequency to give all the necessary velocity increment in the given time. If the specific thrust is low, this frequency will have to be high, requiring a large power drain from the satellite. If the specific thrust is too low, it is possible that because of power conditioner cycling time, the system cannot be pulsed at a high enough frequency to achieve the required ΔV within the time constraint. A high I/E has the added advantage of reducing storage capacitor and power conditioner weight. By reducing the number of times the capacitors must be cycled to produce a given ΔV and by decreasing the amount of energy they must store, the design specifications for the capacitors can be relaxed resulting in lighter capacitors. Similarly, the weight of the power conditioner may be reduced because of the lower power and reduced number of cycles required.

The specific impulse, I_{sp}, relates directly to the weight problem. Being the ratio of thrust to the rate that fuel is required, the higher this ratio, the smaller will be the amount of fuel required to achieve the desired thrust. Especially in long missions, this ratio can be critical. For missions which require a large velocity increment, the fuel weight could be exorbitant, if the specific impulse is too low.

Sometimes a design change will increase the impulse, I, and decrease the specific impulse, I_{sp}, or alternatively increase I_{sp} and decrease I. In these cases, the thruster efficiency becomes an important figure of merit of

the thruster configuration. The efficiency is given by the ratio of the average kinetic energy in the exhaust, based on the average particle velocity, to the energy supplied to the thruster. Losses in efficiency can arise from electrode and capacitor resistance, energy required for ablation, exhaust beam divergence, velocity spread, and unrecovered energy in the form of dissociated and ionized species in the exhaust. In general, an overall thruster improvement can be based on an increase in efficiency. Thus, for a given I_{sp}, the maximum I is found, or alternatively for a given I, the maximum I_{sp} is sought. The designer is also left with the option of selecting a high value of thrust, or specific impulse, as needed, with decreased values of the I_{sp} or the I, respectively, and a reduced efficiency.

In designing the thruster for this thesis, general improvements in specific thrust and specific impulse were sought. Thus, efficiency was used to determine the optimum design. Factors that affect the performance of the cylindrical thruster are: 1) Discharge energy; 2) Fuel configuration including the size and shape of the discharge chamber, its length, and parallel or sloping walls; 3) The addition of a nozzle; the nozzle length; and, 4) The total thruster circuit inductance; by changing the thruster design, the inductance and energy losses of the system would be affected.

The means by which these different parameters were changed is described below.

PROPELLANT CONFIGURATIONS

Design of the propellant (teflon) shapes for the tests was dictated by two requirements, the first was the configuration that was to be tested---circular or rectangular cross-section, tapered walls or straight, etc. The

second requirement was the desirability of obtaining an ablation profile. In order to test the uniformity of ablation in the axial (discharge) direction, the amount of mass ablated as a function of axial distance had to be found.

A. Circular Cross Section

The majority of the tests run were performed on teflon with circular cross sections. The main reasons behind this was the relative ease of machining required, as compared to that needed for rectangular shapes. Since the results for circular cross sections could be applied to rectangular cross sections in many instances, the tremendous time saving was a major consideration. Since the circular shape is very difficult to feed, thus making it impossible to maintain a constant radius, a rectangular shape was used for the final design of the long-life thruster.

In early experiments, a 1 1/2" diameter rod of teflon was bored with a hole of the desired diameter and then sliced into 1/4" thick discs. These discs were numbered and placed in a plexiglas sleeve which kept them together and kept the interior bore (the discharge chamber) aligned. By weighing each disc before and after each run and noting its position, an ablation profile could be plotted. In later experiments, small holes were drilled axially near the outer edge of each disc. Then 1/8" plexiglas rods were placed into them, keeping them together and aligned. The end of each rod was threaded and bolts were used to clamp the entire assembly together. In this way, not only could ablation profiles be found, but tests could be run for different lengths of the propellant discharge chamber.

Diameters of teflon from 0.15" to 0.812" were tested in this way. In addition, lengths from 0.5" to 2.5" were also tested. Using the

same arrangement, different wall taper angles were examined. The angles (full included angle) ranged from 0° to 25°. In addition to teflon, polyethylene, and plexiglas were also tested.

B. Rectangular Cross Section

In testing rectangular cross sections, three cases were examined. These included discharge chambers with two, three and four walls of teflon. In the two wall case, only bars of teflon 0.44" wide by 1.1" high were tested, however, the teflon wall separation was varied from 0.16" to 0.28". Super-mica (a mica composite), boron nitride, and quartz were tested for the two inert walls. In the three teflon wall configuration, one of the inert walls was replaced by teflon.

The four wall design consisted of two-2" by 1" by 1" blocks of teflon, between which were sandwiched two movable teflon inserts, 1" by 1" by (1/4" and 1/8"). The two inserts could be moved apart separately and clamped. In this way, tests were run for chamber sizes of 0.125" by 1.0" to 0.125" by 0.25" and 0.25" by 1.0" to 0.25" by 0.125".

C. Feed Methods

In the course of experimentation, two feed methods were used. The feed provides for a constant supply of fresh propellant as the discharge ablates away teflon. The first method---using coil springs to keep the teflon bars against the shoulder in the cathode was adequate for short term runs but could not be used for long-life tests as the springs did not have large enough deflections. The test was with four teflon bars forming a chamber 1/4" by 1/4" by 1". Smaller 1/8" by 1" pieces of teflon were used to form seals at the corners of the teflon discharge chamber. These were held in place by

coil springs also.

In order to handle longer lengths of teflon, Negator springs were used instead of coil springs. These springs, coiled strips of stainless steel exert an almost constant force, regardless of their deflection. The Negator springs used have a return force of ~6 pounds and a deflection length of 30 inches. A small shoulder (~0.030") in the cathode or anode retained the fuel in proper position. Ablation occurs satisfactorily behind the steps. (See Figure 6.)

NOZZLE DESIGN

A number of different nozzles were designed and constructed in order to improve the performance of the thruster. The first of these was an integral part of the teflon itself. The last three 1/4" discs of the 2.5" fuel element were machined to form a converging throat and diverging parabolic shaped nozzle. The area ratio for this "internal" nozzle was (A_{exit} : A_{throat}) 5.4 : 1. This corresponds to a mach number of 3.85 for gas with a specific heats ratio of $\gamma = 1.4$.

An external nozzle was then constructed, from aluminum and stainless steel. Using the results of G.V.R. Rao[12], two nozzle contours were determined, for optimum thrust, for 0.5" bore and 0.812" bore teflon fuel elements. The respective mach numbers were 3.5 and 2.6. (See Figure 7). Although the design was for the steady flow in a perfect gas, it was believed that the nozzle would perform adequately with the teflon thruster. The first nozzle was tested with both a converging-diverging throat, and simply a diverging throat..

In many resisto-jet designs, a 15° half angle diverging cone is used as an approximation to an ideal nozzle. In order to examine the effect of

nozzle length on performance, a segmented five-inch, 15° conical nozzle was constructed. This nozzle could be used in one, two, three, four, and five inch sections, to determine the optimum length. The throat area was stainless steel, slightly larger in diameter than the teflon bore. It had no converging portion, as seen in Figure 8.

A nozzle was also tried with a rectangular fuel configuration. Having 15° sloping sides (mach number ~3.5), it was constructed of aluminum and was one inch long. (See Figure 9).

THRUSTER CURRENT LOOP CONFIGURATIONS

During most of the tests, the thruster components placement was basically as shown in Figure 2. The front circular plate and the back circular plate carried current from the capacitors to the discharge, which was concentric with and between the capacitors. This design has a low inductance and produces little or no ringing in the circuit discharge, as shown in Figure 10.

However, when first testing the rectangular feed design, the entire discharge chamber was placed on a plexiglas plate on the front of the thruster. The discharge was no longer between the capacitors. Copper wires (1/8" in diameter) carried the current from the capacitors to the plasma. This type of design had a high inductance and produced considerable ringing, as shown in Figure 11, and gave poor results. To circumvent this problem, a low inductance design rectangular feed thruster was designed and constructed. This is shown in Figure 12. The discharge chamber is again surrounded by the capacitors and the copper leads have been eliminated in favor of aluminum plates to decrease the total circuit inductance. See also Figures 13 & 14.

MATERIALS

A variety of materials were tested during the course of optimizing the

thruster's performance. Materials for the electrodes, discharge chamber walls and propellant were examined. The materials tried as propellants were mentioned earlier, teflon, polyethylene, and plexiglas. As the energy required for ablation changes with the type of fuel, the performance of the thruster is modified. In addition, to selecting a fuel with the best performance, care must be taken to find a fuel that also "burns clean", ie., one that does not leave a carbon char or residue in the chamber that may eventually short out the thruster. This is important also with regard to the spark plug. If carbon build-up on the plug is too great, the spark plug will short out and not fire.[13]

Tungsten, stainless steel, aluminum, and Mallory 1000 were tried as electrode materials. The tungsten was used for the anodes only, and it was in the form of 1/16" diameter rods. Stainless steel was used both as an anode and a cathode material. In addition, the nozzle throats were constructed of stainless steel. Aluminum was used as a cathode in the form of the coverplate placed over the spark plug for small chamber diameters. It was also used for the main body of the nozzles. Mallory 1000, an alloy of Tungsten (90%) and copper (10%) was used for both the anode and the cathode. While it has the very good erosion properties of Tungsten, (resistance to the electrical discharge and the high temperature plasma), it is much easier to machine than pure Tungsten and has good thermal conductivity. Its machining qualities are much like those of stainless steel.

Except for the tungsten rods, the anodes were generally fabricated with the same shape as the discharge chamber opening. Being slightly larger in diameter than the chamber, a circular anode was used for round chambers and

flat anodes were used for rectangular fuel configurations. The tungsten rods were generally raised above the front surface of the teflon about 1/16" and slightly recessed from the edge of the chamber (~1/32"). The circular and flat anodes rested on the front face of the teflon and were also recessed from the edge of the chamber by about 1/32".

The cathodes generally took the shape of flat circular plates. With the fuel feed configurations, however, shoulders were milled into the cathode (~0.03" high) to retain the fuel in the proper position. The cathode is pressed against the fuel piece and seals the stagnation end of the discharge chamber.

In the feed designs, an inert wall material was sometimes used in place of a teflon wall. A material was needed that could survive the high energy discharge and also would not build-up a layer of carbon. Quartz, boron nitride, and Super-mica were tried as wall materials. The Super-mica is a mica particle composite, pressed into sheets, with very good dielectric properties and discharge resistance. Super-mica is similar to glass in strength, much stronger than pure mica.

CHAPTER III

PERFORMANCE EVALUATION

To measure an impulse bit on the order of tenths of millipound-seconds, a very accurate and sensitive thrust stand is required. The sequence of operations for such a stand, the one used in the course of work for this thesis, is as follows: The thruster is mounted upon a pendulum in a vacuum chamber and the pendulum is started swinging. After the chamber is evacuated, and the pendulum damping rate has settled to a constant value, thrust measurements are taken by recording the changes in amplitude of the pendulum's swing, produced by periodic firing of the thruster. From these measurements, the impulse bit, I, can be determined. When the mass of the ablated propellant is determined, the amount of mass ablated per shot can be calculated and then used to find the specific impulse, I_{sp}, of the thruster. Oscillograms of the voltage waveform across the thruster's capacitors are also taken. From there, the average total resistance and inductance of the thruster can be computed.

APPARATUS

The vacuum system used is an NRC Model 3316 Vacuum Coater, with a 6" oil diffusion pump and a Welch Duo-Seal mechanical pump (10 cfm). The pendulum is enclosed in an 18" diameter by 30 " high pyrex bell jar. With the diffusion pump warmed-up and the cyro-baffle full of liquid nitrogen, the system operates in the low 10^{-6} torr range. With the thruster firing one shot per second, the steady state pressure rises into the low 10^{-5} torr range.

The pendulum assembly (See Figure 15, 16, 17, & 18) consists of a brass block with a two piece, adjustable length shaft extending from it, and the pendulum support. The shaft consists of a 5/8" diameter, five inch long brass tube, in which slides, and is secured, a 3/8" diameter, four inch long,

aluminum rod. This rod is attached to the thruster.

The brass block is 1 3/4" by 1 1/2" by 1 1/2". Two V-shaped, hardened steel knife edges are pressed into its sides and rest on two parallel aligned cradles attached to the pendulum support. The smoothness and parallel alignment of the knife edges and cradles, are critical factors in obtaining large damping times with this system. The sharp parts of the knife edges are rounded to a Rockwell hardness of 60.

The pendulum support consists of an aluminum angle A-frame upon which the cradles are attached. These cradles are arcs milled into small blocks of carbon steel, 2" by 1/4" by 1/4". The arcs (1 inch diameter) prevent any "walking" of the pendulum, while it is swinging, by keeping it from sliding. As the arcs themselves are only 1/16" wide, their total contact length with the knife edges is only 1/8". Thus the area of contact is small, keeping the friction in the system low. With this system, damping times on the order of 13 hours have been achieved for the pressures in the 2×10^{-6} torr range. This long damping time is also dependent upon the amplitude of the pendulum's swing, which is below 5°. For defections greater than 6°, the damping becomes large.

The thruster is connected to external circuitry through three leads, two for power and one to trigger the thruster. To connect these leads, a terminal strip was glued to the top of the brass block. Copper wires, 0.005 mills in diameter were then run from the terminal strip to the A-frame, where they were attached to the external wiring. These fine wires are large enough to carry the necessary current, but small enough to have little effect upon the damping time of the pendulum. By keeping the wires at least 1/4" apart,

arcing between them is prevented.

One wire connects an NJE, Model S-326, 500-2500 volts, 0-50 ma, power supply to the main thruster storage capacitors. Another wire carries the 500 volts (10 ma) to the trigger circuit storage capacitor. The third wire carries the 6 volt impulse used to trigger the thruster.

A. Thrust Measurement

To measure thrust, a method is needed to measure the changes in pendulum amplitude due to the thruster firing. A very accurate system has been devised to accomplish this. Using a helium-neon laser (University Laboratory Model 240) as a light source, a spot of light is shown through the bell jar and reflected from a first surface mirror attached to the front of the brass block. The spot of light is reflected onto a meter stick three meters away from the pendulum's rest position. With this arrangement very small changes in the amplitude are easily measured. An error analysis (See Appendix) reveals an uncertainty in I of about 2.5% and in the I_{sp} of less than 3%, using this thruster stand.

In order to achieve the most efficient transfer of momentum, the thruster should fire at the bottom of the pendulum's swing, ie., where the velocity is highest. To do this, a focused iodine lamp and a photo cell were placed on opposite sides of the bell jar. An aluminum angle with a 1/4" wide vertical slit in its center is attached to the bottom of the thruster and arranged so that light is only permitted to shine through the slit when the thruster is at the bottom of its swing. The signal from the photo cell is sent to a triggering circuit and a 6 volt impulse is sent to initiate the firing of the thruster,either every cycle or every other cycle. The trigger-

ing circuit is shown in Figure 19. Its operation is explained in a thesis by R.J. Radley.[14] The manual stepper switch is used to change from direct fire to retro fire.

B. Equations of Motion

The equation for the pendulum can be written

$$\frac{d^2\alpha(t)}{dt^2} + 2\nu \frac{d\alpha(t)}{dt} + \omega_c^2 \alpha(t) = \frac{F}{mg} \cdot \frac{\ell'}{\ell} \cdot \omega_c^2 \qquad (3\text{-}1)$$

where:

α= deflection angle from rest

t= time

$1/\nu$= damping time of pendulum

$\omega_c = \omega/(1-\nu^2/\omega^2)$

ω= angular frequency of pendulum= $2\pi/T$

T= period of pendulum assembly

m= pendulum assembly mass

g= acceleration due to gravity

ℓ'= distance from the axis of rotation to the center of thrust

ℓ= distance from the axis of rotation to the center of mass of the pendulum assembly

For a particular period the pendulum starts at an angle of α_{n-1}. Near the bottom of its swing, the thruster begins firing at α_i and finishes at α_f, then completes that swing and swings back to an angle α_n to complete the cycle. Typically, $t_f - t_i \simeq 10$ microseconds. Since the period of the pendulum is ~ 1 second, we can write $\alpha_f - \alpha_i << \alpha_{n-1}$ and therefore $\alpha_i \simeq \alpha_f$. By integrating the equation of motion from t_i to t_f, we can develop an expression for the angle after the N^{th} shot. This expression, together with the

facts that T≃1 second, $1/\nu \simeq 10$ hours, and $\bar{n} \simeq 1000$ shots, leads us to the approximation,[14]

$$\frac{I}{mg} \cdot \frac{\ell'}{\ell} \cdot \frac{2\pi}{\nu T^2} = \alpha_\infty \simeq \frac{\alpha_n - \alpha_o e^{-\nu n T}}{1 - e^{-\nu n T}} \tag{3-2}$$

or

$$I = \alpha_\infty \nu \cdot \frac{mg\ell}{\ell'} \cdot \frac{T^2}{2\pi} \tag{3-3}$$

I is the impulse bit and α_∞ is the asymptotic value of α as N, $t \to \infty$.

If we let nT =t, we can rewrite Eq.(3-2) as,

$$(\alpha_n - \alpha_o) = (\alpha_\infty - \alpha_o)\ (1-e^{-\nu t})$$

or

$$\alpha_n = \alpha_o + (\alpha_\infty - \alpha_o)\ (1-e^{-\nu t})$$

α_n is the deflection angle of the pendulum after n shots. Since $t \ll 1/\nu$, we can approximate α_n by,

$$\alpha_n \simeq \alpha_o + (\alpha_\infty - \alpha_o)\ (\ 1 - (1 - \nu t))$$

For direct fire α_∞ is positive and we have:

$$\alpha_D = \alpha_o(1-\nu t) + \alpha_\infty \nu t$$

where: α_D is the deflection angle after time t of direct fire.

For Retro fire α_∞ is negative and we have:

$$\alpha_R = \alpha_o\ (1-\nu t) - |\alpha_\infty|\ \nu t$$

where: α_R is the deflection angle after time t of retro fire.

We may write these last two equations as:

$$\alpha_D - \alpha_o = (|\alpha_\infty| - \alpha_o)\nu t$$

$$\alpha_R - \alpha_o = (-|\alpha_\infty| - \alpha_o)\nu t$$

Note that the slopes of the direct fire and retro fire curves, respectively, are just,

$$S_D = (|\alpha_\infty| - \alpha_o)\nu$$

$$S_R = (-|\alpha_\infty| - \alpha_o)\nu$$

If we add these together we arrive at

$$\frac{S_D + S_R}{2} = -\alpha_o \nu$$

Subtracting:

$$\frac{S_D - S_R}{2} = \alpha_\infty \nu \qquad (3\text{-}4)$$

From Figure 20 we see that $\alpha_o \nu$ is just the slope of the damping curve. With $\alpha_\infty \nu$, we can now calculate the impulse bit from Eq. (3-3).

If the thruster is only fired once every two cycles, the calculated value of $\alpha_\infty \nu$ must be multiplied by 2 in order to get the correct impulse bit. This arises because, in the development of the solution, we assumed that the thruster fired once every cycle. (Put n/2 shots in place of n in Eq. (3-2).)

To calculate the specific impulse, I_{sp}, we need to know the propellant

mass ablated per shot. This is found by measuring the amount of mass ablated during the run, Δm, and dividing it by the total number of shots, n, which gives the mass ablated per shot, $\Delta m/shot$. The specific impulse is then,

$$\frac{\text{thrust}}{\text{weight of propellant ablated/shot}} = I_{sp} = \frac{I}{\Delta m/shot \cdot g} \qquad (3\text{-}5)$$

A Mettler single pan balance accurate to $5 \cdot 10^{-5}$ grams was used to weigh the propellant. The number of shots was taken from a counter in the triggering circuit.

The efficiency is calculated from the impulse bit and the specific impulse,

$$\frac{\text{Kinetic energy of exhaust}}{\text{energy input}} = \eta = \frac{1/2mu^2}{E_o} = \frac{1/2(I \cdot I_{sp}) \cdot g}{E_o}$$

or

$$\eta = \frac{I \cdot I_{sp} \cdot g}{2E_o} \qquad (3\text{-}6)$$

C. Determination of Circuit Resistance and Inductance

The voltage discharge waveform is found by taking a Polaroid picture of the waveform form trace on an oscilloscope. The oscilloscope was a Tektronix, Type 555 Dual Beam, with a type 53/54g plug-in vertical unit and a Type 21 time base unit. A high frequency compensating probe, Tektronix P6009, with 100x attenuation and a bandwidth of 150 Mhz was also used.

The discharge circuit (Figure 21) can be modeled as a series RLC circuit.[15] In reality the values of the plasma resistance and inductance, R_p

and L_p, change with time, however, in order to arrive at an estimate of the total average resistance and inductance, the approximation was made and it appears adequate.

The voltage variation is measured across the main storage capacitors and is given by:

$$V_m(t) = V_c(t) - i(t)\cdot R_c - L_c\cdot di/dt$$

where: R_c and L_c are the capacitors internal resistance and inductance respectively.

The voltage applied by the capacitors is

$$V_c(t) = L\ di/dt + iR \tag{3-7}$$

where:

$$L = L_{CAP} + L_{PLASMA} + L_{CIRCUIT}$$

$$R = R_{CAP} + R_{PLASMA} + R_{CIRCUIT}$$

It is this voltage, $V_c(t)$, that is desired for analytical purposes. R and L are the sums respectively of resistance and inductance due to the capacitor, the plasma, and the external circuit.

It has been shown[16] that the damping constant ν and the angular frequency ω are approximately the same for both $V_c(t)$ and $V_m(t)$. The current, i(t), in the circuit, is of the form,

$$i(t) = i_o e^{-\nu t}\sin(\omega t)$$

where: $\nu = R/2L$ and $\omega^2 = (1/LC) - \nu^2$ and $i_o = V_o/(L\omega)$

Then, we have for $V_m(t)$,

$$V_m(t) = V_o e^{-\nu t}\cdot \frac{\sin(\omega t + \phi)}{\sin(\phi)}$$

where, neglecting L_c,

$$\phi = \tan^{-1}\left[\frac{\omega}{\nu - R_c C(\nu^2 + \omega^2)}\right]$$

The phase angle ϕ approximately $3\pi/2$ for the values of ν and ω found from the oscillographs ($\sim 10^6$/second). Then, ν and ω can be determined, and the the total resistance and inductance of the circuit can be calculated from $V_m(t)$,

$$V_m(t) \simeq V_o e^{-\nu t} \cos(\omega t) \tag{3-8}$$

(The sine term is neglected, as $\cos(\phi) \simeq 0$)

For the underdamped case, $C > 4L/R^2$, the value of ω can be found directly by measuring the period of the signal trace. (See Figure 22). Then ν can be calculated from the expression:

$$\nu = \frac{\ln(V(t)) - \ln(V_o)}{t_o - t} \tag{3-9}$$

where: $t - t_o = n \cdot 2\pi/\omega$; $n = 0, 1, 2, \cdots$; a multiple of the period T.

By considering as large a combination of points as possible, an average value of ν can be determined and R and L calculated.

If no oscillations are present in the waveform, ω cannot be determined directly. (See Figure 23). For those cases,(the majority of the runs), a value of ω and ν can be found by comparing the waveform to normalized curves of the step responses of a second order system for different values of damping and natural frequency. We can rewrite Eq. (3-7) as:

$$L\,(d^2q/dt^2) + R\,(dq/dt) + q/C = 0$$

or

$$\ddot{q} + 2\xi\omega_n\dot{q} + \omega_n^2 q = 0 \qquad (3\text{-}10)$$

where: $\omega_n^2 = 1/LC$

$\xi = R/2L\omega_n$

The time of the maximum overshoot for such a system is given by:

$$t_{max} = \pi/\omega_n(1-\xi^2) \qquad (3\text{-}11)$$

The percent of overshoot at t_{max} can be written,

$$\%O.S. = 100\cdot\exp[\,-\pi\xi/\sqrt{1-\xi^2}\,] \qquad (3\text{-}12)$$

The percent of overshoot and the time of the maximum overshoot are easily found from the oscillograms, thus average values of R and L can be determined.

For some configurations the discharge was overdamped. (See Figure 24). In these cases a value for resistance and inductance could not be found.

D. Life Test

The same vacuum system is used for the life tests of the thruster. Minor modifications had to be made to the system, however. The pendulum was put on blocks, to prevent it from swinging as the thruster fired. Since the light-photocell arrangement could not be used for triggering, a circuit was designed and constructed to trigger the thruster at the desired frequency. The schematic is shown in Figure 25. The pulse rate frequency could be raised from 8 pulses/minute to 180 pulses/minute. During the life testing, a frequency of 4o pulses/minute was used. A faster rate could not be used because the steady

state pressure increase in the vacuum system became unsatisfactory ($>5 \cdot 10^{-5}$ torr). At this pulse rate, it took approximately 42 hours for 100,000 shots. A continuous liguid nitrogen feed was used to keep the cryo-baffle full.

The longest life test was terminated at 510,000 shots, because the necessary information had been gathered and the pressure in the system was beginning to rise. This was brought about by the degradation of the diffusion pump oil from teflon contamination. Approximately 48 grams of teflon were ablated during the test.

CHAPTER IV: DATA AND ANALYSIS---REVIEW OF EXPERIMENTAL RESULTS

The first part of Chapter IV presents an analysis of the data gathered during the testing of the various thruster configurations. As there was a large amount of data gathered and the analysis is of a detailed nature, the following summary has been included which presents the major relationships between the thruster's performance and its configuration. For a more detailed analysis, the reader may refer to the appropriate section in Chapter IV and the summary at the end of Chapter IV.

Figure 64A presents an overall view of the thruster's performance. The envelope shown encompasses the limits in performance of the thruster configurations tried. The LES-6 and LES-7 data points are included for reference.

The specific impulse of the cylindrical pulsed ablative thruster was found to be mainly a function of h ; where h is the length of the discharge chamber height. The dependence upon energy and the chamber diameter was weak. Typical I_{sp} values range from 250 seconds to 400 seconds for teflon.

The impulse bit is proportional to the discharge energy times $h^{1/2}$. It also had a weak dependence upon chamber diameter. Typical impulse bits range from 100 micro-pound-seconds to 238 micropound-seconds.

The efficiency is approximately a constant, regardless of the configuration changes made. Typical values ranged from ~6% to ~9%.

The addition of different nozzles improved the performance of the thruster and increased the value of three parameters from 10% to 30%.

The mass ablated per shot is proportional to the discharge energy and the chamber length. It is also weakly dependent upon the chamber diameter. Typical values of mass ablated per shot range from 100 micrograms/shot to 300 micrograms per shot.

CHAPTER IV

DATA AND ANALYSIS

During the course of testing, the thruster performance parameters were determined for all of the configurations discussed in Chapter V. The experiments with propellant geometry can be divided into two main groups: Circular and Rectangular. Under the heading, Circular, the tests can be further divided into subgroups defined by their configuration--parallel or sloping walls, variable length, variable diameter, variable energy, type of propellant, and with, or without a nozzle. For the rectangular geometries we have a variable cross-section, variable length, variable number of teflon walls, and the effects of nozzles. In addition, data was gathered on the behavior of materials used for critical components and the practicality of fuel feed. Semi-empirical expressions relating the thruster configurations and the performance parameters are derived and presented.

PRESENTATION OF DATA

The data gathered for all of the runs is presented in Table I at the end of this chapter. Also included at the end of the data is a comments section, further describing each configuration. The data is gathered into the two main categories mentioned above, with the appropriate subheadings as applicable. V_m is the initial voltage applied to the main storage capacitors. Since all runs used 6-2μfarad capacitors, in parallel, the initial energy stored, E, can be calculated directly. I, I_{sp}, and η are calculated from Eqns. (3-3), (3-5), and (3-6). The values of R and L are calculated from Eqns. (3-10), (3-11), and (3-12).

CIRCULAR CONFIGURATION

A. Energy Variation

In Figures 26 and 27, we present the variations in thrust, specific impulse, efficiency, and mass ablated per shot with energy. Figure 28 presents specific mass ablated per shot and specific thrust variations as a function of the discharge energy. The diameters of the chambers for these runs were 0.5" and 0.812". The length of the discharge chamber was 2.5". From Figure 26, it can be seen that the impulse bit is nearly proportional to the discharge energy. The results are similar for both diameters shown. The slope of the 0.5" diameter line is ~ 8.77 μlb-sec/joule. The slope of the 0.812" diameter line is ~ 8.1 μlb-sec/joule. The specific impulse increases also, but not linearly, with increasing energy. A plot of I_{sp} vs. $(\text{energy})^{1/2}$ is shown in Figure 29. The dependence appears to be linear. Neither I, nor I_{sp} appear to be strongly dependent upon the diameters, 0.5" and 0.812", however, their relation with diameter is shown later.

Figure 27 presents the variation of mass ablated as a function of the discharge energy. The amount of mass ablated per shot seems to be proportional to the discharge energy. The efficiency, η, also varies linearly with the discharge energy, however, the relation is weak and η appears almost constant.

Figure 28 presents another view of the variation of mass ablated with energy. The specific mass $\Delta m/E$, decreases slightly as E increases. It is also seen than that the specific thrust, I/E, is only weakly dependent upon the energy in the range shown. Note that in all of the above cases, there appears to be little dependence upon the diameter 0.5" and 0.812".

B. Diameter

The effects upon performance of changes in the teflon bore diameter are shown in Figures 30, 31, 32, and 33. The results are for 15 joules and 20 joules, discharge energy. In all of the parameters, I, I_{sp}, I/E, η, Δm/shot,

and Δm/E, we observe a peaking between 0.2" and 0.4" in diameter, with a sharp decrease for small diameters and a much more gradual tail-off at large diameters. The results of the 0.5" and 0.812" diameter show the gradual decrease in performance as the base diameter becomes large. The curves are suggestive of a square root dependence upon diameter for small diameters, changing to an inverse relationship (1/Diameter) for large diameters.

From Figure 31, one can see that the dependence of I_{sp}, upon the diameter is not strong. The very weak dependence of I/E upon energy is shown here also, as the 15 joule and 20 joule points are evenly mixed throughout the diameter range.

In Figure 33, the dependence of Δm/shot, and Δm/E on diameter is not nearly as strong as with the other parameters, however, the peaking between 0.2" and 0.4" is still observed.

C. Length and Wall Taper

The results for changes in chamber length and wall taper are presented in Figures 34 through 37. The bore diameter for the straight wall case was 0.376". The smaller diameter for the tapered wall runs was close to ~0.39". A discharge energy of 20 joules was used for all of these runs.

In Figure 34, it can be seen that the impulse bit increases with increasing length, h, while the specific impulse, I_{sp}, decreases as h increases. The plot of specific thrust, I/E, would be similar to the plot of I, as the discharge energy was constant in all of these runs.

In Figure 35, η is a convex function of length showing a maximum efficiency around h = 1.0". Figure 36 presents Δm/shot vs. h. Here, as above, Δm/E vs. h, would have a similar form, since E was constant for all of the runs.

From Figures 37, 38, 39, and 40, we can see similar results for tapered wall chambers. In general, the shape of the performance curves versus lengths, for the different lengths, are similar for all of the angles tested. In all cases, the 15° and 20° data points fell very close to each other and sometimes coincided. In the mass ablation curve, the points for 10°, 15°, 20°, and 25° appeared to group around a single line. For one angle 10°, performance was equal to or greater than that for 0°, for almost all of the lengths tested. I_{sp} (10°), was greater than I_{sp} (0°) in all cases. However, the highest efficiency point is h = 1.0" and θ = 0°. The decrease in performance at large angles may be due to a loss of sonic conditions in the bore as a result of the taper.

D. Nozzle Addition

As stated in Chapter III, a number of different nozzles were tested to examine their effect upon performance. Two interesting observations can be made. First, a decrease was noted with every nozzle that had a converging throat diameter smaller than the teflon bore. Second, the addition of nozzles did not in general, change the amount of mass ablated per shot from that of the original configuration. These two facts tend to support the idea that the flow at the end of the discharge chamber is already sonic (choked). Thus, anything constricting in the flow path would introduce losses. This was borne out by the performance improvements achieved with nozzles that simply expanded the flow from the bore diameter.

The teflon nozzle (M ≃ 3) produced an increase in performance of approximately 10%. The parabolic nozzle (Rao, optimum thrust, M ≃ 3.5) gave a specific thrust of 13.45 μlb/watt with a specific impulse of 346 seconds for

a teflon bore diameter of 0.44" and a length of 2.5", (Run #31, Log #76). This amounts to an increase in performance of approximately 30% over the same configuration without the nozzle.

Figures 41 through 43, show the effect on performance of changes in nozzle length, for a 15° half-angle cone. The bore diameter of 0.4" is near the optimum diameter found and is large enough (>0.35") to fit over the spark plug without the use of a coverplate. The length of the teflon was 1". The mass ablated/shot remained almost constant regardless of nozzle length. The best performance resulted with a 2" nozzle. With the optimum teflon diameter of 0.375" and length 1", an impulse bit of 232 μlb-sec was achieved, with I/E = 11.6 μlb/watt and I_{sp} = 477 seconds. This gave an efficiency of 12%, (Run #133, Log #63). This is an improvement of approximately 15% for I and I_{sp} and 30% for efficiency, over the results with the same configuration without the nozzle, (Run #77, Log #49). The performance of the 1" cone nozzle and the 1" parabolic nozzle were compared for h = 1", D = 0.44". The results were about identical, with the straight cone nozzle performing slightly better.

E. Propellants

Polyethylene and plexiglas were the two propellants tried in addition to teflon. With both, carbonization proved to be a problem. With polyethylene, after the first few shots, carbon coating the spark plug would cause a short preventing the sparking action. In order to run polyethylene, the spark plug voltage had to be increased (~700 volts) and the main discharge voltage had to be increased to 2100 volts (26.45 joules). The carbonization with plexiglas proved to be so great that even these adjustments were inadequate. The spark plug short could not be remedied. After a few shots (~10), the sparkplug resistance became so low that no spark was emitted. Upon investigation, the

entire discharge chamber was found to be coated with a film of carbon dust that could be easily wiped off.

An interesting phenomenon occurred when discs of teflon were alternated with discs of polyethylene in forming the discharge chamber. After firing once, the thruster would not fire again even with the main voltage increased to 2500 volts. This occurred for 5-1/4" discs of polyethylene and 5-1/4" discs of teflon, as well as for 1-1/4" inch disc of teflon and 9-1/4" discs of polyethylene. However, once the teflon disc was replaced with a polyethylene disc the thruster fired normally at 2100 volts. With the mixed fuel a thick coating of carbon dust was noted covering the chamber after the first shot. The sparkplug continued to fire but the spark itself appeared weak. No explanation has yet been found to explain the behavior of the mixed fuel as opposed to the behavior of pure teflon or pure polyethylene.

With the higher voltage, the results with polyethylene were as expected. The I_{sp} increased because of the smaller molecular weight and the impulse bit decreased. For a diameter of 0.455" and a 2.5" length, an I_{sp} of 505 seconds resulted, with I/E = 5.25 μlb/watt. This gave an efficiency of 5.77%, (Run #66, Log #152). The values for teflon of approximately the same geometry are I_{sp} = 282 seconds; I = 11.0 μlb/watt and η = 6.9%, (Run #68, Log #35). With a nozzle (1", parabolic), a length of 1" and a bore of 0.38" diameter, and E = 30 joules, polyethylene had an I_{sp} = 810 seconds, I/E = 4.25 μlb/watt and η = 7.62% (Run #116, Log #153). Teflon in the same configuration (Run #115, Log #65), gave an I_{sp} = 470 seconds, I/E = 10.6 μlb/watt and η = 10.9%.

At high discharge energies and small chamber sizes, the teflon surface was often observed to become speckled with small black particles, at the end of the run. They did not scrape off easily and appeared to be carbon particles

imbedded in the teflon. This agrees with Wentink's observations,[17] who found that under certain conditions, $C_2F_4 \rightarrow C + CF_4$. This reaction occurs for pressures greater than 8 atmospheres and temperatures higher than 1350°C. These conditions may well have been present for runs at small diameters. For a 200 μlb-second impulse, lasting 5 μsec, in a 0.3" diameter chamber, an average gasdynamic pressure of about 30 atmospheres is calculated. The temperature is very high also, as evidenced by the amount of mass ablated per shot and the values of specific impulse. (See p. 64).

RECTANGULAR CONFIGURATIONS

It is much more difficult to present data for the rectangular configurations than it is for the circular configurations. This is due to the addition of another parameter in the propellant geometry. Instead of being able to consider only the radius and length of the teflon bore, now, width, height, and length must be considered. A combination of the first two dimensions yields a term that can be thought of as the "diameter" of the rectangular cross-section. This is the hydraulic diameter, given by four times the ratio of the cross-sectional area to the wetted perimeter of the teflon bore. When plotting performance parameters as a function of the rectangular shape, this diameter was used as the independent variable (abcissa). The results for I/E, I_{sp}, $\Delta m/E$, and η are presented in Figures 44 through 49. From Figure 44, it is seen that the specific thrust decreases with the increasing hydraulic diameter. The relationship is fairly linear with a noticeable change in specific thrust for a change in hydraulic diameter. Figure 45 presents the variation of the specific impulse with the diameter, it appears that I_{sp} varies as the square root of the diameter. This in fact is a reasonable statement as shown by Figure 46, where I_{sp} is plotted as a function of the square root of the

diameter. Figure 47 presents the variation of specific mass ablated/shot with the hydraulic diameter. As shown, these are two definite curves corresponding to the four teflon wall and the two teflon wall configurations. In both cases the relationship appears to be one where $\Delta m/E$ is proportional to the inverse of the diameter. This plot is presented in Figure 48, and it correlates well with the data.

The variation of efficiency with hydraulic dimeter (Figure 49) seems to be uncorrelated. An average value of η can be determined to be ~7.7%, but there is no strong relationship discernable.

The optimum performance,(Run #147, Log #134), was for a rectangular cross-section of 0.25" by 0.25". This gave: I_{sp}= 400 seconds, I/E =11.4 μlb/watt, η = 9.95%. The addition of a rectangular nozzle increased the performance of (Run #121, Log #125), (0.25" x 0.7" x 1.0") by about 10% (Run #122, Log #149). As can be seen, the variation in performance parameters is not as drastic with changes in configuration as it is with circular geometries. This is especially true for the I_{sp}, where all rectangular configurations of 0.25" by x" (Run #135 to 139, Log #126 to 130) had an I_{sp} in the range of 365 seconds.

INERT WALLS

Replacing part of the teflon chamber with an inert wall led to decreases in performance of all of the configurations tested. Two inert walls produced poorer performance than just one inert wall. This can be seen by comparing (Run #164, Log #147), using three teflon walls to (Run #163, Log #146), using two teflon walls, and to (Run #137, Log #128), having four teflon walls. The efficiency decreased with each inert wall added. The materials tested as inert walls were boron nitride, Super-mica, and quartz. Boron nitride was not used

extensively, as it would develop a thick carbon coating after a few hundred shots. Since carbon tends to short the discharge, the performance is lowered. The Super-mica did not carbonize like the boron nitride did but after a few thousand shots it began to erode rather severely. This erosion can be seen in Figure 50. The hole in the middle of the wall is for the exhaust of the spark plug discharge. In the runs with the spark plug placed in the backplate, the material from the mica composite slowly builtup over the plug causing it to become inoperative. In addition, the surface of the Super-mica became very rough after erosion began and probably lowered the performance of the thruster.

The quartz side walls appear by far to be the best material of those tested. There was very little carbon buildup on the walls and very little erosion. The walls maintained their smooth surfaces throughout the tests.

ELECTRODE MATERIALS

Only Tungsten and Mallory 1000 were able to survive thousands of discharges without serious erosion. Tungsten rods (Thoriated 2%) were not visibly affected by the discharges, unfortunately Tungsten is difficult to machine. There was some slight pitting of the Mallory 1000, but not serious enough to affect the thruster's performance. Aluminum gave the poorest performance of all the materials tested and is unacceptable as an electrode material for long-life applications. With only a few hundred shots, its surface becomes severely pitted. It was useful as the body of the nozzles, as long as it was not exposed to the direct discharge as an electrode. For this reason, stainless steel was used for all throat or nozzle sections which served as electrodes. Stainless steel performed adequately in short runs (< 10,000 shots), however, for larger numbers of shots, erosion became evident. The anode was affected more than the cathode, becoming severely eroded after approximately 50,000 shots; however, the cathode

eroded also and allowed a deposit buildup, as seen in Figure 51.

FEED MECHANISM

The coil spring feed system demonstrated the feasibility of feeding the teflon, however, it encountered a number of problems. The ablation profile of the teflon was such that more teflon was ablated from the stagnation end of the chamber than the exhaust end, thus a curved surface formed. The use of teflon as a sealing wall at the corners of the chamber was unfortunate, as it began to ablate considerably, as soon as the uneven chamber ablation profile exposed it to the discharge. Since the chamber did not retain its original shape the performance was decreased. However the teflon bars did feed approximately 0.1" to 0.125", as 4.6 gm of teflon were ablated in 19,600 shots.

The Negator spring feed system fared much better. In the majority of runs with this system, two teflon walls and two inert walls formed the discharge chamber. In the long-life test, the thruster fired 510,580 times. Approximately1.4" of teflon was ablated off each bar , (total ablated mass = 48 gm), demonstrating successfully the feed mechanism. Unfortunately, the ablation was uneven in the axial direction, as more teflon ablated off of the bars at the stagnation end of the chamber than at the exhaust end. Thus a converging chamber was formed resulting in very poor performance, (Run #155b, Log #139). In all runs with the Negator springs, the spark plug was mounted onto one of the inert walls forming the side of the discharge chamber. In Figures 52 and 53, the ablation profile of the teflon can be seen. Each grid square is 1/4" x 1/4" in the photographs. The "Front View" denotes that the front surface of the teflon is towards the top of the photograph. Thus the plasma exhaust would be heading toward the top of the photograph. "Spark plug side" refers to the wall side that contained the spark plug. As evid-

enced by the length (~3" total) of teflon that fed and was ablated, ablation behind the retaining shoulders occurs satisfactorily.

It was found that with the spark plug in the side wall position, the spark plug ignition circuit ground had to be partially isolated from the main discharge circuit ground (the cathode). Otherwise, the discharge would not only take place from the anode to the cathode but also from the anode to the sparkplug, as that current path is shorter. Then, even with the isolation transformer, the SCR and diode would be burned out by the discharge-induced back emf generated in them. After a number of shots with the sparkplug in this position, it became evident that more teflon was being ablated on the spark plug side of the fuel bars, than on the opposite side. This probably is the result of the discharge initiating on the sparkplug side of the chamber, where the particles are first ejected. (See Figure 54). To assure even ablation laterally across the face of the teflon, spark plugs should be placed in both inert walls and fired alternately. This arrangement will also give an extra degree of redundancy.

ABLATION PROFILE

Much useful information was found by studying the ablation profiles from circular configuration tests. This information was later applied to solve the previously mentioned rectangular feed ablation problems. It was found with the rectangular life test designs that, as the teflon assumed a shape, as in Figure 52, the performance of the thruster decreased markedly. Thus a means had to be found assuring even ablation in this axial direction. The ablation profile was found to be dependent upon two factors, the diameter of the chamber and the discharge energy. These two factors are interrelated in their effects upon the ablation profile. The results are summarized in Figure 55 and 56.

The profiles were determined for the relative amount of mass ablated from each disc in the fuel element. In general, for a high E and a small D, the discharge chamber began to assume a conical shape with the vertex towards the exhaust end and the base at the stagnation end of the chamber. For a low E and a large D, the exact opposite occurred, with the vertex towards the stagnation end of the chamber. For a very large D, even a high energy (20joules) discharge kept the vertex towards the stagnation end of the chamber. Between these two extremes, for a discharge energy of approximately 15 to 17 joules and a chamber diameter of 0.5", the ablation profile was even.

These results were applied to the rectangular feed design. The discharge energy was lowered from 20 joules to 17.5 joules. The chamber size was 0.44" x 0.160" by 1.0", where the fuel bars had a cross-sectional area of 1.0" x 0.44". After 20,000 shots, the ablation profile appeared almost perfectly even, a considerable improvement over the 20 joule runs. From the circular results, it seems certain that in order to achieve even ablation a new optimum energy will have to be found for each new chamber size. Comparisons with the results from the circular ablation profiles in different chamber sizes may provide a guide.

RESISTANCE AND INDUCTANCE

Figures 57 through 63 present the total circuit resistance and inductance as a function of circular bore diameter, chamber length and hydraulic diameter. Examining changes with diameter first, it must be noted that for a certain range of diameters (0.25" to 0.35") the discharge waveforms were overdamped, and R and L measurements were not made. Fig.57 shows very large values of R and L (0.187 ohms and 385 nanohenries) for small chamber diameters. For large chamber diameters, larger than ~0.3", the resistance and inductance

drop sharply and then tend to level off. Figures 58 and 59 show these regions with an expanded scale. For runs at a diameter where more than one energy was tried, the values of R and L were averaged to produce one value for that diameter. Generally, they were approximately equal for any one diameter, as would be expected, as the geometry was not changed.

Figure 58 shows L proportional to diameter, for small chamber diameters, then assuming a constant value for diameters greater than 0.5". There appears to be a discontinuity in the results between 0.45" and 0.5". This cannot be satisfactorily explained. Figure 59 shows that the circuit resistance increases as diameter decreases, in what appears to be a 1/Diameter relationship. This relationship is seen more clearly in Figure 60, which plots resistance vs. the inverse of the diameter.

The variation of R and L with the chamber length is presented in Figure 61. Both resistance and inductance are seen to vary proportionately with the length of the chamber. The approximation for L is crude, however, the approximation for R is much closer. Figure 62 presents the variation of resistance and inductance with changes in hydraulic diameter (H.D.). The relationship between R and H.D. may be approximated accurately by a straight line, with R decreasing as the diameter increases. R is not linearly proportional to 1/H.D. as can be seen in Figure 63. The results for L vs. H.D. are too scattered to allow definite conclusions, although L seems to follow a relationship to H.D. similar to that of resistance.

It is interesting to note that in the run with the potential reversed on the electrodes (reverse polarity, the cathode was at the exhaust end), (Run #152, Log #161), the plasma resistance dropped to one-half of its value in the previous run, which had the same geometry, The inductance was not

affected.

The result of the low inductance design can be seen by comparing(Runs# 162 to 165, Log # 145 tO 148), the low inductance design, to (Runs #149 to 161, Log #139 to 143 and Log #158 to 163), the high inductance design. The inductances for the low L design are about one-half to one-quarter of those for the high inductance design, while the plasma resistance remains about the same. The lower inductance design helped improve the performance of the thruster. This can be seen by comparing I/E, I_{sp}, and η (respectively, 6.4 to 8.35 μlb/watt, 414 to 392 seconds, and 5.81 to 7.15%), for (Run # 161 to 165, Log # 144 to 148). Although a nozzle was added to the low inductance design to keep the plasma from impinging upon the capacitors, it is believed to have had only a slight contribution to the performance improvement of the thruster. This assumption is based on the fact that the nozzle was circular and has a throat diameter of about one inch. The chamber, however, was rectangular and only 0.44" by 0.23". As expected, changes in energy for a fixed configuration (Runs #2 to 5, Log # 36 to 39) and (Runs # 7 to 10, Log #41 to 44), had no apparent effect upon the circuit resistance and inductance.

ANALYSIS---THEORETICAL CONSIDERATIONS

Figure 64 presents a plot of the performance characteristics of a particular thruster, using the three most important parameters, I/E, I_{sp}, and η. The optimization of the thruster design can be greatly facilitated, if the mechanisms by which it operates are known and understood. For this reason, a model of the operation of the thruster needs to be developed, which will relate the thruster's performance (I/E, I_{sp}, & η), to its configuration. Using the results of the preceding section as a guide, a model for the operation of the thruster will now be developed.

A. Mass Ablated Per Shot

Our first aim will be to establish an expression for the mass ablated per shot as a function of the thruster parameters. The mass ablated can be calculated by evaluating the amount of heat transferred from the hot plasma to the teflon walls, the amount of heat transferred being subsequently equated to the mass of the teflon ablated times the specific energy of ablation of teflon.

The energy, ε, required for the ablation of a mass Δm of teflon will be:

$$\varepsilon = \Delta m \cdot \lambda$$

where:

Δm = mass ablated

λ = heat of ablation; λ = 2180 joules/gm for teflon[17]

The energy transferred per unit time and area as heat from the flow to the walls of the chamber can be written as:

$$q = \rho u(5/2)R \cdot (T_p - T_w) \cdot St$$

where:

ρ = plasma density

u = mass averaged flow velocity

R = Universal gas constant = 8.31 joules/mole · °C

T_p = plasma temperature

T_w = wall temperature << T_p

St = Stanton number = $h_v/(\rho u \frac{5}{2}R$

h_v = heat transfer coefficient;

For turbulent flow in pipes, the Stanton number can be related to the friction coefficient of the flow by the Reynold's analogy, St = f/2, which is reasonably valid for all gases.[18]

Assuming that the plasma flow per unit time and area is zero at the stagnation end of the chamber and increases linearly with distance along the chamber (assuming uniform ablation) becoming $(\rho u)_e$ at the exit, we may write the total enthalpy transferred per unit time as:

$$\dot{\varepsilon} = \int_0^h q(x) \cdot \pi \cdot D \, dx$$

$$= \pi Dh \cdot (\rho u(5/2)RT_p)_e \cdot \overline{St}/2$$

$$= \dot{m}\lambda$$

This can be rewritten:

$$\dot{m} = \frac{1}{2} \frac{\pi Dh}{\pi D^2/4} \cdot \frac{\overline{f}}{2} \cdot \dot{m}(H_p \cdot 5/2 \cdot (\gamma-1)/\gamma)$$

where:

H_p = total enthalpy/unit mass of plasma

$\overline{f}$ = average friction factor

This leads to:

$$\Delta m = (5/2)(h/D) \cdot \bar{f} \cdot (E/\lambda) \cdot (\gamma-1)/\gamma \qquad (4\text{-}1)$$

Where it has been assumed that all of the discharge energy goes into fluid ($E = \Delta m H_p$).

Δm versus $(h/D)E$ is plotted in Figure 64B. The slope of the straight line approximation correlating the data is $2.98 \cdot 10^{-9}$ kg/joule.

Equating this to Eqn. (4-1), we have;

$$\frac{5}{2} \cdot \bar{f} \cdot \frac{\gamma-1}{\gamma} \cdot \frac{1}{\lambda} = 2.98 \cdot 10^{-9} \text{ kg/joule}$$

The ratio of specific heats, γ, was chosen to be 1.2. This value is close to values computed for convential rocket exhausts. The friction coefficient is then:

$$\bar{f} = 1.56 \cdot 10^{-2}$$

or

$$\overline{St} = 0.0078$$

To provide a check on this value, the friction coefficient was compared to a graph of f vs. Reynold's number, with the roughness of the channel as a third variable.[19] The Reynold's number for this flow can be estimated as $\sim 10^5$. With these two values, the relative roughness of the chamber, found from the graph is $E/D \simeq 0.04$. This would mean that the average height of the rough spots in the chamber is approximately four percent of the chamber diameter. For D = 0.5", this would be 0.02", which is a high, but not unreasonable value for the chamber roughness.

The mass ablated per shot is then,

$$\Delta m = (2.98 \cdot 10^{-9} \text{ kg/joule}) \cdot (h/D)E$$

Typically, h/D ≃ 2.5"/0.5" = 5; E = 20 joules, hence

$$\Delta m \simeq 298 \ \mu gm/shot$$

The actual value for this geometry is 310 μgm/shot. Thus, Egn.(4-1) accurately predicts, to first order, the amount of mass ablated per shot.

B. Efficiency

Next an estimate of the thruster efficiency will be derived. Based upon the experiments performed, we can assume that the flow is sonic at the exit, hence, we may estimate the efficiency from the equation:

$$\frac{\Delta mu^2}{2} = \frac{\frac{\gamma-1}{2} M^2}{1+\frac{\gamma-1}{2} M^2} \cdot E$$

where:

$\frac{\Delta mu^2}{2}$ = the kinetic energy of the exhaust

E = the stagnation energy, (= discharge energy)

M = Flow Mach Number

For M = 1, we have: $[(\Delta mu^2)/2)/E = \eta]$

$$\eta = \frac{\gamma-1}{\gamma+1} \qquad (4\text{-}2)$$

For γ = 1.2;the efficiency is $\eta \simeq 9\%$. This value is within the correct order of magnitude for the values of efficiency measured for the thruster (~6-9%). This result also agrees with the graphical data for η, where it has been seen that η was generally constant, regardless of geometry changes. The close agreement between the predicted efficiency and the actual efficiency tends to support the assumption made concerning γ (1.2) and the flow characteristics.

C. Specific Impulse

Knowing the efficiency and the mass ablated per shot, we can calculate the specific impulse from the following relationship:

$$\eta = \frac{I \cdot I_{sp}}{2E} \cdot g$$

We determine that I_{sp} is given by:

$$I_{sp} = \frac{1}{g} \cdot \{\frac{2E}{\Delta m} \cdot \eta\}^{1/2} = \frac{1}{2} \{\frac{D}{h} \cdot \frac{4}{5} \cdot \frac{\lambda}{St} \cdot \frac{\gamma}{\gamma+1}\}^{1/2} \qquad (4\text{-}3)$$

For the values used above, we predict:

$$I_{sp} \simeq 345 \text{ seconds}$$

This is slightly high (Typical values are ~280 seconds), but again it is the right order of magnitude. The model also predicts correctly the variation in I_{sp} as changes in configuration are made. In Eqn. (4-3), there is no dependence of I_{sp} upon energy. This is essentially what Figure 26 shows, as I_{sp} varies only by ~15% from its mean value as the energy is varied from 5 to 20 joules. Thus, I_{sp} is almost independent of the discharge energy.

The dependence of I_{sp} on $D^{1/2}$ agrees with the actual results for the diameters less than 0.4". Above 0.4", the model fails to predict the 1/Diameter dependence of I_{sp} upon the diameter(See Figure 31). Here also, the actual variation of I_{sp} with the diameter is small.

The third relation shows that, $I_{sp} \propto h^{-1/2}$. This agrees with the graph given previously, Figure 34, in predicting a strong dependence in I_{sp} upon h. However, as seen in Figure 66, this relation does not hold precisely.

D. Impulse Bit

The impulse bit can be determined from the efficiency and the mass ablated per shot also. It is given by:

$$I = (2E \cdot (\Delta m/\text{shot}) \cdot \eta)^{1/2}$$

or

$$I = E \cdot (5 \cdot (h/D) \cdot (St/\lambda) \cdot (\gamma-1)^2/(\gamma+1))^{1/2} \qquad (4\text{-}4)$$

This predicts an impulse bit of 1000 μN-seconds. For D =0.5", the actual value is ~750 μN-seconds. Again, the model has been accurate to first order, predicting a value the same order of magnitude as the actual value (~30% in error).

The relations between I, L, D, and E are in agreement with the test results. I is proportional to E as seen in Figure 26. The variation of I with D tends to fit the curve, Figure 30, for d >0.04". The direct relation between I and $\sqrt{h}$ is also shown for the actual thruster in Figure 34. As with I_{sp}, the $\sqrt{h}$ relation does not hold exactly. This is shown in Figure 67.

The fact that these relations predict the performance values , as closely as they do, tends to support the assumptions made in the development of the formulas for the mass ablated /shot and the specific impulse. The heat transfer model, while simple, predicts many of the dependencies between I, I_{sp}, and η and the configuration parameters of h, D, and E.

E. Calculation of Inductance and Resistance

RESISTANCE

Theoretical approximations to the plasma resistance and inductance can also be made. Assuming a uniform plasma column in the discharge chamber, with a conductivity,σ, we can eliminate the total resistance of the plasma as,

$$R_p = \frac{1}{\sigma} \cdot \frac{h}{\pi D^2/4} \qquad (4\text{-}5)$$

The variation of plasma resistance with chamber length is clearly seen in Figure 61. This linear relationship suggests that the conductivity, σ, is a constant. From the slope of the line in Figure 61, we may estimate σ as: $\sigma = 116$ mhos/cm.

INDUCTANCE

The inductance of plasma can be calculated by modeling the plasma as a conductor with uniform properties. Assuming a current density, $\bar{J}$, a conductor of diameter, D, with a concentric return path of diameter, a, (here the capacitors), we may determine the inductance from the following formula.[20]

$$L = \frac{\mu_o h}{2\pi} \cdot \left[\frac{1}{4} + \ell n\left(\frac{a}{D}\right) \right] \qquad (4\text{-}6)$$

A proportional dependence of L on chamber length, h, is predicted. This is, in fact, true for the thruster, as seen in Figure 61. To further check this model, the slope predicted by Eqn. (4-6) for L vs. h $[(\mu_o/2\pi) \cdot (1/4 + \ell n(a/D))]$, is compared to the slope of L vs. h from Figure 61. We predict: a = 5"; D = 0.5").

$$(L/h) \sim 13 \cdot 10^{-9} \text{ henries/inch}$$

From Figure 61; the slope of the curve is approximately:

$$(L/h) \sim 12.8 \cdot 10^{-9} \text{ henries/inch}$$

Thus, the model for the inductance of the thruster yields a result that is very close to the actual value. The dependence of L upon diameter is predicted to be a weak logarithmic function, with L increasing as D decreases. From Figure 58, there appears to be little dependence of L upon diameter.

F. Estimation of Plasma and Electron Temperature

From the models just presented, estimates of the plasma temperature and the electron temperature can be made. The plasma temperature may be

estimated from the specific impulse by the following relation:

$$I_{sp} = 1/g\ [(5/2)RT_p/M]^{1/2} \qquad (4\text{-}7)$$

where:

g = accelaration due to gravity---9.81 m/sec^2

R = Molecular gas constant---8.31 joules/mole °C

T_p = Plasma temperature

M = average molecular weight of plasma (Assuming complete dissociation---$C_2F_4 \rightarrow 2C + 4F$ = 6 particles

M = (100gm/mole/6 particles)
= 16.7 gm/mole

The plasma temperature is then, for I_{sp} = 300 seconds.

$T_p \simeq 7000°K$

The electron temperature may be calculated from the following relation between the plasma conductivity and the electron temperature.[21]

$$\sigma = 3000 \cdot T_e^{3/2} \qquad (4\text{-}8)$$

where:

σ is in mhos/meter

T_e = electron temperature in electron volts

The coefficient of 3000 is based upon a reasonable estimate of the electron density of $\sim 2 \cdot 10^{19}$/cc and the plasma temperature of 10^4°K.

The electron temperature is then:

$T_e \simeq 2.46$ ev

$\simeq 28{,}500$ °K

where:

1 ev ≃ 11,606 °K

CHAPTER IV---DATA AND ANALYSIS---SUMMARY OF EXPERIMENTAL RESULTS

The following summary presents a brief review of the experimental and analytical results presented in Chapter IV. The major relationships between each configuration examined and the thruster performance parameters are given, as well as the results of the material studies. The basic features of the model representing the operation of the thruster are present also.

CONFIGURATION PARAMETER	PERFORMANCE PARAMETER
1.Circular	
A. Discharge Energy (Figures 26-29)	I, $\Delta m/shot \propto Energy$ $I_{sp}, \propto \sqrt{Energy}$ $\eta \simeq$ constant
B. Chamber Diameter (Figures 30-33)	All parameters (I, I_{sp}, η, $\Delta m/shot$), relatively insenstive to changes in diameter for D > 0.4". A peaking was observed between 0.2" and 0.4". $\Delta m/shot$ more insentive than other parameters to changes in D.
C. Chamber Length (Figures 34-36)	All parameters strongly related I--increases as h decreases I_{sp}--decreases as h increases $\Delta m/shot \propto h$ $\eta \simeq$ constant
D. Chamber Wall Taper Angle (Figures 37-40)	Same relations with length as for the 0° case(1c). For half angles >5°, performance was decreased from the 0° case. For half angles 0° to 5° performance parameters were approximately constant.
E. Nozzle (Figures 41-43)	Any form of constricting throat, decreases performance. Performance improvements of~30% were

	obtained using an optimum length (2"), 30°(full angle) conical nozzle.
2. Rectangular	
A. Hydraulic Diameter	I--linear with H.D.; decreasing as H.D. increases I_{sp}--constant, 0.2"<H.D.<0.5"--decreases, H.D. <0.2" $\Delta m/shot \propto 1/H.D.$ $\eta \simeq$ constant
B. Teflon Fuel Feed	Life test--(two teflon wall, Negator spring feed) successfully completed ~510,000 shots, 48 gm teflon ablated; ~1 1/2" off of each bar. Problems with ablation profile.
C. Inert Chamber Walls	Performance decreases with each inert wall added. Quartz--best inert wall material tested. Super-mica--erosion problems. Boron nitride--becomes coated with carbon.
D. Electrode Material	Tungsten and Mallory 1000 performed best. Stainless steel--serious erosion problem for > 50,000 shots Aluminum--serious erosion after few hundred shots.
3. Ablation Profile	Dependent upon discharge energy & chamber diameter. As E increases D decreases, stagnation end of chamber ablates more than exhaust end. As E decreases, D increases, the exhaust end ablates more than the stagnation end.
4. Resistance and Inductance (Figures 57-63)	$R \propto 1/D$; $R \propto h$; R decreases with increases to H.D. L increases with increasing D, and increasing H.D. $L \propto h$.

5. Thruster Performance Model

$$\Delta m/\text{shot} = (2.98 \cdot 10^{-9}\ \text{kg/joule}) \cdot (h/D) \cdot E$$

$$\eta = (\gamma-1)/(\gamma+1) \simeq 9\% \simeq \text{constant}$$

$$I_{sp} = (2.51 \cdot 10^{-3}\ \text{seconds}) \cdot (D/h)^{1/2}$$

$$I = (2.32 \cdot 10^{-5}\ \text{sec/meter}) \cdot (h/D)^{1/2} \cdot E$$

6. Characteristics

Plasma Temperature $\simeq$ 7000°K

Electron Temperature $\simeq$ 24,000°K

TABLE I: SUMMARY OF EXPERIMENTAL RESULTS

Section I: Circular Configuration, Straight Bore, No Nozzle

Log Number	1	2	3	4	5	6	7	8	9	10
Run Number	35	36	37	39	38	40	41	43	45	46
Diameter, inches	0.15	0.15	0.25	0.25	0.25	0.30	0.30	0.33	0.33	0.33
Length, inches	2.5	2.5	2.5	2.5	2.5	2.5	2.5	2.5	2.5	2.5
V_m, volts	1581	1825	1581	1581	1825	1581	1825	1581	1581	1581
E, joules	15	20	15	15	20	15	20	15	15	15
I, μN-second	628	855	756	735	994	791	1035	755	700	703
I, μlb-second	142	193	171	166	224	179	234	171	158	159
I_{sp}, seconds	201	239	228	234	261	266	274	260	239	233
I/E, μlb/watt	9.46	9.65	11.4	11.1	11.2	11.9	11.7	11.4	10.5	10.6
Δm/shot, μgm	318	365	337	313	388	303	384	296	298	307
Δm/E, μgm/joule	21.2	18.3	22.4	20.8	19.4	20.2	17.2	19.7	19.9	20.5
η, %	4.14	5.01	5.65	5.63	6.35	6.9	6.95	6.41	5.48	5.35
L, 10^{-9} henries	431	334	248	Critical	276	Critical	Critical	Critical	Critical	Critical
R, 10^{-2} ohms	16.7	14.4	18.7	Critical	18.5	Critical	Critical	Critical	Critical	Critical

Section I continued: Circular Configuration, Straight Bore, No Nozzle

Log Number	11	12	13	14	15	16	17	18	19	20
Run Number	44	47	48	49	50	51	52	53	54	55
Diameter, inches	0.33	0.344	0.345	0.357	0.360	0.362	0.362	.383	.383	.386
Length, inches	2.5	2.5	2.5	2.5	2.5	2.5	2.5	2.5	2.5	2.5
V_m, volts	1825	1825	1825	1581	1825	1581	1581	1581	1581	1825
E, joules	20	20	20	15	20	15	15	15	15	20
I, μN-second	1058	955	992	643	981	715	718	711	718	955
I, μlb-second	238	216	224	145	222	162	162	161	162	216
I_{sp}, seconds	276	255	258	212	262	246	245	236	248	275
I/E, μlb/watt	11.9	10.8	11.2	9.66	11.1	10.7	10.8	10.7	10.8	10.8
Δm/shot, μgm	389	381	391	310	382	297	299	307	295	354
Δm/E, μgm/joule	19.5	19.1	19.6	20.6	19.1	19.8	20.0	20.4	19.65	17.7
η, %	7.17	5.98	6.3	4.45	6.32	6.95	6.04	5.49	5.82	6.45
L, 10^{-9} henries	Critical	Critical	20.4	Critical	26.0	Critical	Critical	Critical	20.3	25.4
R, 10^{-2} ohms	Critical	Critical	7.0	Critical	7.55	Critical	Critical	Critical	7.0	7.2

Section I continued: Circular Configuration, Straight Bore, No Nozzle

Log Number	21	22	23	24	25	26	27	28	29	30
Run Number	56	57	59	58	60	61	62	64	63	65
Diameter, inches	.386	.393	.399	.400	.403	.419	.420	.422	.422	.422
Length, inches	2.5	2.5	2.5	2.5	2.5	2.5	2.5	2.5	2.5	2.5
V_m, volts	1825	1581	1825	1581	1825	1581	1581	1581	1825	1825
E, joules	20	15	20	15	20	15	15	15	20	20
I, μN-second	976	645	895	701	950	715	719	205	975	987
I, μlb-second	221	146	206	159	211	162	163	159	220	223
I_{sp}, seconds	256	236	269	242	265	259	257	254	277	284
I/E, μlb/watt	11.05	9.7	10.3	10.6	10.55	10.8	10.9	10.6	11.0	11.15
Δm/shot, μgm	388	279	339	295	365	281	285	283	359	354
Δm/E, μgm/joule	19.4	18.6	17.0	19.7	18.25	18.7	19.0	18.9	17.95	17.7
η, %	6.15	4.98	5.92	5.54	6.18	6.07	6.05	5.86	6.62	6.88
L, 10^{-9}henries	36.5	16.3	26.6	20.8	27.7	14.6	39.0	35.1	42.0	36.0
R, 10^{-2}ohms	7.95	6.4	5.8	6.7	5.7	3.1	8.1	7.7	7.8	7.0

Section I continued: Circular Configuration, Straight Bore, No Nozzle

Log Number	31	32	33	34	35	36	37	38	39	40
Run Number	33	34	42	67	68	3	2	5	4	1
Diameter, inches	.44	.44	.44	.447	.449	.5	.5	.5	.5	.5
Length, inches	2.5	2.5	2.5	2.5	2.5	2.5	2.5	2.5	2.5	2.5
V_m, volts	1581	1581	1825	1581	1825	912	1290	1472	1581	1825
E, joules	15	15	20	15	20	5	10	13	15	20
I, μN-second	723	646	924	755	980	143	337	430	497	725
I, μlb-second	162	146	209	170	220	33.2	75.8	96.8	111.5	163
I_{sp}, seconds	284	264	286	280	282	166	203	211	223	237
I/E, μlb/watt	10.8	9.74	10.5	11.3	11.0	6.64	7.58	7.45	7.44	8.15
Δm/shot, μgm	259	250	329	275	355	90.3	169	208	228	312
Δm/E, μgm/joule	17.3	16.7	16.5	18.3	17.8	18.1	16.9	16.0	15.2	15.6
η, %	6.61	5.29	6.5	6.91	6.9	2.39	3.36	3.42	3.62	4.2
L, 10^{-9}henries	48.5	40.0	39.2	38.6	40.8	16.0	25.4	24.6	28.2	---
R, 10^{-2}ohms	5.0	5.5	7.7	7.1	6.8	5.8	6.1	5.7	5.5	---

Section I continued: Circular Configuration, Straight Bore, No Nozzle

Log Number	41	42	43	44	45	46	47	48	49	50
Run Number	9	10	7	8	74	75	76	79	77	78
Diameter, inches	.812	.812	.812	.812	.376	.376	.376	.383	.375	.383
Length, inches	2.5	2.5	2.5	2.5	2.5	2.0	1.5	1.5	1.0	0.5
V_m, volts	1290	1290	1581	1825	1825	1825	1825	1825	1825	1825
E, joules	10	10	15	20	20	20	20	20	20	20
I, μN-second	351	324	511	700	1045	995	935	933	908	656
I, μlb-second	79	73	115	157	235	224	210	210	204	148
I_{sp}, seconds	195	195	216	244	285	334	378	340	419	495
I/E, μlb/watt	7.9	7.3	7.66	7.85	11.75	11.2	10.5	10.5	10.2	7.4
Δm/shot, μgm	182	169	241	293	373	329	252	279	221	135
Δm/E, μgm/joule	18.2	16.9	16.1	14.7	18.65	16.45	12.6	13.95	11.1	7.75
η, %	3.36	3.11	3.62	4.18	7.31	8.15	8.67	7.79	9.34	7.97
L, 10^{-9} henries	26.1	25.2	25.8	25.4	38.6	36.6	28.2	26.6	20.6	12.6
R, 10^{-2} ohms	4.1	3.8	4.2	4.1	8.2	6.7	4.8	4.4	4.2	2.2

Section II: Circular Configuration, Straight Bore, With Nozzle

Log Number	51	52	53	54	55	56	57	58	59	60
Run Number	13	15	12	6	14	11	18	19	20	17
Diameter, inches	0.5	0.5	0.5	0.5	0.5	0.5	0.5	0.5	0.5	0.5
Length, inches	2.5	2.5	2.5	2.5	2.5	2.5	2.5	2.5	2.5	2.5
V_m, volts	1290	1472	1581	1581	1708	1825	1290	1581	1581	1581
E, joules	10	13	15	15	17.5	20	10	15	15	15
I, μN-second	371	545	633	527	722	772	400	599	619	602
I, μlb-second	83.5	123	142	125	162	174	90	135	139	136
I_{sp}, seconds	221	267	273	239	263	254	236	262	254	242
I/E, μlb/watt	8.35	9.45	9.46	8.34	9.25	8.7	9.0	9.0	9.28	9.07
Δm/shot, μgm	171	208	247	238	280	311	173	233	248	254
Δm/E, μgm/joule	17.1	16.0	16.5	15.8	16.0	15.6	17.3	15.5	16.5	16.9
η, %	4.03	5.49	5.93	4.35	5.32	4.68	4.63	5.14	5.15	4.75
L, 10^{-9}henries	23.6	26.4	28.2	29.6	27.5	26.0	30.2	26.4	27.5	28.8
R, 10^{-2}ohms	5.6	5.8	5.4	3.6	5.5	5.4	6.6	6.4	5.3	6.3

Section II continued: Circular Configuration, Straight Bore, With Nozzle

Log Number	61	62	63	64	65	66	67	68	69	70
Run Number	16	134	133	114	115	117	126	127	128	129
Diameter, inches	0.5	0.36	0.375	0.378	0.380	0.385	0.390	0.390	0.40	0.40
Length, inches	2.5	1.0	1.0	1.0	1.0	0.5	0.5	1.0	1.0	1.0
V_m, volts	1825	1825	1825	1825	2240	1825	1825	1825	1825	1825
E, joules	20	20	20	20	30	20	20	20	20	20
I, μN-second	782	955	1025	996	1419	737	625	818	900	921
I, μlb-second	176	216	232	224	318	166	141	191	203	208
I_{sp}, seconds	243	372	477	457	470	596	501	397	426	445
I/E, μlb/watt	8.8	10.8	11.6	11.2	10.6	8.3	7.05	9.55	10.15	10.4
Δm/shot, μgm	328	262	219	222	308	126	127	210	215	211
Δm/E, μgm/joule	16.4	13.1	10.95	11.1	10.3	6.3	6.35	10.65	11.85	10.55
η, %	4.66	8.71	12.0	11.2	10.9	10.8	7.69	7.85	9.41	10.1
L, 10^{-9}henries	32.6	18.9	20.8	21.9	18.5	17.4	16.3	19.8	20.0	21.9
R, 10^{-2}ohms	6.3	3.3	3.2	3.3	2.6	2.3	2.1	3.0	3.4	3.4

Section II: Circular Configuration, Straight Bore, With Nozzle

Log Number	71	72	73	74	75	76	77	78	79	80
Run Number	130	131	132	32	30	31	112	113	28/29	27
Diameter, inches	0.40	0.40	0.40	0.44	0.44	0.44	0.453	0.455	0.5	0.5
Length, inches	1.0	1.0	1.0	2.5	2.5	2.5	1.03	1.04	2.5	2.5
V_m, volts	1825	1825	1825	1290	1581	1825	1825	2240	1581	1825
E, joules	20	20	20	10	15	20	20	30	15	20
I, μN-second	880	930	865	530	884	1196	907	1380	465	723
I, μlb-second	199	210	194	119	199	269	204	310	105	162
I_{sp}, seconds	434	454	422	274	324	346	407	465	216	231
I/E, μlb/watt	9.95	10.5	9.7	11.9	13.3	13.45	10.2	10.3	6.97	8.1
Δm/shot, μgm	207	209	209	197	278	352	227	302	219	319
Δm/E, μgm/joule	10.35	10.45	10.45	19.7	18.6	17.6	11.35	10.1	14.6	15.95
η, %	9.36	10.4	8.95	7.4	9.37	10.2	9.05	10.5	3.2	4.09
L, 10^{-9} henries	18.7	21.1	18.4	55.2	28.2	51.7	23.8	21.0	31.0	31.0
R, 10^{-2} ohms	2.9	3.1	3.0	4.2	6.8	5.7	3.2	3.1	5.1	4.9

Section II continued: Circular Configuration, Straight Bore, With Nozzle

Log Number	81	82	83	84	85	86
Run Number	24	23	26	25	21	22
Diameter, inches	0.5	0.5	0.812	0.812	0.812	0.812
Length, inches	2.5	2.5	2.5	2.5	2.5	2.5
V_m, volts	1581	1581	1825	1290	1581	1825
E, joules	15	15	20	10	15	20
I, μN-second	393	417	514	197	307	430
I, μlb-second	89	94	115	44	69	97
I_{sp}, seconds	171	171	175	120	135	145
I/E, μgm/joule	5.9	6.24	5.75	4.42	4.6	4.84
Δm/shot, μgm	234	248	299	167	228	302
Δm/E, μgm/joule	15.6	16.6	14.45	16.7	15.2	15.1
η, %	2.2	2.33	2.2	1.16	1.35	1.53
L, 10^{-9}henries	29.2	28.2	36.6	34.7	22.0	34.7
R, 10^{-2}ohms	5.8	5.3	4.7	4.2	3.3	4.2

Section III: Circular Configuration, Tapered Bore

Log Number	87	88	89	90	91	92	93	94	95	96
Run Number	80	81	82	83	85	84	87	88	89	90
θ, degrees	10°	10°	10°	10°	10°	10°	10°	10°	15°	15°
Length, inches	2.5	2.0	1.5	1.0	1.0	0.5	1.5	0.5	2.5	2.0
V_m, volts	1825	1825	1825	1825	2100	1825	1825	1825	1825	1825
E, joules	20	20	20	20	26.45	20	20	20	20	20
I, μN-second	1005	998	868	834	1120	630	899	603	925	945
I, μlb-second	226	224	195	187	252	142	202	135	208	212
I_{sp}, seconds	329	363	386	447	471	549	378	544	304	356
I/E, μlb/watt	11.3	11.2	9.75	9.35	9.52	7.1	10.1	6.75	10.4	10.6
Δm/shot, μgm	311	280	229	190	242	117	242	113	310	271
Δm/E, μgm/joule	15.5	14.0	11.45	9.5	9.15	5.85	12.1	5.65	15.5	13.55
η, %	8.11	8.90	8.23	9.15	9.80	8.49	8.31	8.04	6.9	8.25
L, 10^{-9}henries	27.2	22.1	24.1	18.0	13.2	42.3	20.4	8.0	29.6	30.6
R, 10^{-2}ohms	4.9	4.7	3.7	4.5	3.4	3.6	3.6	3.9	4.5	4.3

Section III continued: Circular Configuration, Tapered Bore

Log Number	97	98	99	100	101	102	103	104	105	106
Run Number	91	92	93	94	95	96a	96b	97	98	99
θ, degrees	15°	15°	15°	15°	15°	15°	15°	15°	15°	15°
Length, inches	1.5	1.0	1.0	0.5	2.5	2.1	2.1	1.7	1.1	.523
V_m, volts	1825	1825	1825	1825	1825	1825	1825	1825	1825	1825
E, joules	20	20	20	20	20	20	20	20	20	20
I, μN-second	877	734	683	493	879	864	836	819	749	569
I, μlb-second	197	165	154	111	198	195	189	185	169	128
I_{sp}, seconds	351	416	390	448	305	328	333	340	402	471
I/E, μlb/watt	10.15	8.25	7.7	5.55	9.9	9.75	9.45	9.25	8.45	6.4
Δm/shot, μgm	255	180	178	112	294	269	256	245	190	123
Δm/E, μlb/watt	12.75	9.0	8.9	5.6	14.7	13.45	12.8	12.25	9.5	6.15
η, %	7.55	7.49	6.55	5.42	6.57	6.95	6.82	6.84	7.40	6.59
L, 10^{-9} henries	20.8	18.9	20.0	12.1	26.6	21.7	31.7	25.2	23.6	46.4
R, 10^{-2} ohms	3.2	2.8	2.8	1.8	5.0	3.9	4.8	3.8	4.0	3.5

Section III continued: Circular Configuration, Tapered Bore

Log Number	107	108	109	110	111	112	113	114	115	116
Run Number	100	101	102	103	105	104	106	107	108	109
θ, degrees	20°	20°	20°	20°	20°	20°	25°	25°	25°	25°
Length, inches	2.5	2.1	1.7	1.1	1.1	0.52	2.5	2.5	2.1	1.7
V_m, volts	1825	1825	1825	1825	1825	1825	1825	1825	1825	1825
E, joules	20	20	20	20	20	20	20	20	20	20
I, μN-second	881	863	820	690	719	566	787	748	720	714
I, μlb-second	199	194	185	156	162	128	177	169	162	161
I_{sp}, seconds	304	354	351	372	392	511	286	274	290	321
I/E, μlb/watt	9.95	9.7	9.25	7.8	8.1	6.4	8.85	8.45	8.1	8.05
Δm/shot, μgm	295	248	238	189	187	112	280	278	253	227
Δm/E, μgm/joule	14.75	12.4	11.9	9.45	9.35	5.6	14.0	13.9	12.65	11.35
η, %	6.57	7.50	7.07	6.3	6.92	7.10	5.52	5.03	5.13	5.62
L, 10^{-9} henries	20.4	24.9	21.9	21.0	19.0	13.2	35.2	26.9	27.2	21.9
R, 10^{-2} ohms	4.9	3.9	3.03	3.1	2.8	1.8	4.7	3.8	3.7	3.3

Section III continued: Circular Configuration, Tapered Bore

Log Number	117	118	119	120	121	122
Run Number	110	111	69	70	71	72
θ, degrees	25°	25°	10°	10°	16°	16°
Length, inches	1.1	0.52	2.5	2.5	2.5	2.5
V_m, volts	1825	1825	1581	1825	1581	1825
E, joules	20	20	15	20	15	20
I, μN-second	640	467	728	990	740	920
I, μlb-second	144	105	164	223	167	208
I_{sp}, seconds	366	429	272	341	270	266
I/E, μlb/watt	7.2	5.25	10.9	11.15	11.1	10.4
Δm/shot, μgm	178	111	273	296	279	352
Δm/E, μgm/joule	8.9	5.55	18.2	14.8	18.6	17.6
η,%	5.75	4.91	6.49	8.28	6.54	6.00
L, 10^{-9} henries	19.0	16.3	29.5	30.6	29.2	28.5
R, 10^{-2} ohms	2.8	2.1	4.5	4.2	4.1	3.9

Section IV: Rectangular Configuration, Straight Bore, No Nozzle

Log Number	123	124	125	126	127	128	129	130	131	132
Run Number	119	120	121	135	136	137	138	139	140	141
Length, inches	1.0	1.0	1.0	1.0	1.0	1.0	1.0	1.0	1.0	1.0
Height, inches	0.5	0.5	0.69	0.25	0.30	0.40	0.70	1.0	0.30	0.25
Width, inches	0.375	0.25	0.25	0.25	0.25	0.25	0.25	0.25	0.125	0.125
V_m, volts	1825	1825	1825	1825	1825	1825	1825	1825	1825	1825
E, joules	20	20	20	20	20	20	20	20	20	20
I, μN-seconds	750	865	840	925	866	804	765	671	975	1070
I, μlb-seconds	169	195	189	208	195	181	172	151	220	242
I_{sp}, seconds	390	390	398	374	365	366	384	354	314	324
I/E, μlb/watt	8.45	9.75	9.45	10.4	9.75	9.85	8.6	7.55	11.0	12.1
Δm/shot, μgm	196	226	215	252	242	224	203	193	316	336
Δm/E, μgm/joule	9.8	11.3	10.75	12.6	12.1	11.2	10.15	8.65	15.8	16.8
η, %	7.2	8.27	8.2	8.50	7.76	7.22	7.21	5.84	7.51	8.50
L, 10^{-9} henries	20.0	19.4	20.2	25.7	25.4	28.4	23.1	19.6	24.1	25.4
R, 10^{-2} ohms	2.9	3.1	2.8	4.5	4.2	3.9	2.9	2.5	5.1	5.8

Section IV: Rectangular Configuration, Straight Bore, No Nozzle

Log Number	133	134	135	136	137
Run Number	142	143	144	145	146
Length, inches	1.0	2.0	2.0	2.0	2.0
Height, inches	0.25	1.0	1.0	1.0	0.5
Width, inches	0.19	---	---	---	---
V_m, volts	1825	1825	1825	1825	1825
E, joules	20	20	20	20	20
I, μN-second	904	595	785	859	761
I, μlb-second	203	134	177	193	172
I_{sp}, seconds	302	262	252	263	280
I/E, μlb/watt	10.15	6.7	8.85	9.65	8.6
Δm/shot, μgm	305	231	318	333	277
Δm/E, μgm/joule	15.25	11.55	15.9	16.65	13.85
η, %	6.7	3.82	4.85	5.55	5.24
L, 10^{-9} henries	24.9	26.9	23.6	26.9	44.4
R, 10^{-2} ohms	5.3	4.8	5.8	6.0	9.5

Section V: Rectangular Configuration, Straight Bore, With Feed Mechanism

Log Number	138	139	140	141	142	143
Run Number	147	155b	156	157	158	160
Length, inches	1.0	1.1	1.1	1.1	1.1	1.1
Height, inches	0.25	0.44	0.44	0.44	0.44	0.44
Width, inches	0.25	---	---	---	---	---
V_m, volts	1825	1825	1708	1708	1708	1708
E, joules	20	20	17.5	17.5	17.5	17.5
I, μN-second	1015	229	403	452	469	279
I, μlb-second	228	51.5	91	102	106	263
I_{sp}, seconds	400	248	395	362	316	245
I/E, μlb/watt	11.4	2.6	5.18	5.83	6.05	3.6
Δm/shot, μgm	258	94.0	104	127	151	116
Δm/E, μgm/joule	12.9	4.7	5.95	7.24	8.65	6.63
η, %	9.95	1.39	4.46	4.59	4.16	1.92
L, 10^{-9} henries	25.1	41.9	67.6	89.0	89.5	98.0
R, 10^{-2} ohms	4.6	3.1	3.1	5.1	5.1	4.1

Section V: Rectangular Configuration, Straight Bore, With Feed Mechanism

Log Number	144	145	146	147	148
Run Number	161	162	163	164	165
Length, inches	1.1	1.1	1.1	1.1	1.1
Height, inches	0.44	0.44	0.44	0.44	0.44
Width, inches	---	---	---	---	---
V_m, volts	1709	1709	1825	1815	1709
E, joules	17.5	17.5	20	20	17.5
I, μN-second	496	517	645	720	650
I, μlb-second	112	118	145	162	146
I_{sp}, seconds	418	390	419	382	392
I/E, μgm/joule	6.4	6.6	7.25	8.1	8.35
Δm/shot, μgm	**121**	**136**	**157**	**192**	**169**
Δm/E, μgm/joule	6.91	7.8	7.85	9.6	9.66
η, %	5.81	5.72	6.63	6.75	7.15
L, 10^{-9} henries	56.0	22.3	22.6	22.6	17.1
R, 10^{-2} ohms	4.0	3.7	3.6	3.6	3.4

Section VI: Rectangular Configuration, Straight Bore, With a Nozzle

Log Number	149	150	151
Run Number	122	123	125
Length, inches	1.0	1.0	1.0
Height, inches	0.69	0.69	0.69
Width, inches	0.25	0.25	0.25
V_m, volts	1825	2240	1825
E, joules	20	30	20
I, μN-second	918	1320	931
I, μlb-second	207	298	210
I_{sp}, seconds	444	452	444
I/E, μgm/joule	10.35	9.95	10.5
Δm/shot, μgm	211	298	214
Δm/E, μgm/joule	10.55	9.95	10.7
η, %	10.0	9.75	10.1
L, 10^{-9} henries	20.8	12.8	20.2
R, 10^{-2} ohms	2.6	2.1	2.8

Section VII: Miscellaneous Configurations, Propellants

Log Number	152	153	154	155	156
Run Number	66	116	118	124	86
V_m, volts	2100	2240	1825	1825	1825
E, joules	26.45	30	20	20	20
I, μN-second	615	574	378	705	800
I, μlb-second	139	129	85	159	180
I_{sp}, seconds	505	810	782	368	388
I/E, μgm/joule	5.25	4.3	4.25	7.95	9.0
Δm/shot, μgm	124	72.1	49.3	195	210
Δm/E, μgm/joule	4.69	2.4	2.46	9.75	10.5
η, %	5.77	7.62	7.25	6.36	7.60
L, 10^{-9} henries	34.2	13.9	20.8	16.5	21.0
R, 10^{-2} ohms	4.4	2.2	2.5	2.7	3.1

Section VIII: RECTANGULAR CONFIGURATIONS, WITH FEED MECHANISMS---LIFE TESTS

Log #	Run #	Configurations	Number of Shots	Mass Ablated	Comments
157	148	20 joules; 4-wall teflon, (.25 x .25" x 1"); Coil spring feed; sparkplug in cathode to retain fuel; Tungsten rod anode; Stain-steel cathode.	19,570	6.64 gm	Ablation Uneven (Axial & lateral); Teflon seals ablated unevenly--Ended because of poor ablation profile.
158	149	Two teflon wall(1.1" x .44") Negator springs; Wall (teflon) separation--0.30"; Super-mica sidewalls--not exposed to discharge initially; Tungsten anodes; Fuel faces rounded to oval chamber; sparkplug in cathode.	53, 795	9.18 gm 3/16" Feed each bar	Ablation uneven axially, formed converging chamber, Teflon ablated to form almost flat walls--Super-mica eroded where exposed to the blast; Ended because of carbon shorting sparkplug.
159	150	Same as Log #158; Teflon wall separation--0.25"; Stainless steel anode with step to retain fuel; sparkplug in fuel.	8,220	1.94 gm	As in Log #158; Supermica exposed and eroded; non-stainless steel portion of sparkplug eroded; uneven ablation; Ended because of sparkplug misfire.

Section VIII: Rectangular Configurations, With Feed Mechamisms--Life Tests

Log #	Run #	Configurations	Number of Shots	Mass Ablated	Comments
160	151	Same as Log #159; with stainless steel cover-plate over base plate.	71,650	13.65 gm	Ended because of spark plug shorting to cover (mica-like material and carbon); uneven ablation.
161	152	Same as Log#160 but polarity on electrodes reversed; Cathode in exhaust; anode at back of chamber.	~9,000	---------	Stopped after 4000 shots, electrodes very hot to touch, main discharge not ocurring; Rerun after cool until ~9000th shot---very eratic firing---very little carbon on plug; Reverse polarity configurations did not fire with coverplate over sparkplug.
162	153	Same as Log#160 with spark plug now attached to inert sidewall, with hole for spark material to be ejected into chamber; New stainless steel anodes with shoulders to retain fuel.	133,800	15.69 gm 1 1/2 " Feed each bar	Ended because anode steps eroded severely, allowing fuel to slip into chamber; Sparkplug clean--uneven ablation--mostly at base & on sparkplug side.

Section VIII continued: Rectangular Configurations, With Feed Mechanisms---Life Tests

Log Number	Run Number	Configurations	NO. of Shots	Mass Ablated	Comments
163	154	Boron Nitride replaced Super-mica.	1,000	--------	Boron Nitride covered with carbon.
164	155a	Same as Log#162; however, cathode and anode with Mallory 1000 (Tungsten/copper) step-in anode for fuel retention.	510,580	48.01 gm	Ended because difficult to maintain vacuum at reasonably high level; uneven ablation, forming converging chamber; Satisfactory electrode wear.
165	159	Flat teflon wall---Super-mica sidewalls; Chamber = 1.1" x .44" x .205"; E = 17.5 joules.	15,100	3.13 gm	Even axial ablation; spark-plug side of chamber ablated more.

TABLE I: COMMENTS ON CONFIGURATIONS

Section I: Circular Configuration, Straight Bore, No Nozzle

Log Number

1-18---Aluminum cover plate over spark plug----Six Tungsten anodes (1/16" diameter rods).

19-20---Stainless steel cover plate over spark plug; same anodes as #1.

21-30---Aluminum cover plate over spark plug; same anodes as #1.

31---Stainless steel back plate, no cover plate over spark plug; same anodes as #1.

32-35---Aluminum cover plate over spark plug; same anodes as #1.

36-50---Stainless steel back plate, no cover plate over spark plug; same anodes as #1.

Section II: Circular Configuration, Straight Bore, With Nozzle

Log Number

51-56---Internal nozzle--Front three discs parabolically flared-M = 3; γ = 1.66; no throat; same anodes as #1.

57-58---Same as #51, but converging-diverging throat added--0.375" Dia; M = 3.85.

59---Same as #57, but Anode (Tungsten electrodes) replaced by Aluminum Ring anode.

60-61---Same as #57.

62-63---External nozzle--2" long, 15° full angle cone; no converging throat; diameter at throat--0.44".

64-66---External nozzle, 1" long, parabolic (RAO), diverging throat; diameter at throat--0.443".

67---External nozzle; 15° conical; diverging throat--0.44" dia; Length = 5".

68---Same as #67; Length = 4".

69---Same as #67; Length = 3".

70---Same as #67; Length = 2".

71---Same as #67; Length = 1".

72---Same as #67, Length = 2".

73-78---Same nozzle as #64.

79-80---Parabolic Rao Nozzle; Length = 1"; With throat for chamber diameter = 0.5".

81-86---Parabolic Rao nozzles, with converging throat---for chamber diameters of D = 0.5" and D = 0.812"); Length = 1".

Also Tungsten Electrodes used--nozzle rested on top of electrodes.

Section III: Circular Configuration, Tapered Bore

Log Number

87-91---Stainless steel Backplate, no cover plate over sparkplug, 6-Tungsten rods formed the anode; small end diameter--~0.40" against backplate.

93-94---Same as #81, with small end diameter--~0.42".

95-100--Same as #81, with small end diameter--~0.43".

101-102--Same as #81, New teflon, anode has 12 Tungsten rods; small end diameter = 0.38".

103--Same as #101, but anode has 6 Tungsten rods.

104-105--Same as #81---with small end diameter = 0.385".

106--Small end diameter = 0.39".

107-109---Small end diameter = 0.40".

110-112---Small end diameter = 0.41". (Note: Very small diameter (<0.05") caused by ablation, large changes from machining).

113-116---Small end diameter = 0.49".

117-118---Small end diameter = 0.50".

119-122---Same as #81.

Section IV: Rectangular Configuration, Straight Bore, No Nozzle

Log Number

123-133---Stainless steel backplate, no coverplate over sparkplug; anodes of Tungsten rods. Annulus of semiconductor material in sparkplug entirely covered with epoxy cement except for one small section ~1/16" x 1/8" long.

134---Same as #123 except two inert walls of Boron nitride replace two two teflon walls. Separation between remaining two teflon walls is 0.25",

135-137---Same as #134; wall separation is 0.125".

Section V: Rectangular Configuration, Straight Bore, With Feed Mechanism

Log Number

138---4 wall teflon feed; square step-in cathode retains teflon to form chamber. Tungsten rod anodes.

139---2 wall teflon feed, Mallory 1000 electrodes; step-in anodes (exhaust end) to retain fuel. Teflon bar separation = 0.4"; Sparkplug mounted on one of the two Super-mica inert walls.

140---Same as #139, with wall separation = 0.28".

141---Wall separation = 0.205".

142---Wall separation = 0.160".

144---Same as #139, with step-in cathode and quartz side walls. Wall separation = 0.23".

145-146---Same as # 144, however, thrust chamber/electrode assembly placed in low inductance configuration between the capacitors.

147-148---Same as #145, with one quartz wall replaced with teflon.

Section VI: Rectangular Configuration, Straight Bore, With Nozzle

Log Number

149-150---Stainless steel backplate as cathode; nozzle also anode; 15° taper walls; 1.0" high; throat section 0.3" x 0.7"; Mach number = 3.5: γ = 1.4; nozzle rested on teflon and had no converging portion.

151---Same as #144, with nozzle extended to 2.0" long.

Section VII: Miscellaneous Configurations, Propellants

Log Number

152---Same configuration as #31 with teflon replaced by polyethylene; Length = 2.5"; diameter = 0.46".

153---Same as #65, with teflon replaced by polyethylene; length = 1.0"; diameter = 0.38".

154---Same as #153.

155---Same as #123, with the rectangular configuration replaced by a cross, 0.69" high and 0.625" wide Each arm of the cross was 1/4" wide.

156---Same as #91, with the 2", 10° taper teflon fuel piece reversed, so that the flow is constricted at the exit; for mass ablation study.

CHAPTER V

SATELLITE-THRUSTER SYSTEM

Using the results of the experiments performed, a flight thruster can be designed to fulfill the objectives stated in the introduction. A rectangular design with fuel feed is necessary in order to meet the requirements for long-life and high total impulse. The basic configuration is shown in the schematic in Figure 65. The cross-section of each bar of the four wall feed system is typically 1" by .25" to 1" by .44". The seals at each corner are constructed of quartz. The spark plug placement is in the cathode. Even axial ablation can be assured by using the optimum ablation energy. As found in Run #160, this will be approximately 17.5 joules. The main storage capacitors should be placed circularly around the discharge chamber, to minimize circuit inductance. The performance of this system can be estimated by Run #147 (Log #134). With the fuel size 1.0" by .25", using Run #162 (Log #145) and Run #163 (Log #146), as an example, we must derate the performance parametersof Run #147 by approximately 10% to take into account the lower discharge energy. This gives I≃ 200μlb-second; I_{sp} = 360 seconds. This will result in I/E ≃ 11μlb/watt and η ≃ 9%. With the addition of a properly designed rectangular nozzle, these values can be raised by at least 10%, based on previous results, Run #121 and #122 (Log #125 and #149 respectively). This will give an I = 220μlb-second and I_{sp} = 400 seconds; I/E = 12.5μlb/watt and η= 11%.

WEIGHT CALCULATIONS

Rough estimates can be made to approximate the weight of this system. For the thruster itself, the weight may be approximated by the LES-7 thruster[2], as an upper limit, since it includes two nozzles. The thruster mass,

without fuel, is then approximately 4 kilograms (8.8 lbm), including capacitors (~20 joule/kg → ~1 kg)[2] , nozzle, electrodes, Negator springs, and case, plus the ignition circuitry. The power conditioner mass can be estimated at ~3 lbm (1.3 kg) with 20 to 40 watts of conditioned power supplied at 85% efficiency.[2, 21]

The power necessary for the thruster's operation can be provided from the power bus already present in most satellites. Communications satellites, especially, have large power requirements, usually met by the use of solar cell arrays. Lightweight 1.5 kilowatt arrays have been flight tested.[6] In some cases large thruster power drains can be timed to occur during periods of low power drain by the satellite itself.

This type of configuration has the added advantage over LES-6 and LES-7 types of thrusters in that the propellant is not directed radially into the satellite. Instead it is oriented tangent to the satellite's surface. Thus for high total impulse systems, the configuration will not require large parts of the satellite's volume, as would an axially fed design.[6]

THRUSTER/SATELLITE MISSIONS

There are a number of missions that a pulsed ablative thruster, such as the one described above, can perform satisfactorily. Typical missions are[22, 23]

a) Precision Satellite Pointing; As narrow beam widths are employed in communications satellites to reduce transmitter power, the satellite must be accurately stabilized with very fine altitude controls of greater than 0.1° accuracy. The pulsed thruster, with its very small and sharply defined im-

pulse bit, is well suited for this task.

b) Precession Control of Spinning Satellites; Spinning spacecraft require spin-axis precession control. Very short pulse durations are needed to precisely increment the spin-axis pointing direction. The pulsed ablative thruster performs the task well, as its pulse length is on the order of microseconds.

c) North-South Station Keeping; The orbits of geosynchronous satellites are affected mainly by three forces; one arising from earth's oblateness, solar/lunar gravity fields, and solar radiation pressure. The primary disturbance is the effect of the moon. Typical rates of change of inclination are on the order of 0.9° per year.[22] Velocity increments of approximately 170 feet/second/year[4] are needed to counteract this drift.

d) East-West Station Keeping; Because of disturbances caused by earth's gravitational field (from the asphericity of the earth), the satellite's longitude will be affected and need maintenance to counteract daily drift, eccentricity, accelerations.[23] A velocity increment on the order of ~ 6.8 ft/sec/yr (2.1 m/sec/yr) is required.

The design requirements for East-West Station Keeping for typical satellites are shown below. Using the design thruster, with teflon 1" by .25" in cross-section, it is assumed that the total satellite weight is 1000 lbm and the mission is five years long. Then the total velocity increment required is 34.0 ft/sec = ΔV. The propellant required is given by:

$$M_p = M_o(1 - e^{-\Delta V/u})$$

where:

M_p = propellant mass

M_o = total satellite mass

ΔV = velocity increment

u = average exhaust velocity = $I_{sp} \cdot g$

For the design thruster, (I_{sp} = 400 seconds), $M_p = M_o(\Delta V/u)$, for $\Delta V/u << 1$. Then $M_p \simeq$ 2.64 lbm of teflon (~1.2 kg). Assuming the satellite carries four thrusters for East-West Station Keeping (like LES-6), and a cross section area of each propellant bar of 0.25 inches^2, each bar will be approximately 9 inches in length. (A total of 38"/thruster is needed). The total number of shots required would be given by the total impulse required, which is 1055 lb_f-second. this requires a total of $4.8 \cdot 10^6$ shots. To fully utilize the capabilities of the thrusters, they would also be used for precession or altitude control. The optimum design is for the propellant mass required to equal the thruster's fixed weight (essentially the capacitors). A typical thrusting program for East-West Station Keeping is shown in Figure 66.[4]

The design requirements for North-South Station Keeping are now investigated. Using the same system as described above, with a velocity increment of 170 ft/sec/year, the total impulse needed is 26,400 lb_f-second. This would require a propellant mass of 133 lbm (~60kg) and approximately $1.22 \cdot 10^8$ shots would be needed. It would be impractical to carry straight bars of teflon of the necessary length (~100" long, each). So in order to be practical, either a larger teflon cross-sectional area must be used, or a higher I_{sp} engine is needed. A shorter mission would be necessary for the

thruster to be practical for North-South Station Keeping. The problem of unwieldly fuel bar lengths has also occurred with other teflon thrusters, thus, investigations are being carried out on the possibilities of coiling the teflon bars in circular shapes.[24] A typical thrust program for North-South Station Keeping is shown in Figure 67.[4] Since the coiled teflon technique has proved unreliable so far,[4] and because of the I_{sp}, requirements, the design would not be suitable for a North-South Station Keeping.

THRUSTER EFFECTS UPON THE SPACECRAFT

There are three main effects that the thruster can have on the spacecraft. These include the contamination of spacecraft surfaces, interference with light sensors, and RFI noise generation. From investigations by Lyon[25, 26] and Hall,[27] on the LES-6 thruster, a number of design considerations can be listed. The most reactive components of the exhaust appear to recombine within a few inches of the exhaust opening and little recombination takes place further downstream. Anything placed in the path of the exhaust, will become coated with exhaust material. This material has been found to be unreactive and non-erosive on surfaces coated with the exhaust. As virgin teflon is very pure, impurities should not present a problem. Most of the ablated material is contained within a 40° included angle.[26] In the spacecraft design, a cone of 40° to 50° semiangle around the exhaust centerline should be kept free of components, preferably a 90° semiangle cone should be used. Some reflection is possible from objects placed in the exhaust path, but as the beam is neutral, there are no space charge buildup effects to attract the particles back to the spacecraft.

As a visible light plume is evident from the exhaust for a few μseconds

and a few inches from the nozzle, when the thruster fires. This must be taken into consideration when placing light sensors that may be affected by the short pulse. Electromagnetic noise interference behavior to be expected from such a thruster is still uncertain. With the high energy discharge, some RFI noise is certainly generated. Its effects upon the satellite will depend greatly upon the thruster-antenna configurations. The LES-6 thruster presented no problems.[26] To prevent stray RFI noise leakage from the thruster case, the case was machined from a solid piece of aluminum. Similar care will have to be taken with the present thruster.

CHAPTER VI

CONCLUSION

A practical pulsed ablative thruster, suitable for satellite control, has been designed and tested. It derives its thrust from gasdynamic forces generated by the ablation and heating of teflon in a high energy electrical discharge. By this means it produces a higher specific thrust than previous pulsed teflon microthrusters, which rely on both electromagnetic and gasdynamic forces. This high thrust is obtained at relatively low values of specific impulse, but the efficiency is comparable to that of more conventional geometries (LES-7). Specific thrusts on the order of 11.4 micropounds/watt, with a specific impulse of 400 seconds, and an efficiency of 10%, have been achieved in a thruster with teflon feed. In life tests, a thruster operated for more than 510,000 shots, feeding and ablating two and one-half inches of teflon (48 grams). This successfully demonstrated that the thruster was capable of being fed with teflon.

This thruster would find applications in satellite control, particularly where a high impulse, pulsed thruster is needed. While requiring a larger mass of teflon because of a lower specific impulse, weight savings are achieved over higher specific impulse pulsed thrusters, because of reduced capacitor and power conditioner weight. This latter is a consequence of fewer shots being required by a high specific thrust engine, over a low specific thrust engine, to achieve a desired thrust.

Further investigation is necessary to develop the full potential of this thruster. A more precise mathematical model describing the thruster's operation would be helpful in guiding optimization experiments. The development of an efficient nozzle compatible with the rectangular discharge chamber is

of prime importance. The choices of quartz, as a sidewall material, and Mallory 1000, as an electrode material should be confirmed with further testing. The development of a four-wall teflon feed design should be pursued in light of the performance losses in designs incorporating inert discharge chamber walls. Finally, a life test of the thruster system should be conducted to at least 10^7 shots.

APPENDIX

ERROR ANALYSIS

An error analysis was performed by Radley[14], in 1969, to determine the accuracy of thrust measurements found by using the thrust stand described in Chapter III. The same analysis is valid here except for changes in the magnitudes of some of the quantities used:

1. The total firing time for the thruster was reduced to ~30 minutes, with approximately 1000 shots.
2. Readings were taken every minute, rather than every five minutes, to 1-second accuracy.

The relative error in the impulse bit is found from:

$$\frac{\Delta I}{I} = \frac{\Delta A}{A} + \frac{\Delta(\nu\alpha_\infty)}{(\nu\alpha_\infty)} \qquad \text{(A-1)}$$

where:

$$I = A\alpha_\infty \nu$$

$$A = Mg \cdot \frac{\ell}{\ell'} \cdot \frac{T^2}{2\pi}$$

$$\frac{\Delta A}{A} = \frac{\Delta M}{M} + \frac{\Delta \ell}{\ell} + \frac{\Delta \ell'}{\ell'} + \frac{2\Delta T}{T}$$

and:

$$\frac{\Delta(\nu\alpha_\infty)}{(\nu\alpha_\infty)} \simeq .007; \text{ (no change from Radley)}$$

where: M, ℓ, ℓ', and T are the same quantities as defined in Chapter III.

In computing the value of $\Delta A/A$, only $\Delta T/T$ is affected. $\Delta T/T$ is equal to the uncertainty in the firing time measurement plus the uncertainty of the

reading for the number of shots. This is given by:

$$\frac{\Delta T}{T} = \frac{\Delta t_f}{t_f} + \frac{\Delta N}{N}$$

From number 1 above, this is;

$$\frac{\Delta T}{T} = \frac{5 \text{ seconds}}{30 \text{ minutes}} + \frac{1 \text{ shot}}{1000 \text{ shots}}$$

$$= .003 + .001$$

$$= 0.4\%$$

Then;

$$\frac{\Delta A}{A} = .003\% + 0.25\% + 0.7\% + 0.8\%$$

$$= 1.75\%$$

Then;

$$\frac{\Delta I}{I} = \frac{\Delta A}{A} + \frac{\Delta(\alpha_\infty \nu)}{(\alpha_\infty \nu)}$$

$$= 0.0175 + 0.008$$

$$= 2.6\%$$

For the specific impulse, $I_{sp} = I/\Delta mg$

$$\frac{\Delta I_{sp}}{I_{sp}} = \frac{\Delta(\Delta m)}{\Delta m} + \frac{\Delta I}{I}$$

$$= \frac{\Delta(\Delta M)}{\Delta M} + \frac{\Delta N}{N} + \frac{\Delta I}{I} \qquad \text{(A-2)}$$

where:

$$\Delta m = \Delta M/N$$

This gives, using the previous value found for $\Delta I/I$;

$$\frac{\Delta I_{sp}}{I_{sp}} = 0.001 + 0.001 + 0.026$$

$$= 2.8\%$$

Thus the uncertainty in the measurements of both I and I_{sp} is less than 3%.

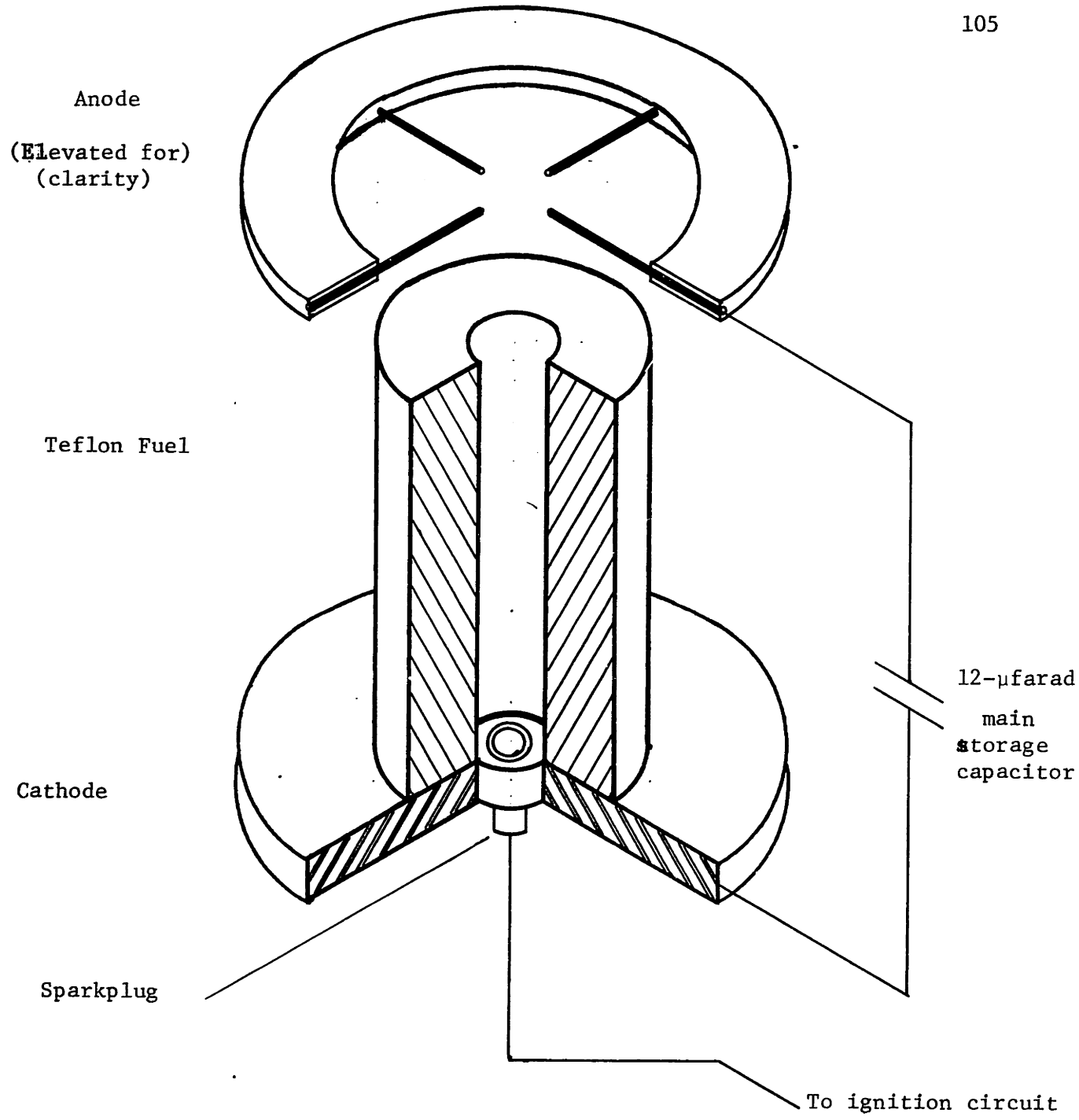

Figure 1: SCHEMATIC OF THRUSTER COMPONENTS

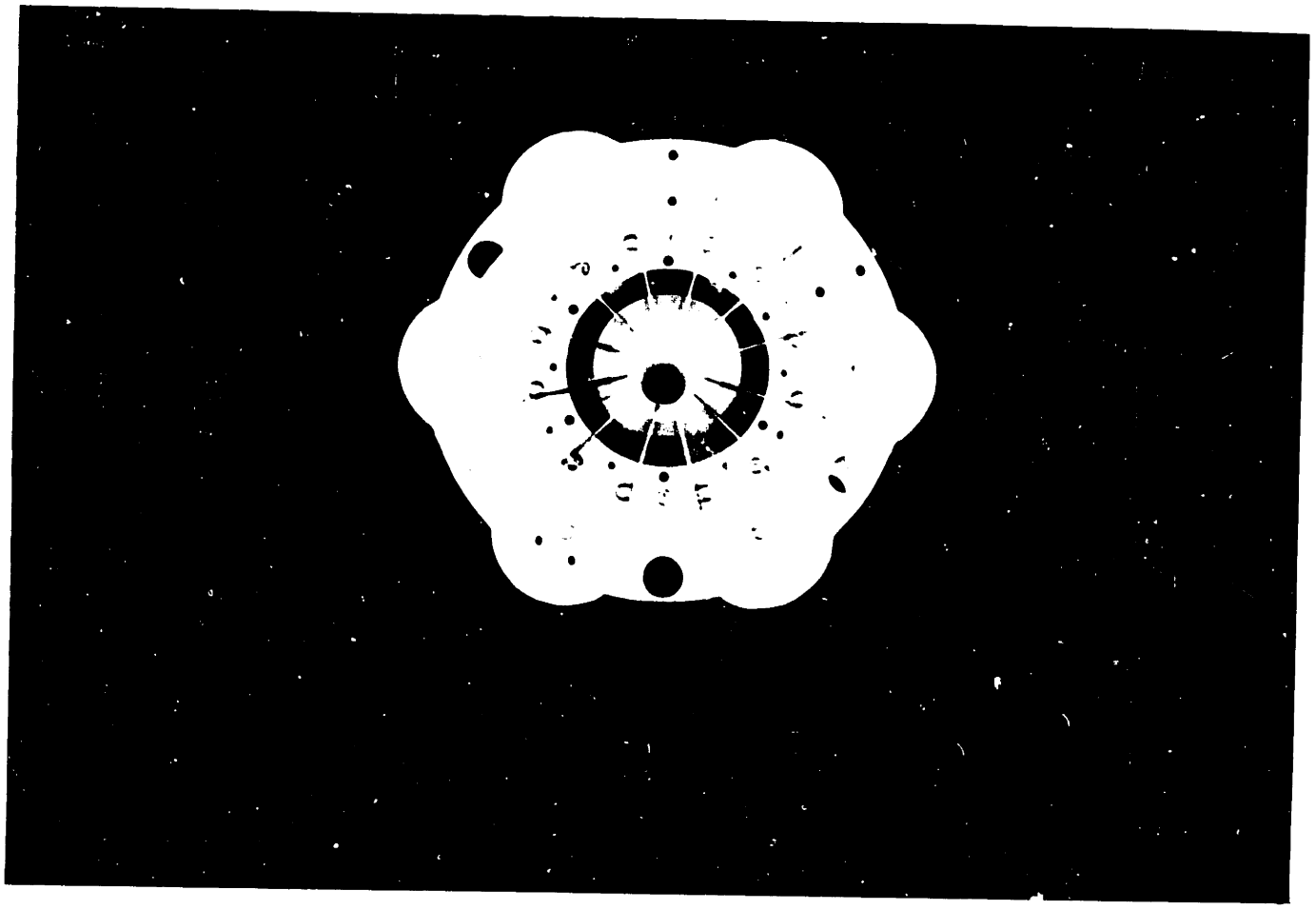

FIGURE 2: FRONT VIEW OF TEST THRUSTER---CIRCULAR CONFIGURATION

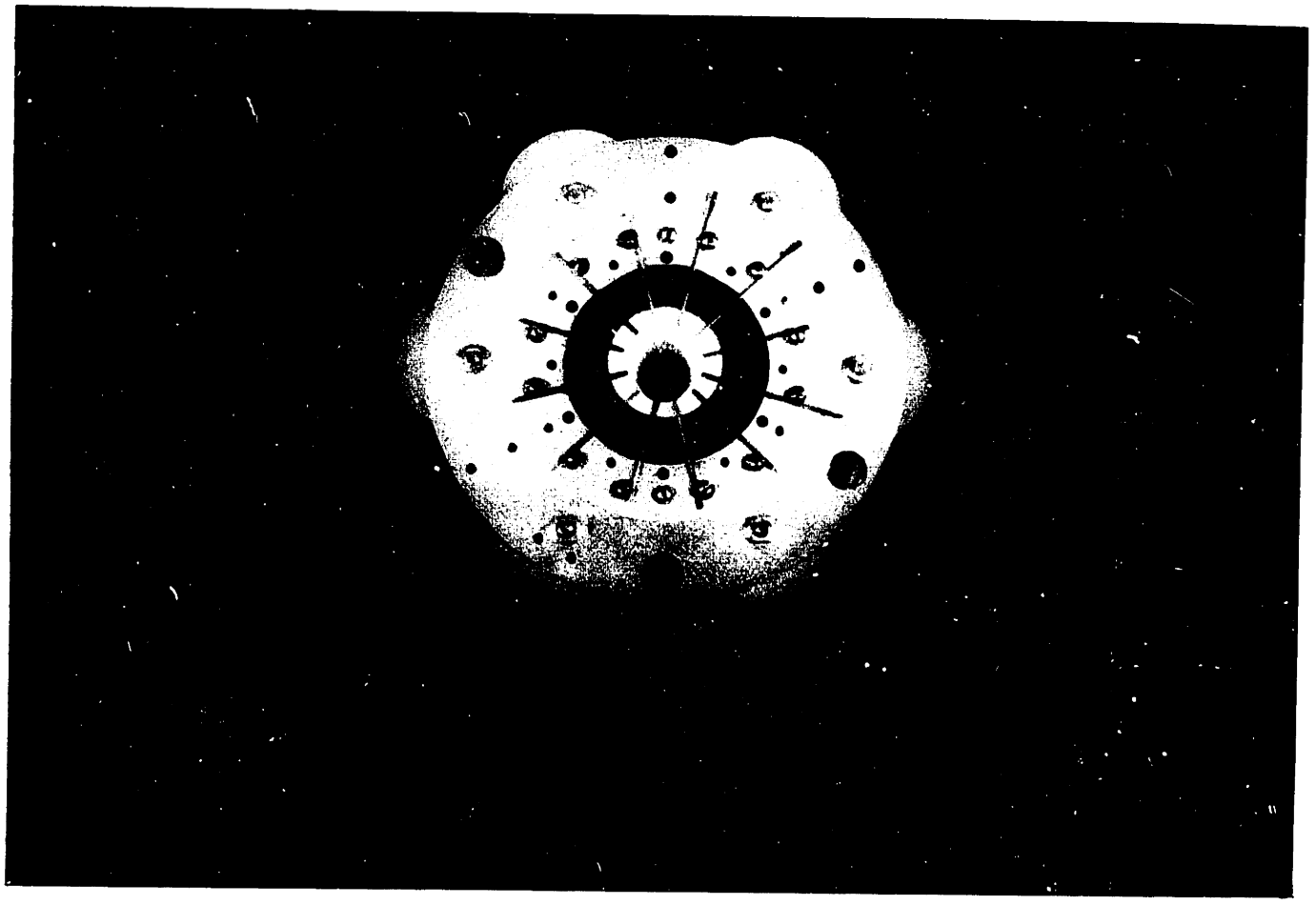

FIGURE 2: FRONT VIEW OF TEST THRUSTER---CIRCULAR CONFIGURATION

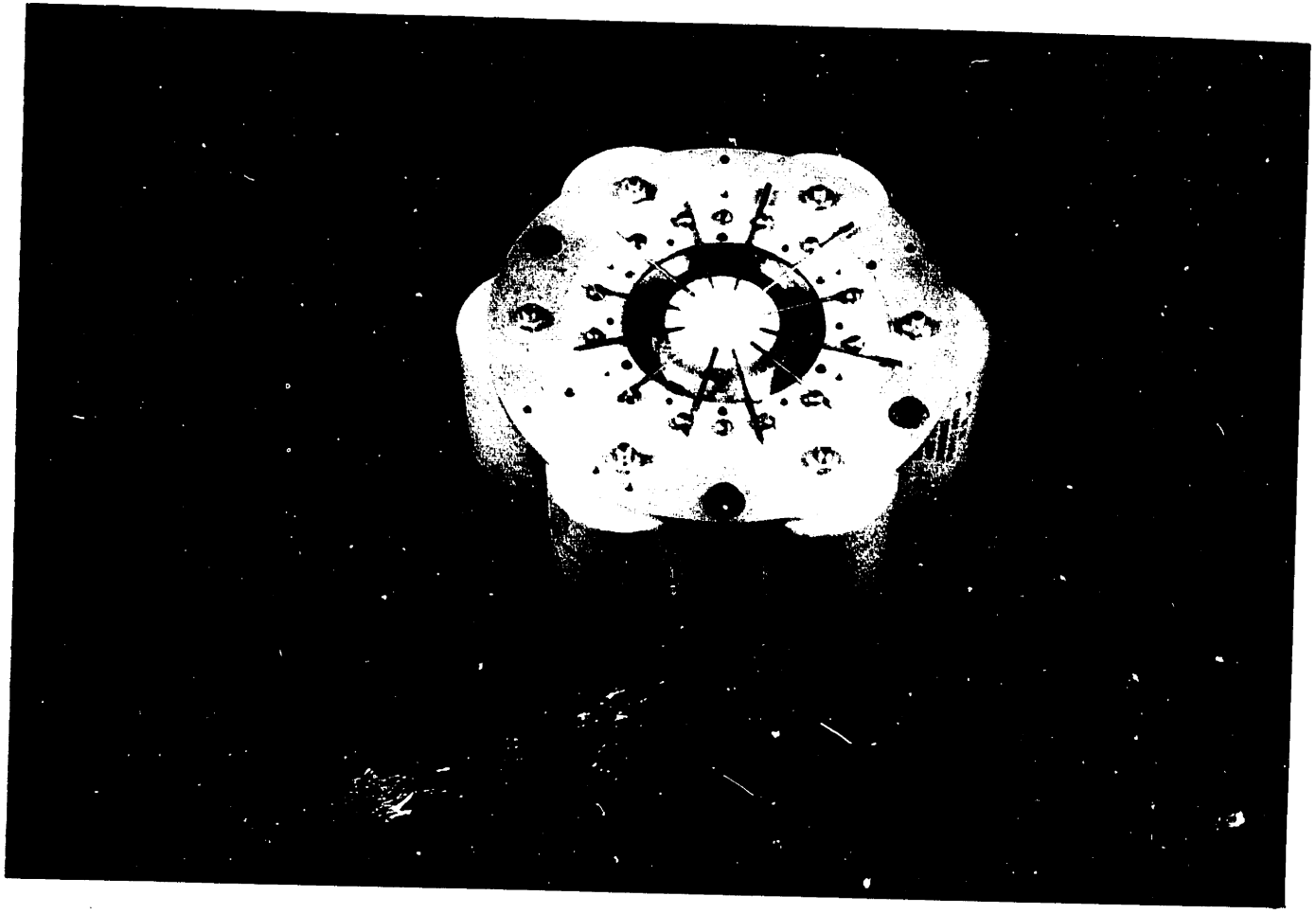

FIGURE 3: SLANT VIEW OF TEST THRUSTER---CIRCULAR CONFIGURATION

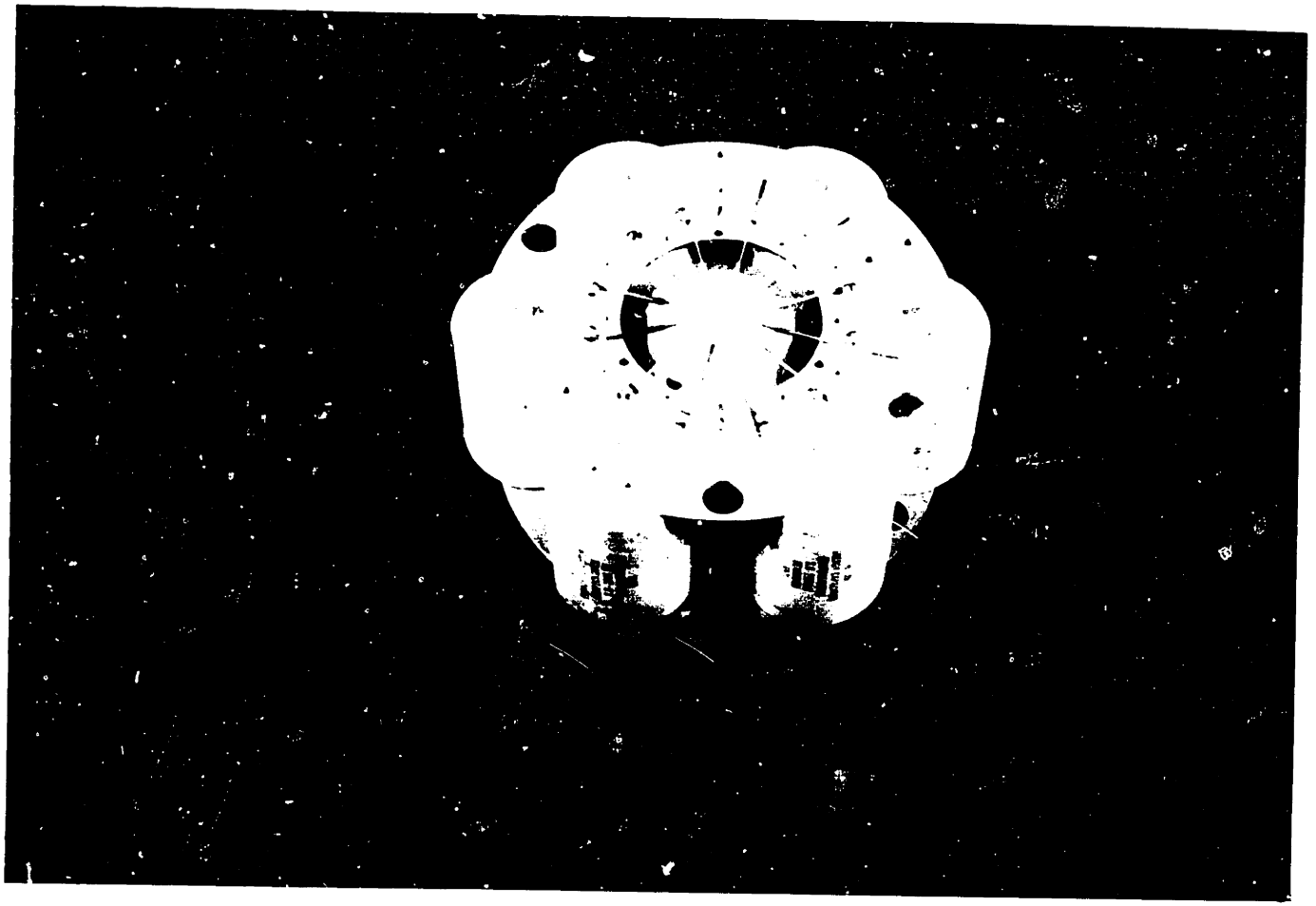

FIGURE 3: SLANT VIEW OF TEST THRUSTER---CIRCULAR CONFIGURATION

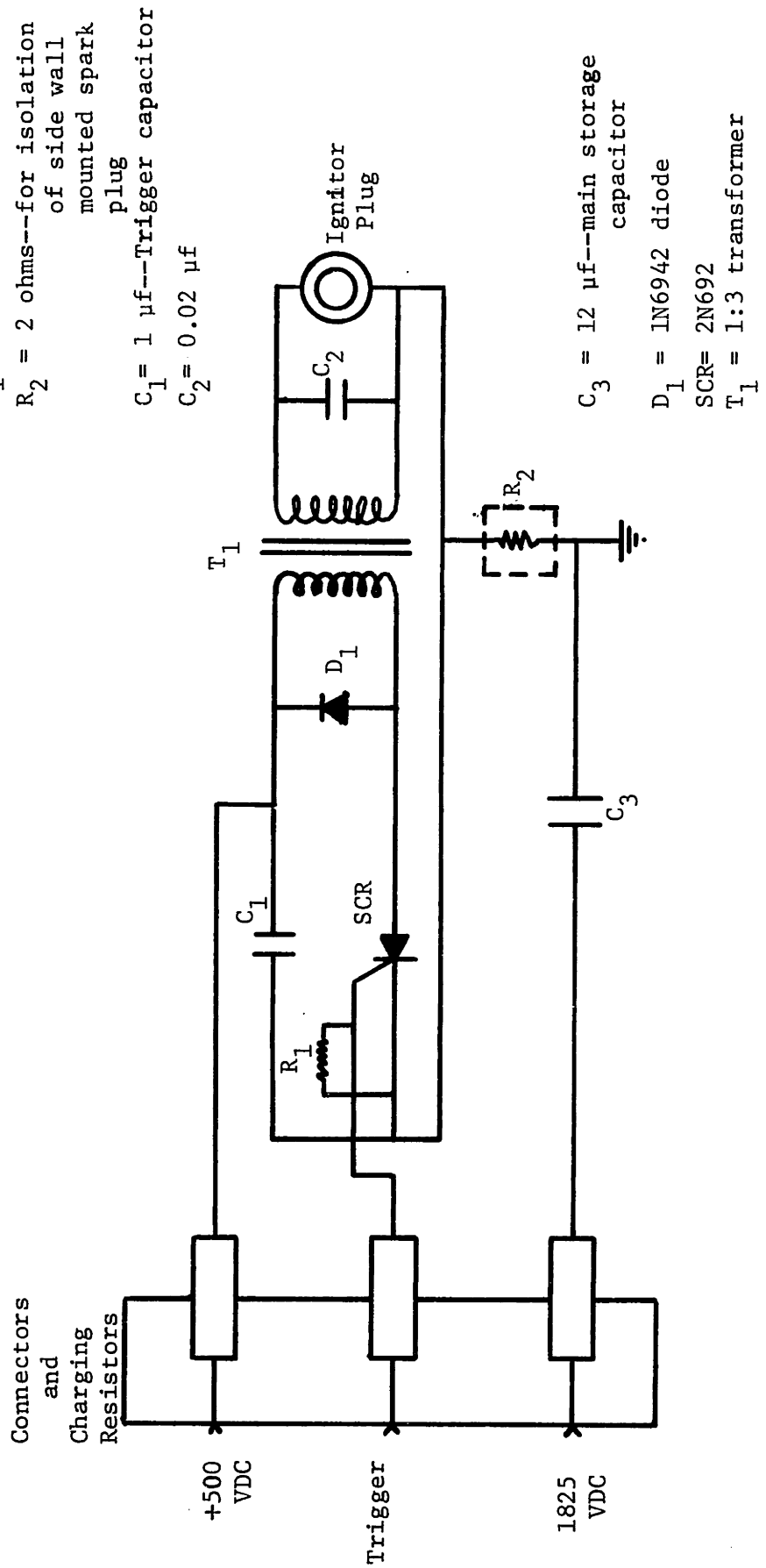

Figure 4: IGNITION CIRCUIT SCHEMATIC

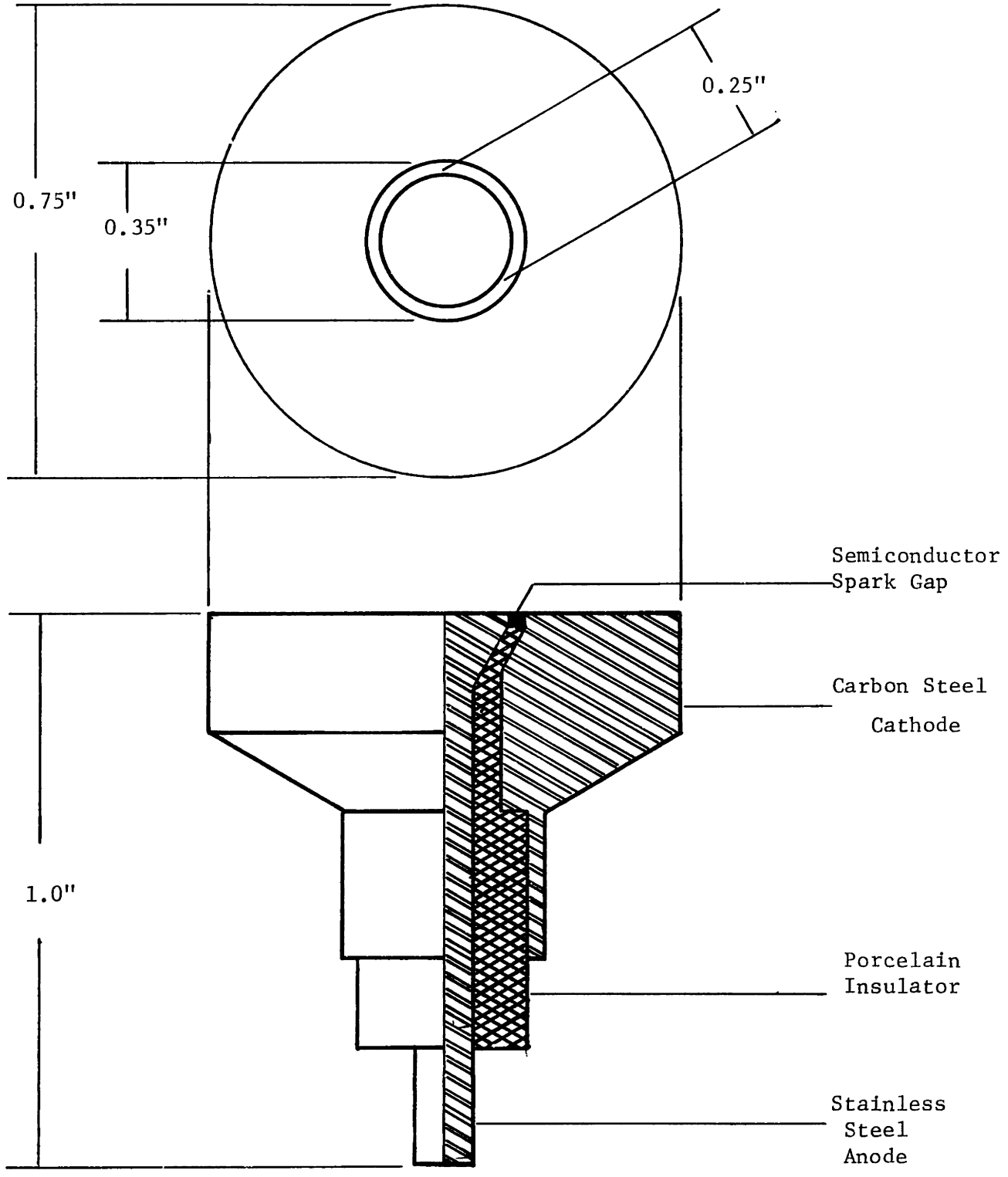

Figure 5: BENDIX IGNITOR PLUG

FIGURE 6: CIRCULAR CONFIGURATION MODIFIED FOR FUEL FEED

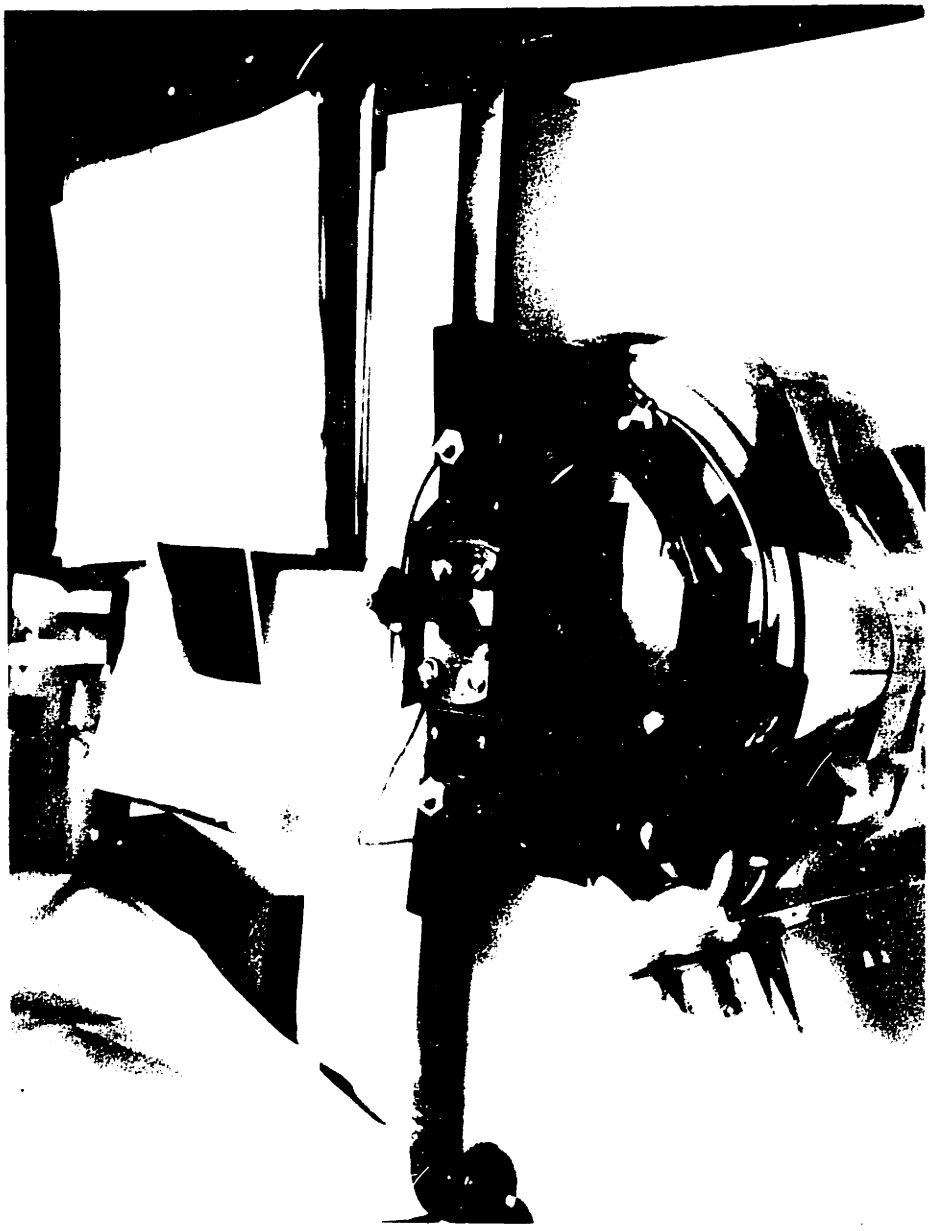

FIGURE 6: CIRCULAR CONFIGURATION MODIFIED FOR FUEL FEED

For $\gamma = 1.23$

Nozzle #1--M ≃ 2.6 (Chamber Diameter-0.812")
Nozzle #2--M ≃ 3.5 (Chamber Diameter-0.5")

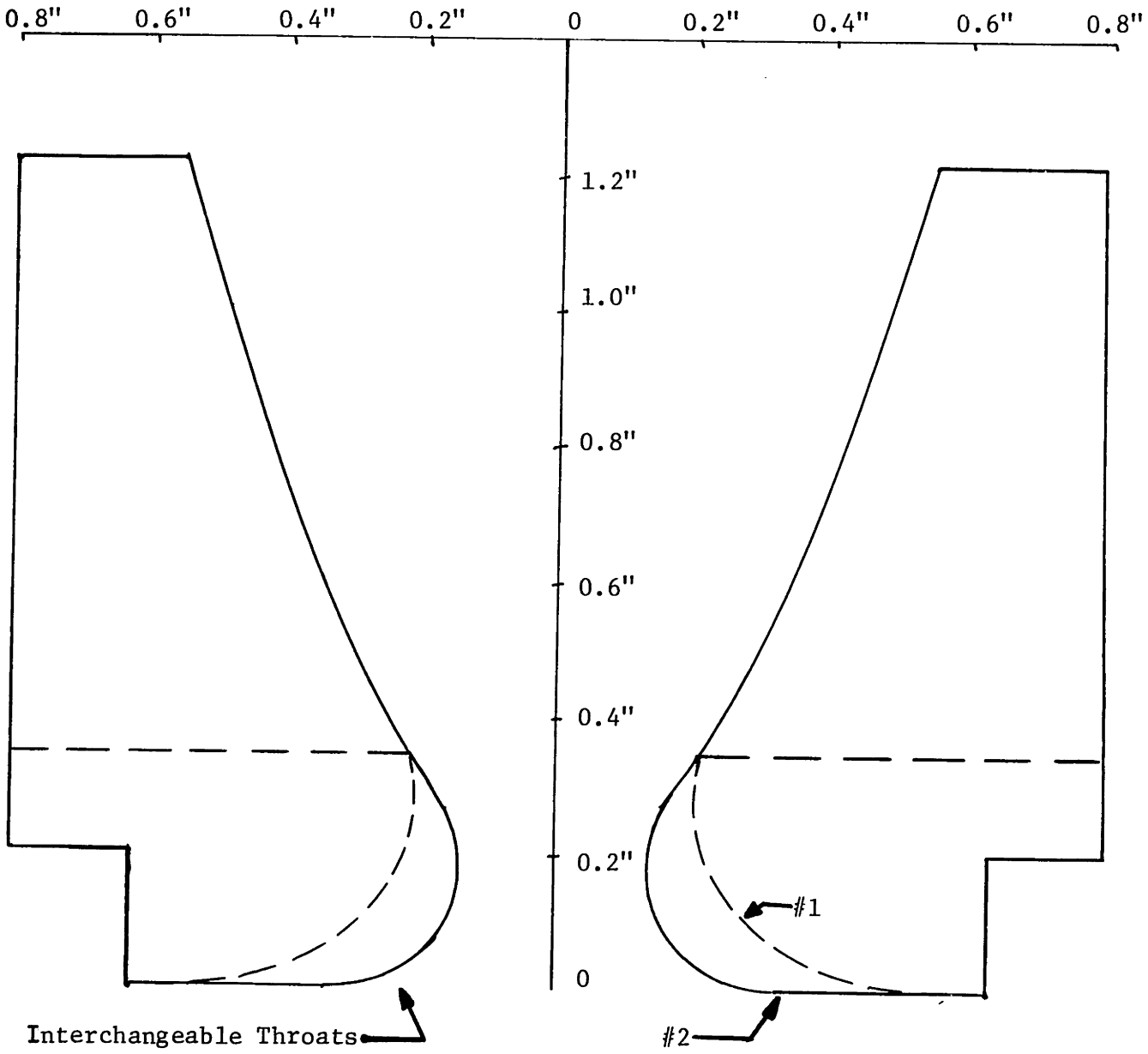

Figure 7--TWO NOZZLES (For 0.5" and 0.812" Dia. Chamber) BASED ON RAO[12] CALCULATIONS WITH INTERCHANGEABLE THROATS AND COMMON EXIT PIECE

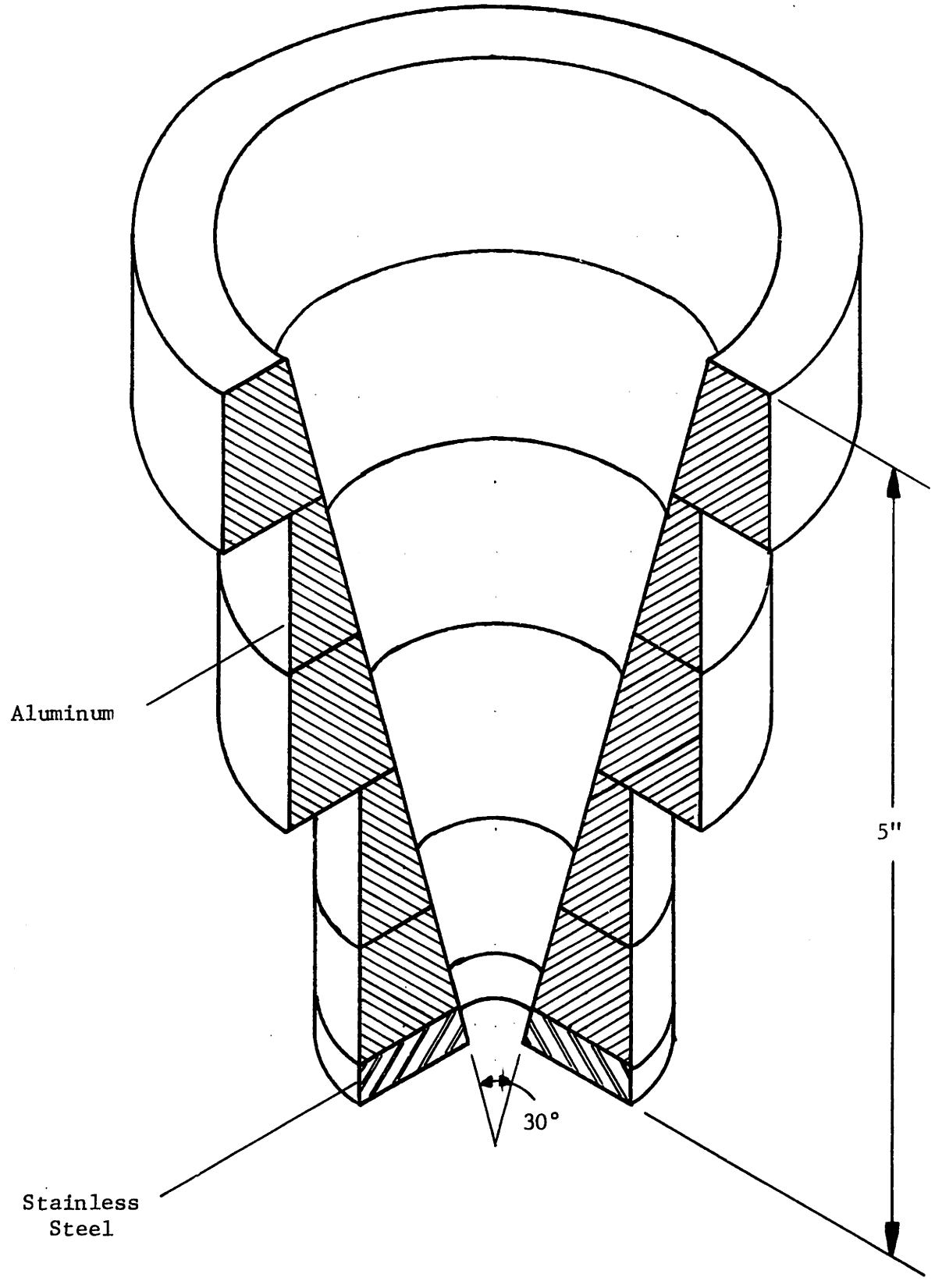

Figure 8: Five-inched, Sectioned, 30° Full Angle Test Nozzle--Full Size

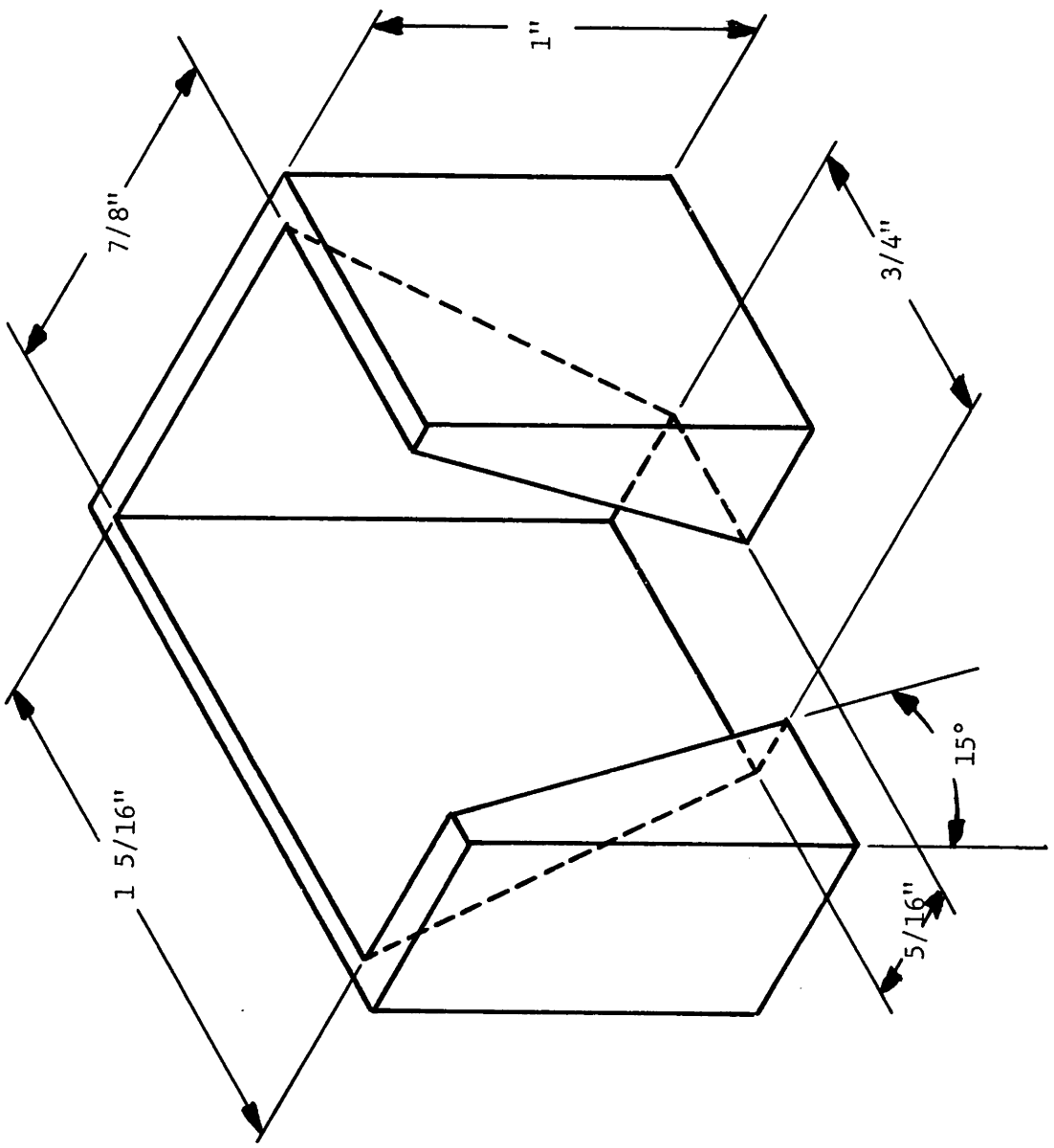

Figure 9: RECTANGULAR NOZZLE--ALUMINUM, Scale 2:1

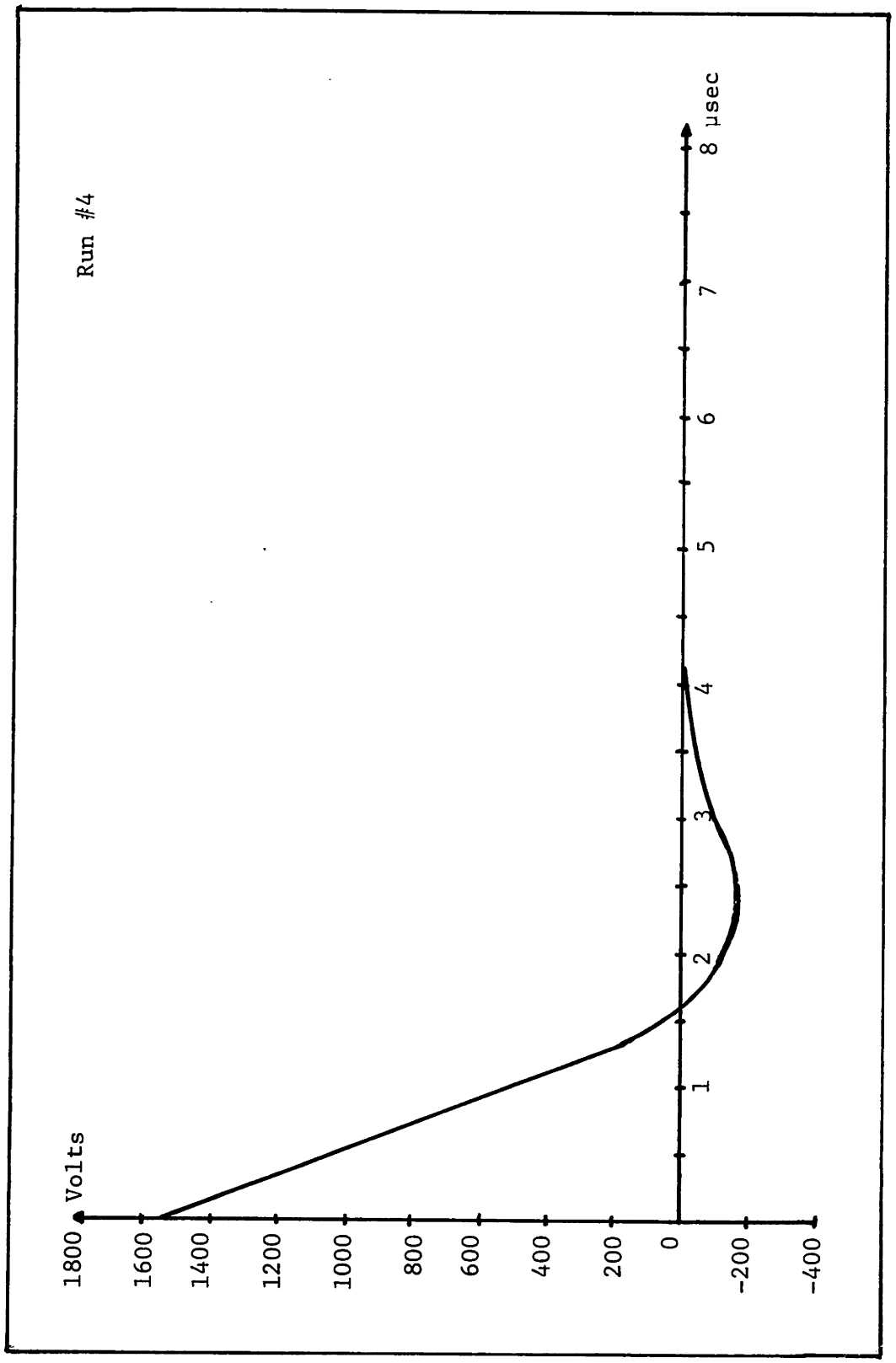

Figure 10--Discharge Waveform (High Damping)

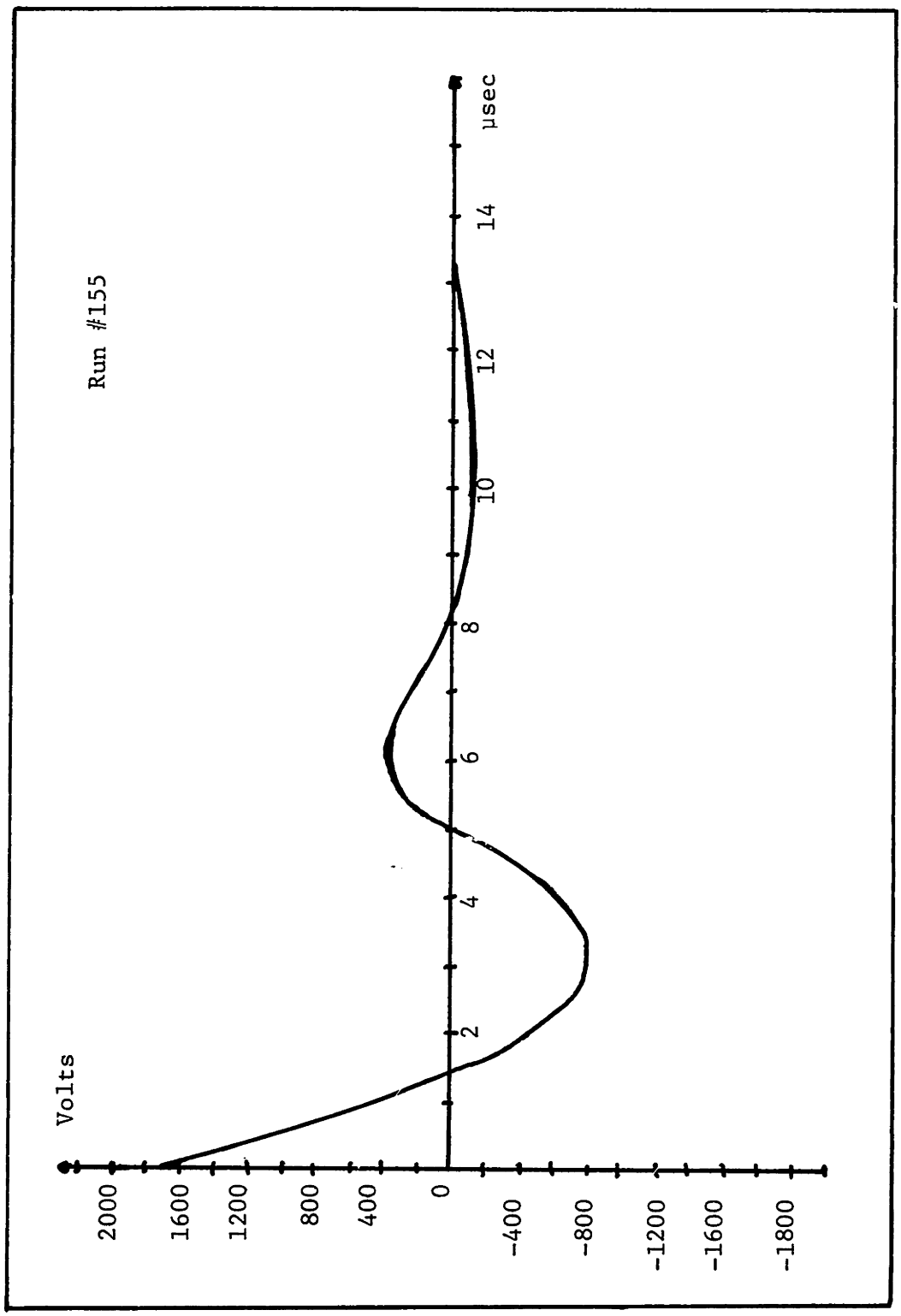

Figure 11--Discharge Waveform (Low Damping)

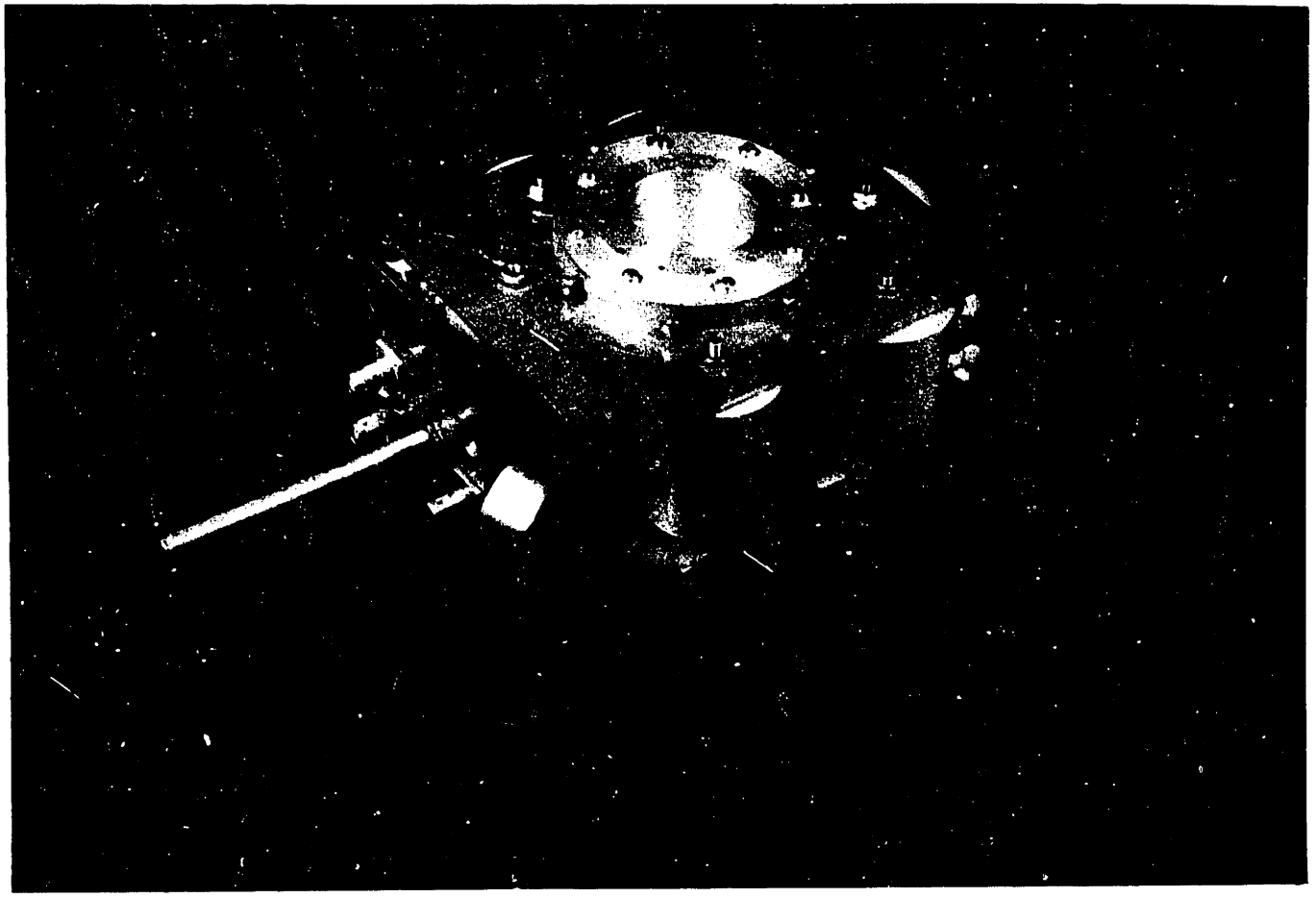

FIGURE 12: SLANT VIEW OF TEST THRUSTER---RECTANGULAR CONFIGURATION

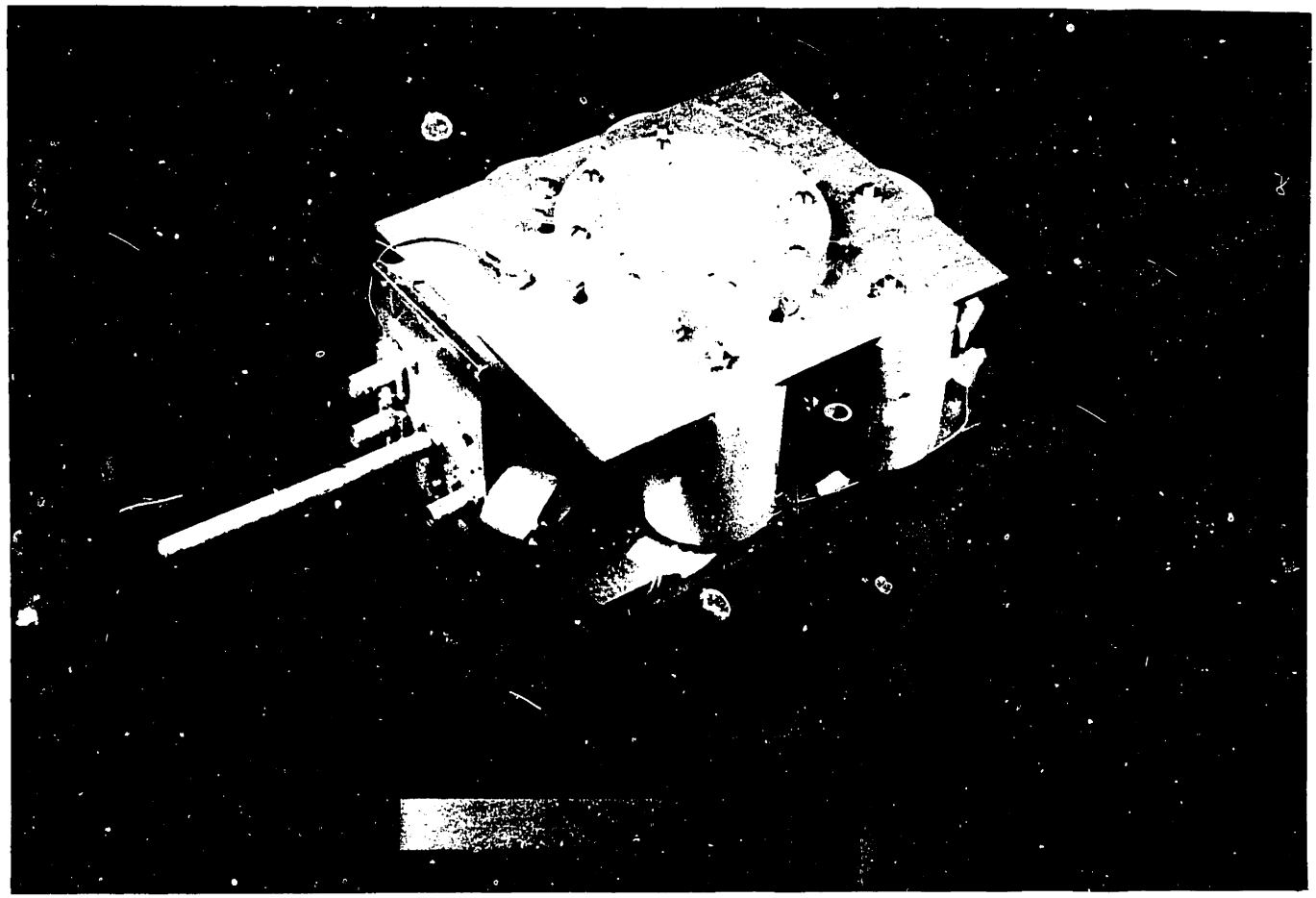

FIGURE 12: SLANT VIEW OF TEST THRUSTER---RECTANGULAR CONFIGURATION

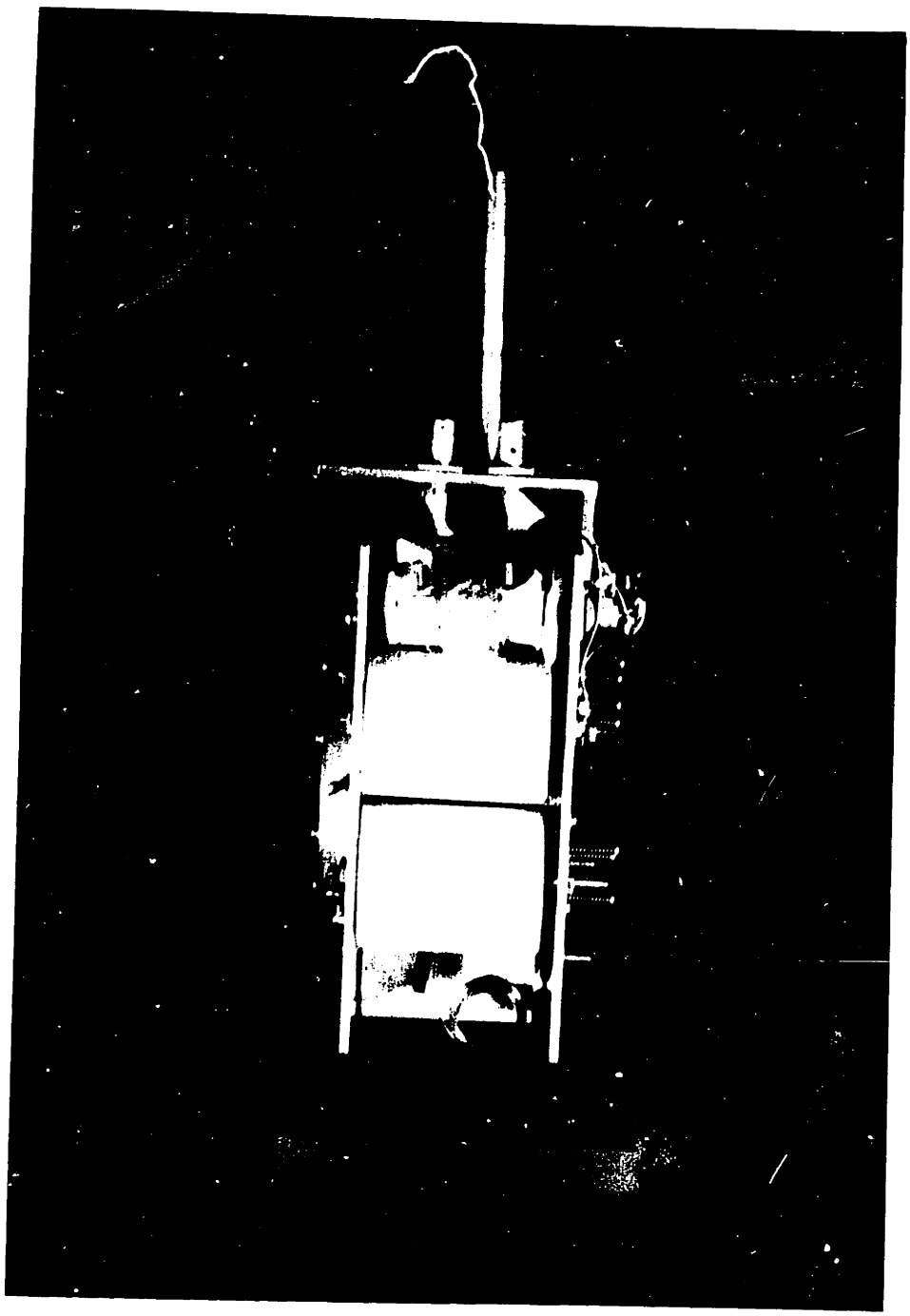

FIGURE 13: SIDE VIEW OF TEST THRUSTER---RECTANGULAR CONFIGURATION

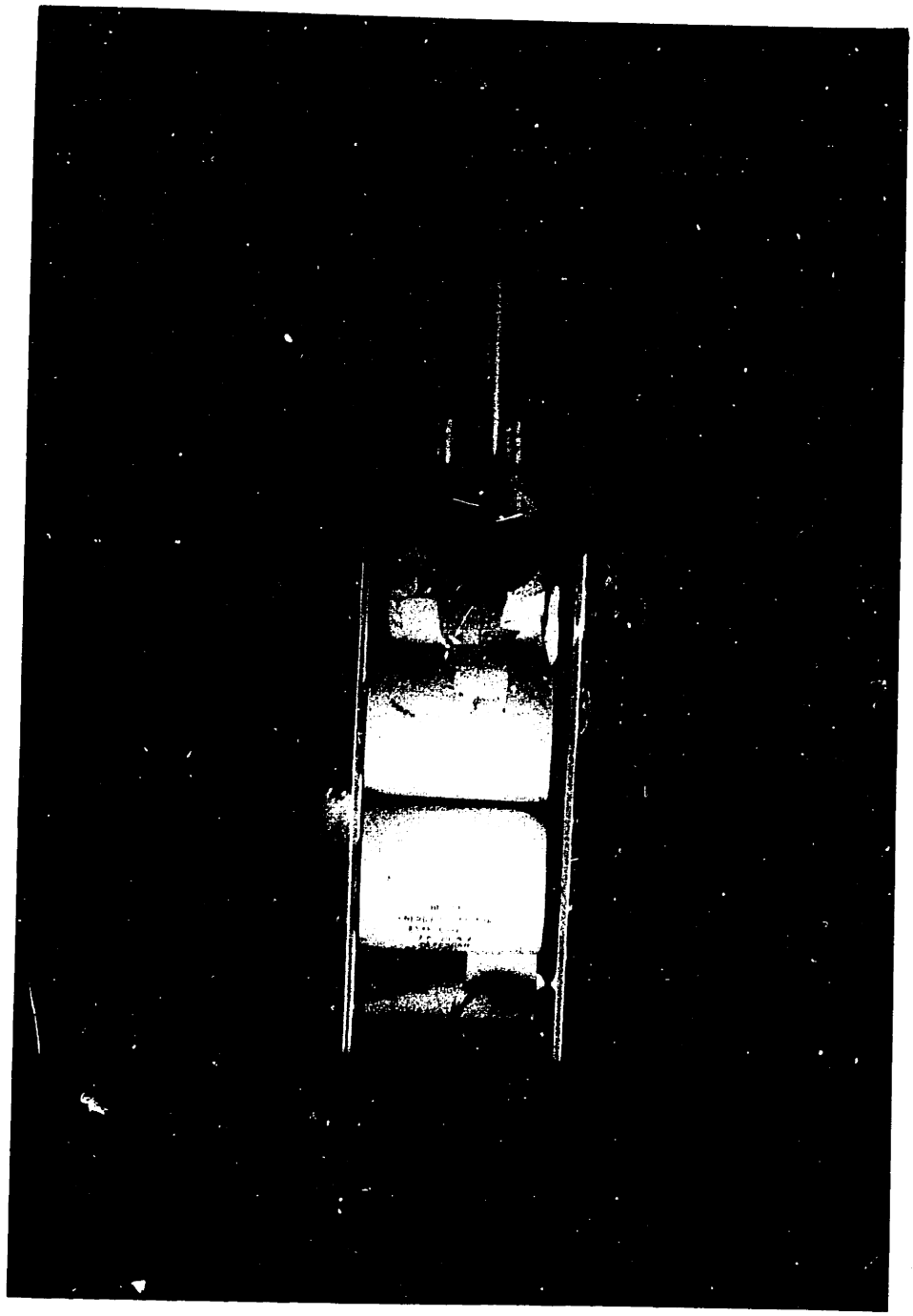

FIGURE 13: SIDE VIEW OF TEST THRUSTER---RECTANGULAR CONFIGURATION

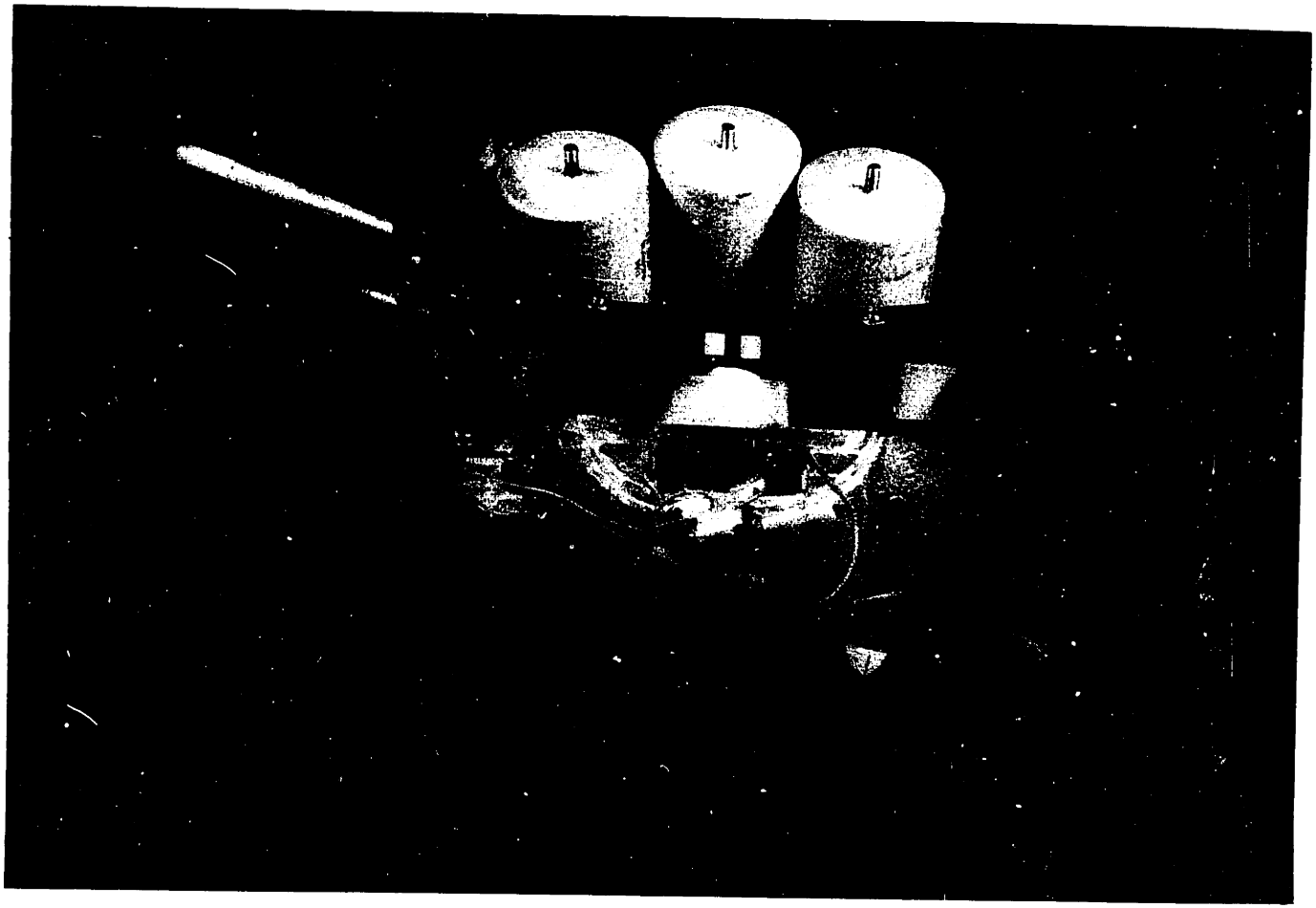

FIGURE 14: RECTANGULAR TEST THRUSTER DISASSEMBLED TO SHOW COMPONENT PLACEMENT

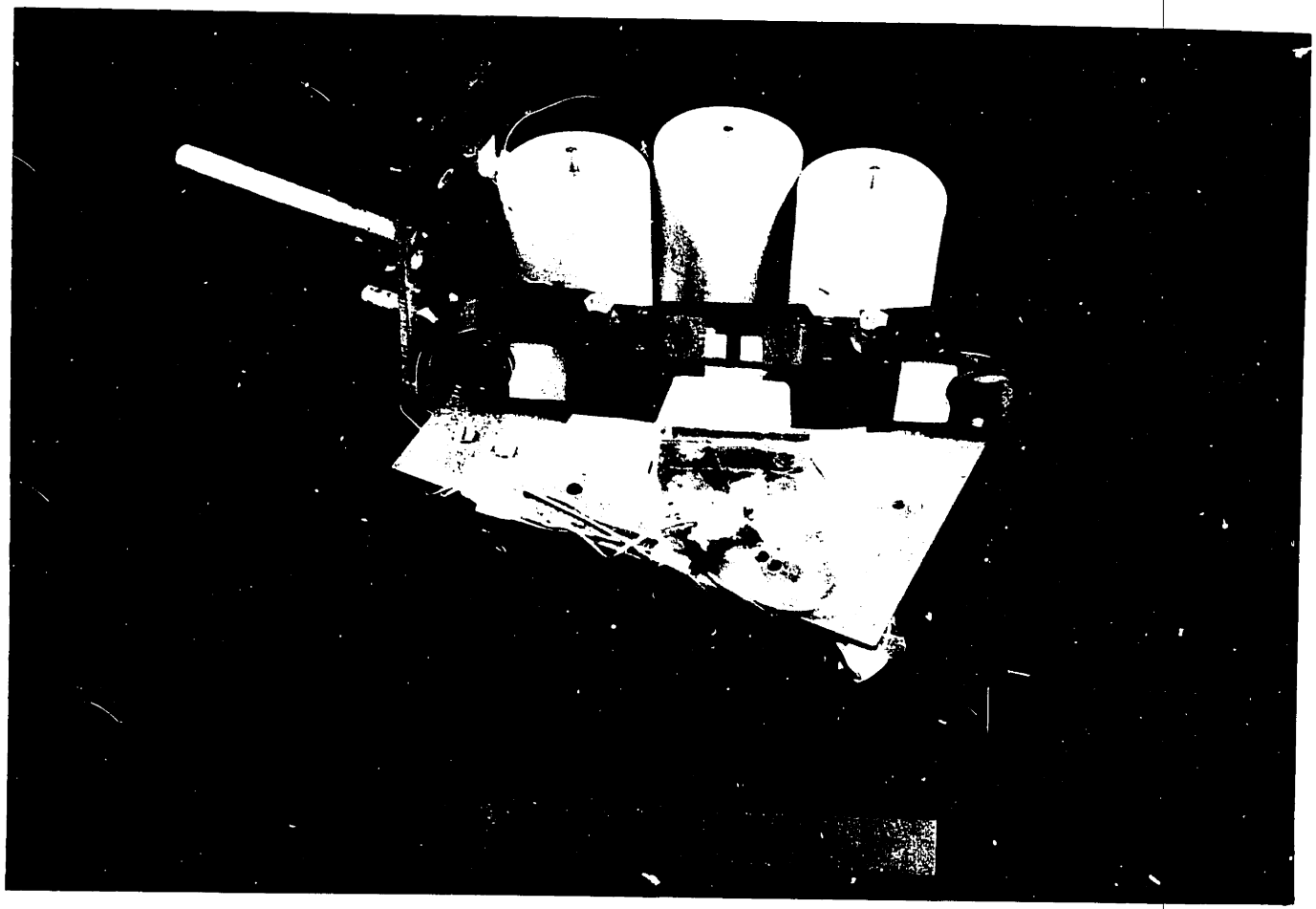

FIGURE 14: RECTANGULAR TEST THRUSTER DISASSEMBLED TO SHOW COMPONENT PLACEMENT

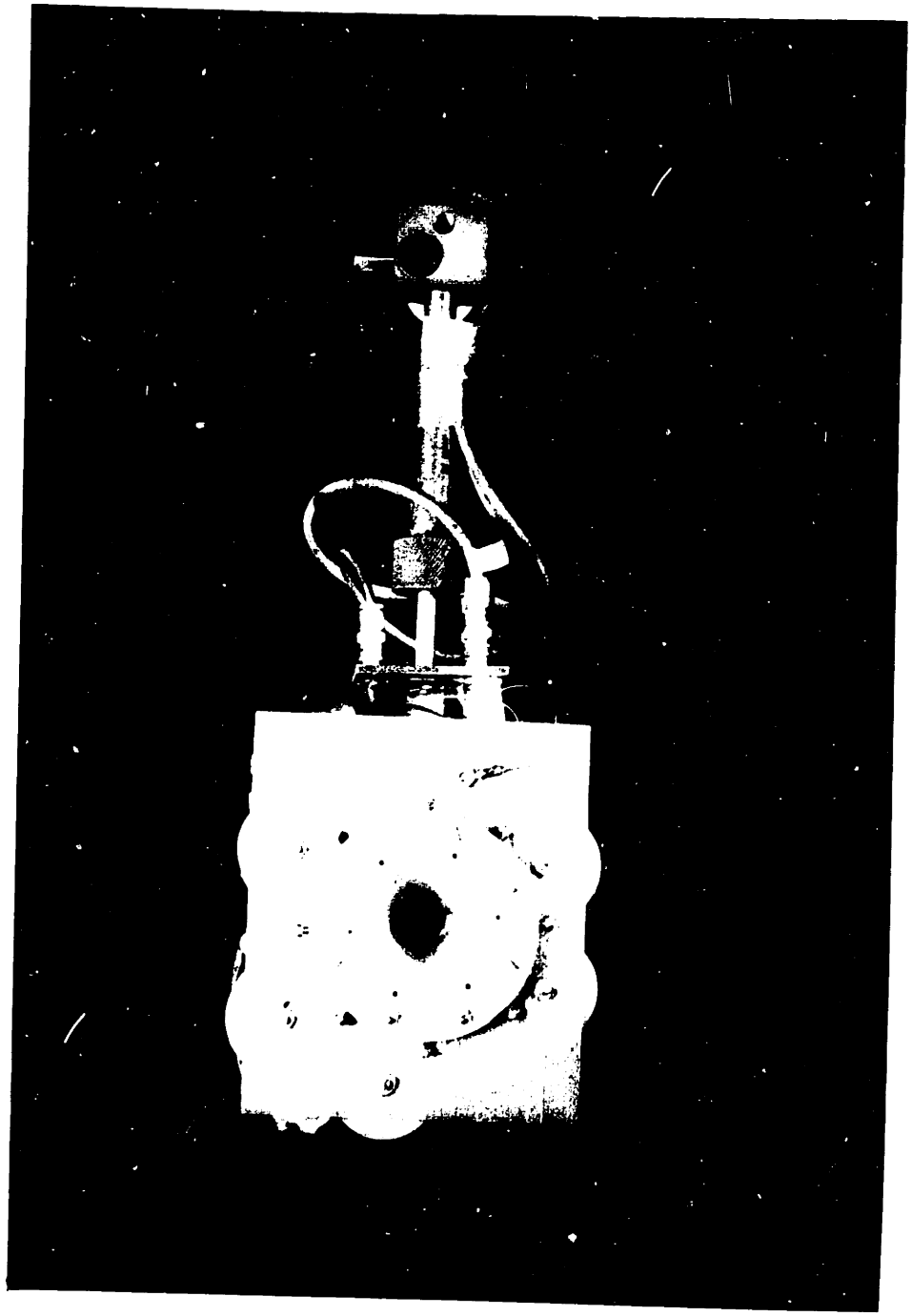

FIGURE 15: THRUSTER ATTACHED TO PENDULUM

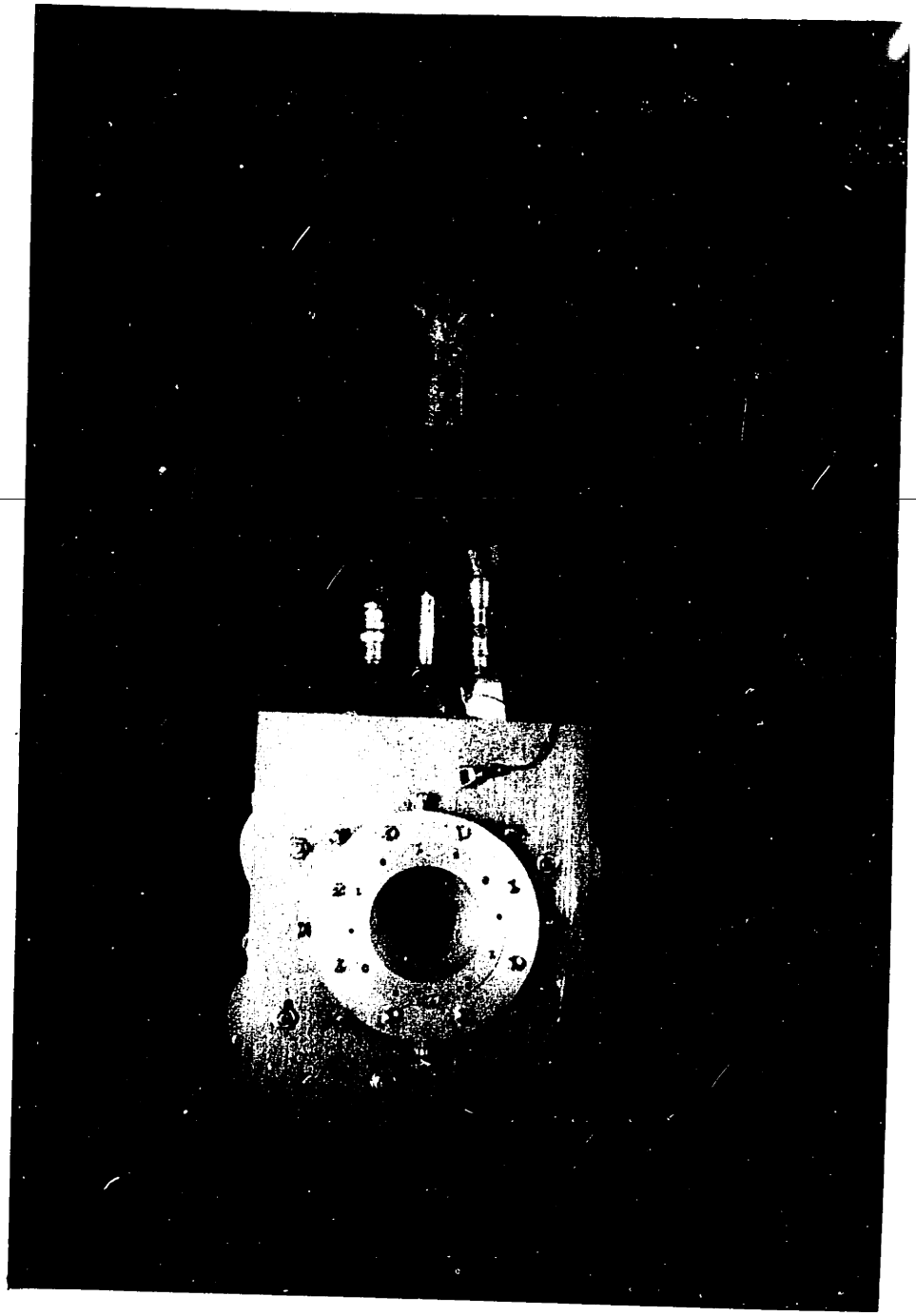

FIGURE 15: THRUSTER ATTACHED TO PENDULUM

FIGURE 16: THRUST STAND--SHOWING THRUSTER MOUNTED ON PENDULUM RESTING ON CRADLES

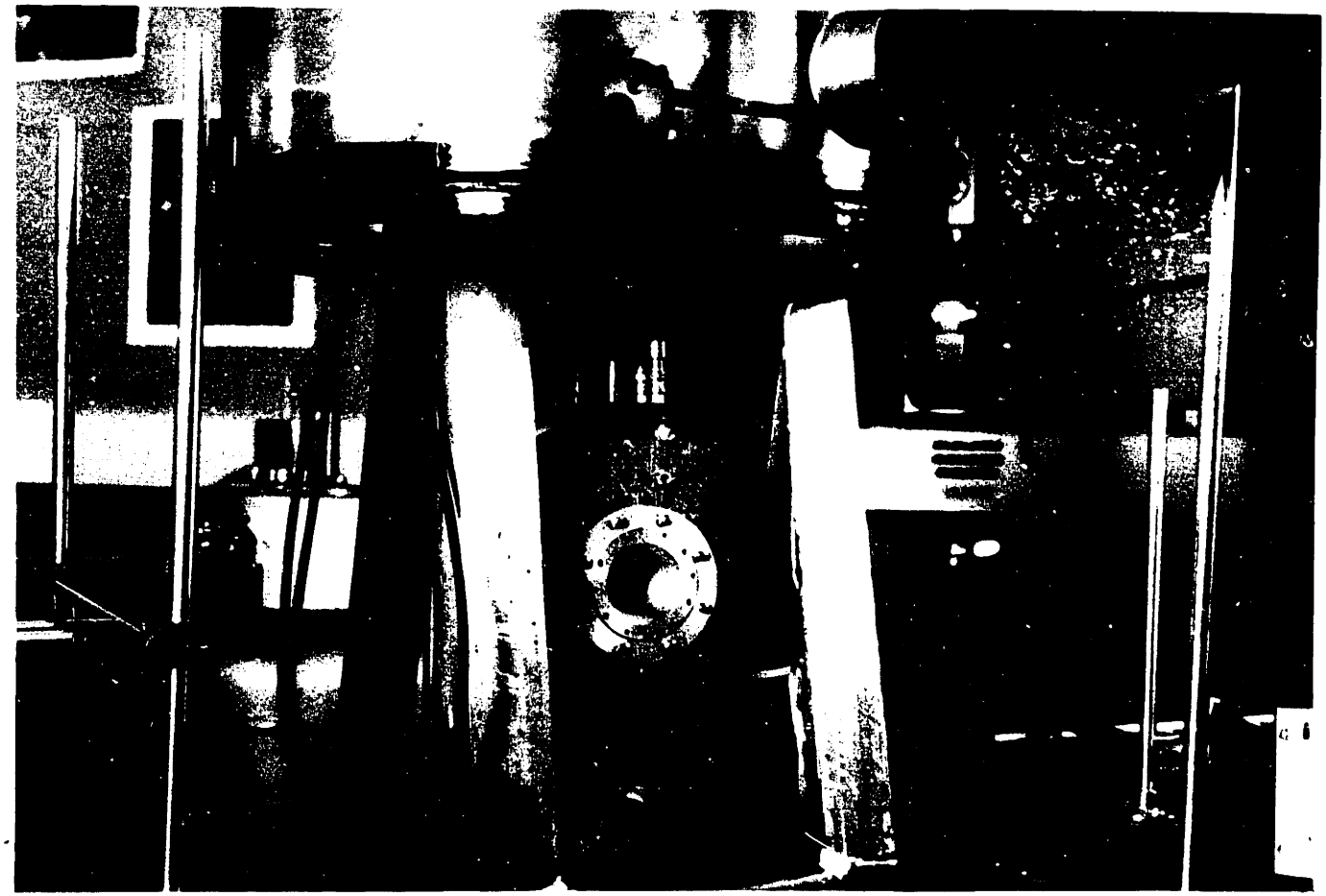

FIGURE 16: THRUST STAND--SHOWING THRUSTER MOUNTED ON PENDULUM RESTING ON CRADLES

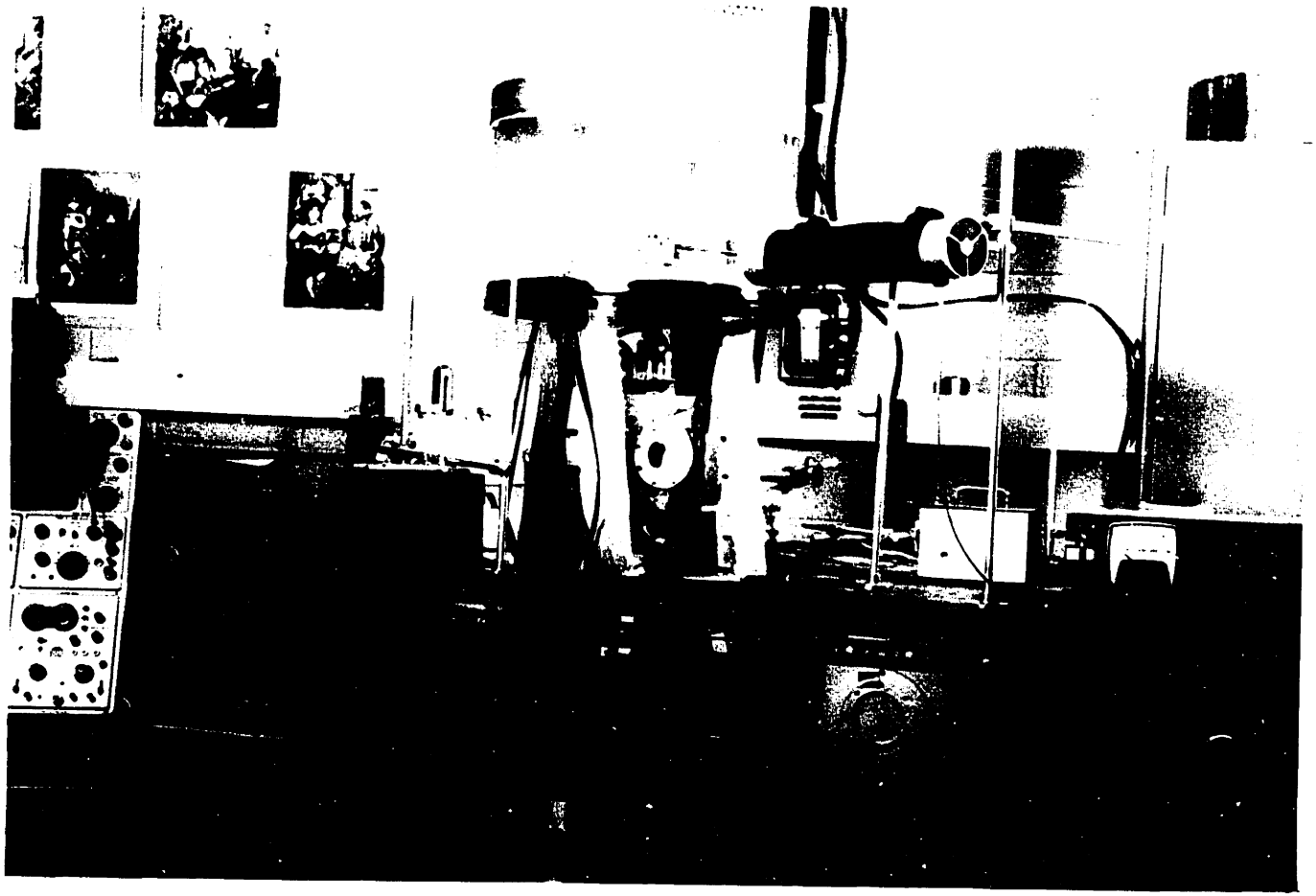

FIGURE 17: THRUST STAND--SHOWING LASER-MIRROR ARRANGEMENT

FIGURE 17: THRUST STAND--SHOWING LASER-MIRROR ARRANGEMENT

FIGURE 18: THRUST STAND/VACUUM SYSTEM--SHOWING METER STICK --LASER--ARRANGEMENT

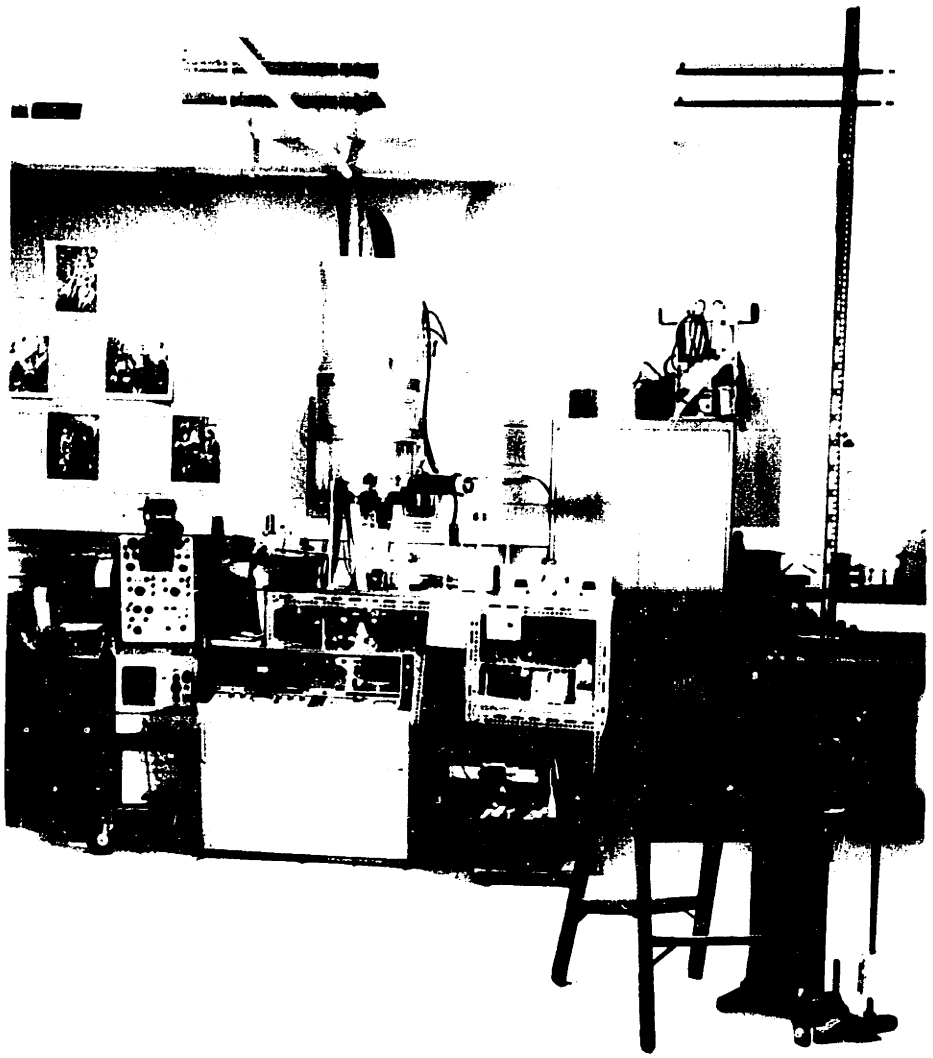

FIGURE 18: THRUST STAND/VACUUM SYSTEM--SHOWING METER STICK --LASER--ARRANGEMENT

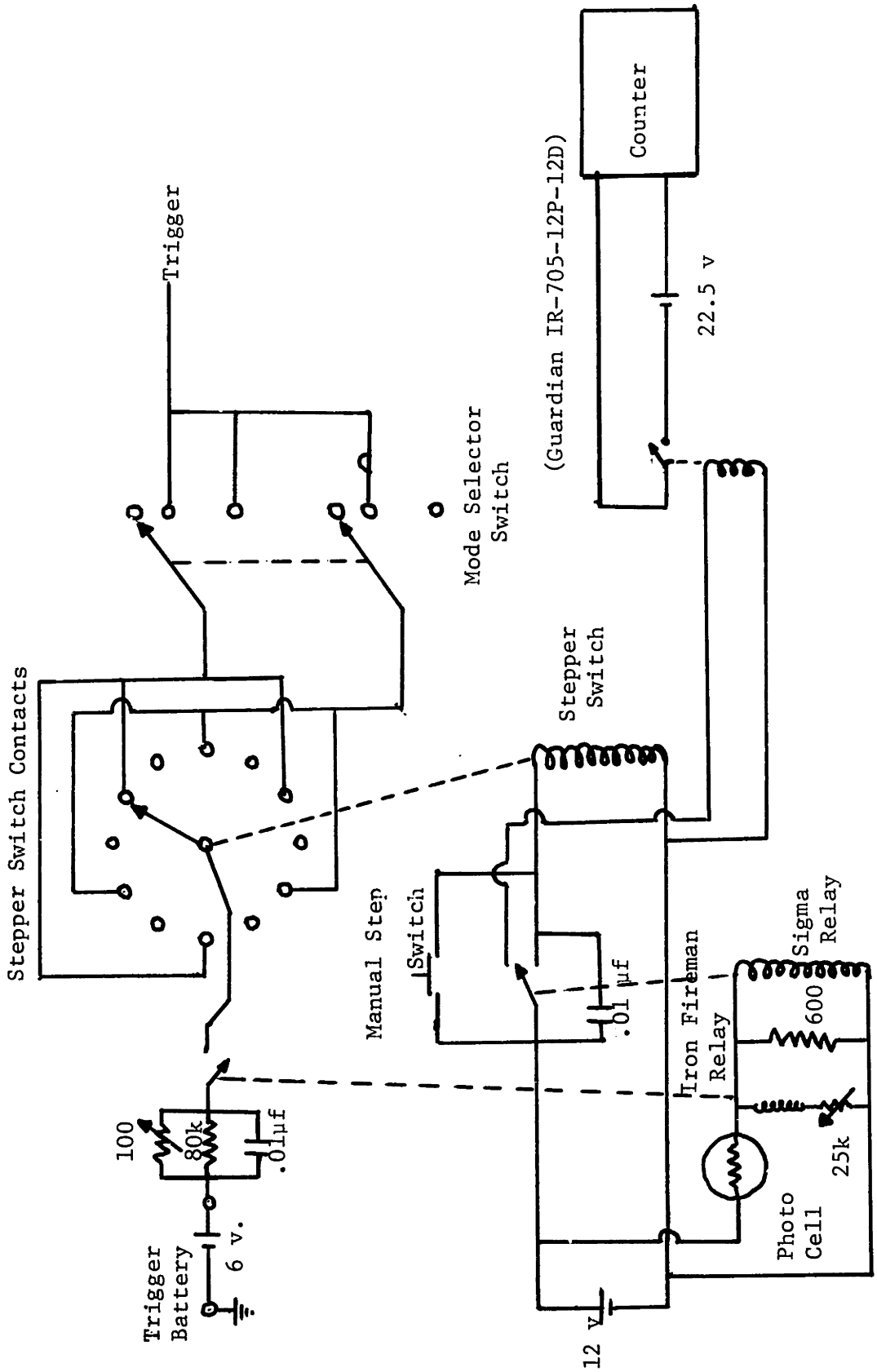

Figure 19--TRIGGERING CIRCUIT SCHEMATIC

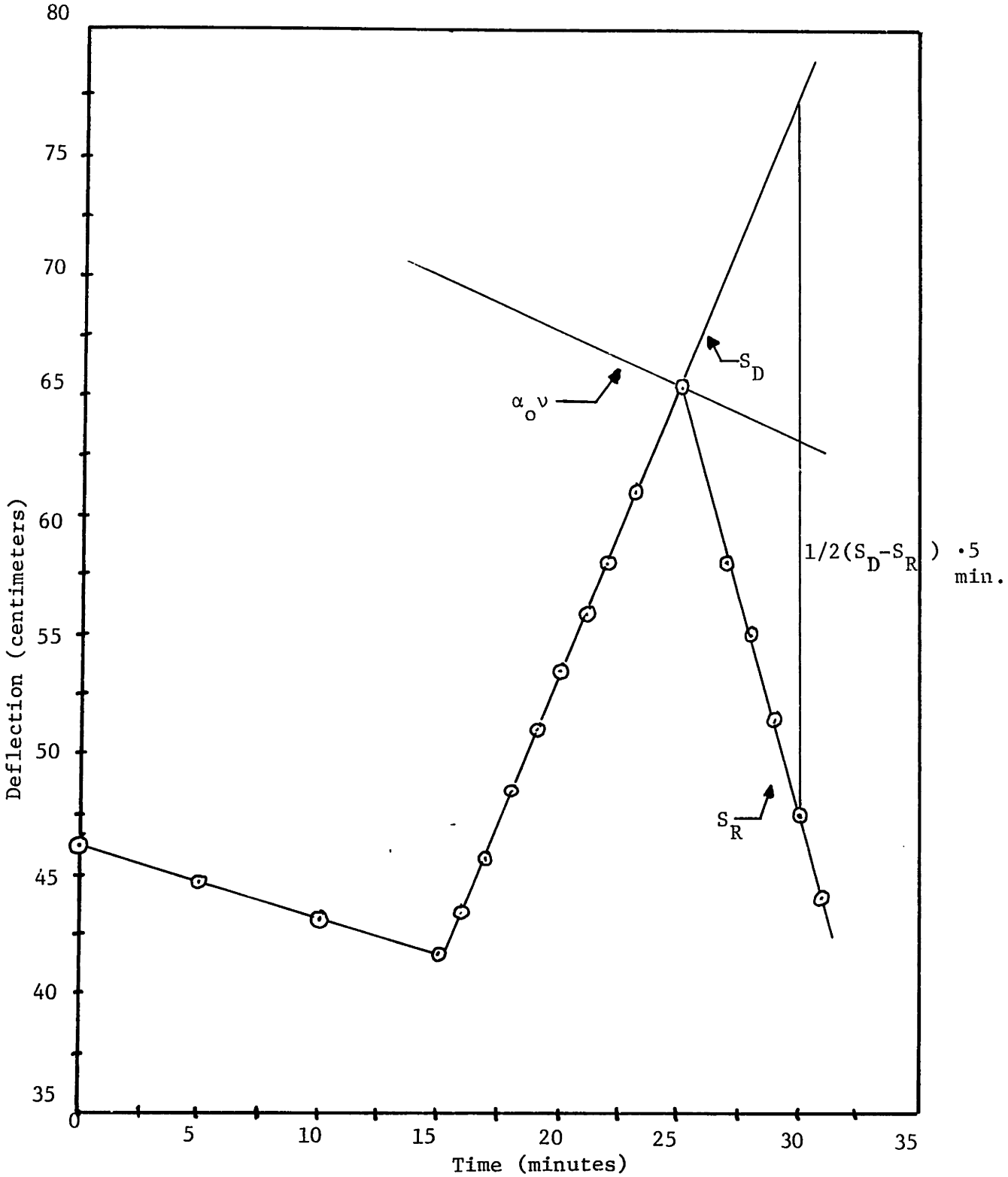

Figure 20--METER STICK READING VS. TIME

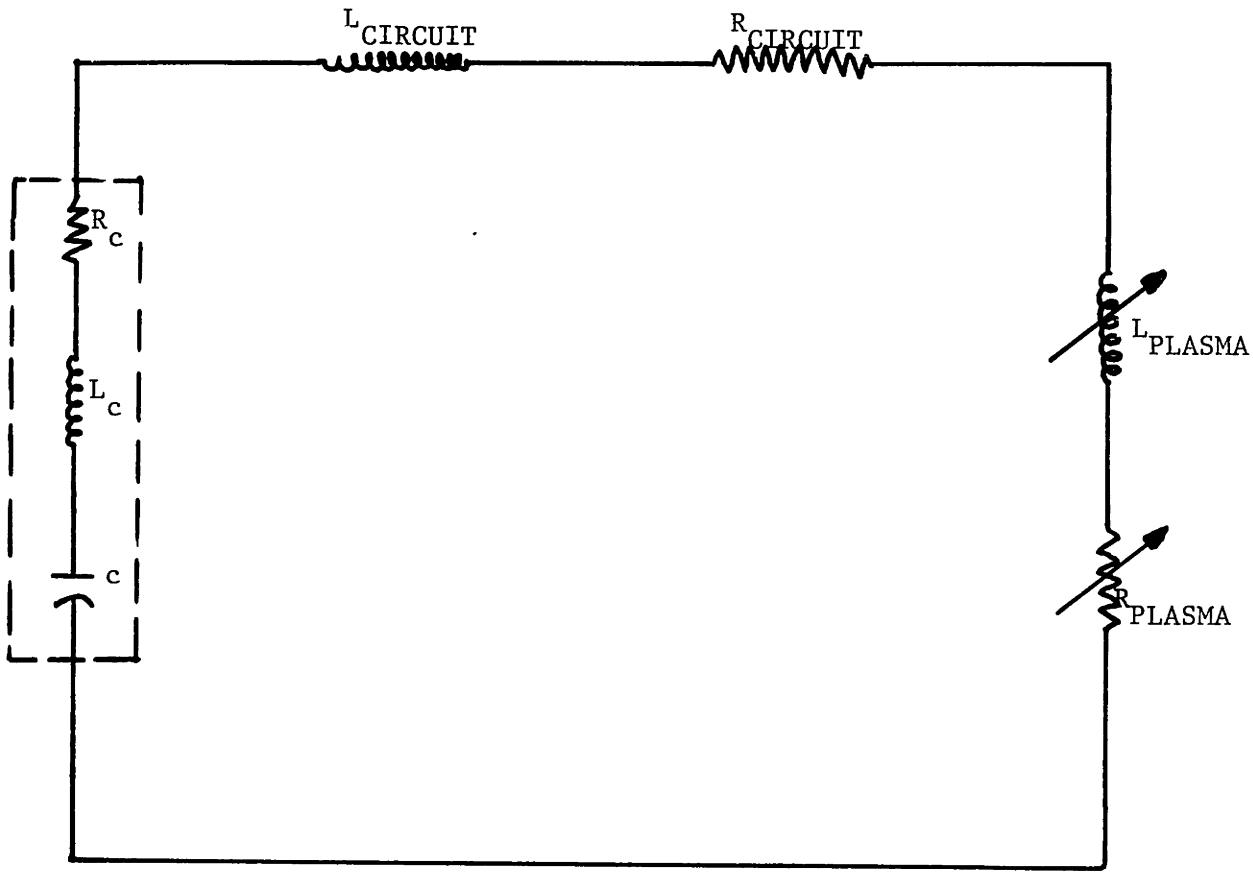

$$V_m(t) = V_c(t) - i(t) \cdot R_c - L_c \, di/dt$$

where: $V_c(t) = L \, di/dt + iR$

with: $L = L_c + L_{circuit} + L_{plasma}$

$$R = R_c + R_{circuit} + R_{plasma}$$

Figure 21--RLC REPRESENTATION OF THRUSTER DISCHARGE CIRCUIT

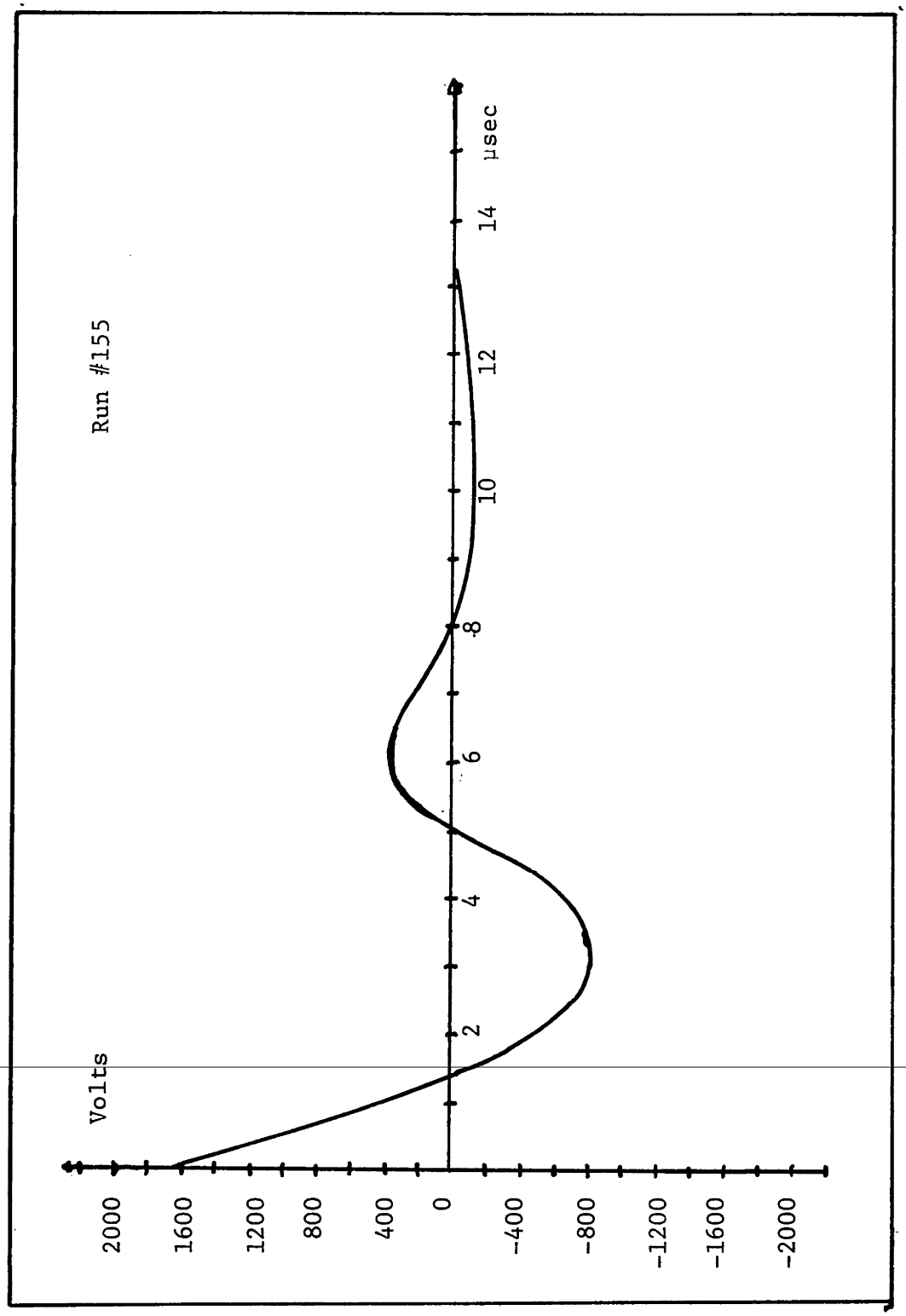

Figure 22--DISCHARGE WAVEFORM (Low Damping)

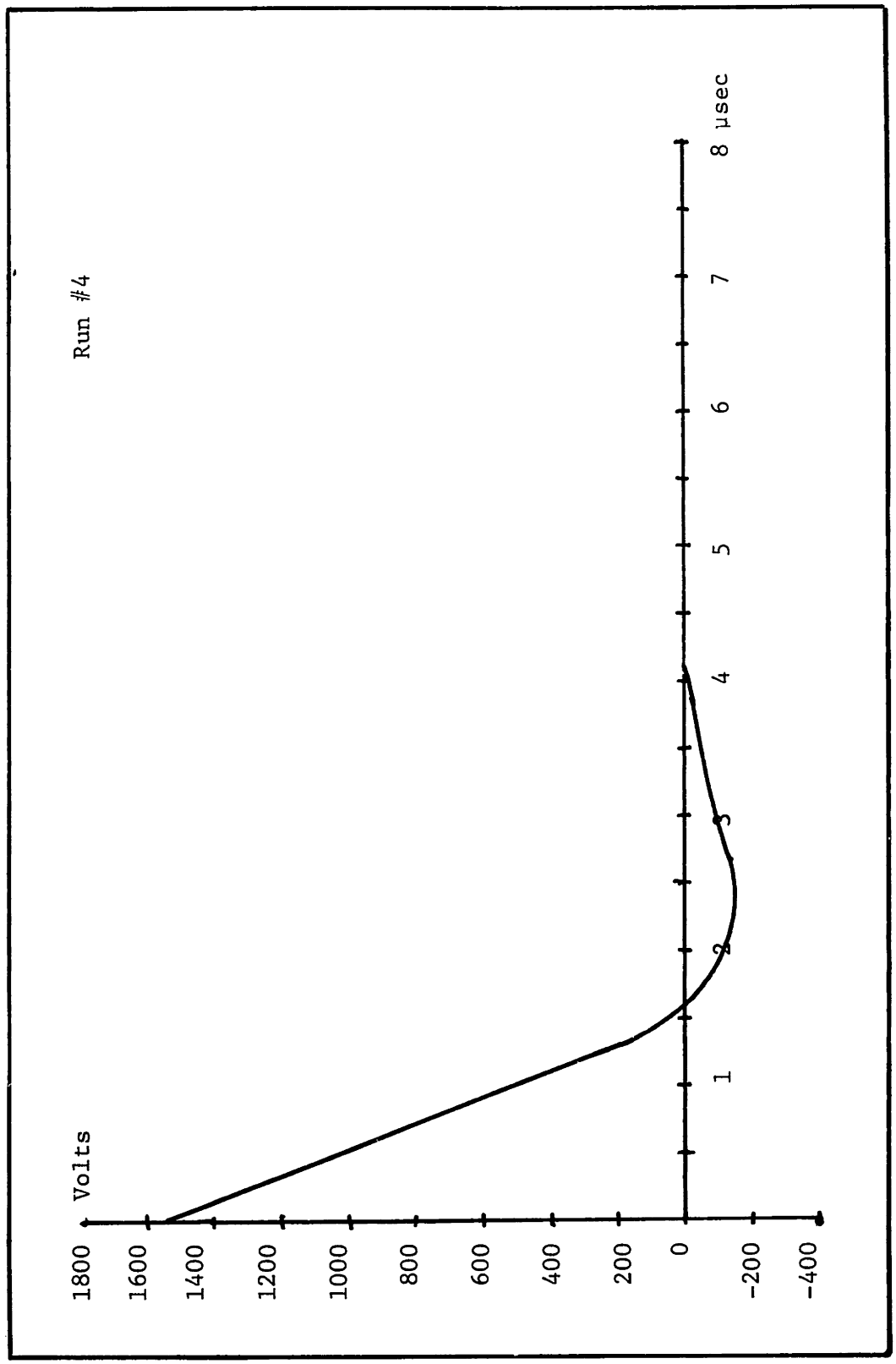

Figure 23--DISCHARGE WAVEFORM (High Damping)

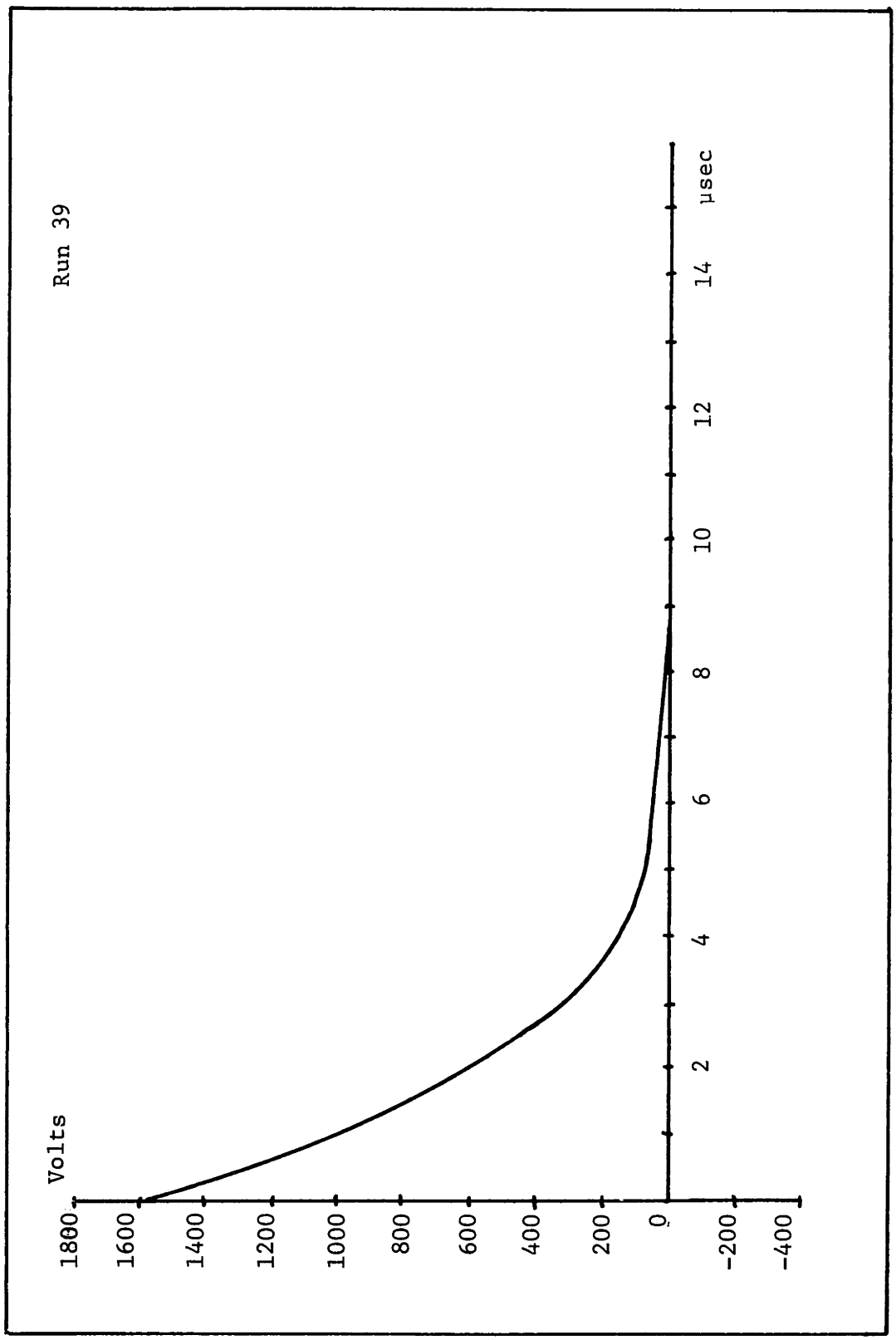

Figure 24--DISCHARGE WAVEFORM (OVERDAMPED)

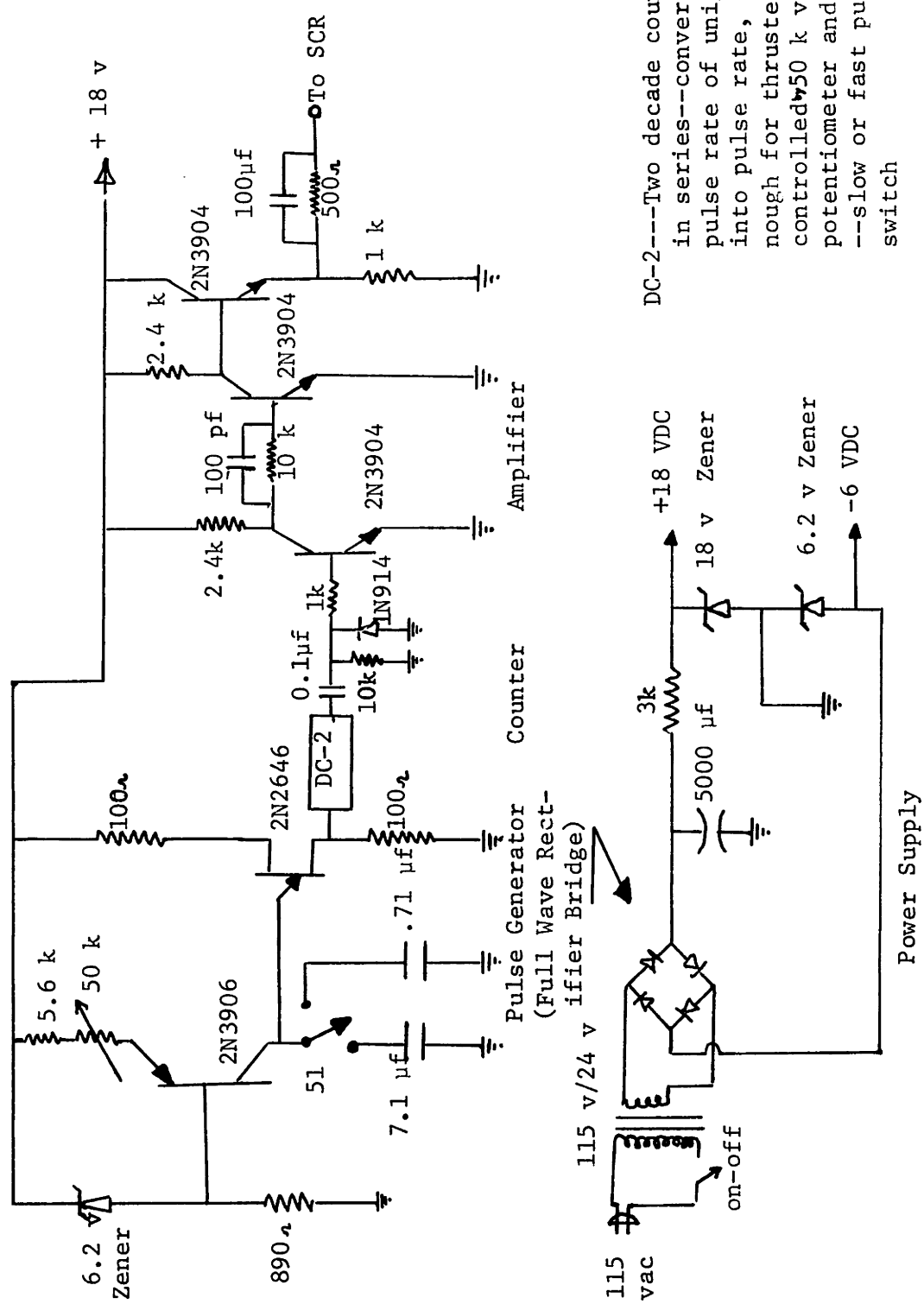

Figure 25--SCHEMATIC OF LIFE TEST TRIGGERING (PULSER) CIRCUIT

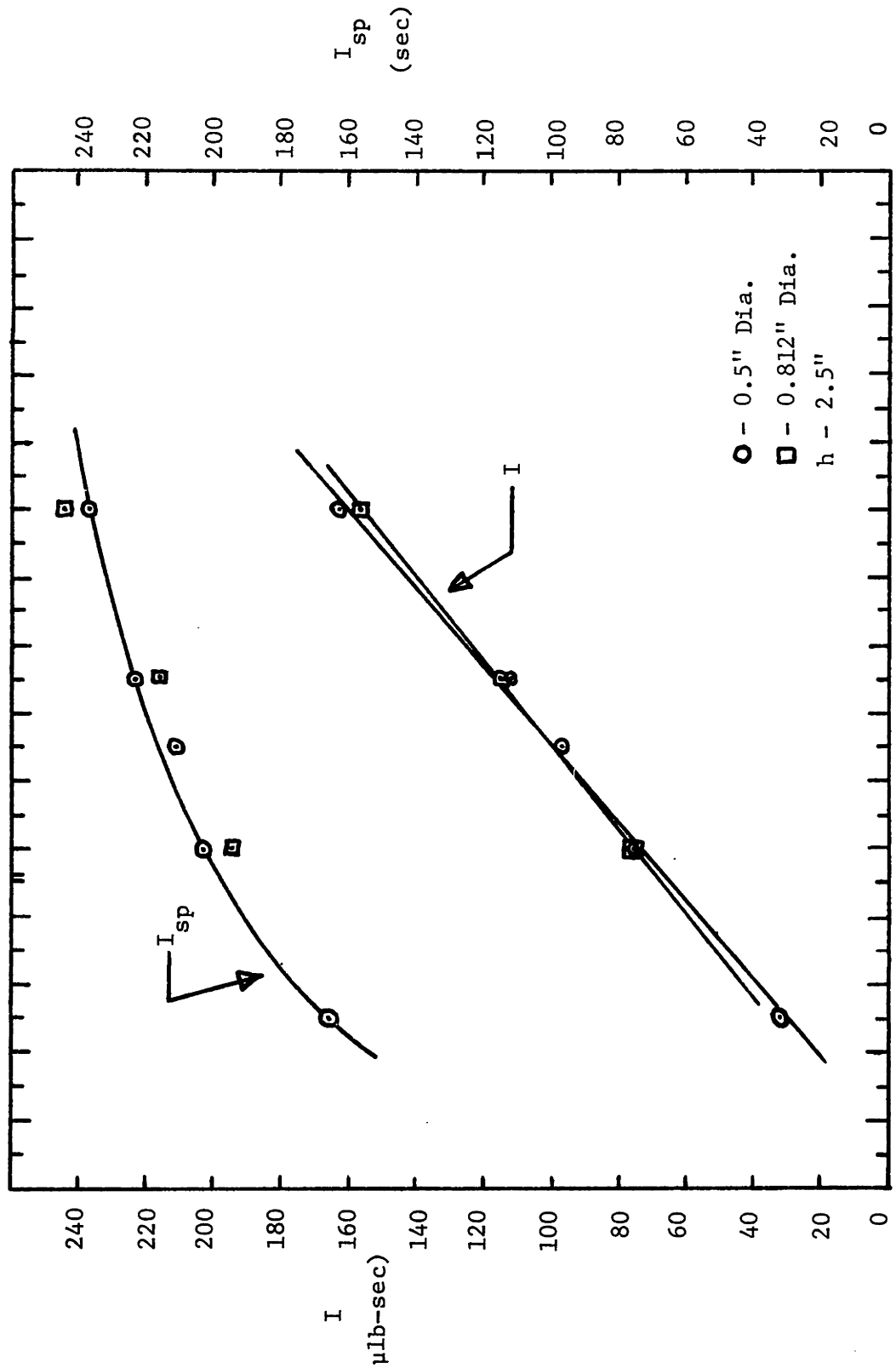

FIGURE 26--IMPULSE BIT AND SPECIFIC IMPULSE VS. DISCHARGE ENERGY

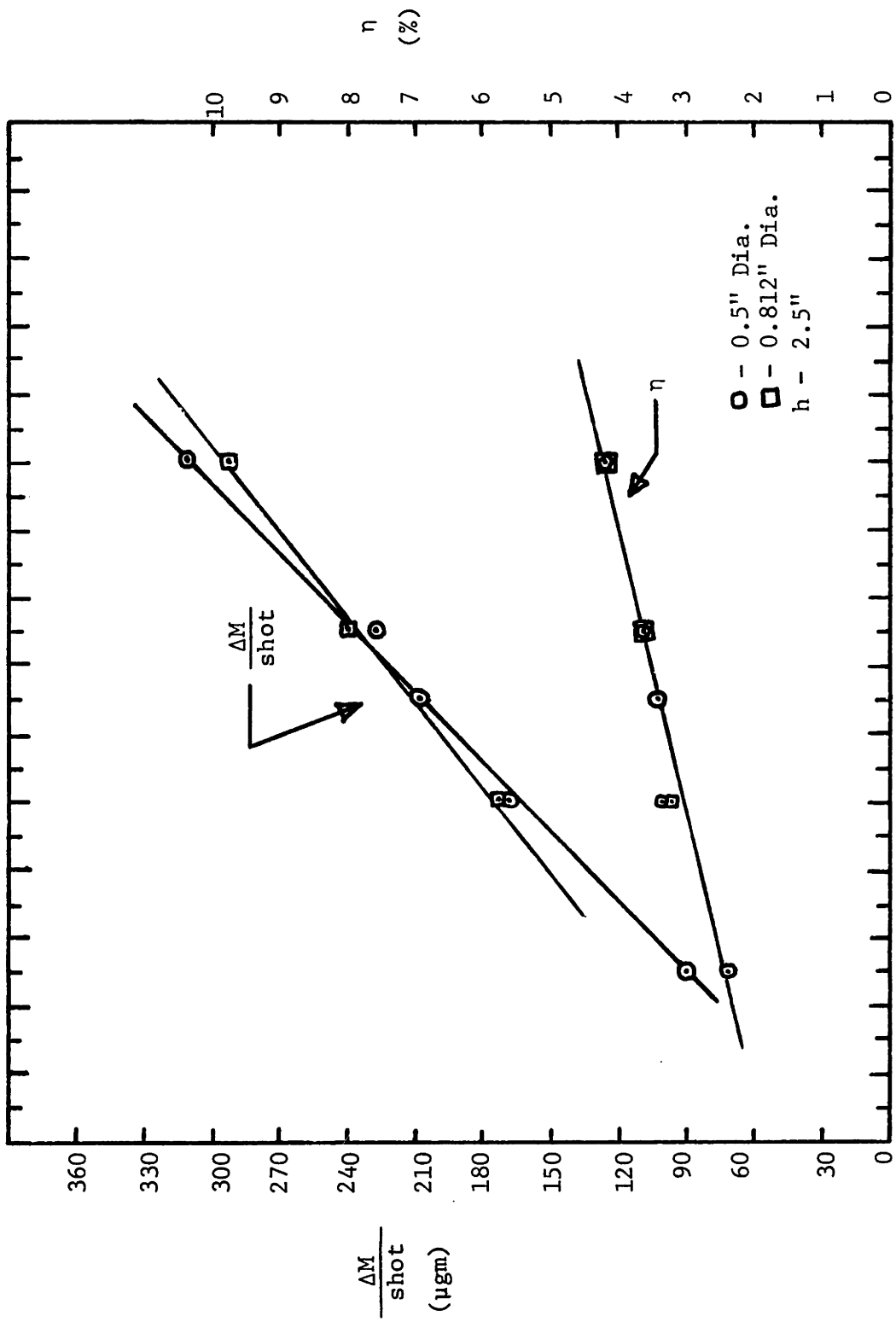

FIGURE 27--MASS ABLATED PER SHOT AND EFFICIENCY VS. DISCHARGE ENERGY

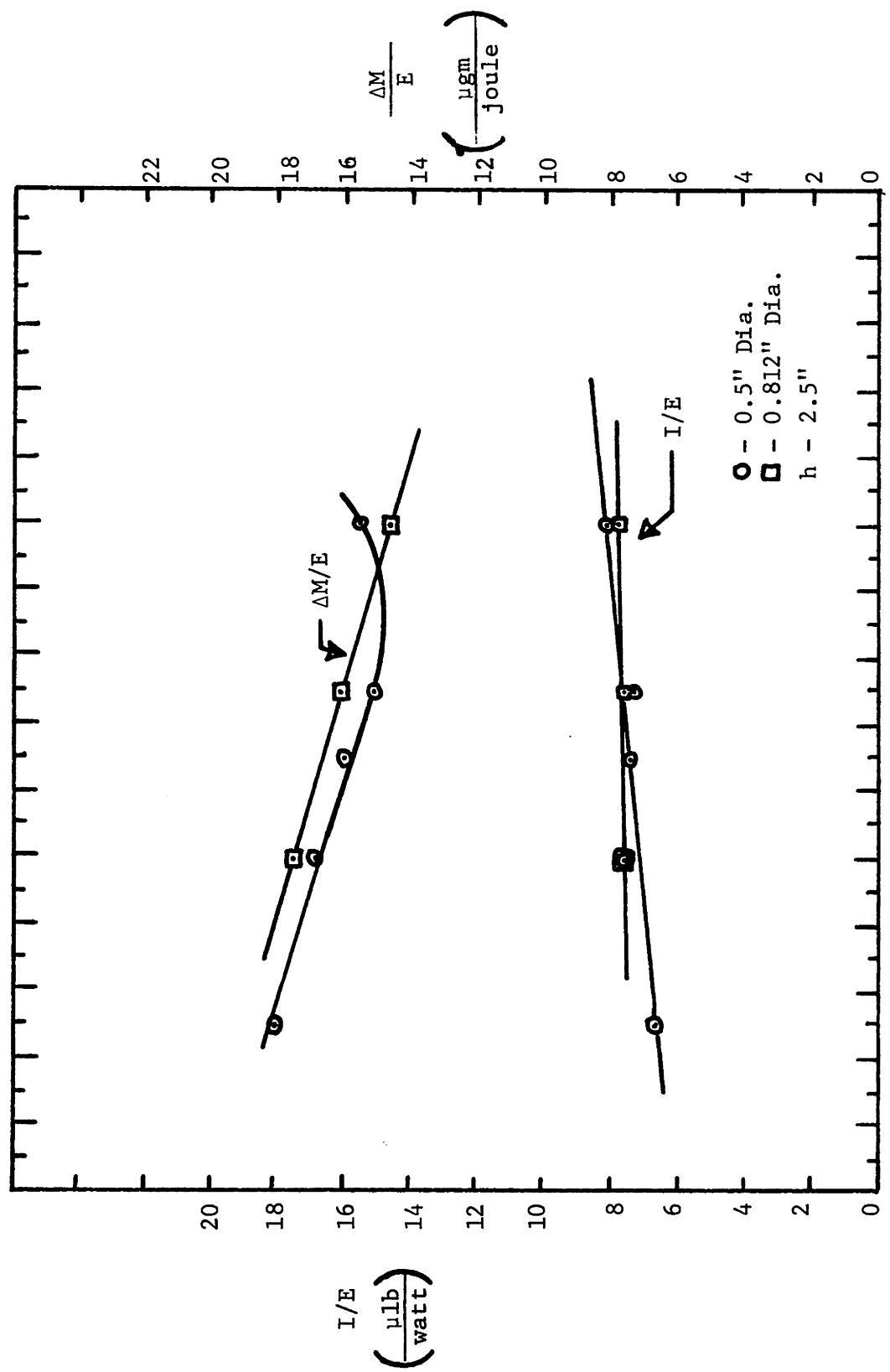

FIGURE 28--SPECIFIC THRUST AND SPECIFIC MASS VS. DISCHARGE ENERGY

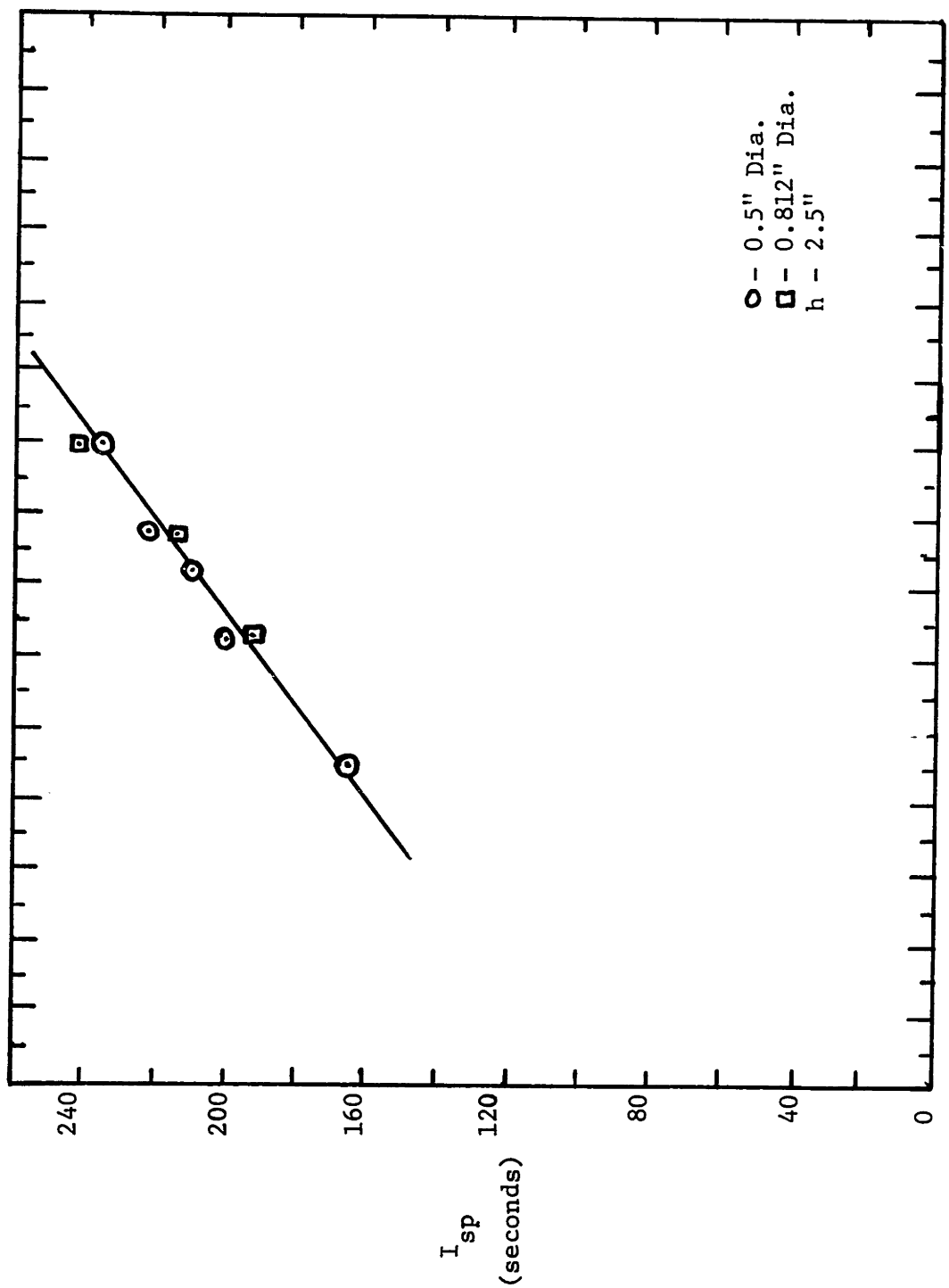

FIGURE 29--SPECIFIC IMPULSE VS. (DISCHARGE ENERGY)$^{1/2}$

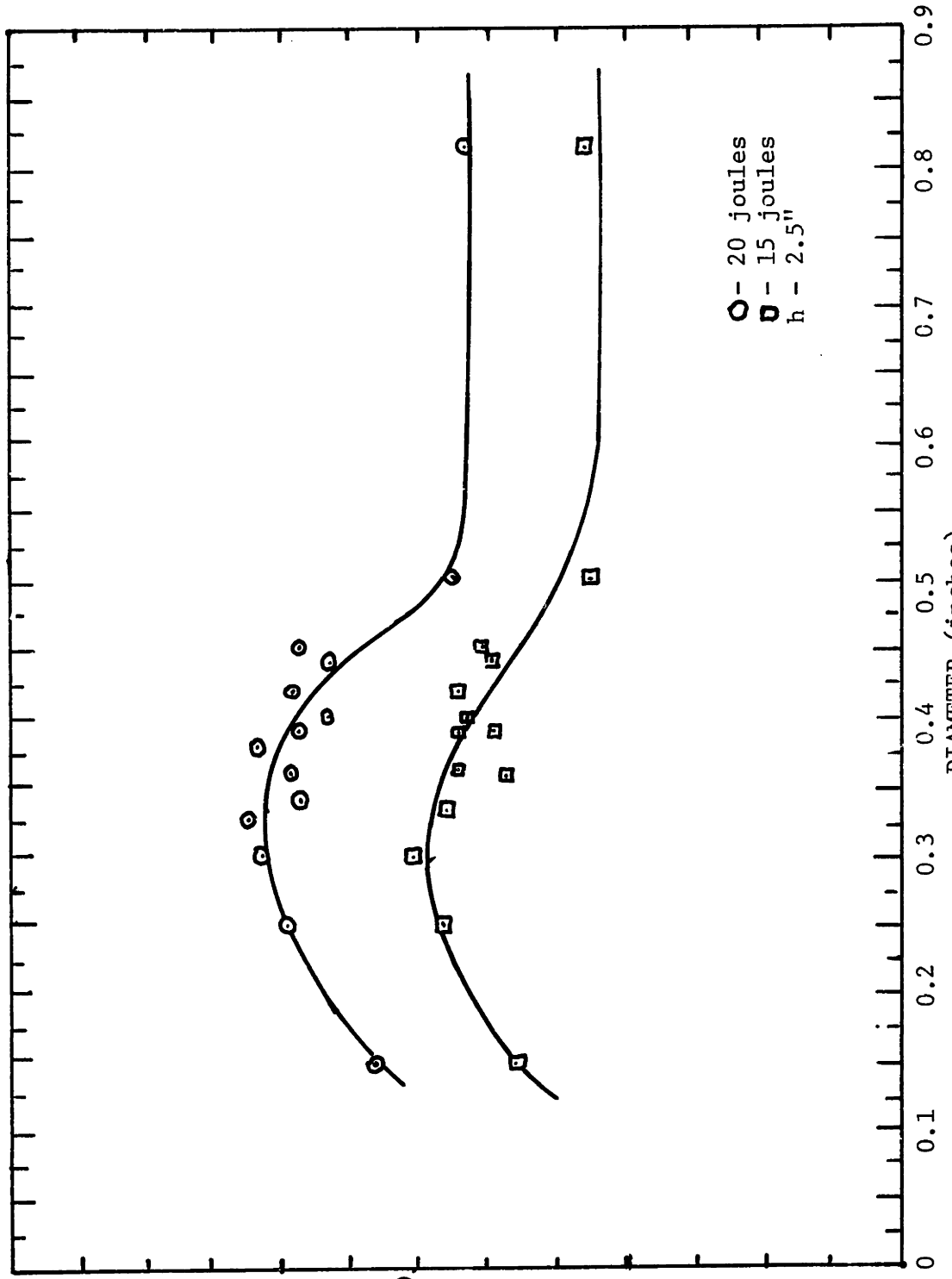

FIGURE 30--IMPULSE BIT VS. CHAMBER DIAMETER

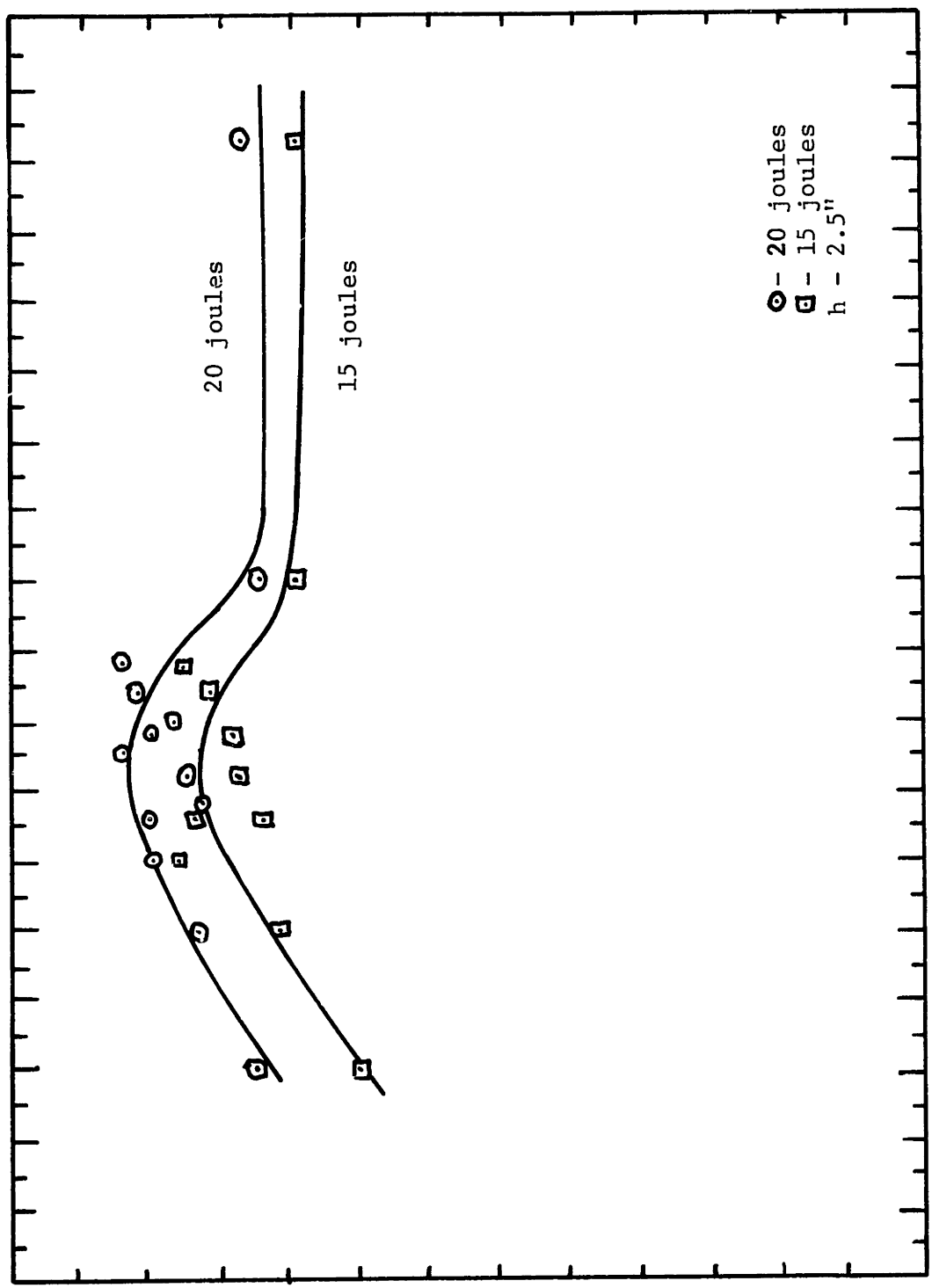

Figure 31--SPECIFIC IMPULSE VS CHAMBER DIAMETER

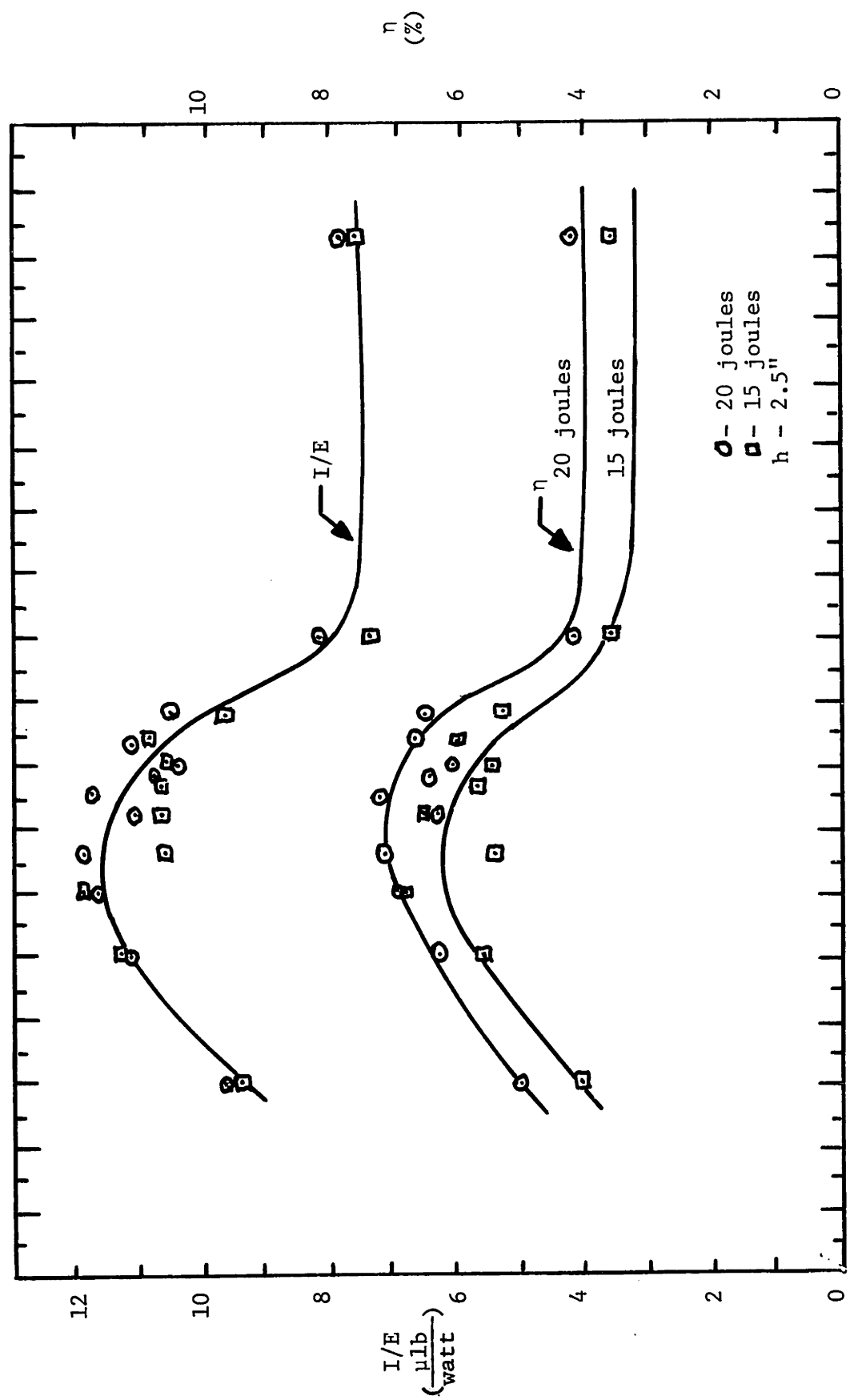

Figure 32--SPECIFIC THRUST AND EFFICIENCY VS. CHAMBER DIAMETER

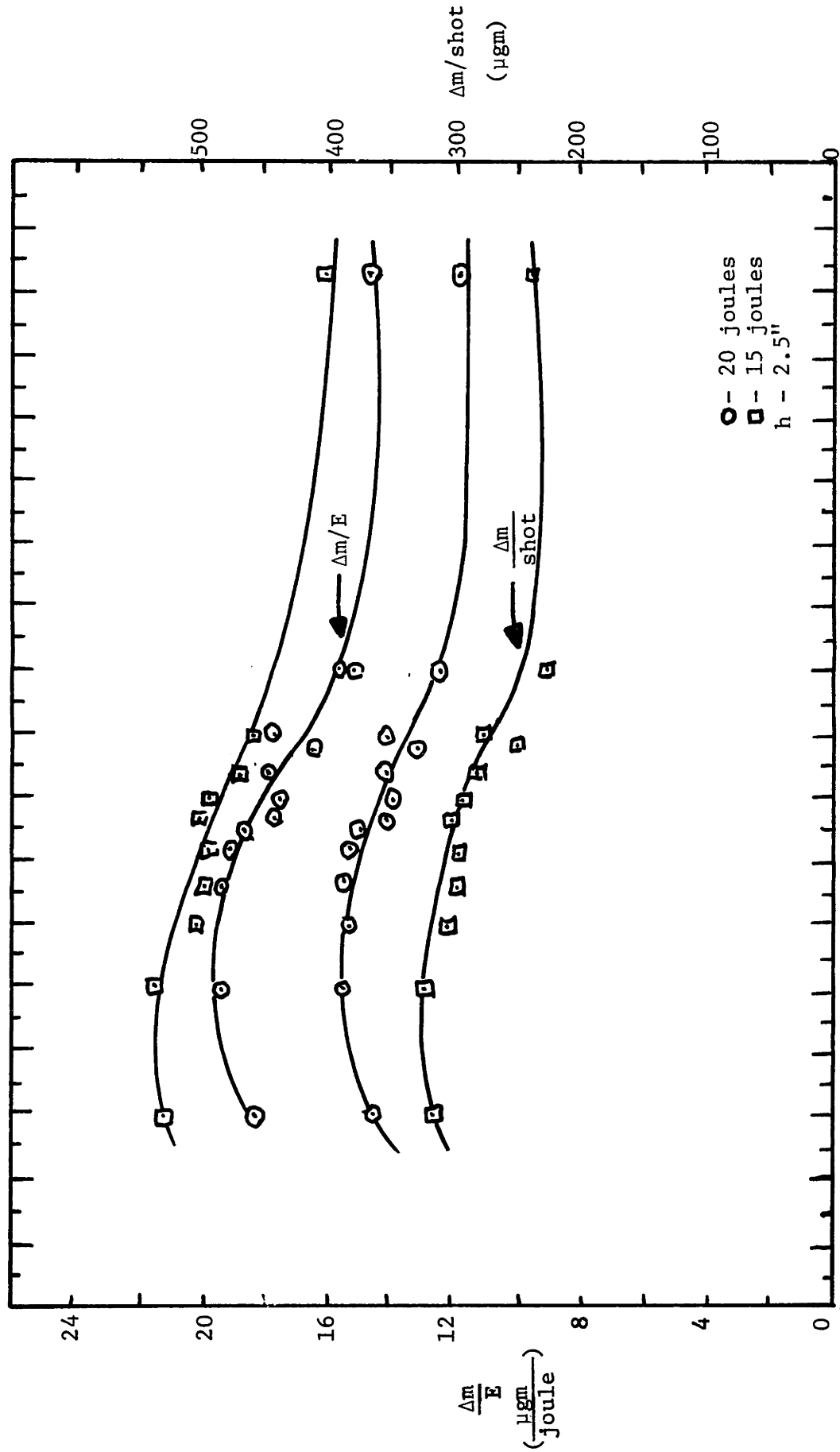

Figure 33--MASS ABLATED/SHOT AND SPECIFIC MASS ABLATED/SHOT VS. CHAMBER DIAMETER

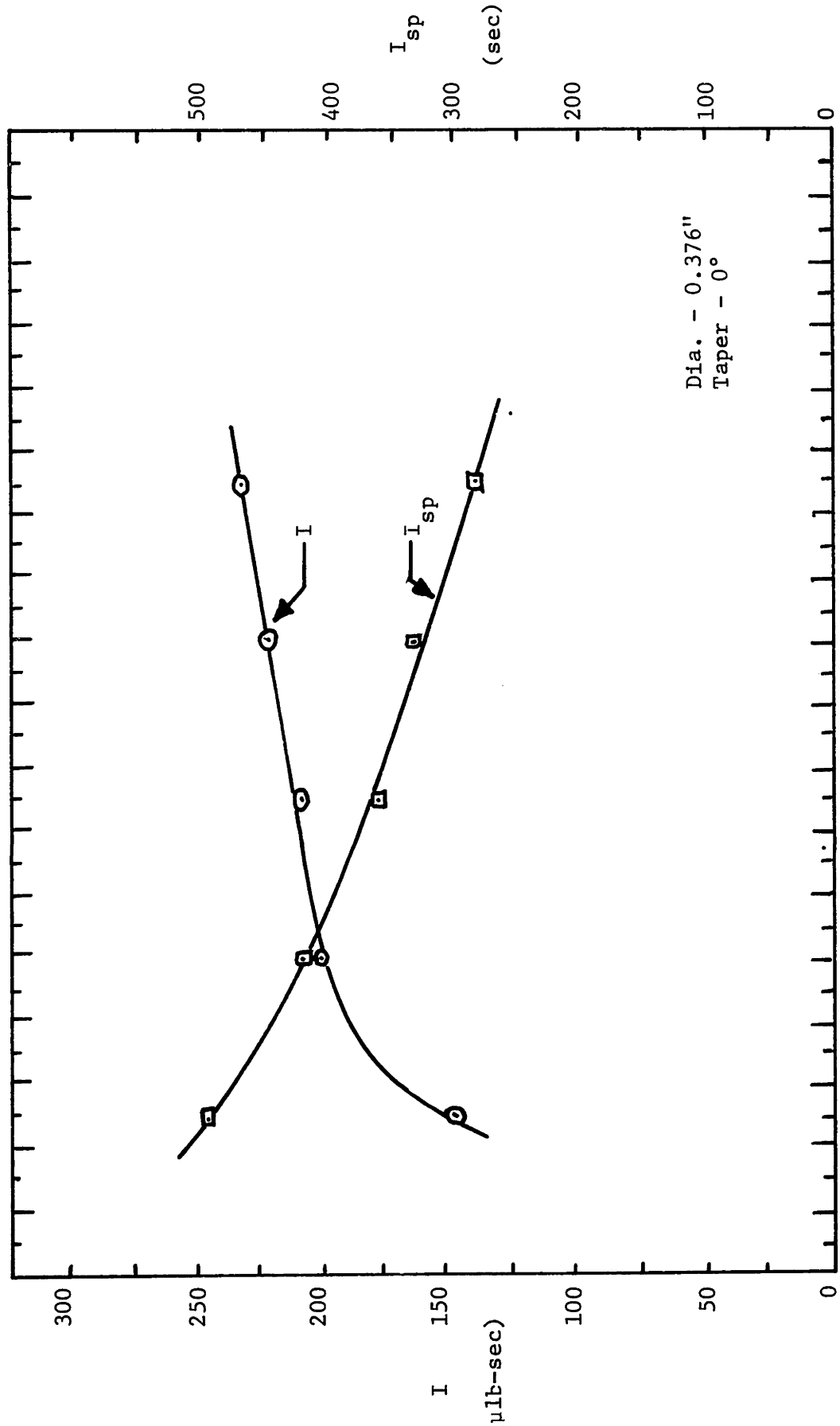

Figure 34--IMPULSE AND SPECIFIC IMPULSE VS. LENGTH OF CHAMBER

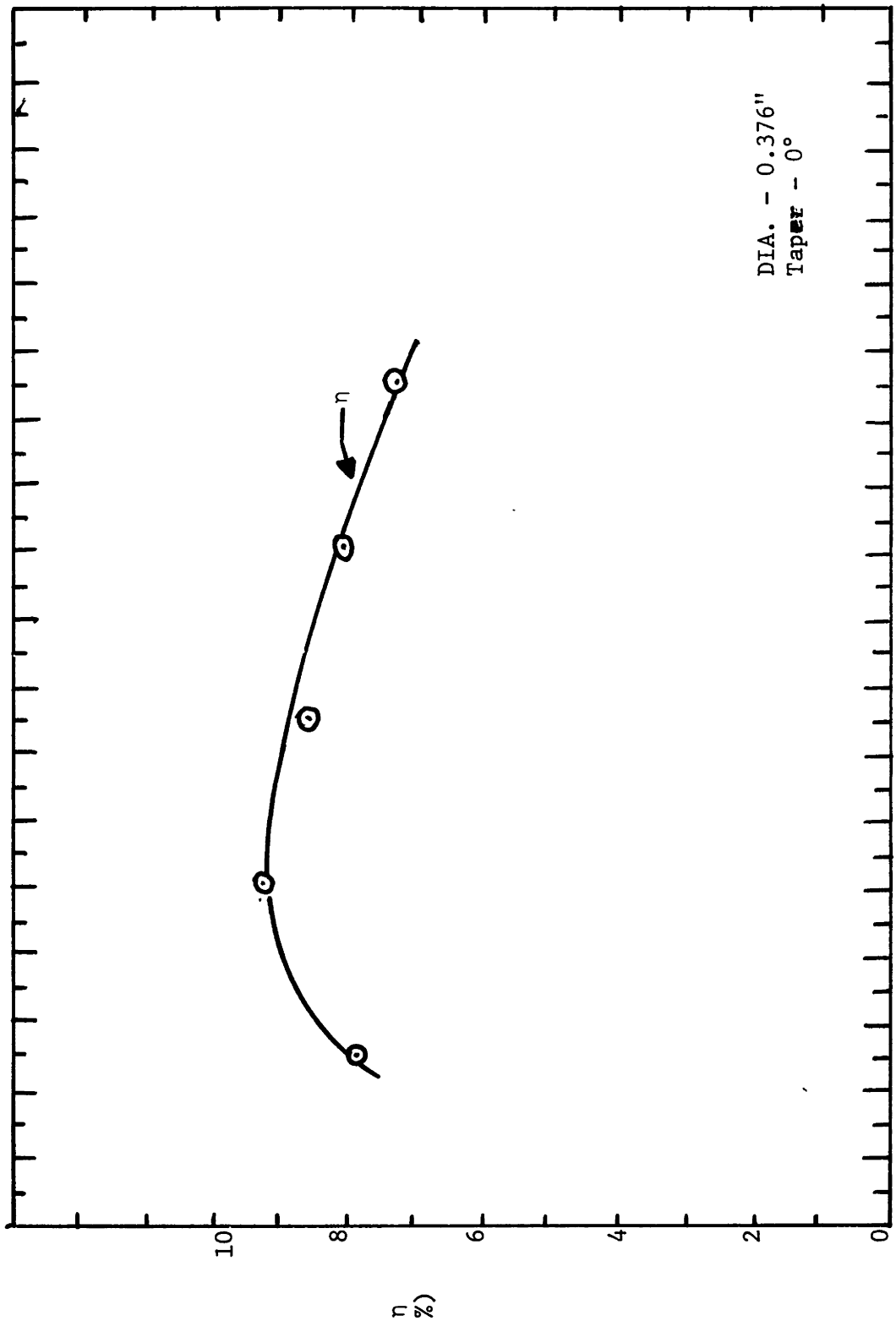

Figure 35--EFFICIENCY VS. CHAMBER LENGTH

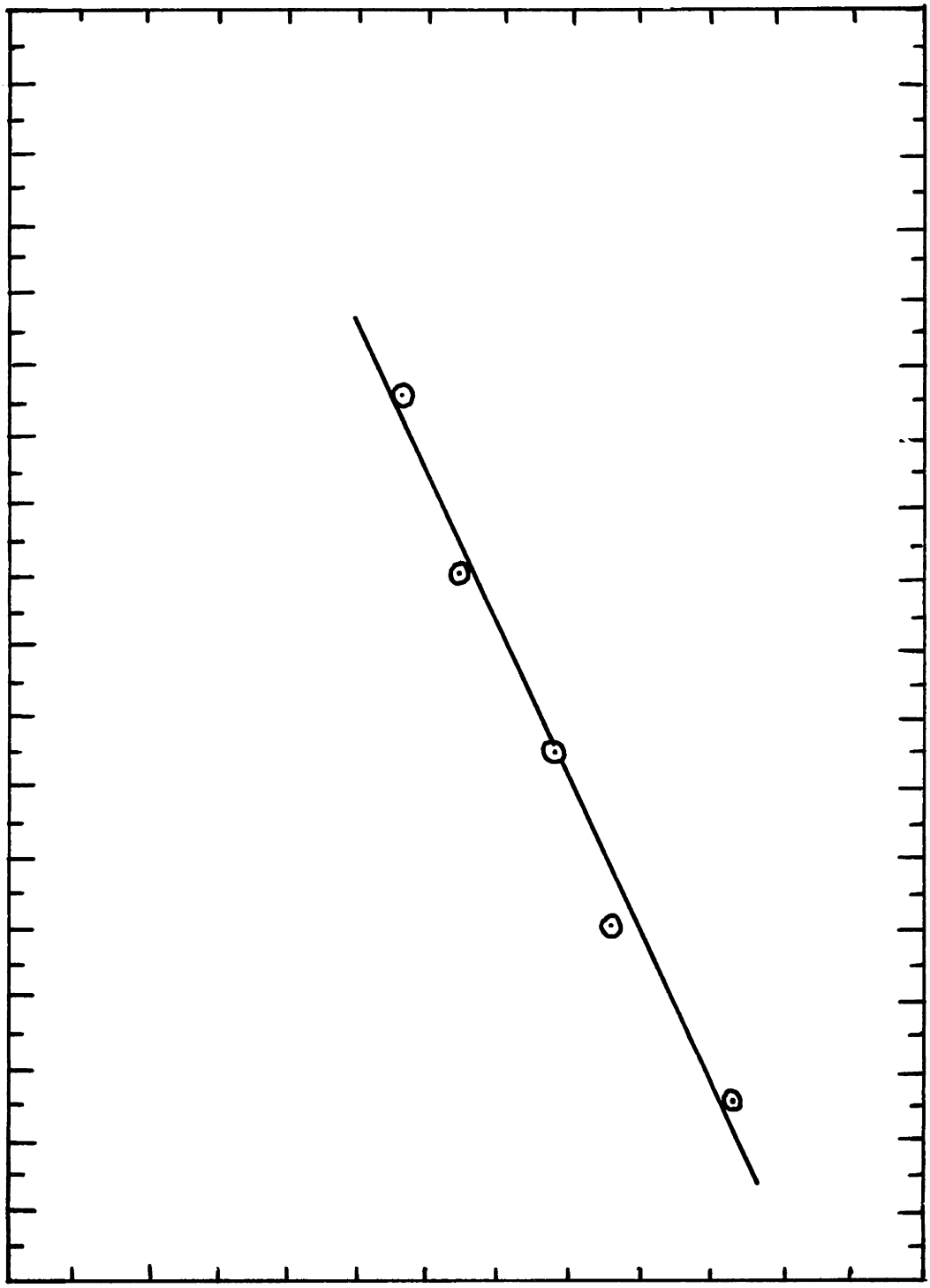

Figure 36--MASS ABLATED/SHOT VS. CHAMBER LENGTH

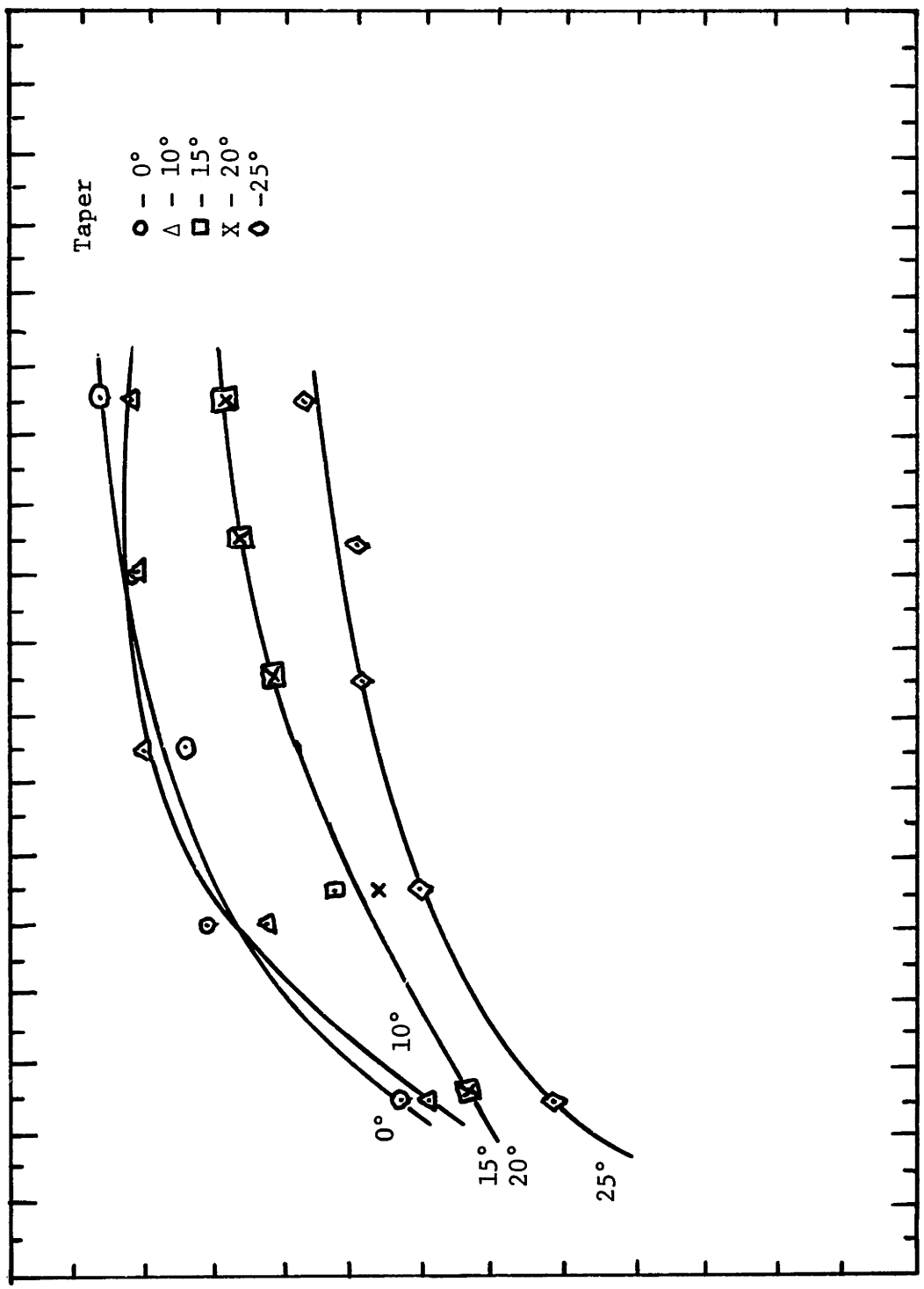

Figure 37--SPECIFIC THRUST VS. CHAMBER LENGTH

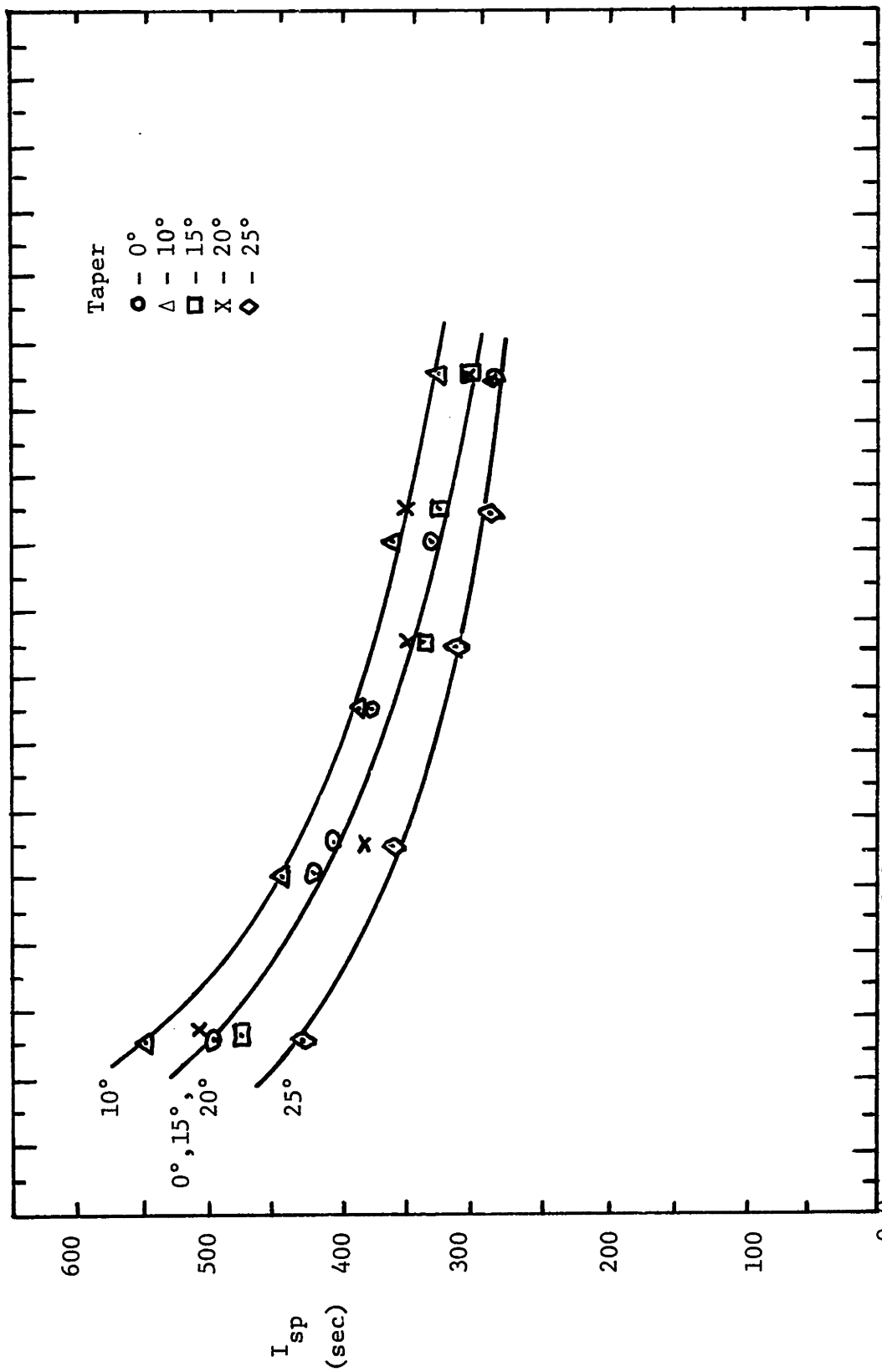

Figure 38--SPECIFIC IMPULSE VS, CHAMBER LENGTH

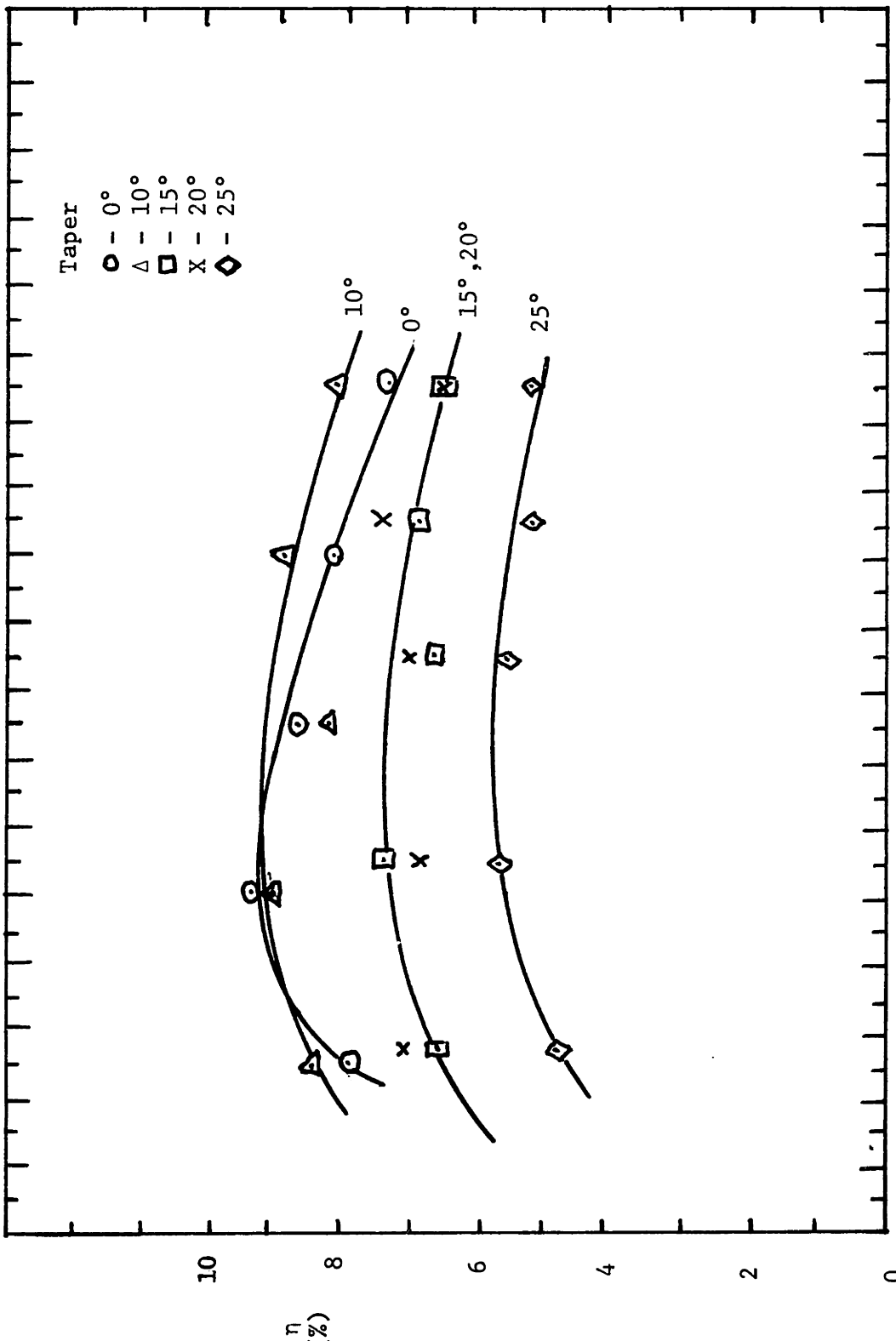

Figure 39--EFFICIENCY VS. CHAMBER LENGTH

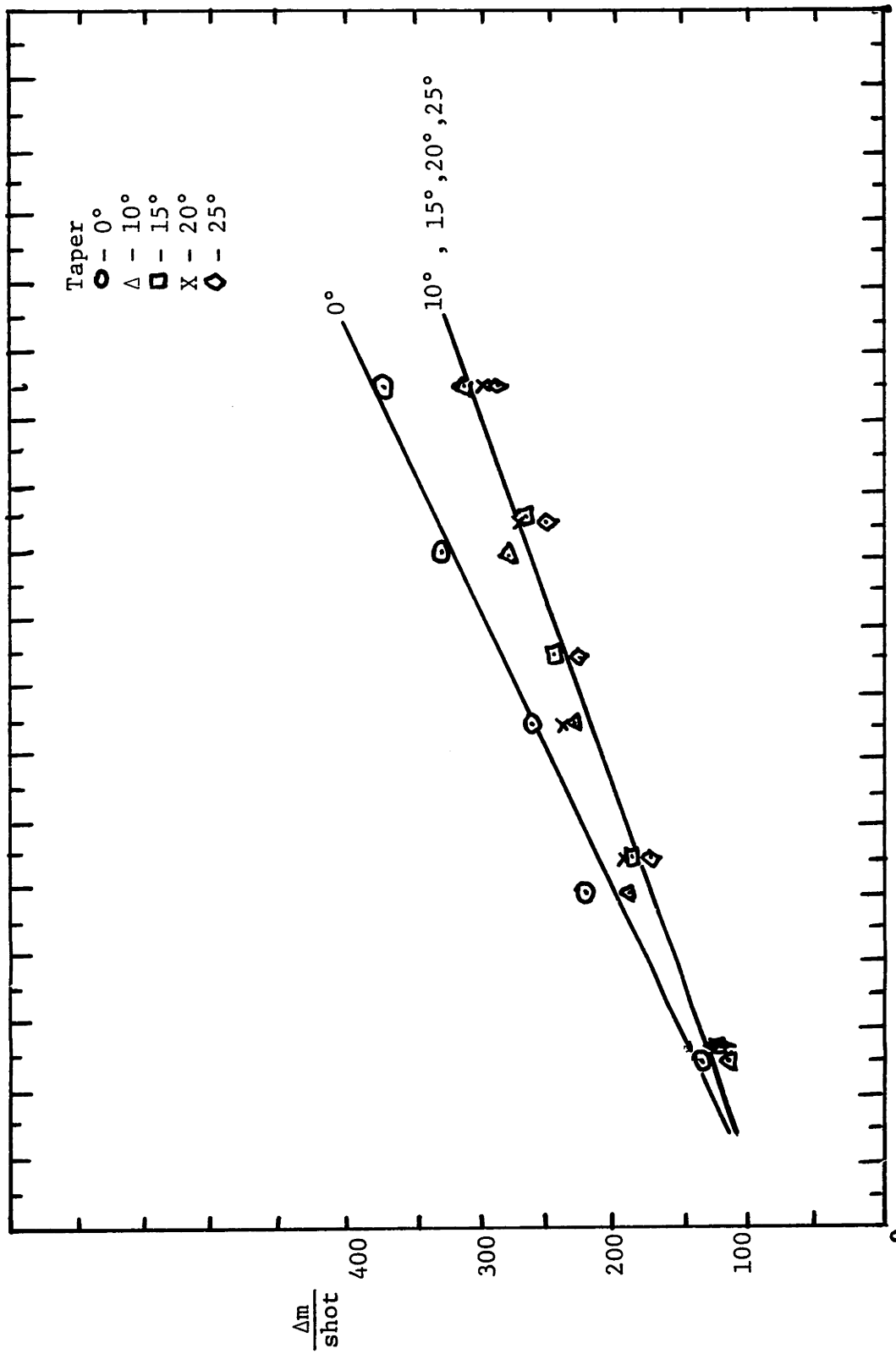

Figure 40--MASS ABLATED /SHOT VS. CHAMBER LENGTH

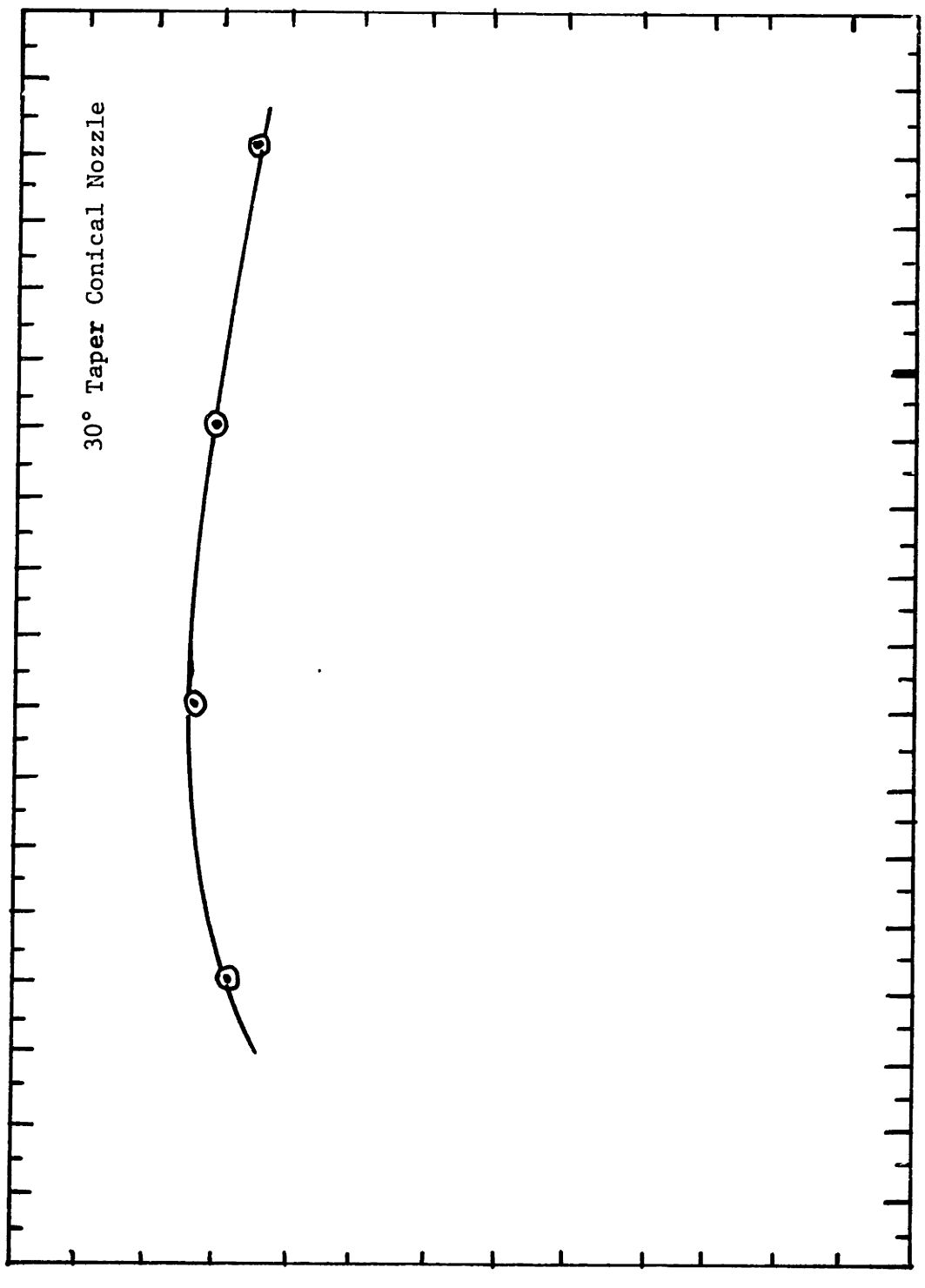

Figure 41--SPECIFIC THRUST VS. NOZZLE LENGTH

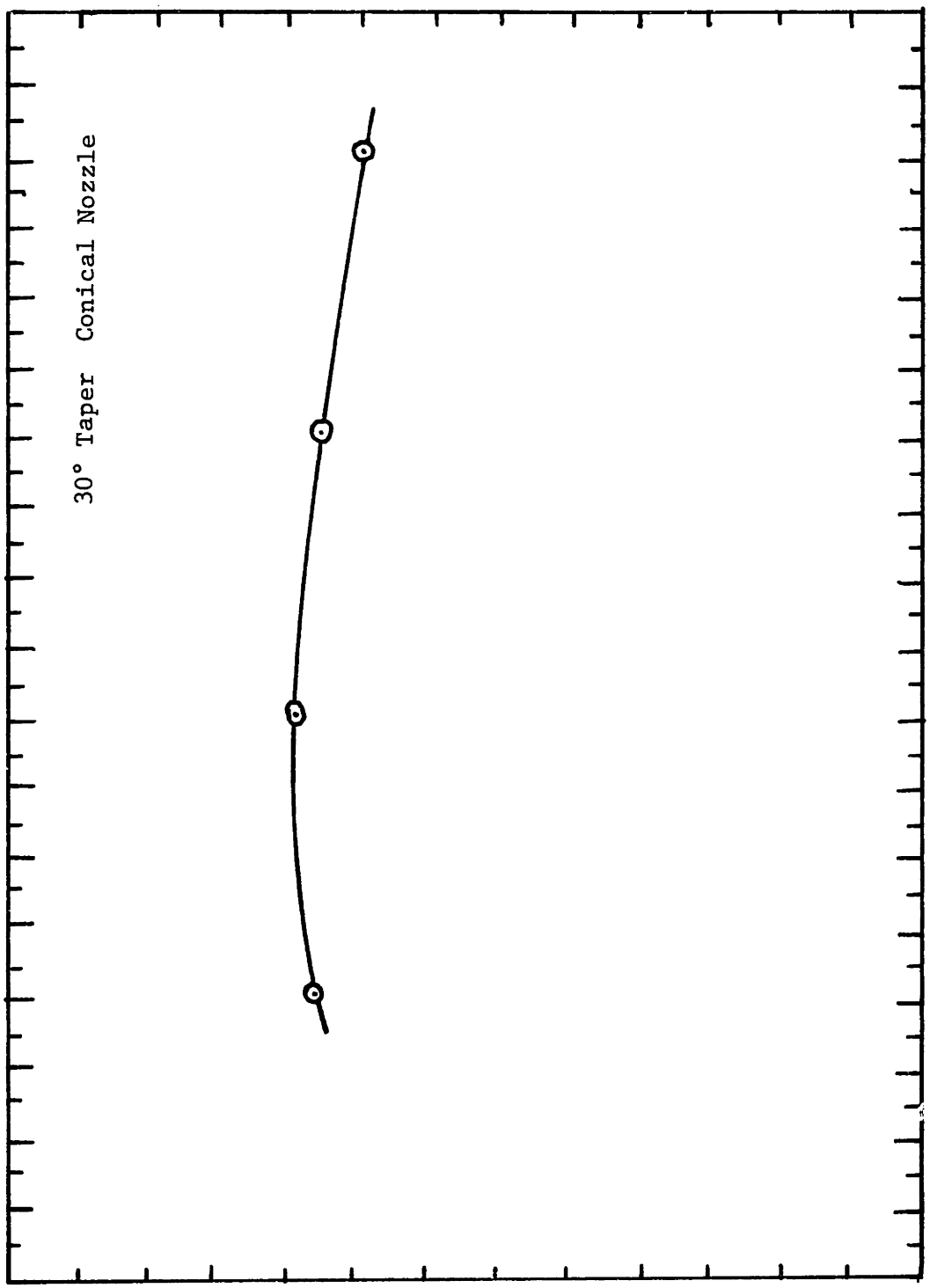

Figure 42--SPECIFIC IMPULSE VS. NOZZLE LENGTH

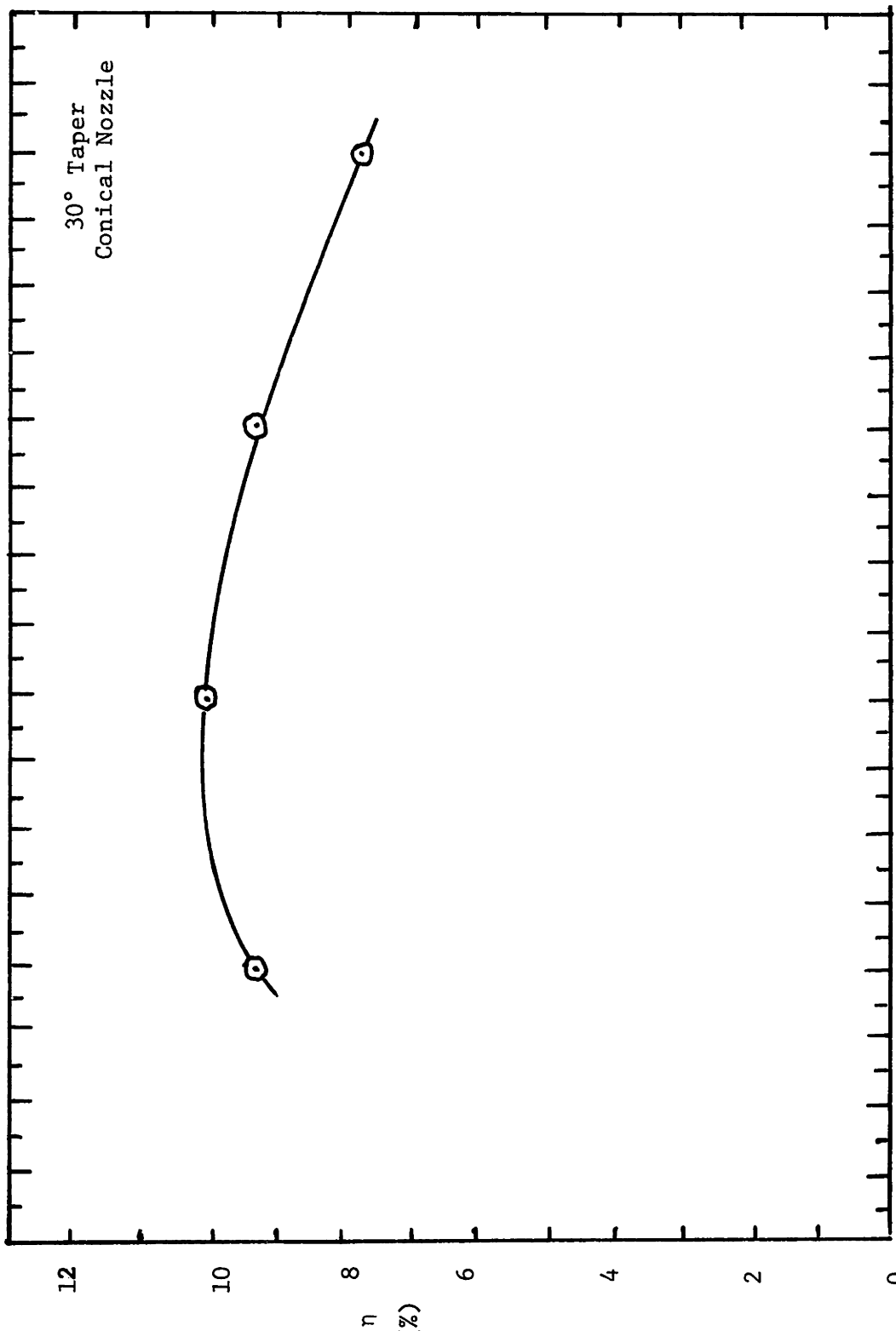

Figure 43--EFFICIENCY VS. NOZZLE LENGTH FOR 15° HALF ANGLE NOZZLE

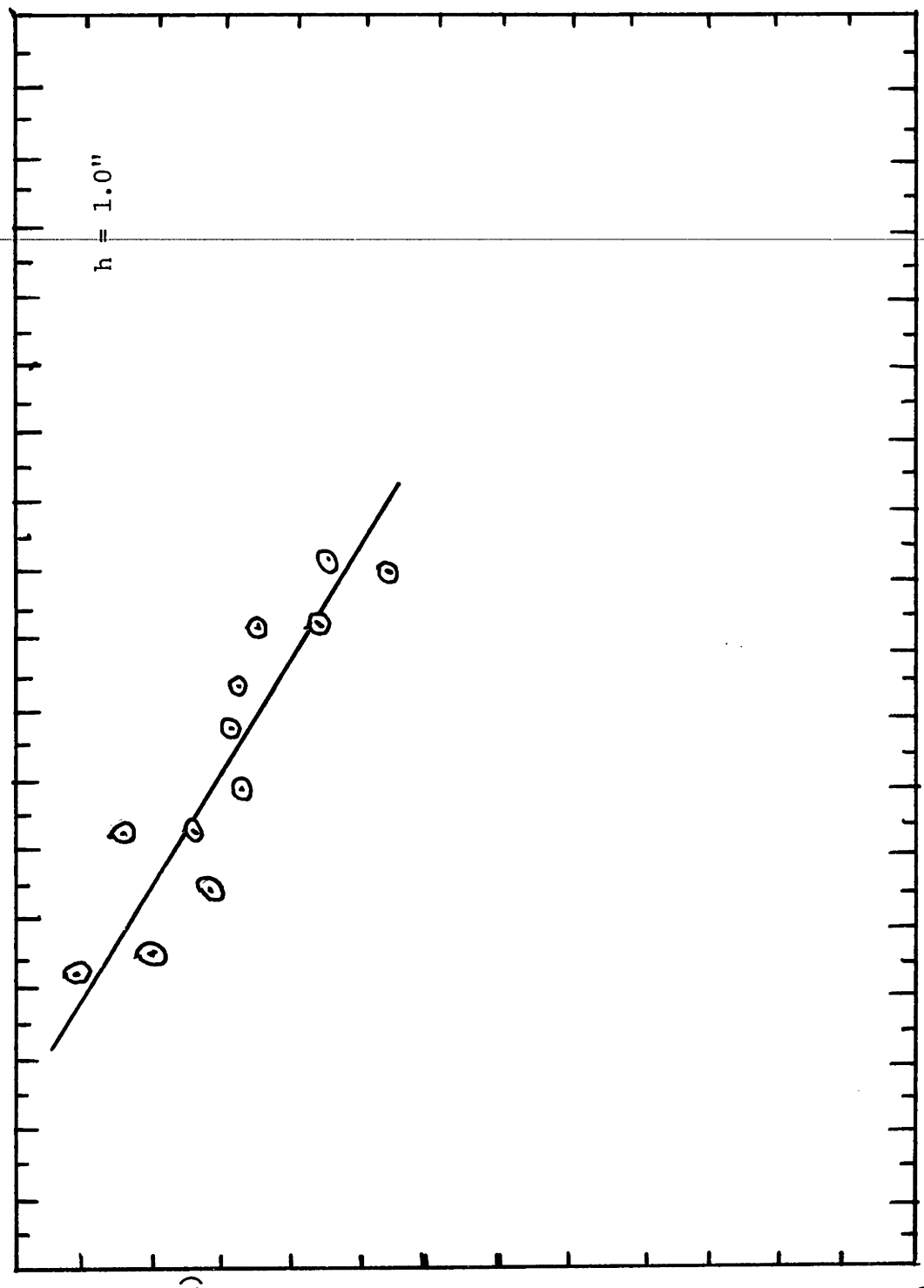

Figure 44--SPECIFIC THRUST VS. HYDRAULIC DIAMETER ---RECTANGULAR GEOMETRY

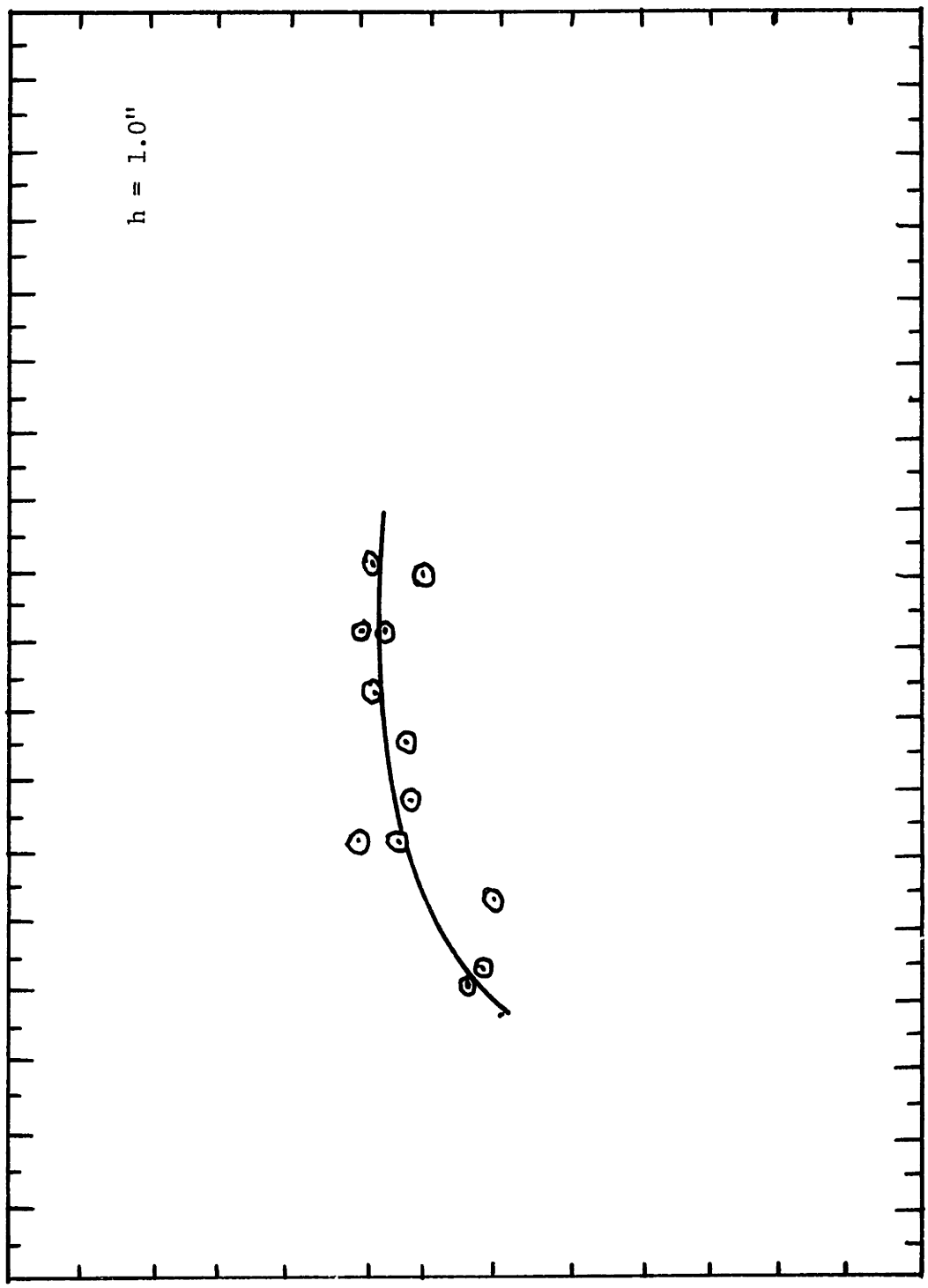

Figure 45--SPECIFIC IMPULSE VS. HYDRAULIC DIAMETER---RECTANGULAR GEOMETRY

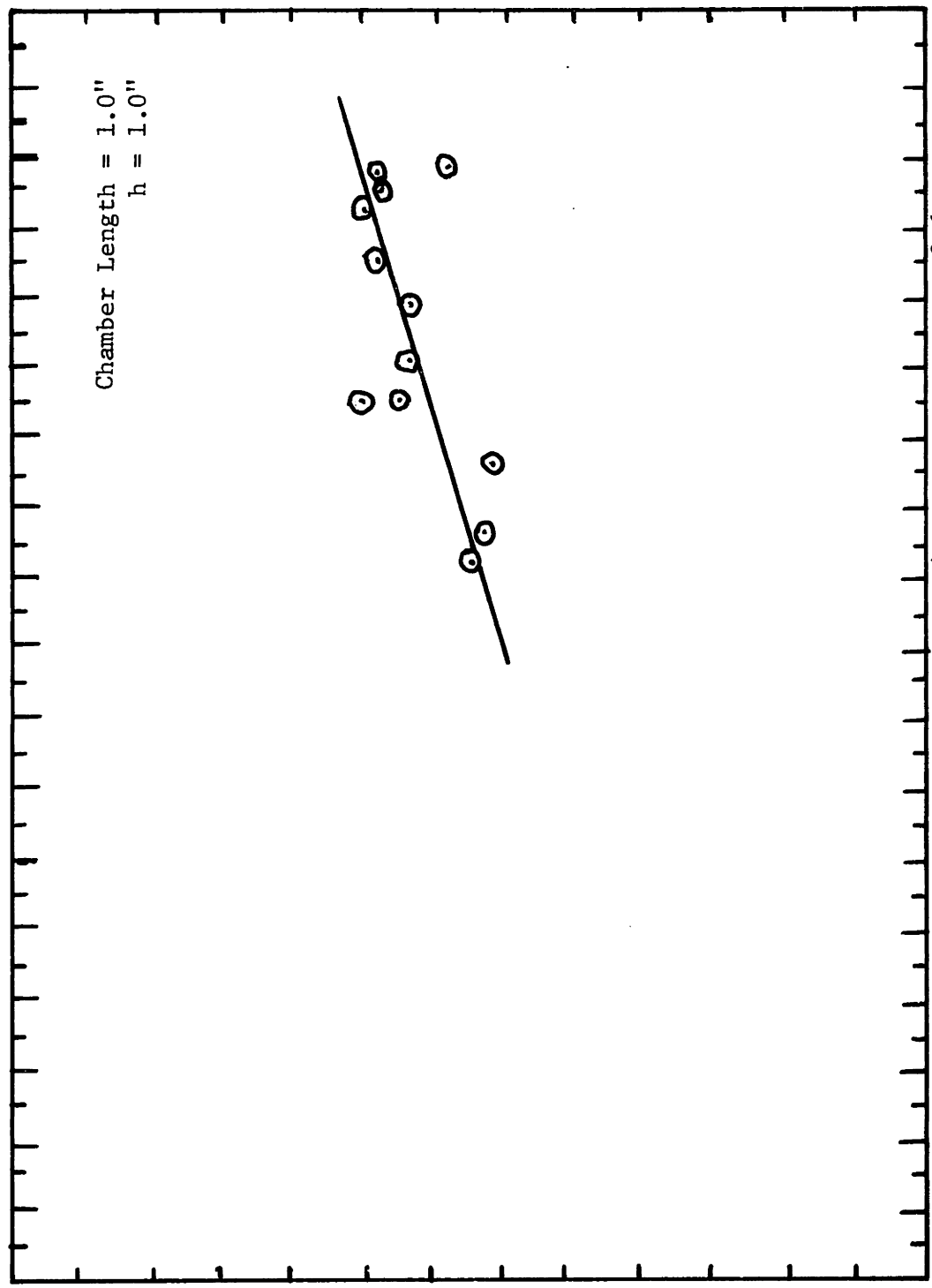

Figure 46--SPECIFIC IMPULSE VS. (HYDRAULIC DIAMETER)$^{1/2}$

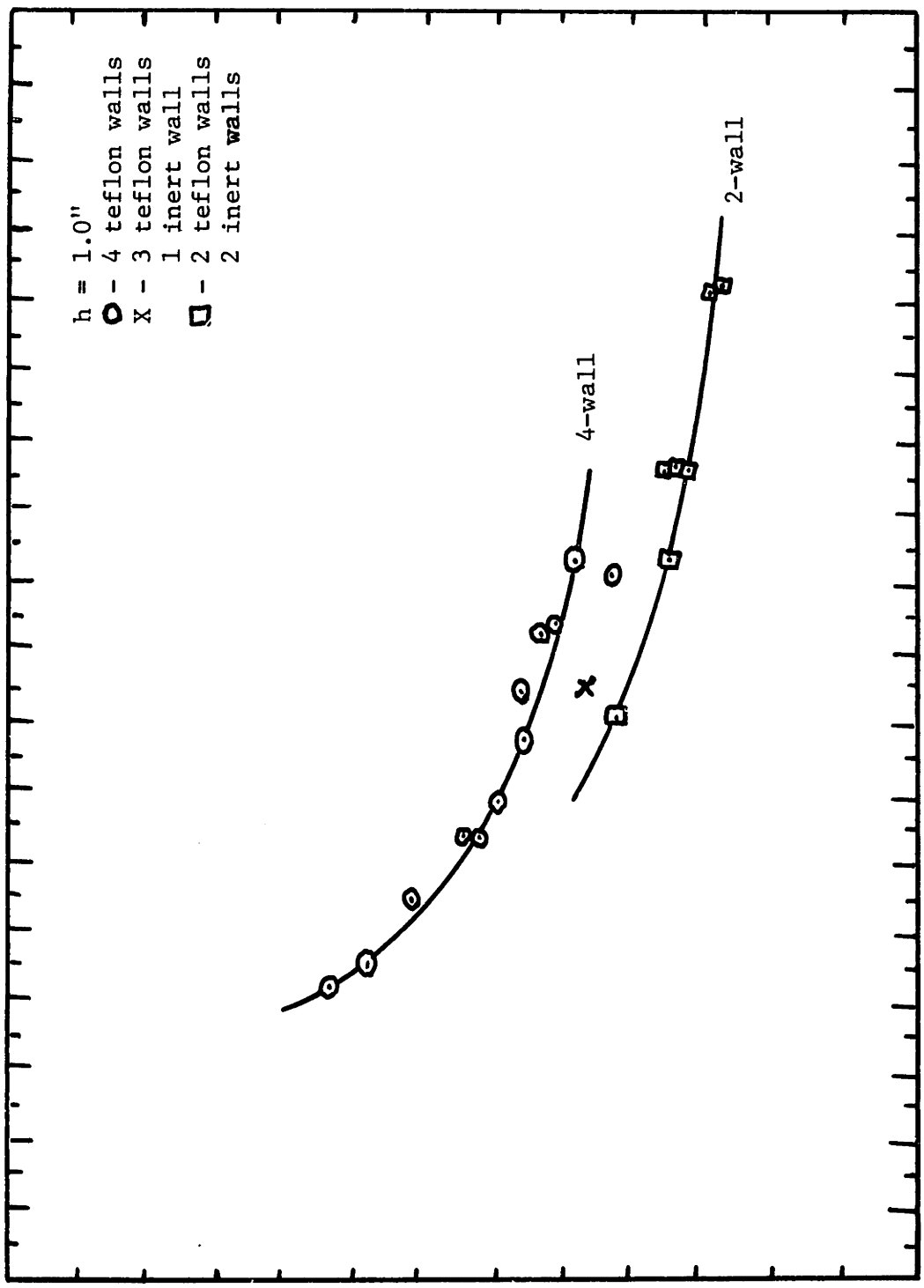

Figure 47--SPECIFIC MASS ABLATED/SHOT VS. HYDRAULIC DIAMETER---RECTANGULAR GEOMETRY

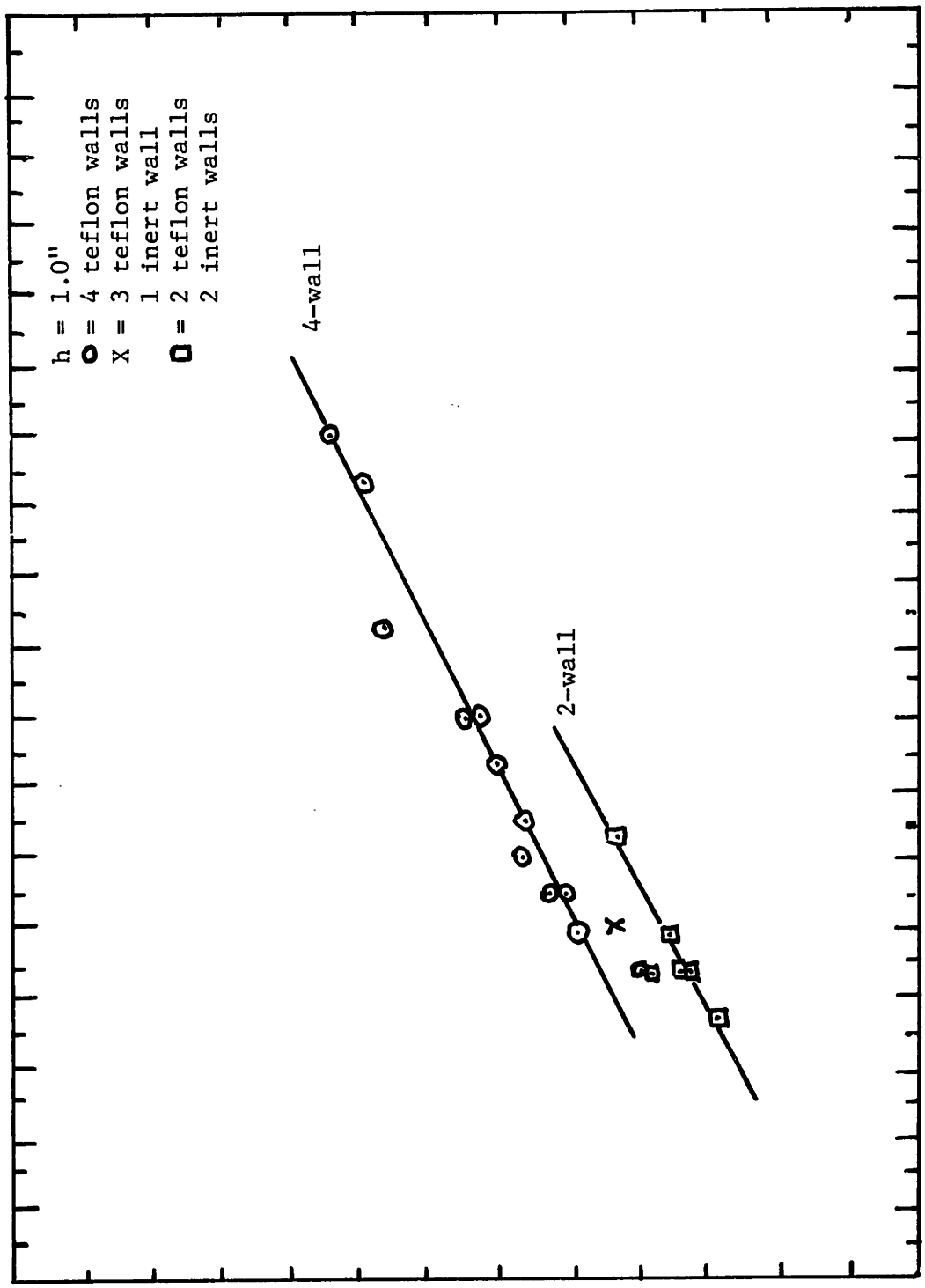

Figure 48--SPECIFIC MASS ABLATED/SHOT VS. $(\text{HYDRAULIC DIAMETER})^{-1}$---RECTANGULAR GEOMETRY

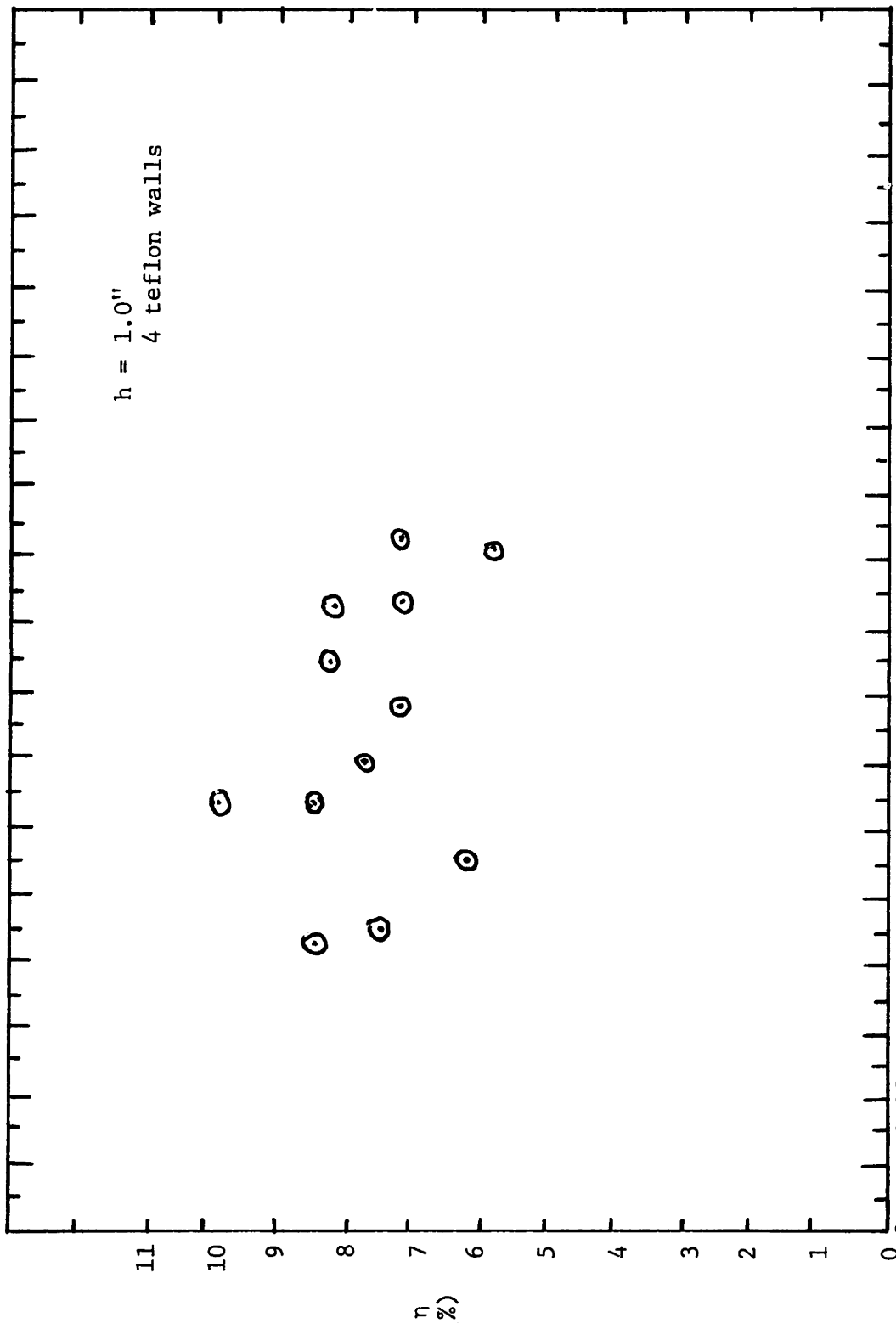

Figure 49--EFFICIENCY VS. HYDRAULIC DIAMETER---RECTANGULAR GEOMETRY

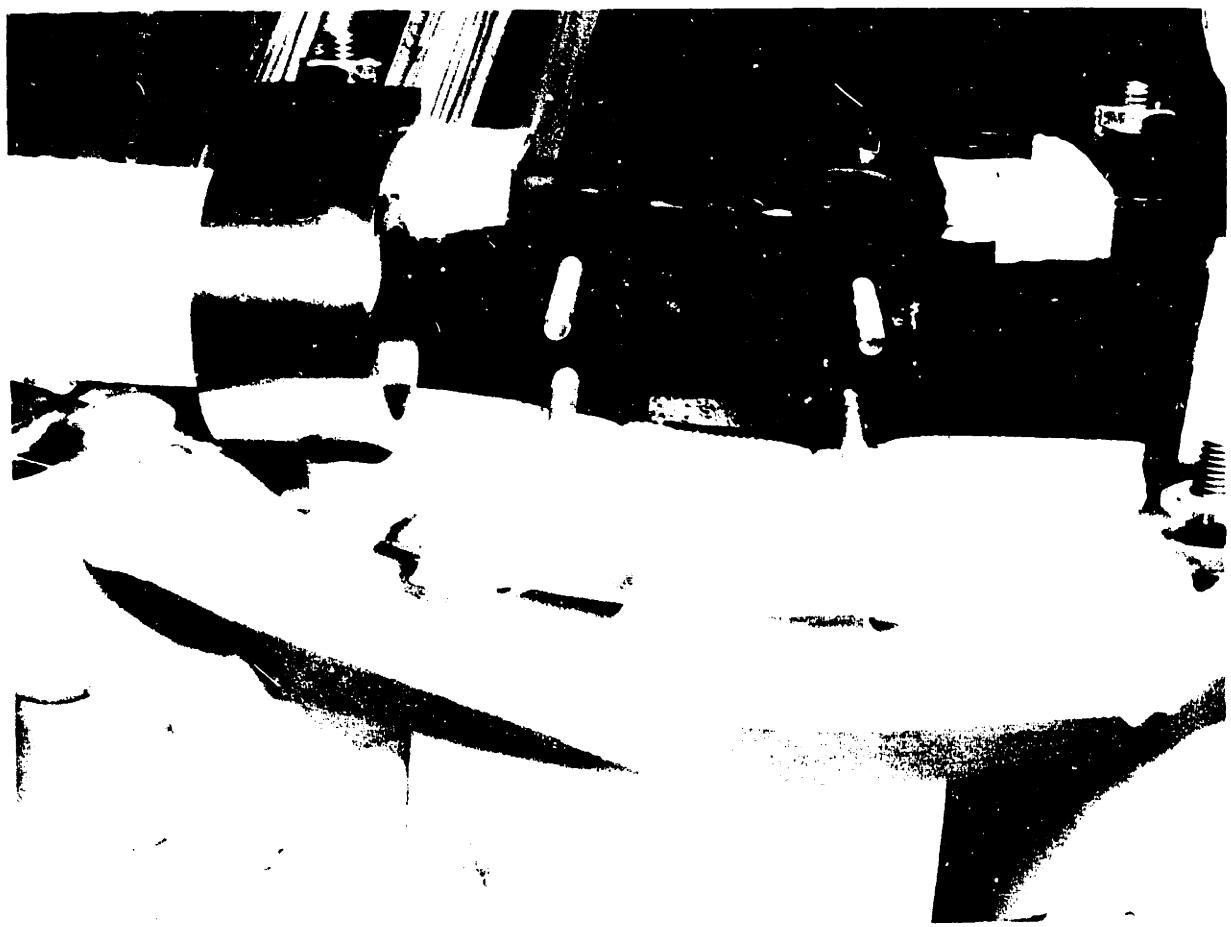

Figure 50—EROSION OF SUPER-MICA SIDEWALL (The Hole in the Wall Allows the Spark Plug Discharge to Enter Chamber)

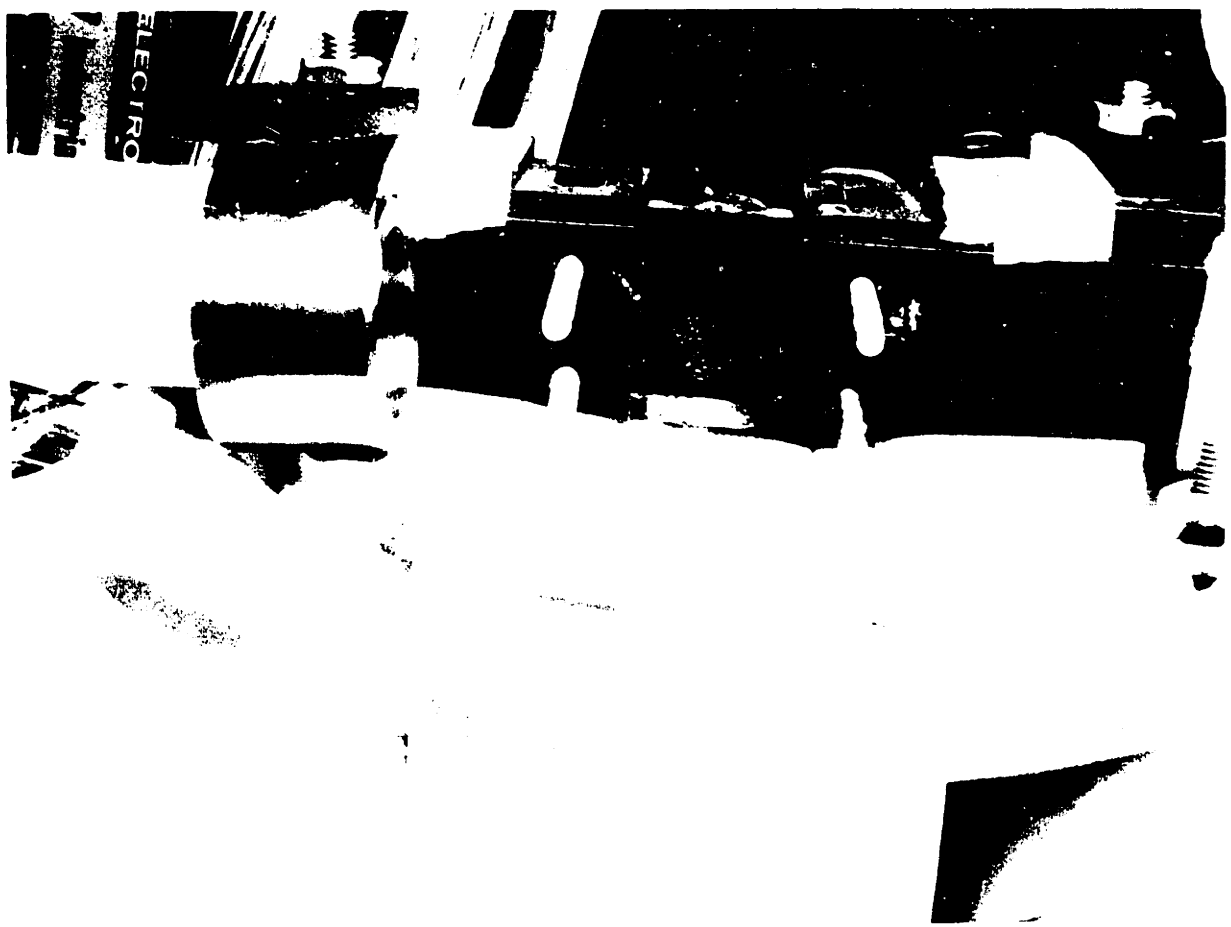

Figure 50—EROSION OF SUPER-MICA SIDEWALL (The Hole in the Wall Allows the Spark Plug Discharge to Enter Chamber)

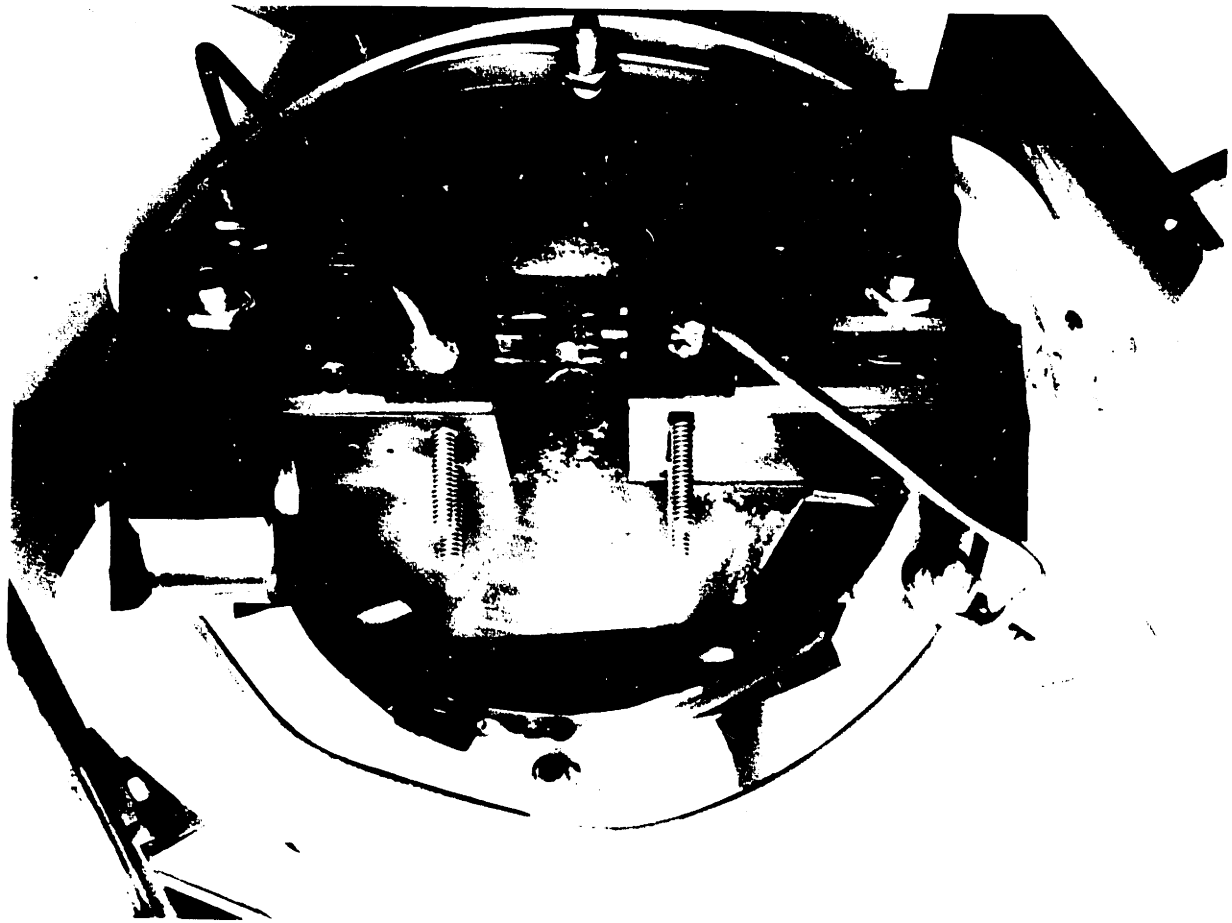

Figure 51: EROSION AND MICA DEPOSITS ON STAINLESS STEEL CATHODE

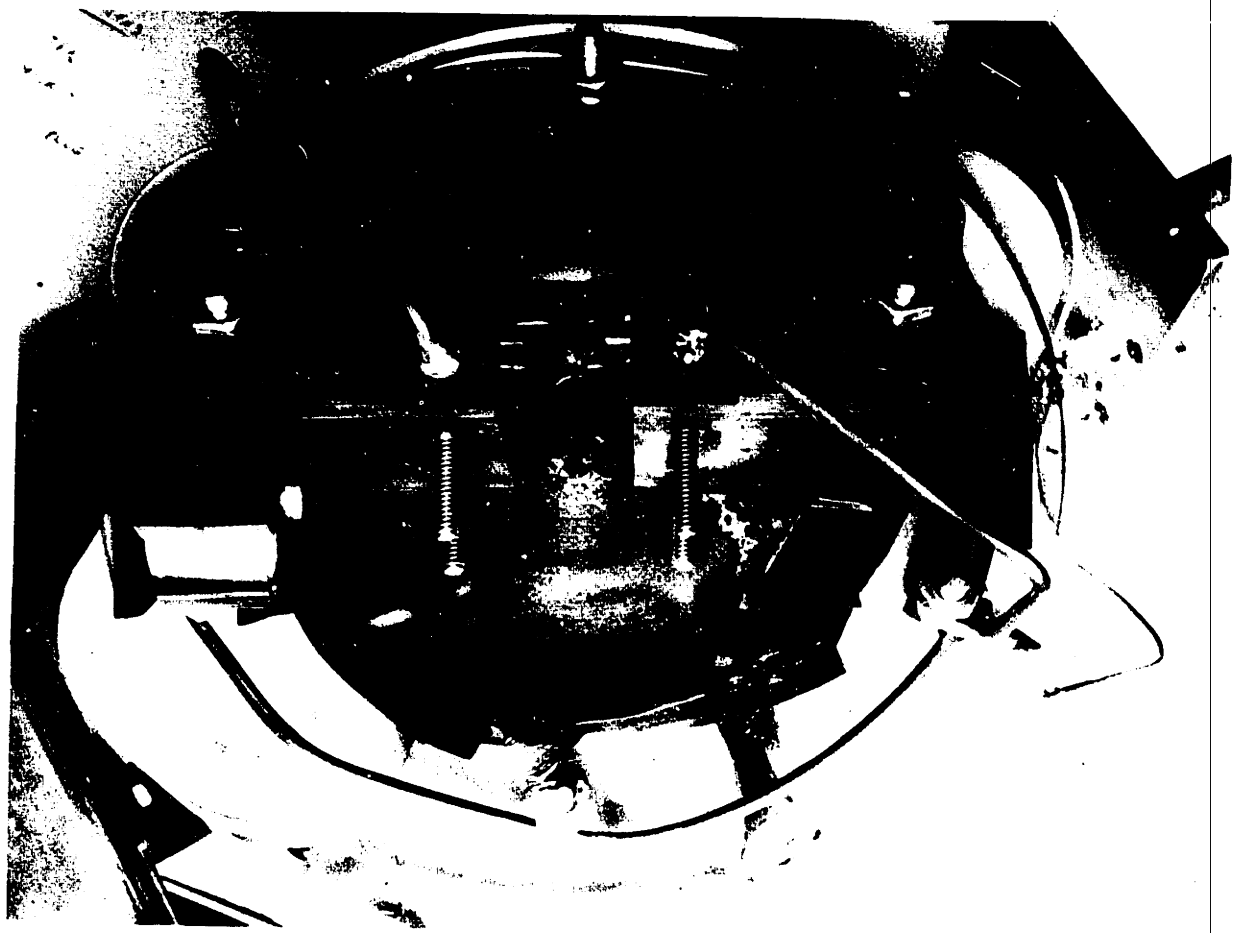

Figure 51: EROSION AND MICA DEPOSITS ON STAINLESS STEEL CATHODE

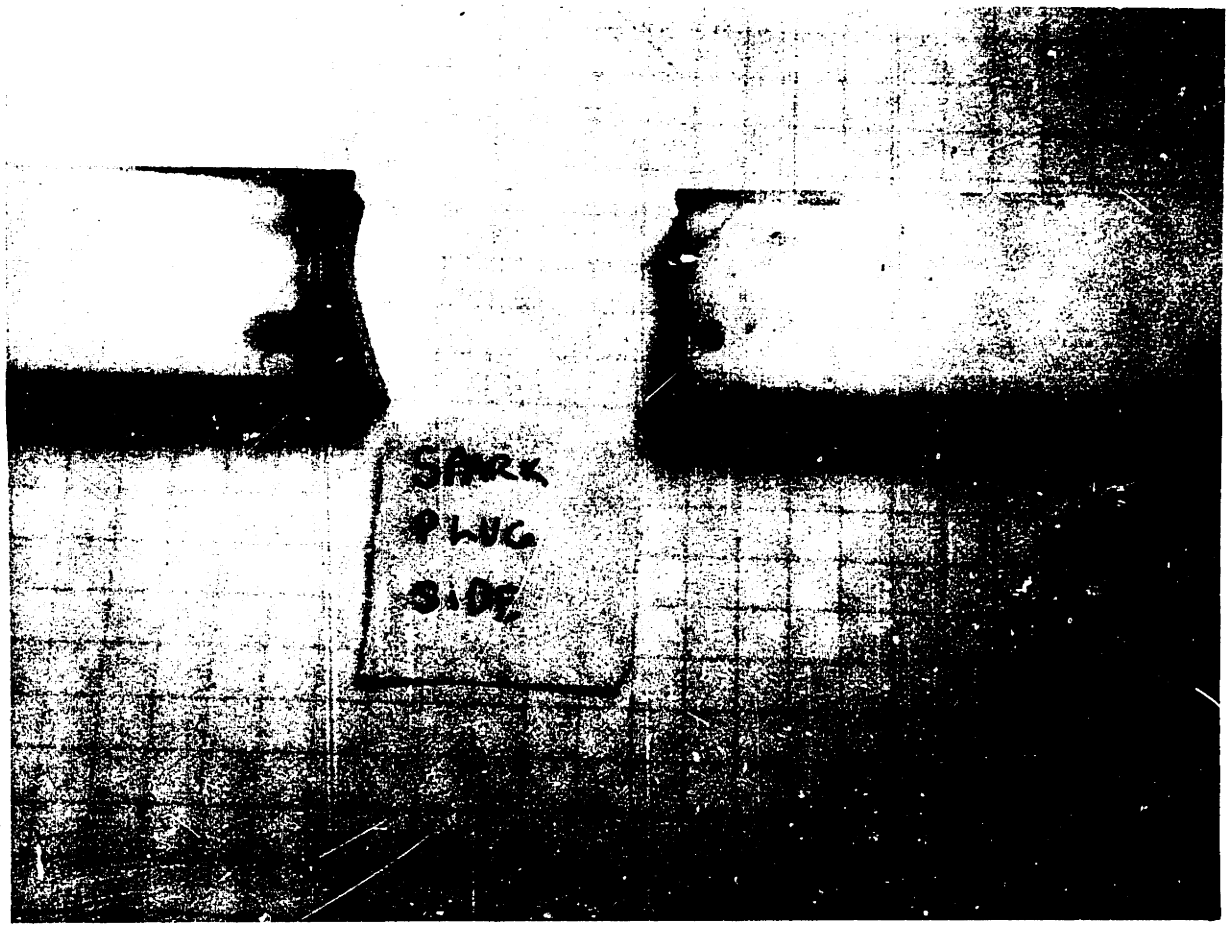

Figure 52: UNEVEN TEFLON ABLATION PROFILE---SIDE VIEW EACH GRID SQUARE 1/4" x 1/4", EXHAUST TOWARDS BOTTOM OF PHOTOGRAPH

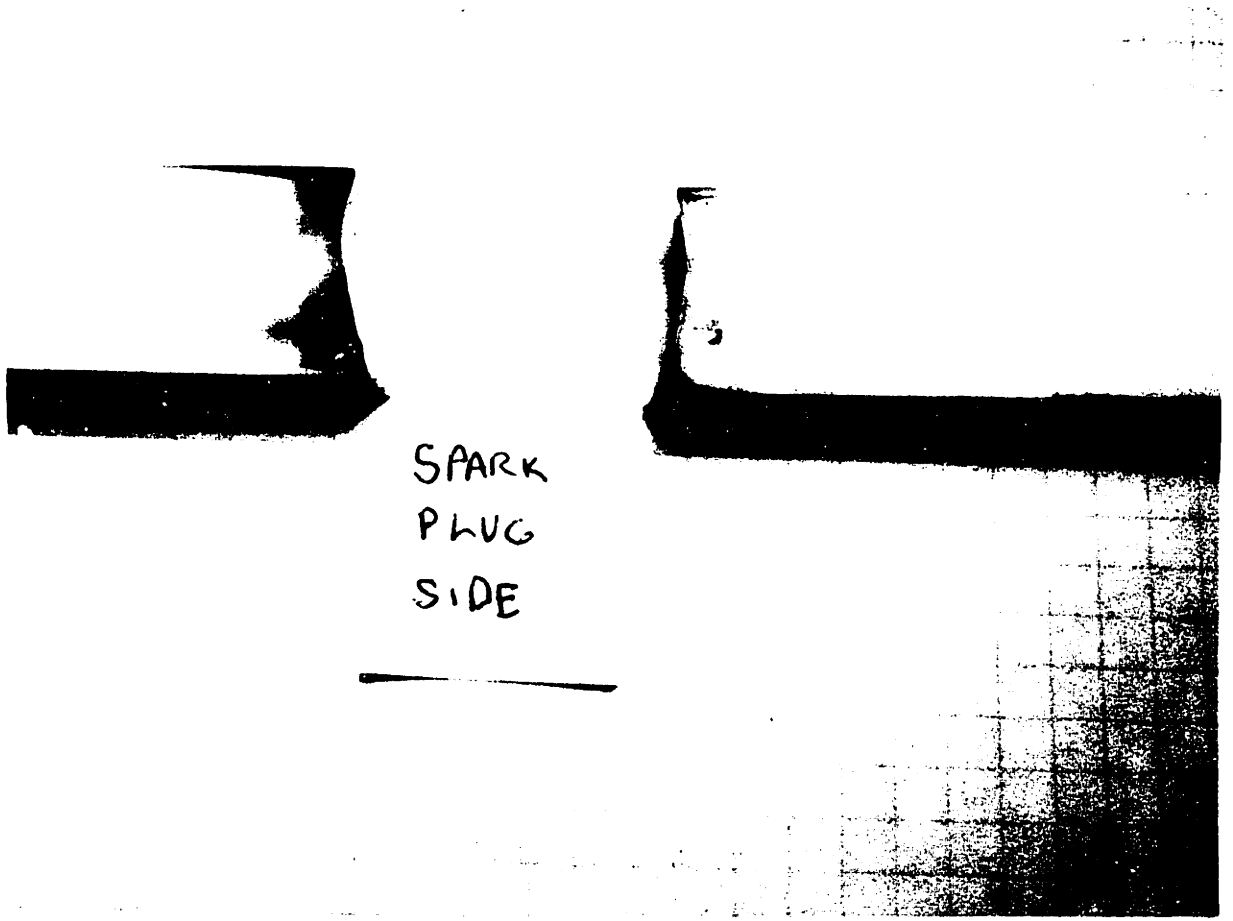

Figure 52: UNEVEN TEFLON ABLATION PROFILE---SIDE VIEW EACH GRID SQUARE 1/4" x 1/4", EXHAUST TOWARDS BOTTOM OF PHOTOGRAPH

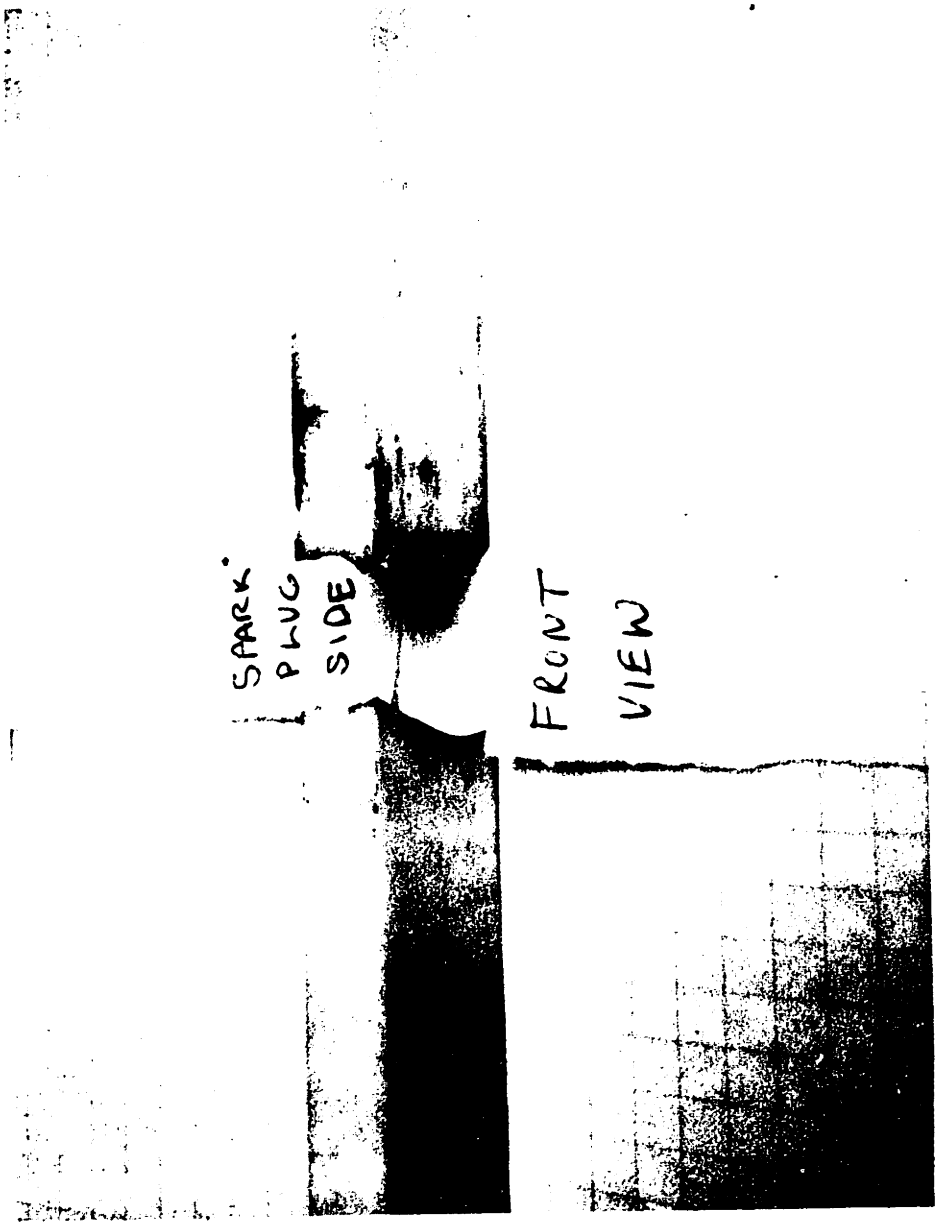

Figure 53: UNEVEN ABLATION OF TEFLON---SLANT VIEW

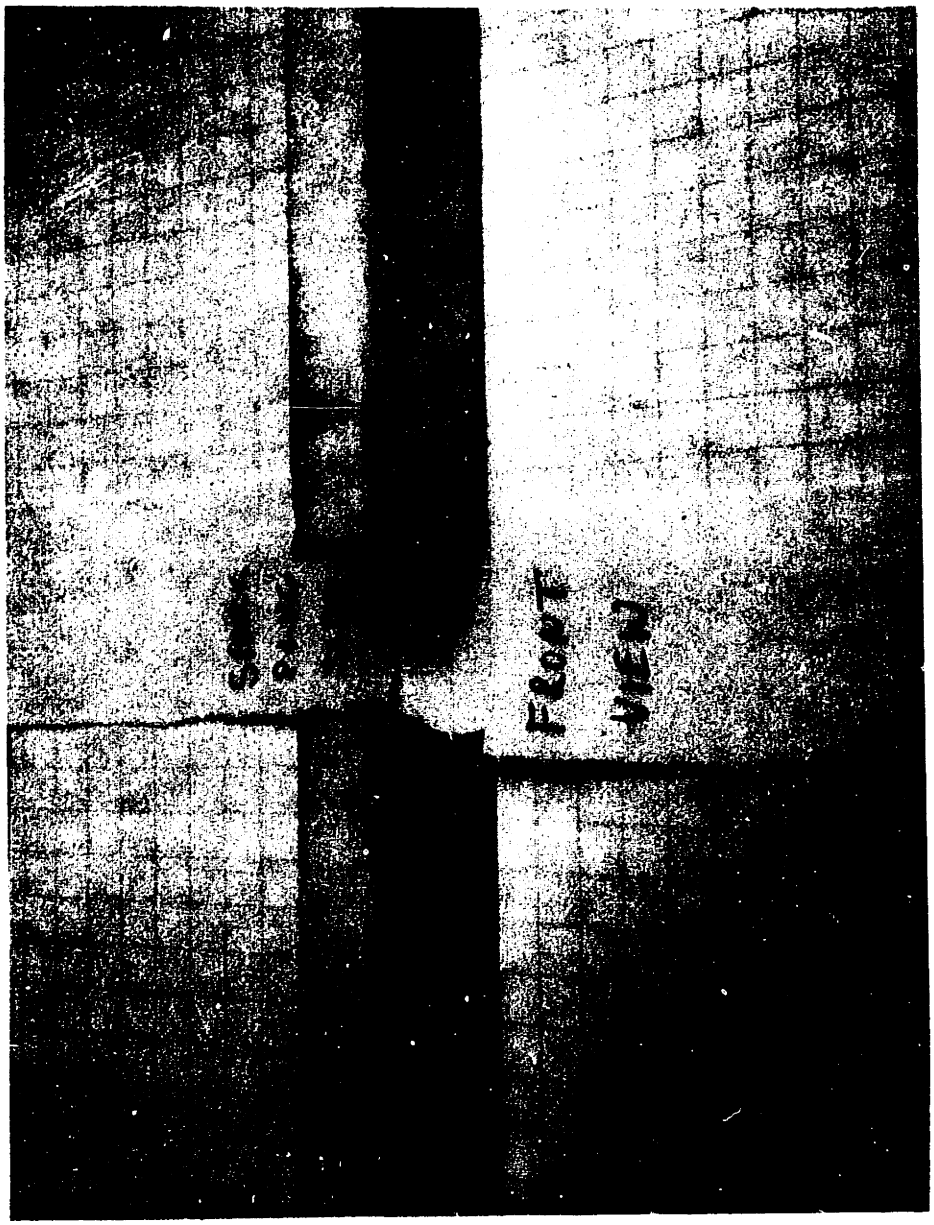

Figure 53: UNEVEN ABLATION OF TEFLON---SLANT VIEW

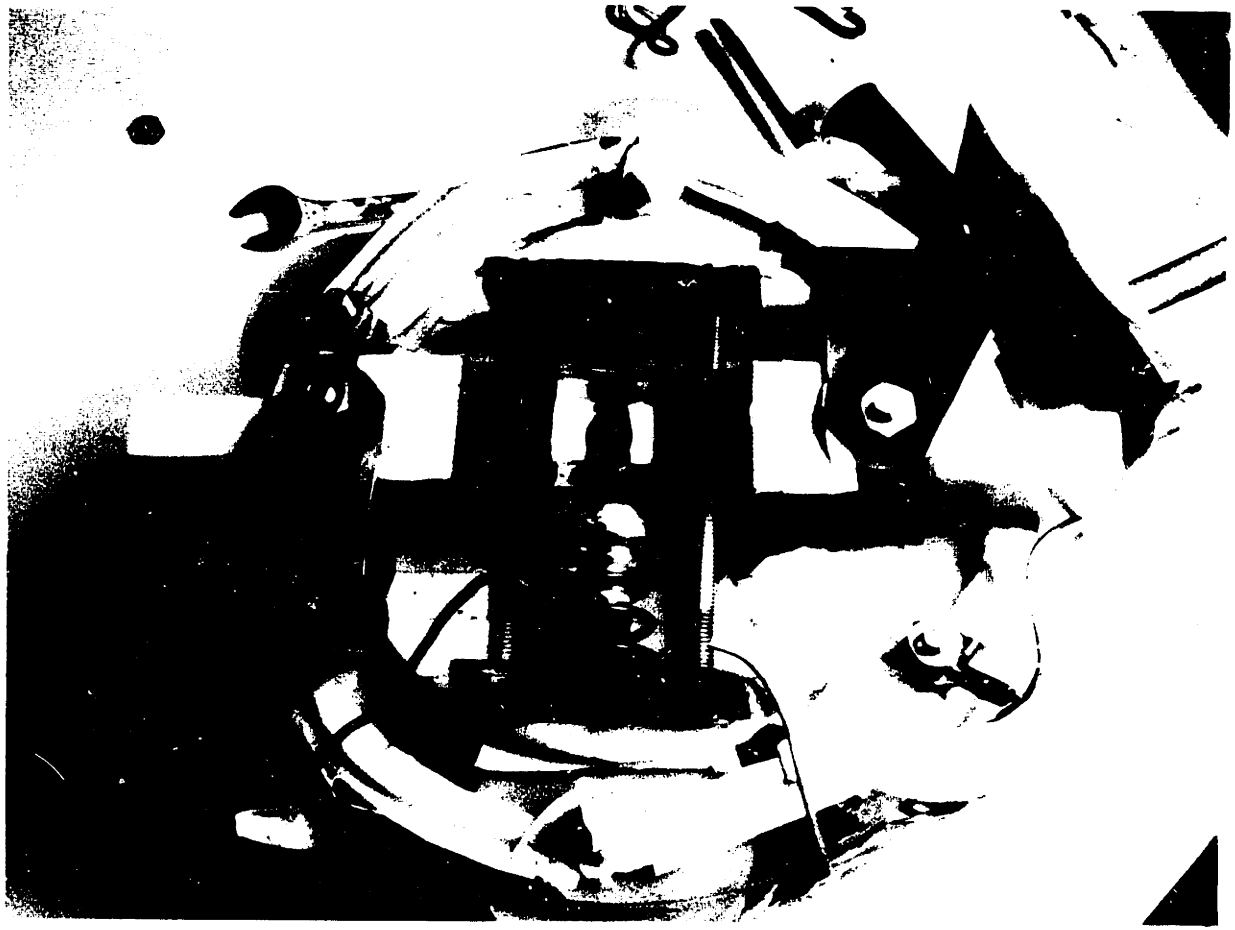

Figure 54: FRONT VIEW---TEFLON ABLATION PROFILE---(Note--Faster Ablation on Spark Plug Side)

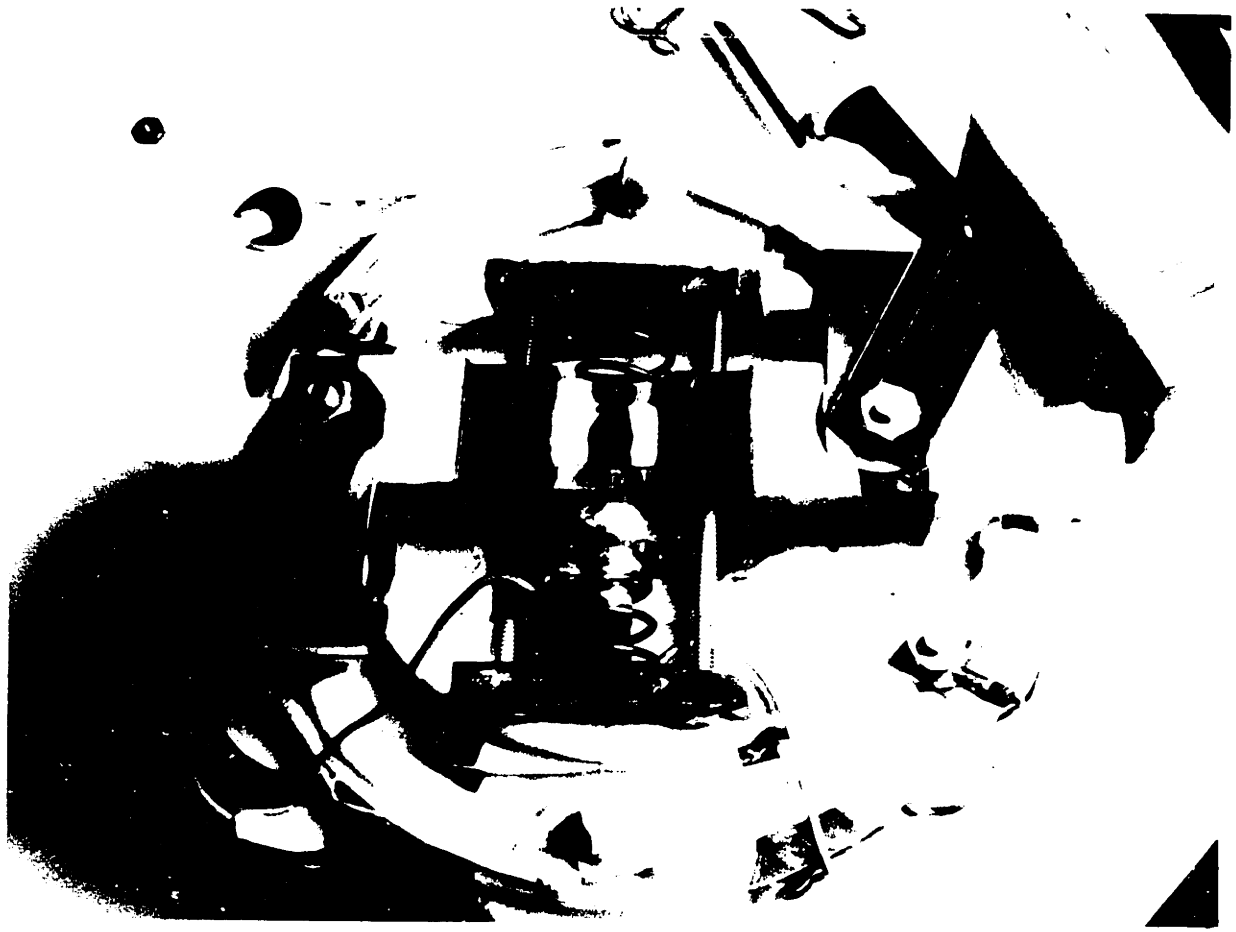

Figure 54: FRONT VIEW---TEFLON ABLATION PROFILE---(Note--Faster Ablation on Spark Plug Side)

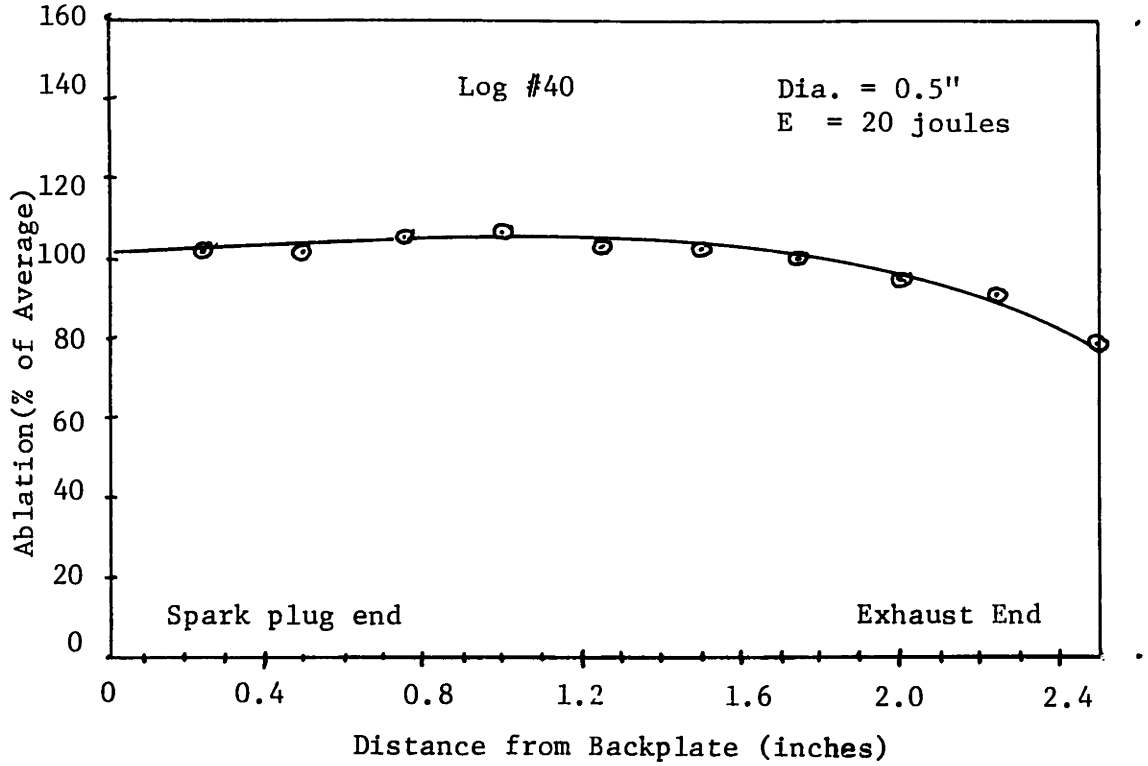

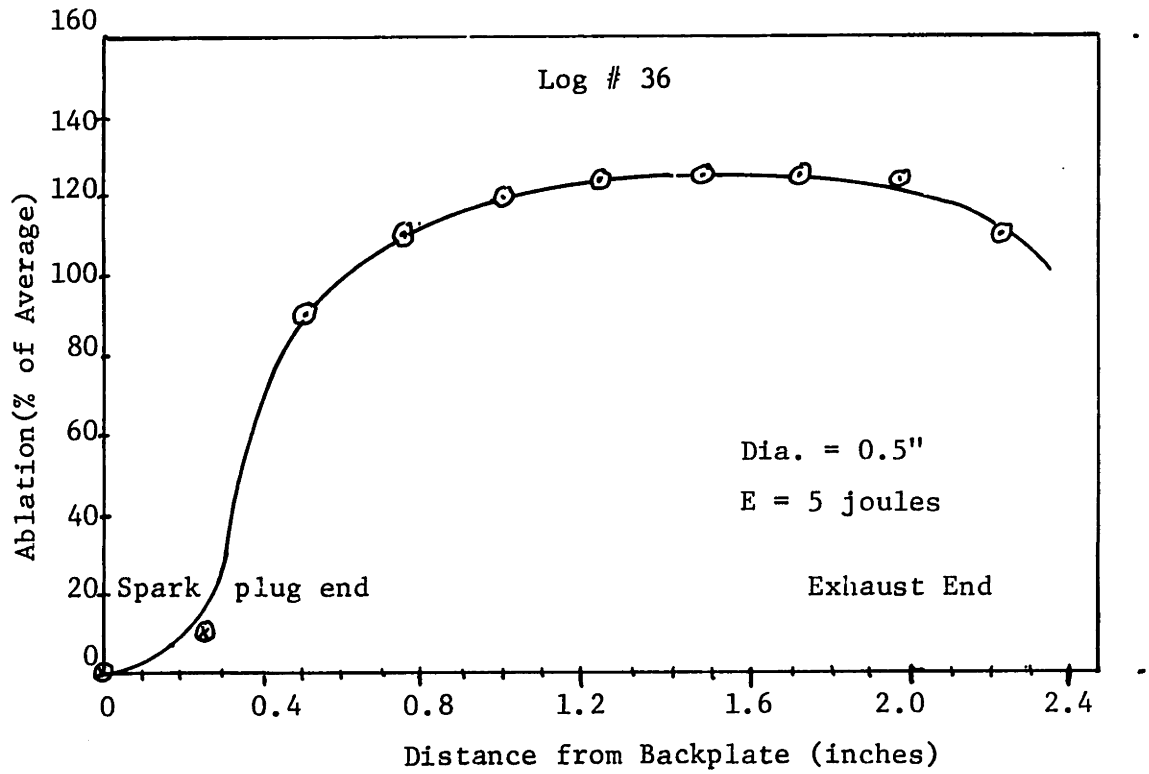

Figure 55--ABLATION PROFILE--ENERGY EFFECTS (Vertical Coordinate Exaggerated)

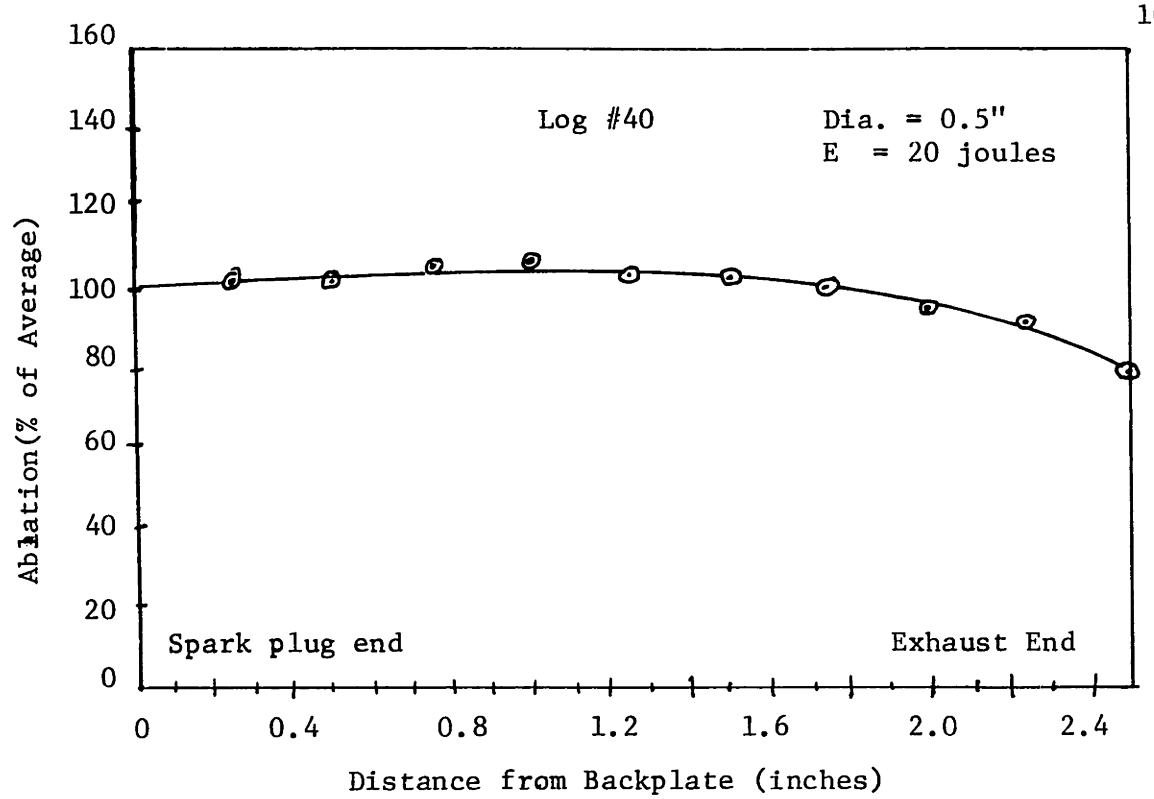

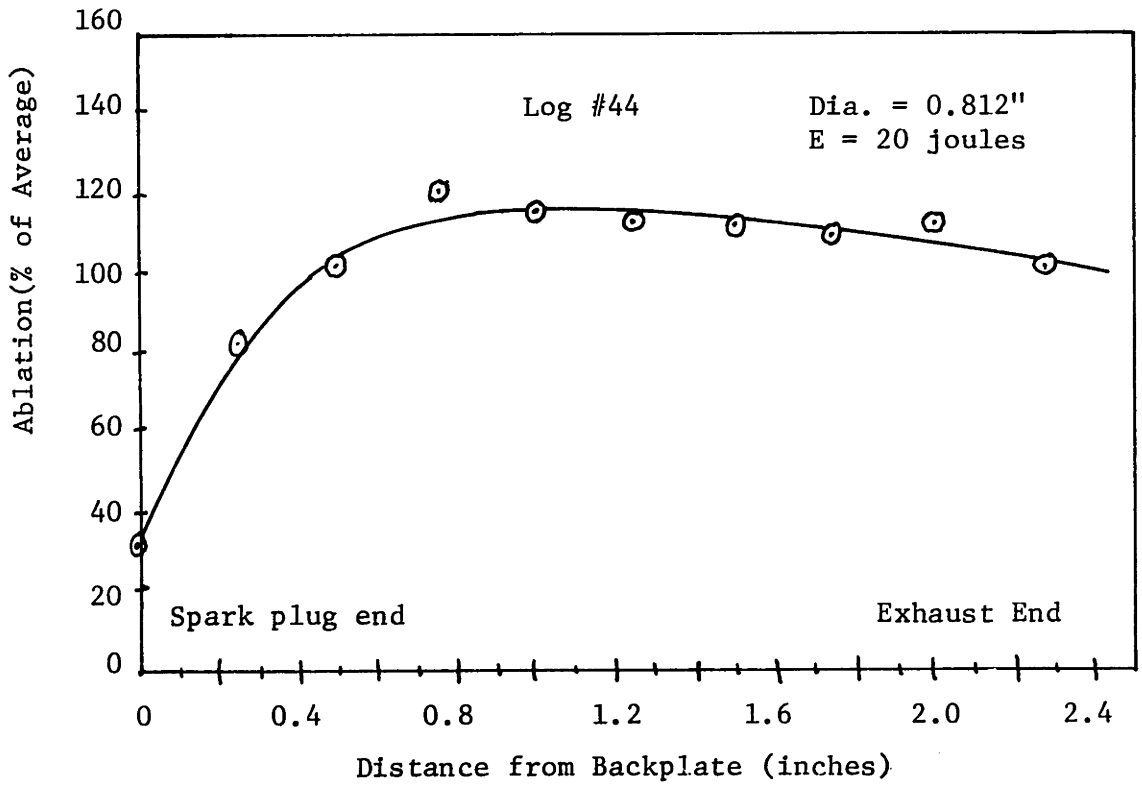

Figure 56--ABLATION PROFILE---DIAMETER EFFECTS

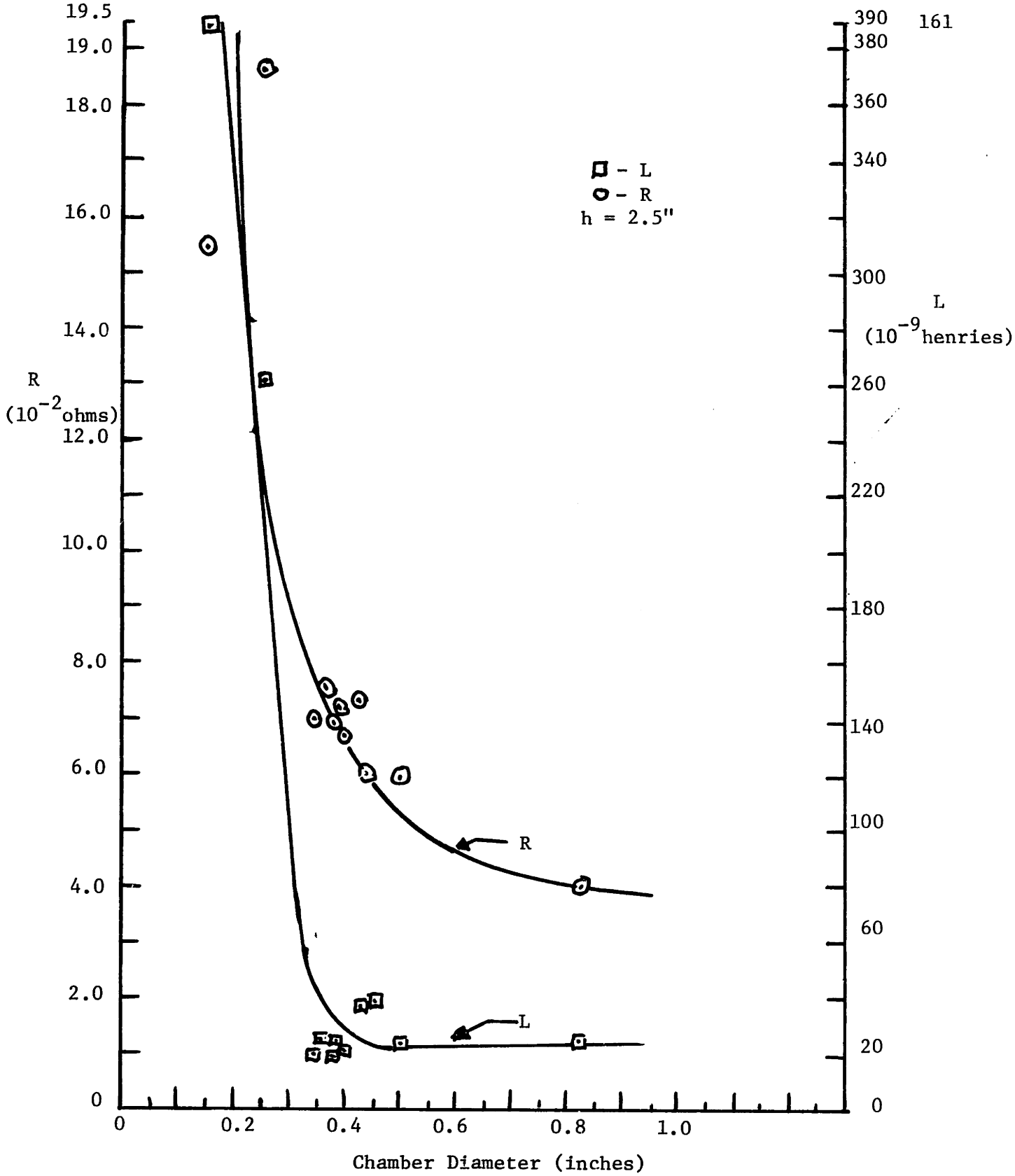

Figure 57--RESISTANCE AND INDUCTANCE VS. CHAMBER DIAMETER

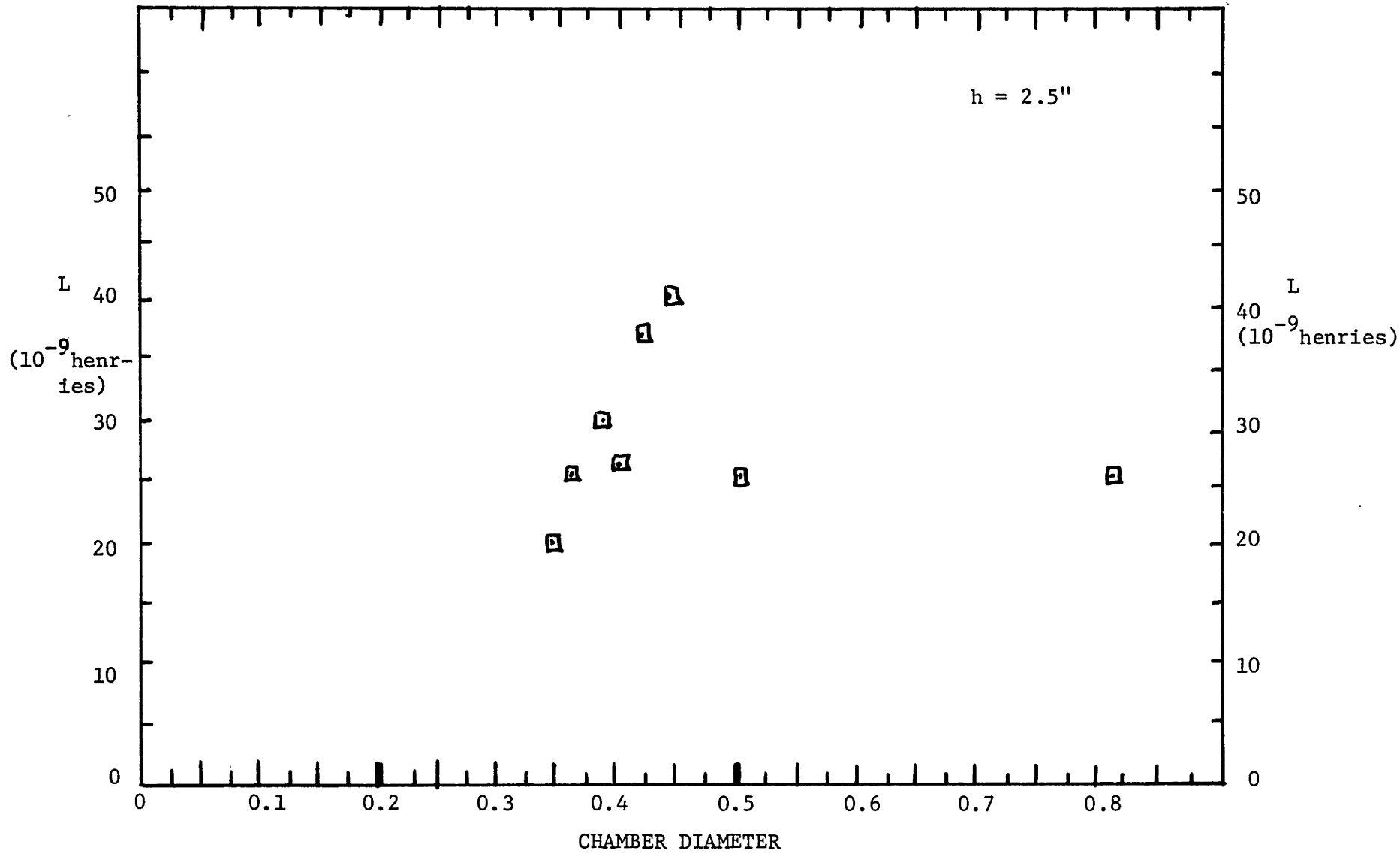

Figure 58--INDUCTANCE VS. CHAMBER DIAMETER

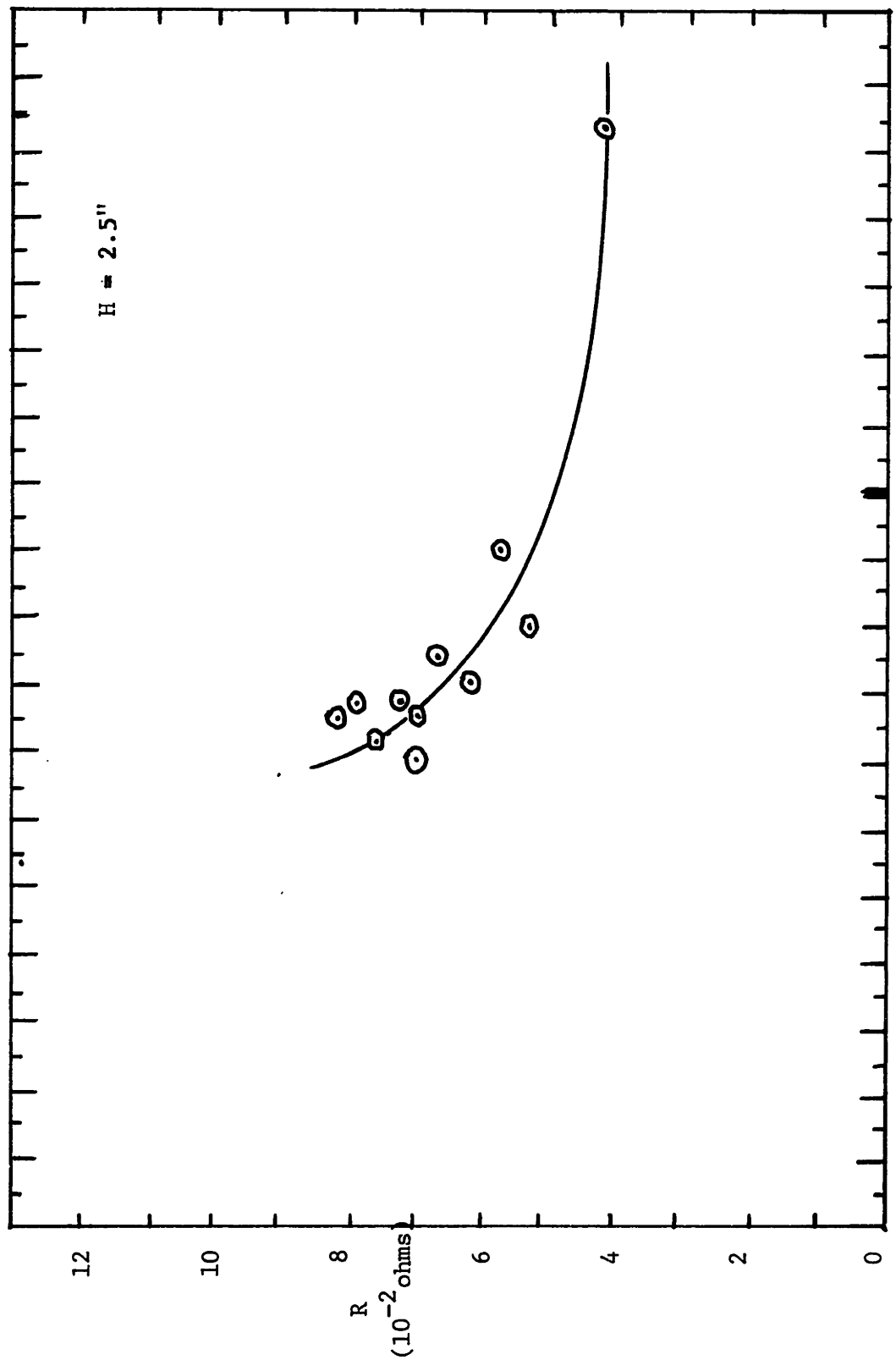

Figure 59--RESISTANCE VS. CHAMBER DIAMETER

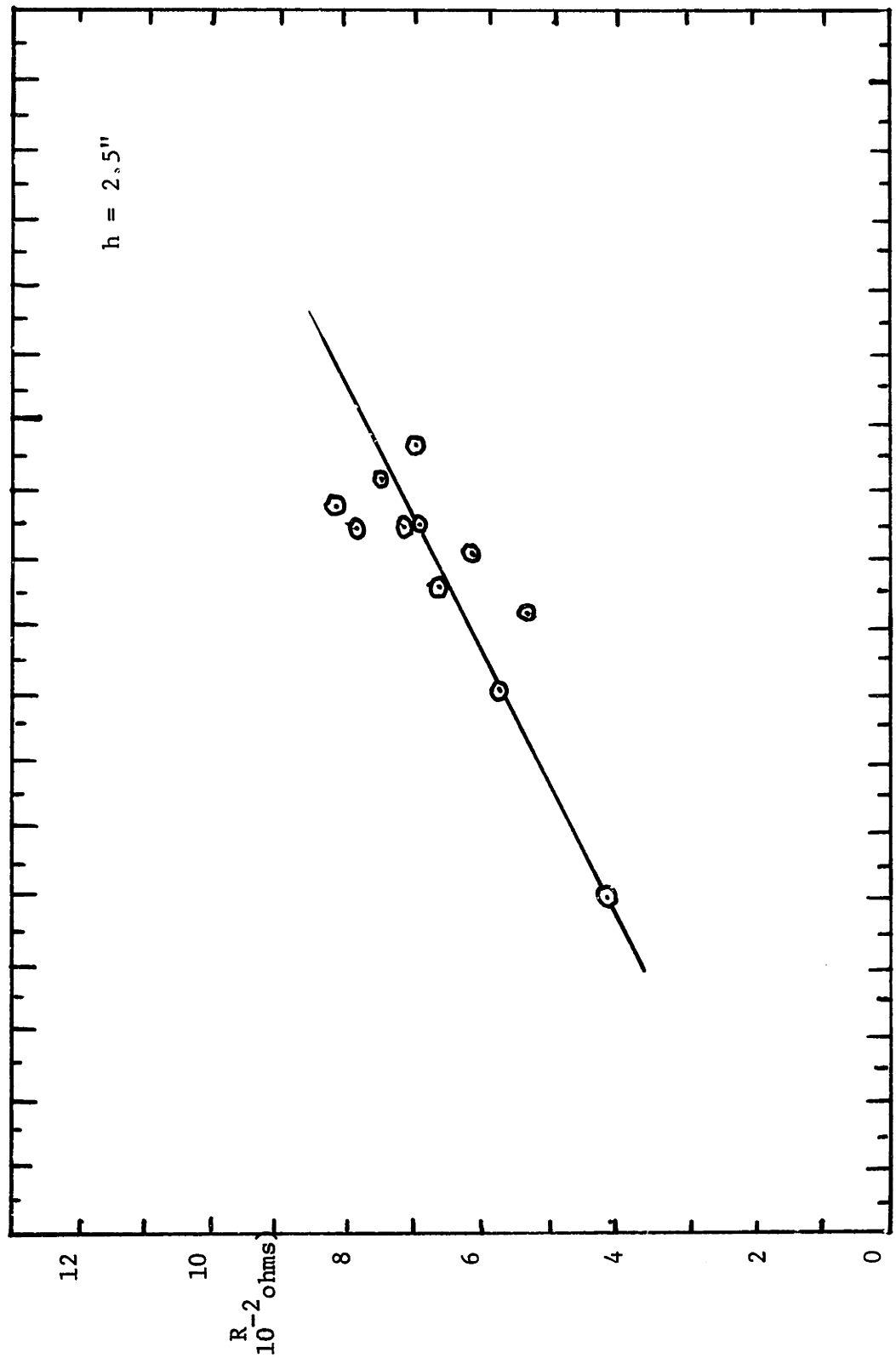

Figure 60--RESISTANCE VS. (CHAMBER DIAMETER)$^{-1}$

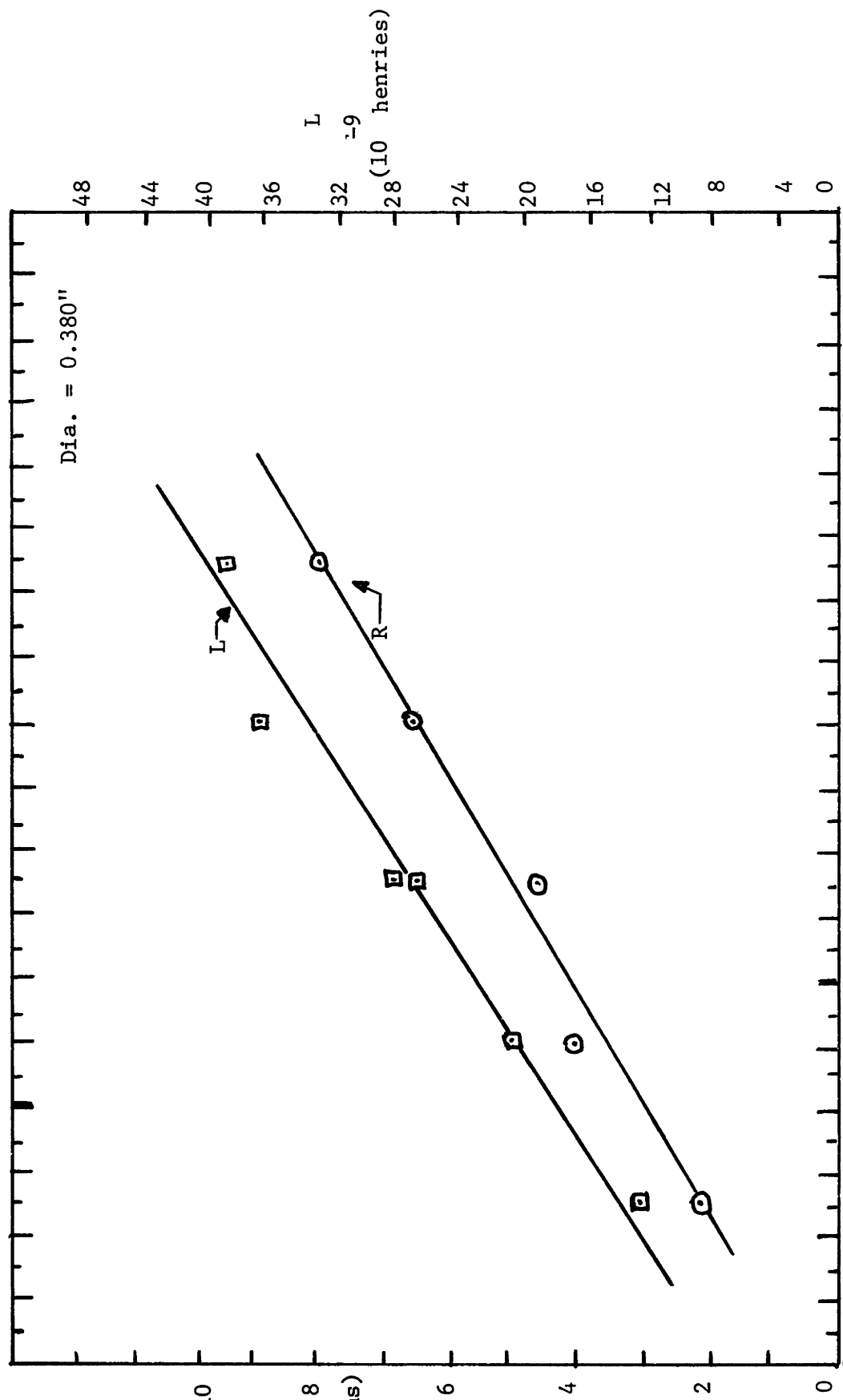

Figure 61--RESISTANCE AND INDUCTANCE VS. CHAMBER LENGTH

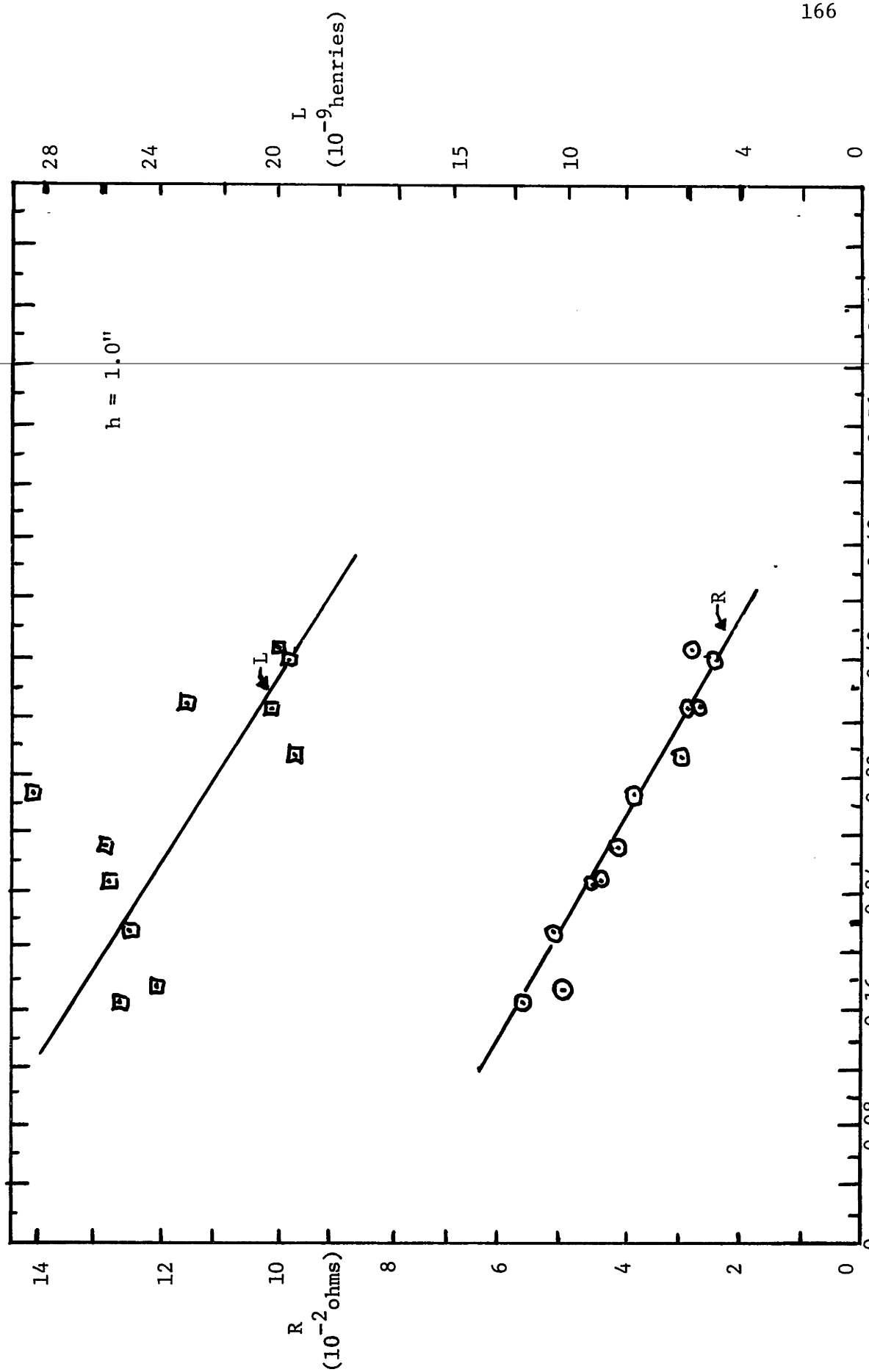

Figure 62--RESISTANCE AND INDUCTANCE VS. HYDRAULIC DIAMETER---RECTANGULAR GEOMETRY

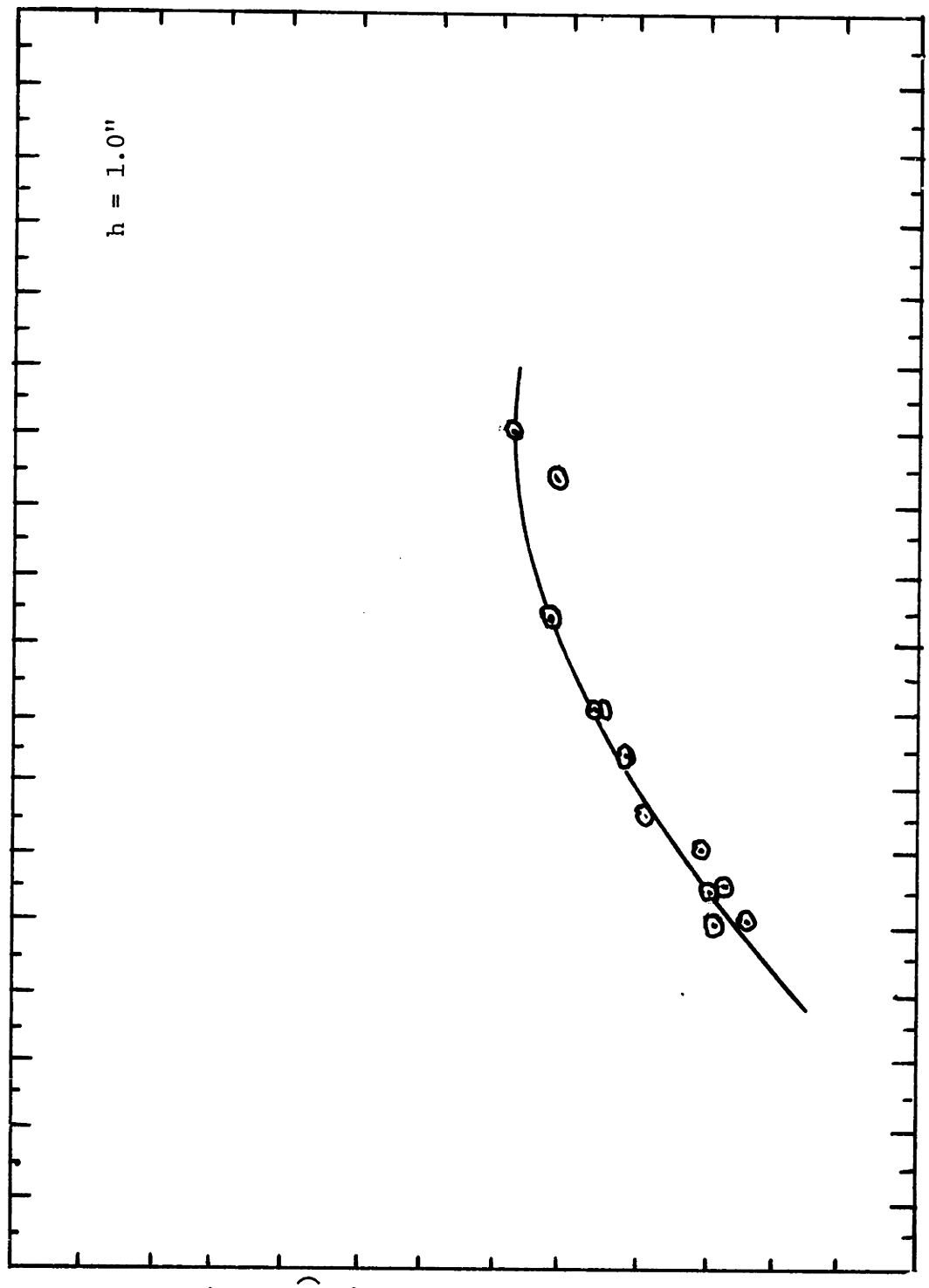

Figure 63--RESISTANCE VS. (HYDRAULIC DIAMETER) $^{-1}$---RECTANGULAR GEOMETRY

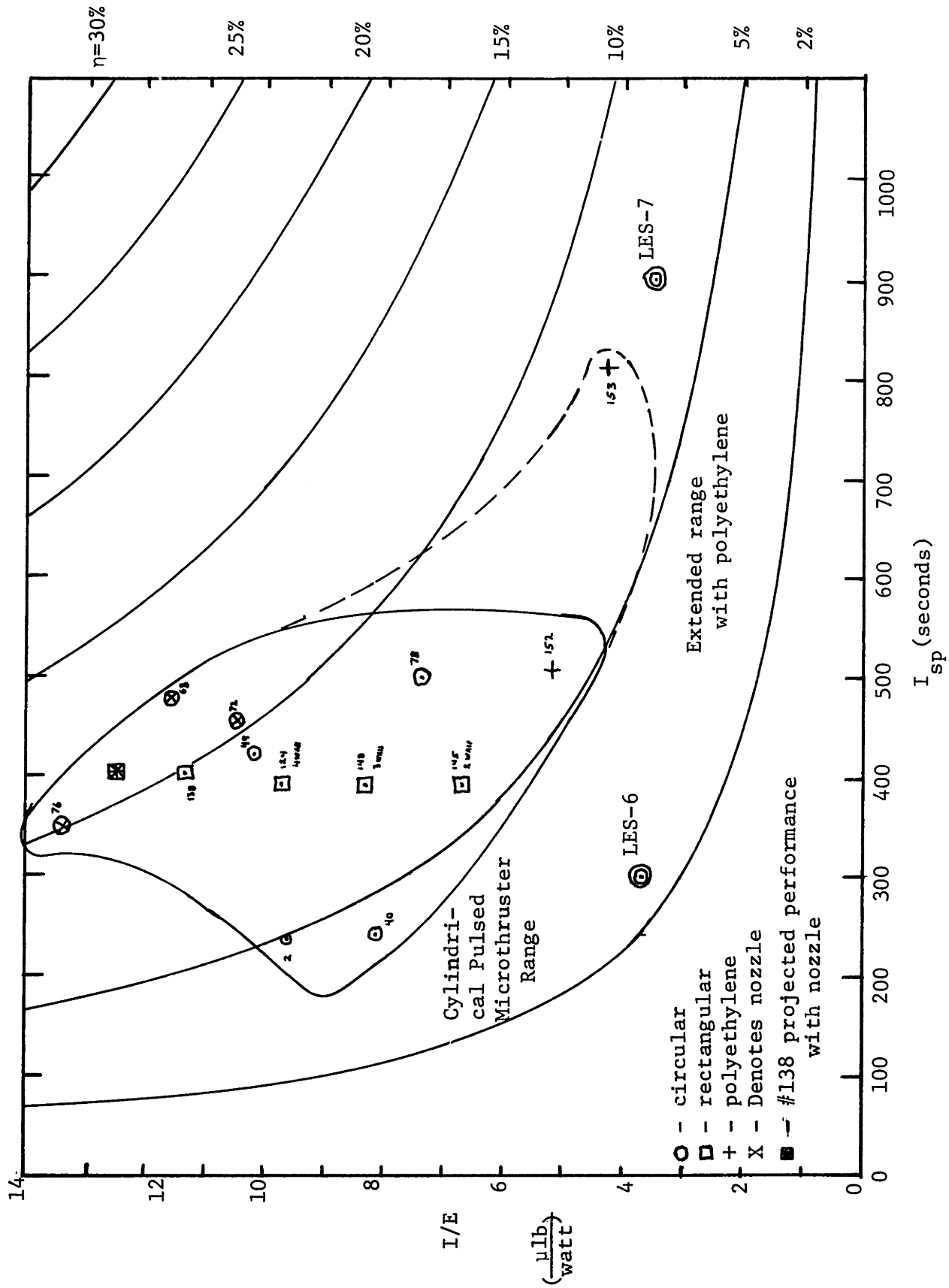

Figure 64A--Thruster Performance Range

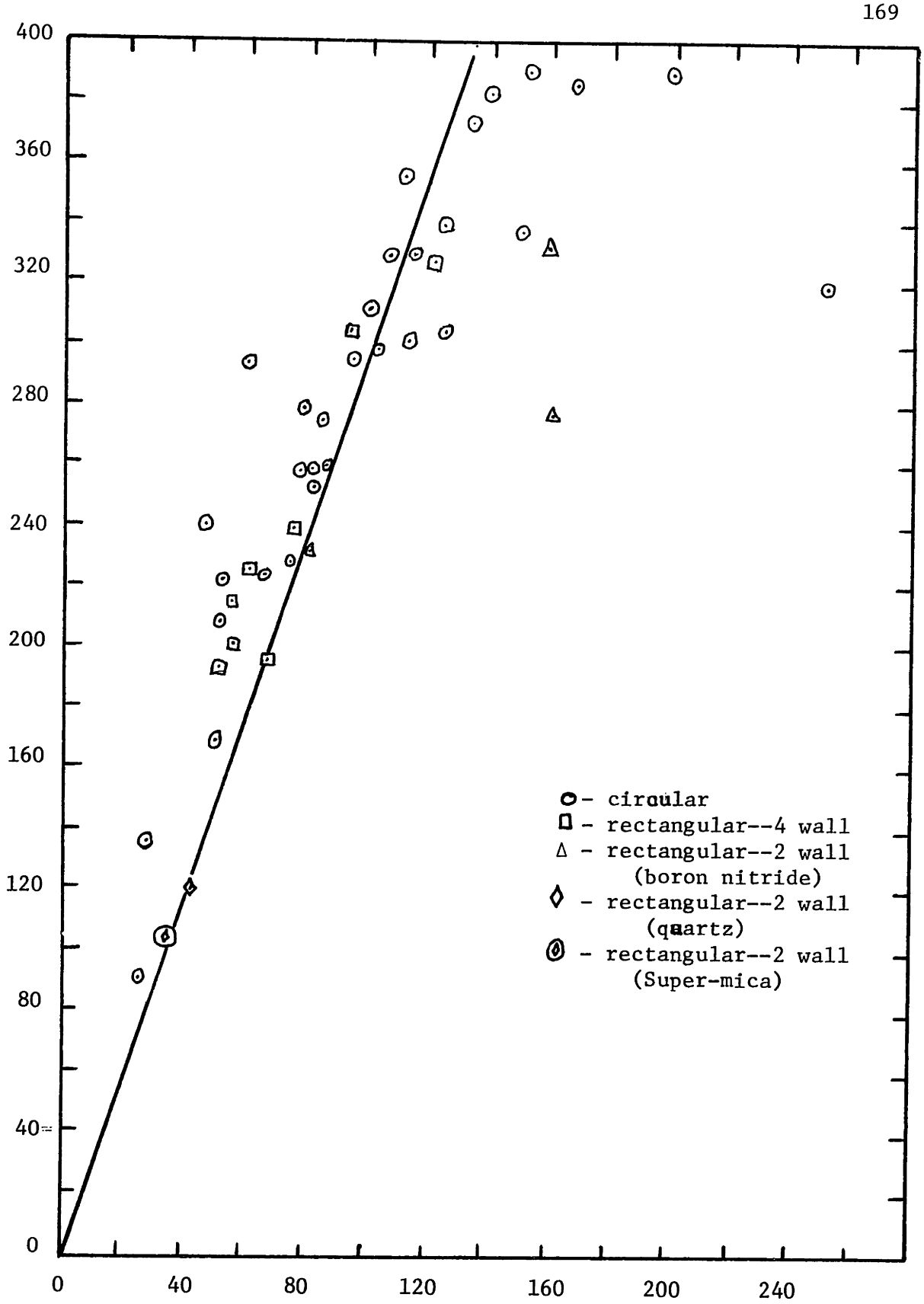

Figure 64B--MASS ABLATED/SHOT VS. hE/D---Circular & Rectangular Configuration

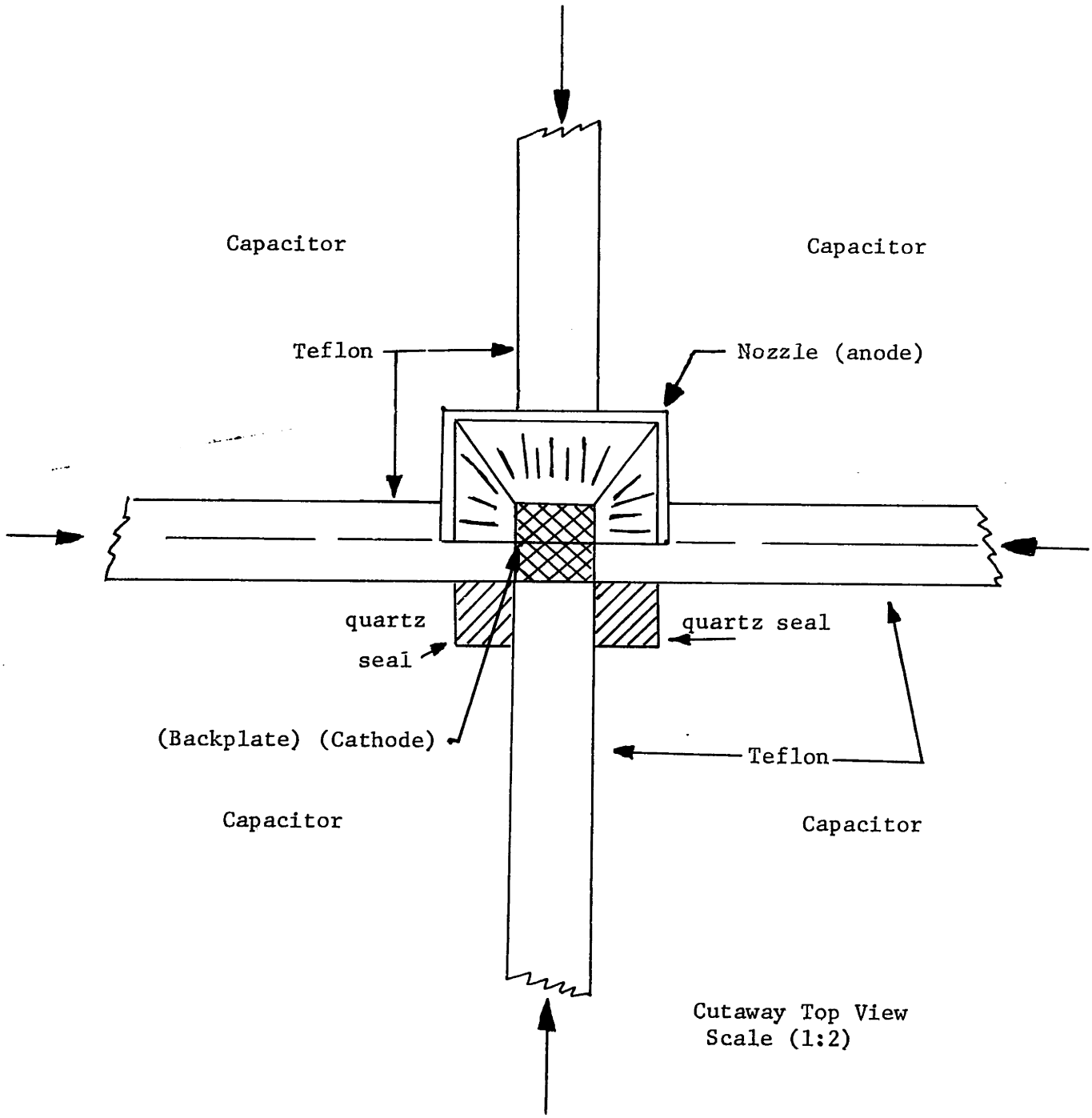

Figure 65--SCHEMATIC OF FOUR-WALL TEFLON FEED THRUSTER

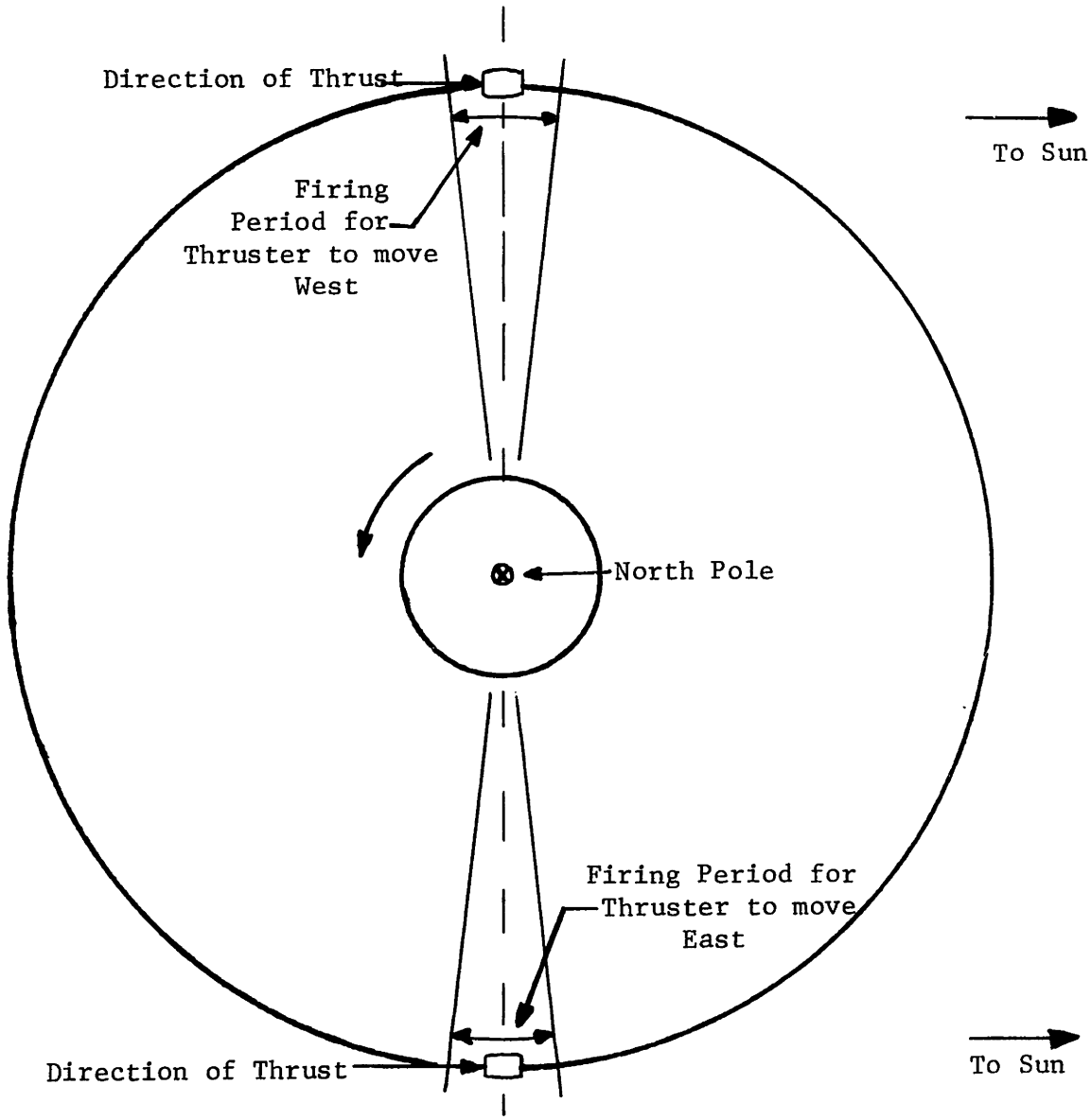

Figure 66--TYPICAL THRUSTING PROGRAM FOR EAST-WEST STATION_KEEPING

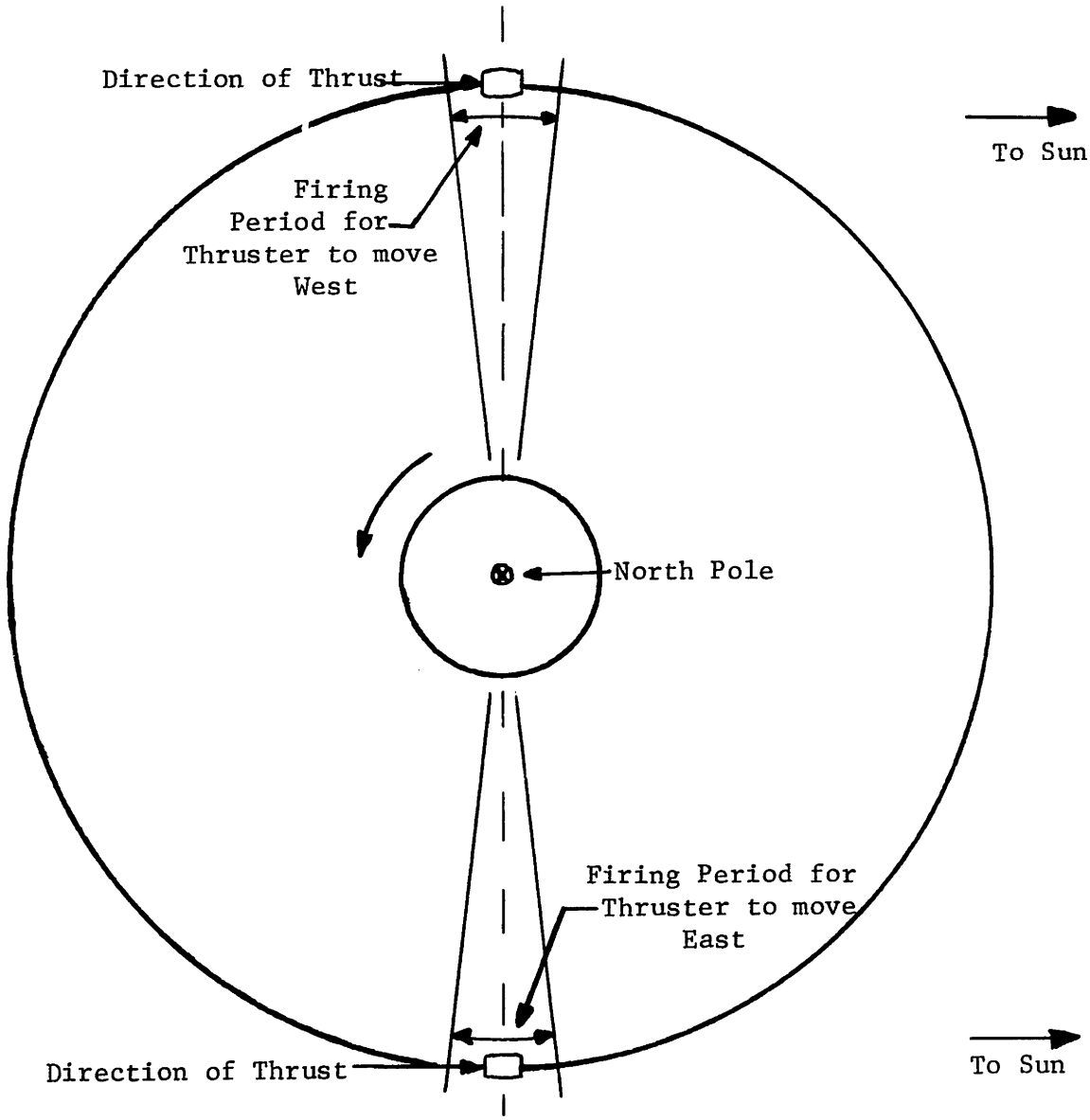

Figure 66--TYPICAL THRUSTING PROGRAM FOR EAST-WEST STATION_KEEPING

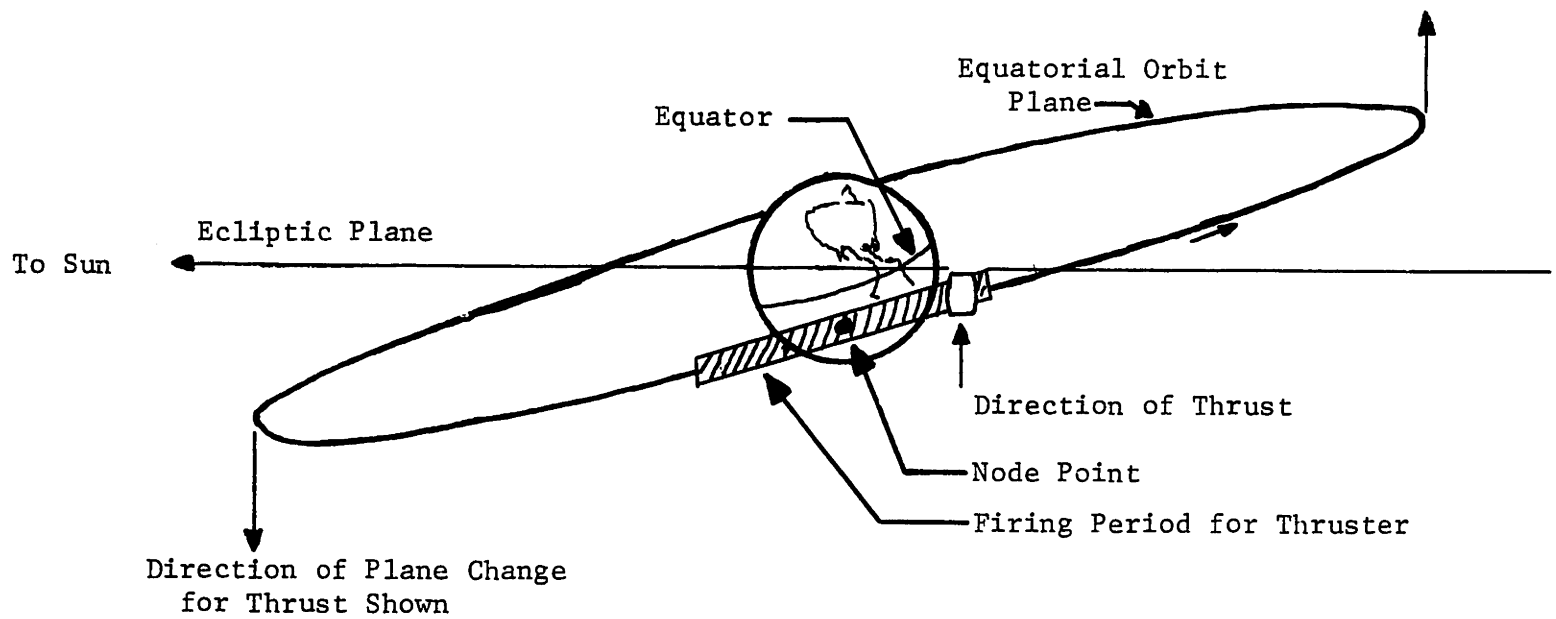

Figure 67--TYPICAL THRUSTING FOR NORTH-SOUTH STATION_KEEPING

REFERENCES

1. Palumbo, D.J. and Guman W.J., "Propellant Sidefeed-Short Pulse Discharge Thruster Studies, NASA Contractor's Report, No. CR-112035, January, 1972.

2. Holcomb, Lee B., Satellite Auxillary--Propulsion Selection Techniques, Addendum Survey of Auxillary Electric Propulsion Systems, Technical Report 32-1505, Addendum, Jet Propulsion Laboratory, Pasadena, Calif., July 15, 1971.

3. Palumbo, D.J., and Guman, W.J., "Continuing Development of Short-Pulsed Ablative Space Propulsion Systems, AIAA Paper No. 72-1154, AIAA/SAE 8th Joint Propulsion Conference, New Orleans, La., Nov. 29-Dec. 1, 1972.

4. Holcomb, Lee B., Satellite Auxillary-Propulsion Selection Techniques, Applications of Selection Techniques to the ATS-H Satellite, Technical Report 32-1505, Supplement I, Jet Propulsion Laboratory, Pasadena, Calif., Oct. 1, 1972.

5. Vondra, Robert, Personal Communication, December 10, 1972. MIT Lincoln Labs, Cambridge, Mass.

6. Hawk, C. et. al., "System Study of Electric Propulsion for Military Space Vehicles", AIAA Paper No. 72-493, AIAA 9th Electric Propulsion Conference, Bethesda, Md., April 17-19, 1972.

7. Guman, W.J. and Nathanson, D.M., "Pulsed Plasma Microthruster System for Synchronous Orbit Satellite, AIAA Paper No. 69-288, AIAA 7th Electric Propulsion Conference, Williamsburg, Va., March 3-5, 1969.

8. Holcomb, Lee B., "Survey of Satellite Auxillary Propulsion Systems", Journal of Spacecraft and Rockets, Volume 9, No. 3, March, 1972.

9. Thomassen, K.I. and Tong, D., "Interferometric Density Measurements in the Arc of a Pulsed Plasma Thruster", AIAA Paper No. 72-463, AIAA 9th Electric Propulsion Conference, Bethesda, Md., April 17-19, 1972.

10. Vondra, Robert, Thomassen, Keith, and Solbes, Albert, "A Pulsed Electric Thruster for Satellite Control", Proceedings of the IEEE, Vol. 59, No. 2, February, 1971, pp. 271-277.

11. Waltz, P.M., "Analysis of a Pulsed, Electromagnetic Plasma Thruster", Master's Thesis, 1969, Department of Electrical Engineering, M.I.T., Cambridge, Mass.

12. Rao, G.V.R., "Exhaust Nozzle Contour for Optimum Thrust", Jet Propulsion, Vol. 28, No. 6, June, 1958, p. 377.

13. Williams, T.E. and Callens, R.A., "Performance Testing of a Solid Propellant Pulsed Plasma Microthruster", AIAA Paper No. 72-460, AIAA 9th Electrical Propulsion Conference, Bethesda, Md., April 17-19, 1972.

14. Radley, R.J., Jr., "A Study of a Pulsed Solid Fuel Microthruster", Master's Thesis, 1969, Department of Aeronautics and Astronautics, M.I.T., Cambridge, Mass.

15. Jahn, Robert G., Physics of Electric Propulsion, (New York: McGraw-Hill Book Co.,)1959, pp. 266-267.

16. Metzler, John, "A Parametric Study of the Performance of a Pulsed Solid Fuel Microthruster", Master's Thesis, 1971, Department of Aeronautics and Astronautics, M.I.T., Cambridge, Mass.

17. Wentink, Tunis, Jr., "High Temperature Behavior of Teflon", AVCO-Everett Research Laboratory Reasearch Report #55, July, 1959.

18. Rohsenow, W.M. and Choi, H.Y., Heat, Mass, and Momentum Transfer, (Englewood Cliffs: Prentice-Hall, Inc., 1961), p. 185.

19. Kreith, Frank, Principles of Heat Transfer, (Scranton: International Textbook Co., 1969), p.377.

20. Smythe, W., Static and Dynamic Electricity, (New York: McGraw-Hill Book Co., 1968), p.340.

21. Landsman, Manny, Personal Communication, September 20, 1972. M.I.T. Lincoln Labs, Cambridge, Mass.

22. Isley, William C. and Duck, Kenneth I., "Propulsion Requirements for Communication's Satellites", AIAA Paper No. 72-514, AIAA 4th Communication's Satellite Systems Conference, Washington, D.C., April 24-26, 1972.

23. Free, Bernard and Huson, George, "Selected Comparisons Among Propulsion Systems for Communications Satellites", AIAA Paper No. 72-517, AIAA 4th Communications Satellite Systems Conference, Washington,D.C., April 24-26, 1972.

24. Guman, W.J., Vondra, R.J., and Thomassen, Keith, Pulsed Plasma Propulsion Systems Studies, AIAA Paper No. 70-1148, AIAA 8th Electric Propulsion Conference, Stanford, Calif., August 31-Sept. 2, 1970.

25. Lyon, Wanen C., "Thruster Exhaust Effects Upon Spacecraft", AIAA Paper No. 70-1143, AIAA 8th Electric Propulsion Conference, Stanford, Calif., August 31-Sept. 2, 1970.

26. Lyon, Warren C., "Monopropellant Exhaust Effects Upon Spacecraft", Journal of Spacecrafts and Rockets, Vol. 8, No. 7, July, 1971, p. 689.

27. Hall, D.F. and Lyon, W.C., "Low Thrust Propulsion System Effects on Communication Satellites", AIAA Paper No.72-519, AIAA 4th Communication Satellite Systems Conference, Washington D.C., April 24-26, 1972.